FINITE ELEMENT ANALYSIS OF STRUCTURES IN THE PLASTIC RANGE

by H. Armen, Jr., A. Pifko, and H. S. Levine

1. Report No. NASA CR-1649	2. Government Accession No.	3. Recipient's Catalog No.
4. Title and Subtitle FINITE ELEMENT ANALYSIS OF STRUCTURES IN THE PLASTIC RANGE		5. Report Date February 1971
		6. Performing Organization Code
7. Author(s) H. Armen, Jr., A. Pifko, and H. S. Levine		8. Performing Organization Report No.
9. Performing Organization Name and Address Grumman Aerospace Corporation Bethpage, New York 11714		10. Work Unit No. 126-14-16-03
		11. Contract or Grant No. NAS1-7315
12. Sponsoring Agency Name and Address National Aeronautics and Space Administration Washington, D. C. 20546		13. Type of Report and Period Covered Contractor Report
		14. Sponsoring Agency Code

15. Supplementary Notes

16. Abstract

This study represents an extension of finite-element methods to provide analytical means for determining the nonlinear response of aircraft structures. Consideration is given to material and geometric nonlinearity, acting separately or in combination.

The methods developed are applicable to loading conditions that cause either membrane stresses or pure bending, or both in combination. The finite-element analysis methods for material nonlinearity can account for the Bauschinger effect for biaxial stress states by using the Prager-Ziegler kinematic hardening theory of plasticity.

Application of the methods is made to several simple structures including notched bars and rectangular, circular, and annular plates, although it should be noted that these methods are fully capable of being applied to complex, built-up structures. Good correlation is obtained between results from the present analysis and existing experimental and/or analytical results.

17. Key Words (Suggested by Author(s)) Plasticity, Finite Element Methods, Nonlinear Structural Analysis, Stress Concentrations	18. Distribution Statement Unclassified - Unlimited		
19. Security Classif. (of this report) Unclassified	20. Security Classif. (of this page) Unclassified	21. No. of Pages 281	22. Price* $ 3.00

FOREWORD

This report was prepared by the Grumman Aerospace Corporation, Bethpage, New York, under Contract NAS 1-7315, entitled, "A Research Study for the Development of a Digital Method of Analysis of Supersonic Transport Aircraft Structures in the Plastic Range." The work was performed by the Research Department of Grumman Aerospace Corporation, with support from the Computing Sciences Department.

The authors wish to acknowledge the valuable contribution of Joseph S. Miller of the Computing Sciences Department for digital computer programming. Thanks also go to Dr. Gabriel Isakson, Head of the Applied Mechanics Group, for helpful comments during the course of the investigation, and to Catherine O'Regan for drafting services.

This volume presents the development of the methodology and results obtained in the application of these methods to some representative sample structures.

TABLE OF CONTENTS

vi

SUMMARY

The present report is concerned with the development of finite-element methods for the treatment of the nonlinear behavior of complex structures. It represents an extension of a previous study reported in NASA Contractor's Report CR-803. The nonlinearity may be of two types, material nonlinearity associated with plastic deformation and geometric nonlinearity associated with the changing geometry of the structure as it deforms, or it may involve a combination of the two. Effects due to creep and other time-dependent material properties are neglected.

The methods developed are applicable to loading conditions that cause membrane stress states or pure bending, or both in combination. The Prager-Ziegler kinematic hardening theory of plasticity is incorporated in the finite element methods to allow for consideration of the plastic response of structures subjected to realistic loading conditions, including cyclic loadings that cause stress reversals into the plastic range. Ideally plastic behavior is also included to provide capability for predicting the collapse load of structures. The plasticity theory is implemented in the finite element analysis by using an incremental approach in conjunction with the initial strain concept, with plastic strains interpreted as initial strains.

The treatment of geometric nonlinearity requires use of an incremental technique in which the internal forces and configuration of the structure are continuously updated to account for its changing geometry.

The methods developed are applied to a number of sample structures. For membrane stress states alone, the analysis employs a triangular finite element in which stress and strain vary linearly. This element is used for the plastic analysis of a variety of structures characterized by regions of rapid stress variation and subjected to cyclic loading resulting in reversed plasticity. Comparisons between the results of the analysis and experimental data indicate good correlation.

Plastic analyses have also been performed for a variety of beam and plate structures. These problems make use of refined rectangular and triangular finite elements. Among the problems considered are rectangular, circular, and annular plates with

various boundary conditions. Once again, comparisons with results of other available analyses are favorable.

Problems of combined bending and stretching of plates are also considered. Results are obtained for rectangular and circular plates. Results for combined geometric and material nonlinearity are presented for beams and arches.

1. INTRODUCTION

Redundant structures constructed of ductile materials can, as is well known, withstand substantial increases in loading, as compared with similar structures constructed of equal strength, brittle materials. The ability to determine the reserve strength of these structures accurately and provide the technology for predicting their failure loads under a variety of realistic loading conditions has stimulated substantial efforts toward developing methods for the analysis of structures in the plastic range.

Considerable progress has been made recently in developing general methods of plastic analysis. This progress is largely attributable to advances in the field of numerical methods of structural analysis, specifically, the finite-element method. The treatment of nonlinearities, both physical and geometric, within the framework of existing finite element techniques, permits analysis of structures of arbitrary shape and consideration of a variety of loading and boundary conditions.

References 1 through 20 are representative of recent investigations concerned with incorporating the effects of plastic behavior in finite-element analysis. These studies describe techniques to treat plasticity by means of various algorithms that linearize the basically nonlinear problem.

This report is an extension of a previous study made under NASA Contract NAS 1-5040 and reported in Ref. 11. The earlier study developed discrete-element methods for the plastic analysis of complex built-up structures in states of biaxial membrane stress, with particular emphasis on the effect of cyclic loading causing stress reversals in the plastic range. To accommodate this case, the methods implemented a plasticity theory that can take into account the Bauschinger effect. This theory is the kinematic hardening theory of Prager (Refs. 21 and 22) as modified by Ziegler (Ref. 23). It can represent the salient features of the plastic behavior of structural metals, and is readily implemented in a discrete-element analysis.

Although the methods developed in Ref. 11 can treat cyclic loading and accommodate ideally plastic or strain-hardening material behavior, they have substantial limitations, viz.,

• The structural idealizations considered in Ref. 11 were limited to bar elements, in which only axial stress is present (uniform and linearly varying), and to thin planar elements that carry only a uniformly distributed biaxial membrane stress. Thus strain variation in the middle surface of a thin planar element or through its thickness as a result of bending was not treated.

• The effect of geometric nonlinearity was not taken into account. Thus the change in the structure's stiffness properties due to the nonlinear strain-displacement relations and to the changing geometry of the deformed structure was neglected.

As a result of the current investigation, these restrictions have been removed and the methods developed in Ref. 11 have been extended. Two principal areas are discussed in this report.

First, plastic analysis methods are developed in which a nonuniform strain distribution is assumed to exist within each element. Two types of strain variation are considered within the framework of this assumption. In the first, a linear variation in the middle surface of a thin planar element is assumed. Using an element with a linearly varying strain distribution has a two-fold advantage over the constant strain element: it can provide a more accurate description of the state of stress in a structure, particularly in regions of high stress gradient, than the constant strain element used previously; and it provides a more easily interpreted description of the state of stress. These features are desirable since accurate representation of stress is particularly important in plasticity analyses.

The second type of strain variation considered is that through the thickness of the element and is intended for application to structures with plate or shell components in which bending effects may be significant. Plastic strains are assumed to vary linearly from the upper and/or lower surface of the element to an elastic-plastic boundary located at some point through the thickness. The finite elements chosen for use in the plastic bending analysis include a beam element of rectangular cross section, a 16 degree-of-freedom rectangular plate element, and an 18 degree-of-freedom triangular bending element.

2

The second area here discussed is the development of finite element methods to treat geometrically nonlinear behavior of elastic and plastic structures. To this end, an incremental procedure is used that involves linearizing the problem within each of a series of steps associated with an incrementation of the applied loading.

Simultaneous treatment of plasticity and geometric nonlinearity is accomplished by combining the initial strain concept with the incremental geometric nonlinear procedure. The resulting incremental procedure involves solving a new linear problem at each step of the loading process, with changing geometry causing changes in the stiffness-influence coefficient matrices, and with plasticity accounted for by means of the initial strain-plastic strain analogy in conjunction with subsidiary constitutive relations from an appropriate plasticity theory.

Application of the methods has been made to a broad spectrum of sample structures. By this means it is possible to determine the limits of applicability of the methods and consequently to single out those deficiencies which might otherwise be undetectable in a numerical method of analysis such as the finite element method.

LIST OF SYMBOLS

a	length of beam or rectangular plate; radius of circular plate
b	width of rectangular plate; inner radius of annular plate
c	hardening coefficient
d	generalized displacement
e^e	elastic strain
e^o	initial elastic strain
e^T	total strain
E	Young's modulus
f	yield or loading function
h	plate thickness
K_T	theoretical elastic stress concentration factor based on nominal net section stress
K_p, $K_p{}'$	plastic stress concentration factor based on nominal net section stress for initial tensile loading and reversed loading from initial tension, respectively
ℓ	length of beam finite element
M_o	fully plastic moment $\left[M_o = \sigma_o t^2 \right]$
M^*	yield moment $\left[M^* = \frac{2}{3} \sigma_o t^2 \right]$
n	shape parameter used in Ramberg-Osgood stress-strain relation
N_x, N_y, N_{xy}, N_r	components of membrane stress resultants

N_{crit}	elastic buckling stress resultant
p	applied load intensity
P_{rq}	area integral $\left[P_{rq} = \iint x^r y^q dA \right]$
P, P_o	nodal generalized forces
q	effective plastic load
r	radial coordinate
S	nominal net section stress
t	half-thickness of plate
u, v	in-plane displacement components
U	strain energy
w	transverse displacement
x, y, z	local coordinates of finite element
$\bar{z}$	depth of elastic-plastic boundary for beams and plates
α	ratio of applied membrane stress resultant to buckling membrane stress resultant
α_{ij}	coordinates of center of loading surface
Δ	denotes an incremental quantity
ϵ_{ij}	plastic strain
θ^2	nonlinear terms in strain-displacement relations
$d\lambda$	differential of scalar quantity appearing in flow rule
$d\mu$	differential of scalar quantity appearing in Ziegler's hardening rule

6

ν	Poisson's ratio
σ_{ij}	components of stress
σ_o	yield stress
$\sigma_{0.7}$	parameter in Ramberg-Osgood stress-strain relation
σ_∞	free field stress
ω_i	triangular area coordinate (see Appendix F)

Matrices:

$[A]$	matrix relating total strains in structure to applied load
$[B]$	matrix relating stresses in structure to applied load
$[C]$	matrix relating plastic strain increments to stress increments in strain-hardening finite element [Eq.(A.8)]
$[E]$	matrix relating elastic strains to stresses in a finite element [Eq. (A.19)]
$[\bar{E}]$	matrix expressing condition of tangency of stress increment vector to yield or loading surface in an individual ideally-plastic element [Eq. (A.11)]
$[\tilde{E}]$	matrix expressing condition of normality of plastic strain increment vector to yield or loading surface in an individual ideally-plastic finite element [Eq. (A.14)]
$[E^*]$	matrix defined by Eq. (A.23)
$[k]$	elastic stiffness matrix for a finite element
$[\bar{k}]$	initial strain stiffness matrix for a finite element based on an assumed distribution for increment of initial (plastic) strain

$[k^{*}]$ initial strain stiffness matrix for a finite element based on an assumed distribution for initial (plastic) strain

$[k^{(1)}]$ initial stress stiffness matrix for a finite element

$[R]$ matrix relating stress increments to total strain increments for a strain-hardening material [defined in Eq. (A.22)]

$[W]$ matrix relating element strain to nodal generalized displacements

$[\bar{W}_p]$ matrix relating element initial (plastic) strain increment to initial (plastic) strain increment at nodes

$[W_p^{*}]$ matrix relating element total plastic strain to total plastic strain at nodes

$[T]$ orthogonal transformation matrix relating generalized nodal displacements in the local co-ordinates axes to the global axes

$\{\Delta\omega\}$ vector defined in Eq. (A.15)

Matrix Notation:

$\{\ \}$ column vector

$[\ ]$ square or rectangular matrix

$\lceil\ \rfloor$ diagonal matrix

$[\ ]'$ transpose

$[\ ]^{-1}$ inverse

d used as a subscript denotes a diagonally partitioned matrix

o used as a subscript denotes nodal quantities

i used as a superscript denotes ith incremental load step

8

2. METHODS OF ANALYSIS

The methods developed here are of the incremental type, since solutions to problems involving material nonlinearity, when it is present alone or in combination with geometric nonlinearity, are best obtained by solving a sequence of linear problems associated with an incremental application of the loading. The formulation of the governing matrix equation is developed within the framework of the displacement method of finite-element analysis. As in a linear elastic analysis, assumptions are made concerning the displacement field within an individual finite element in terms of discrete quantities at node points. In addition, assumptions may be made concerning the distribution of plastic strain (or its increment corresponding to an increment in loading) within each element. Plasticity is included by introducing the effects of initial strains into the governing matrix equation and then interpreting these initial strains as plastic strains. Stiffness matrices additional to the usual elastic stiffness matrices for small displacements are introduced to treat problems of combined nonlinearity involving small strains and large displacements.

Formulation of General Matrix Equation

As a first step in the analysis, the assumptions concerning displacements and initial strains are used to derive the force-displacement relations for an individual finite element. This is accomplished by application of the principle of virtual work or through a consistent energy approach. Here we use the latter and, in accordance with an incremental approach, the equations are derived from the expression for the increment of strain energy.

The increment in elastic strain energy ΔU from an initial elastic strain state $\{e^o\}$ may be written as

$$\Delta U = \iiint_V \left[\int_{\{e^o\}}^{\{e^o\}+\{\Delta e^e\}} \{\sigma\}' \{de^e\} \right] dV \qquad (1)$$

9

where $\{\sigma\}$ represents the stresses, $\{\Delta e^e\}$ is the increment in elastic strain, and the triple integration is carried out through the volume V of the element.

Strictly interpreted, Eq. (1) is valid only for linear elastic material behavior. However, by analogy with the equivalence between temperature gradients and body forces in causing a strain field in thermoelasticity, plastic strains can similarly be related to fictitious body forces (Refs. 24 and 25). This permits application of known analytical techniques of elasticity to the analysis of bodies subjected to plastic strain.

In the presence of plastic strains, the increment of elastic strain can be written as

$$\left\{\Delta e^e\right\} = \left\{\Delta e^T\right\} - \left\{\Delta\epsilon\right\} , \qquad (2)$$

where $\{\Delta e^T\}$ is the increment of total strain and $\{\Delta\epsilon\}$ is the increment of plastic strain. The stresses $\{\sigma\}$ are related to the elastic strain by the linear stress-strain relation, written as

$$\left\{\sigma\right\} = [E] \left\{e^e\right\} , \qquad (3)$$

where the elements of the matrix $[E]$ are the usual elastic coefficients. Similarly, the stresses present in the structure at the beginning of the load increment are related to the corresponding elastic strains as follows,

$$\left\{\sigma^o\right\} = [E] \left\{e^o\right\} . \qquad (4)$$

The following expression for the increment of strain energy is obtained by substituting Eq. (3) into Eq. (1), integrating between the prescribed limits of strain, and then substituting Eqs. (2) and (4) into the resulting equation.

10

$$\Delta U = \frac{1}{2} \iiint_V \left\{ \Delta e^T \right\}' [E] \left\{ \Delta e^T \right\} dV - \iiint_V \left\{ \Delta e^T \right\}' [E] \left\{ \Delta \epsilon \right\} dV$$

$$+ \frac{1}{2} \iiint_V \left\{ \Delta \epsilon \right\}' [E] \left\{ \Delta \epsilon \right\} dV + \iiint_V \left\{ \sigma^o \right\}' \left\{ \Delta e^T \right\} dV \qquad (5)$$

$$- \iiint_V \left\{ \sigma^o \right\}' \left\{ \Delta \epsilon \right\} dV$$

It is at this stage that the assumptions concerning the displacement and plastic strain fields must be made. These assumptions, although independent of each other, are dependent upon the class of problem to be considered (i.e., bending or membrane stress) and serve to define the stiffness properties of the finite element. Specific assumptions made and results for some sample structures are discussed in subsequent sections.

Once the assumption concerning the variation of displacement within the element is made, the total strain distribution can be expressed in terms of nodal displacements by making use of the appropriate strain-displacement relations in conjunction with the assumed displacement function. These relations can be written in matrix form as follows,

$$\left\{ \Delta e^T \right\} = [W] \left\{ \Delta d_o \right\} + \left\{ \Delta \theta^2 \right\} \qquad (6)$$

where $\{ \Delta d_o \}$ is the vector of generalized incremental nodal displacements, $[W]$ is a function matrix (that is, a matrix in which the elements are functions rather than constants) that is obtained from the linear component of the strain-displacement relations, and $\{ \Delta \theta^2 \}$ symbolically represents the nonlinear contribution to the strain-displacement relations, i.e., squares and products of increments of rotation. The increments of rotation $\{ \Delta \theta \}$ are related to the generalized displacement increments, and may be represented as

$$\{\Delta\theta\} = [\tilde{W}] \{\Delta d_o\} \tag{7}$$

where $[\tilde{W}]$ is a function matrix.

In a plasticity analysis, assumptions may also be made concerning the distribution of the increment of initial strain (or plastic strain) within each element. These assumptions are made independently of those concerning the distribution of total strain, Eq. (6). The assumed distribution of plastic strain increments can be written in terms of their values at nodes, as follows,

$$\{\Delta\epsilon\} = [\bar{W}_p] \{\Delta\epsilon_o\} \tag{8}$$

where $\{\Delta\epsilon_o\}$ represents the nodal plastic strain increments, and $[\bar{W}_p]$ is a function matrix that explicitly depends upon the assumptions made concerning the distribution of plastic strain increments.

Substituting Eqs. (6) through (8) into Eq. (5), neglecting the higher order contributions of displacement increments in each of the integrals, and neglecting as well all terms that are independent of displacement increments, we are led to the following expression,

$$\Delta U = \frac{1}{2} \{\Delta d_o\}' [k^{(0)}] \{\Delta d_o\}$$

$$- \{\Delta d_o\}' [\bar{k}] \{\Delta\epsilon_o\} \tag{9}$$

$$+ \frac{1}{2} \{\Delta d_o\}' [k^{(1)}] \{\Delta d_o\} + \ldots$$

12

where

$$[k^{(0)}] = \iiint_V [W]'[E][W]\,dV$$

$$[\bar{k}] = \iiint_{V_p} [W]'[E][\bar{W}_p]\,dV \tag{10}$$

$$[k^{(1)}] = \iiint_V [\tilde{W}]'[\sigma^0][\tilde{W}]\,dV \ .$$

The matrix $[k^{(0)}]$ is the conventional elastic stiffness matrix, obtained from the linear components of the strain-displacement relations; $[\bar{k}]$ is the initial strain stiffness matrix and accounts for the effects of the presence of initial strains; $[k^{(1)}]$ represents the initial stress stiffness matrix and appears as a result of the nonlinear terms of the strain-displacement relation. This last matrix can be considered as an additional component of the element stiffness matrix that accounts for the effect that the presence of stresses has on subsequent deformations. The elements of the matrix $[\sigma^0]$ are components of the stress state existing at the beginning of the incremental change in energy. V_p is the volume of the plastic region in each element.

Application of Castigliano's first theorem to Eq. (9) yields the following governing incremental linear matrix equation for an individual finite element,

$$\frac{\partial(\Delta U)}{\partial\{\Delta d_o\}} = \{\Delta p_o\} = \left[[k^{(0)}] + [k^{(1)}]\right]\{\Delta d_o\} - [\bar{k}]\{\Delta\epsilon_o\} \tag{11}$$

where $\{\Delta p_o\}$ represents the vector of increments in the generalized nodal forces.

13

This form is convenient to use if the assumptions associated with the plastic strain distribution are applied to their incremental values. For some types of analysis, such as bending and combined bending and stretching, it is convenient to use assumptions concerning the distribution of total plastic strain rather than of incremental plastic strain. This requires that Eq. (8) be replaced by

$$\{\epsilon\} = [W_p^*] \{\epsilon_o\} \tag{12}$$

where the elements of the matrix $[W_p^*]$ represent the assumed functional representation of the total plastic strains $\{\epsilon\}$ in terms of their nodal values $\{\epsilon_o\}$. At any step of the loading process, the increment of plastic strain may be written as

$$\{\Delta\epsilon\}^i = \{\epsilon\}^i - \{\epsilon\}^{i-1} \tag{13}$$

where the superscripts i and $i-1$ refer to current and preceding load steps, respectively.

Substituting Eqs. (12) and (13) into the expression for strain energy, Eq. (5), and applying Castigliano's first theorem leads to the following equation,

$$\{\Delta p_o\} = \left[[k^{(0)}] + [k^{(1)}] \right] \{\Delta d_o\}$$

$$- \left([k^*]^i \{\epsilon_o\}^i - [k^*]^{i-1} \{\epsilon_o\}^{i-1} \right) \tag{14}$$

where

$$[k^*] = \iiint_{V_p} [W]'[E][W_p^*]dV \tag{15}$$

14

and represents the initial strain stiffness matrix developed on the basis of assumptions made concerning the distribution of total plastic strain.

In general, the initial strain stiffness matrices $[\bar{k}]$, Eq. (10), and $[k^*]$, Eq. (15), may differ substantially. This is not the case, however, when the assumed distribution of the increment of plastic strain is the same as that for total plastic strain and when the initial strain stiffness matrix $[k^*]$ does not change with each load increment. The following equivalence is then valid

$$[k^*]^i \left\{\epsilon_o\right\}^i - [k^*]^{i-1} \left\{\epsilon_o\right\}^{i-1} = [k^*] \left\{\Delta\epsilon_o\right\} = [\bar{k}] \left\{\Delta\epsilon_o\right\} \tag{16}$$

and Eqs. (11) and (14) can be used interchangeably.

Material Nonlinearity

If we initially neglect the effects of changing geometry and write the elastic stiffness matrix as

$$[k^{(0)}] + [k^{(1)}] = [k_e] \tag{17}$$

then Eqs. (11) and (14) may be rewritten as

$$\left\{\Delta p_o\right\}^i = [k_e] \left\{\Delta d_o\right\}^i - [\bar{k}] \left\{\Delta\epsilon_o\right\}^i \tag{18}$$

and

$$\left\{\Delta p_o\right\}^i = [k_e] \left\{\Delta d_o\right\}^i - \left([k^*]^i \left\{\epsilon_o\right\}^i - [k^*]^{i-1} \left\{\epsilon_o\right\}^{i-1}\right) . \tag{19}$$

It should be noted that the initial stress stiffness matrix $[k^{(1)}]$ is not necessarily associated only with geometric nonlinearity, but may be required in such other cases as the bending of plates subjected to membrane stress.

<u>Displacement method — predictor procedure.</u> — Equations (18) and (19) may be put into alternative forms suitable for numerical solution; associated with each of these forms, there are alternative procedures for effecting a solution. In the following discussion, we distinguish between the basic forms employed by using the term "method"; we distinguish between the solution procedures employed by using the term "procedure." Thus we define a "displacement method" and a "strain method," and associated with each there is a "predictor procedure" and a "direct substitution procedure." In the first "method" to be treated, the product of the initial strain stiffness matrix and the vector of plastic strains (or their increments) can be considered as an "effective plastic loading," represented in Eq. (18) as

$$\{\Delta q\}^i = [\bar{k}] \{\Delta \epsilon_o\}^i \tag{20a}$$

or in Eq. (19) as

$$\{\Delta q\}^i = \{q\}^i - \{q\}^{i-1} = [k^*]^i \{\epsilon_o\}^i - [k^*]^{i-1} \{\epsilon_o\}^{i-1} . \tag{20b}$$

In Eq. (20b) the increment of the effective plastic loading is determined at any step by taking the difference in the products of the initial strain stiffness matrix and the vector of total plastic strains in two consecutive steps. In this way, only total values of plastic strain are utilized in the governing linear matrix equation.

The desired form of the equation is obtained by grouping together the increments of generalized nodal forces and effective plastic loads, resulting in the following equation,

$$[k_e] \{\Delta d_o\}^i = \{\Delta p_o\}^i + \{\Delta q\}^{i-1} . \tag{21}$$

Here it can be seen that the values of the increments of fictitious loads introduced into Eq. (21) are taken to be equal to those computed in the preceding load increment and are thus known quantities in this equation. The use of this type of "predictor procedure" obviates the necessity of introducing the plastic stress-strain relations explicitly into the governing matrix equation.

16

Equation (21) is written for each element in the structural idealization, and then, by an appropriate process of assemblage, the over-all linear matrix equation for the entire structure is formed. This resulting equation is identical in form to that of Eq. (21) and can be written as

$$[K_e] \left\{ \Delta D \right\}^i = \left\{ \Delta P \right\}^i + \left\{ \Delta Q \right\}^{i-1} \tag{22a}$$

where capitalization of the symbols in this equation represents the corresponding assembled or "stacked" matrices. The above equation may be written in terms of total quantities, rather than in the incremental form, for the case when the elastic stiffness matrix $[K_e]$ remains constant, i.e.,

$$[K_e] \left\{ D \right\}^i = \left\{ P \right\}^i + \left\{ Q \right\}^{i-1} . \tag{22b}$$

The incremental solution technique using either of Eqs. (22) reduces to a sequence of linear problems in which the applied loading is constantly modified by the effective plastic load vector. Thus, with the increments of generalized displacement obtained from Eqs. (22), the linear matrix equation, Eq. (6), together with Eqs. (A.22) and (A.8), and the constitutive plasticity relations presented in Appendix A are used to obtain the complete solution for increments of total strain, stress and plastic strain, respectively, assuming elastic strain-hardening material behavior. The corresponding relations [replacing Eqs. (A.22) and (A.8)] for an elastic, ideally-plastic material are given in Eqs. (A.23), (A.16), and (A.17). After summing all incremental quantities to determine current values of the pertinent variables, new values of the increments of fictitious load $\{\Delta q\}$ are determined for each element in the plastic range, and the procedure is repeated until the end of the loading process is reached.

Strain method — predictor procedure. — The predictor procedure solution technique can also be applied in an alternative formulation of the problem involving a direct solution for the increments of total strain. This alternative formulation is applicable to those problems in which an explicit solution for displacements, or their increments, is not required, and where the

initial strain stiffness matrix $[\bar{k}]$ does not change throughout the loading range. The governing matrix equation in this formulation is determined by substituting Eq. (17) into Eq. (11), performing the necessary stacking operation for application to the entire structure, then solving for displacements, as follows,

$$\{\Delta D\} = [K_e]^{-1} \left(\{\Delta P\} + [\bar{K}] \{\Delta \epsilon_o\} \right) \tag{23}$$

and finally substituting Eq. (23) into the linear portion of the strain-displacement relations, Eq. (6) (evaluated at nodes or alternatively at some point within each element and assembled to apply to the whole structure), yielding the following expression for the vector of increments of total strain:

$$\{\Delta e_o^T\} = [A] \{\Delta P\} + [J] \{\Delta \epsilon_o\} \tag{24}$$

where

$$[A] = [W_o][K_e]^{-1}$$

and

$$[J] = [W_o][K_e]^{-1}[\bar{K}] .$$

If we wish to use a predictor procedure to solve Eq. (24), we must write this relation in the following form,

$$\{\Delta e_o^T\}^i = [A] \{\Delta P\}^i + [J] \{\Delta \epsilon_o\}^{i-1} . \tag{25}$$

Using values of $\{\Delta \epsilon_o\}$ estimated in this way, we can find the unknown total strain increments from Eq. (25), and then find the increments of stress and plastic strain from Eqs. (A.22) and (A.8) for strain-hardening behavior, or from Eqs. (A.23), (A.16), and (A.17), for ideally plastic behavior.

The predictor procedure, involving the use of estimated values of plastic strain in Eq. (22) or Eq. (25), has computational advantages since the solution requires only matrix

18

multiplication in each load step once the corresponding effective plastic load vector is formed, provided the matrix $[K_e]$ is constant and thus need be inverted only once. This differs from the direct substitution procedure to be discussed below, in which matrix inversion or simultaneous equation solution is required at each load step. However, a disadvantage associated with the predictor procedure solution technique is a propagation of error as plastic straining proceeds. Hence it may be necessary to use small load increments for improved accuracy, thereby reducing the computational advantage of this procedure.

In Refs. 1, 4, 5, and 11 the predictor procedure is also formulated in terms of a governing matrix equation relating increments of stress to increments of load and plastic strain, as follows,

$$\left\{\Delta\sigma_o\right\}^i = [B]\left\{\Delta P\right\}^i + [H]\left\{\Delta\epsilon_o\right\}^{i-1} . \tag{26}$$

This procedure, referred to as a "constant stress" procedure, has been shown to lead to a characteristic numerical instability (Refs. 1, 5, and 11). No such instability occurs when the predictor procedure is used in conjunction with Eq. (22) or Eq. (25).

A detailed discussion of the formulation of the coefficient matrices of Eqs. (25) and (26) is presented in Appendix B for a triangular membrane element in which a linear strain variation is assumed.

Displacement method — direct substitution procedure. — The use of Eqs. (22), (25), or (26) is usually associated with the initial strain method of finite-element plasticity analysis. An alternative approach, commonly referred to as the tangent modulus method, involves the direct substitution of the incremental constitutive plasticity relations into the governing matrix equation, Eq. (18). For an elastic, strain-hardening material, Eqs. (A.8) and (A.22) may be combined to yield an incremental relation between plastic strains and total strains, as follows,

$$\left\{\Delta\epsilon\right\} = [C][R]^{-1}\left\{\Delta e^T\right\} . \tag{27}$$

19

The strain-displacement relation of Eq. (6) (considering only the linear component) can be substituted into Eq. (27) to yield the following relation,

$$\{\Delta\epsilon\} = [C][R]^{-1}[W] \{\Delta d_o\} .$$ (28)

Equation (28) must be evaluated at each plastic node of any element, and can be written as

$$\{\Delta\epsilon_o\} = [\Gamma_j] \{\Delta d_o\}$$ (29)

where

$$[\Gamma_j] = 0 \qquad \text{if node } j \text{ is elastic and}$$

$$[\Gamma_j] = [C_j][R_j]^{-1}[W_j] \qquad \text{if node } j \text{ is plastic.}$$

Substituting Eqs. (17) and (29) into Eq. (11) yields the following incremental load-deflection relation for an individual element,

$$\{\Delta P_o\} = \left([k_e] - [k_p] \right) \{\Delta d_o\}$$ (30)

where

$$[k_p] = [\bar{k}][\Gamma] ,$$

and the matrix $[\Gamma]$ represents the assembled nodal $[\Gamma_j]$ matrices for the element.

For an elastic, ideally-plastic material the incremental relation between plastic strains and total strains is obtained by substituting Eq. (A.23) into Eq. (A.17) to yield the following equation,

20

$$\left\{\Delta\epsilon\right\} = [\tilde{E}][E^*]^{-1} \left\{\Delta e^T\right\} . \tag{31}$$

The corresponding incremental plastic strain-displacement relation, obtained by substituting the strain-displacement relation [the linear portion of Eq. (6)], into Eq. (31), may be written as

$$\left\{\Delta\epsilon\right\} = [\tilde{E}][E^*]^{-1}[W] \left\{\Delta d_o\right\} . \tag{32}$$

The nodal plastic strain increments can again be written in terms of displacement increments, as in Eq. (29), where now

$$[\Gamma_j] = 0 \qquad \text{if node } j \text{ is elastic, and}$$

$$[\Gamma_j] = [\tilde{E}][E^*]^{-1}[W_j] \qquad \text{if node } j \text{ is plastic.}$$

The matrix $[k_p]$ in Eq. (30) may be looked upon as a "plastic stiffness matrix" since it explicitly contains the effect of plasticity and enters into the analysis as an additional component of the total stiffness matrix. Further, since the elements of $[k_p]$ are functions of the instantaneous stress state, they must be evaluated at each incremental step.

Equation (30) represents a form that is associated with the displacement method used in conjunction with the "direct substitution" or tangent modulus procedure. An alternative formulation of this method and procedure that avoids any explicit assumption as to the distribution of plastic strains is obtained by reforming Eq. (11) without making use of Eq. (8), and excluding consideration of $[k^{(1)}]$, to yield the following relation,

$$\left\{\Delta P_o\right\} = \iiint_V \left[[W]'[E][W] \left\{\Delta d_o\right\} - [W]'[E] \left\{\Delta\epsilon\right\} \right] dV . \tag{33}$$

For an elastic, strain-hardening material, the incremental plastic strain-nodal displacement relation of Eq. (28) may be

substituted into Eq. (33), which results in the following incremental load-displacement relation,

$$\left\{\Delta p_o\right\} = [k_T] \left\{\Delta d_o\right\}$$ (34)

where, after some manipulation, we find that

$$[k_T] = \iiint_V [W]'[R]^{-1}[W]dV .$$ (35)

It should be noted from Eq. (A.22) of Appendix A that $[R]^{-1}$ is the matrix relating increments of stress to increments of total strain in an elastic, strain-hardening material.

Similarly, for an elastic, ideally-plastic material the matrix relating load increments to increments of displacement is given as

$$[k_T] = \iiint_V [W]'[\bar{E}][E^*]^{-1}[W]dV$$ (36)

where the product $[\bar{E}][E^*]^{-1}$ is used to relate increments of stress to increments of total strain for an elastic, ideally-plastic material.

Although Eqs. (30) and (34) both relate increments of load to increments of displacement, in general, with the exception of uniform stress elements,

$$[k_T] \neq [k_e] - [k_p] .$$ (37)

The matrix $[k_T]$ represents a reduced or tangent modulus stiffness matrix. The effect of plasticity is explicitly contained in it through the matrix $[R]^{-1}$ (or $[\bar{E}][E^*]^{-1}$), obtained from

22

the constitutive relations corresponding to the plasticity theory used. This matrix represents the new material stiffness properties and replaces the elastic material coefficient matrix $[E]$ in the expression for $[k_e]$.

Since the elements of $[R]^{-1}$ (or $[\bar{E}][E^*]^{-1}$) are nonlinear functions of stress, the expression for $[k_T]$ is not readily integrable for finite elements other than those that involve the assumption of a uniform stress field. Consequently, the elements of $[k_T]$ are determined on the basis of values of stress at some point within the element, usually taken at the centroid.

Strain method — direct substitution procedure. — The direct substitution procedure may also be applied to the matrix equation represented in Eq. (24). For an elastic, strain-hardening material, the incremental plastic strain-total strain relation given in Eq. (27) is substituted into Eq. (24) to yield the following relation

$$[Y] \left\{ \Delta e_o^T \right\} = [A] \left\{ \Delta P \right\} \tag{38}$$

where

$$[Y] = \lceil I \rfloor - [J][C_d][R_d]^{-1}$$

and the subscript d denotes a diagonally partitioned matrix.

Similarly, for an elastic, ideally-plastic material, Eq. (24) is written in a form identical to that of Eq. (38), where now

$$[Y] = \lceil I \rfloor - [J][\tilde{E}_d][E_d^*]^{-1} .$$

An equation similar in form to Eq. (38), relating stress increments directly to applied loads, was developed in Ref. 11. For strain-hardening behavior this equation takes the form:

$$[Z] \left\{ \Delta \sigma \right\} = [B] \left\{ \Delta P \right\} \tag{39}$$

23

where

$$[Z] = \lceil\ I\ \rfloor - [H][C_d]$$

The method of solution using this equation is called the "stress method." Based upon the direct substitution procedure, it does not exhibit the characteristic numerical instability associated with the predictor type of solution procedure presented in Eq. (26). The strain and stress methods are equivalent when used in conjunction with the direct substitution procedure.

Summary of Methods for Plastic Analysis

Starting with an expression for the increment of strain energy, several alternative governing equations have been presented. Three of these equations, namely, Eqs. (21), (30), and (34), are written in terms of increments of displacement. Although these equations are interrelated, a basic distinction associated with their formulation does exist. In the case of Eqs. (21) and (30), an assumption is made concerning the distribution of the initial strains (or their increments), while in the case of Eq. (34) no such assumption is required; however, in the latter case the expression for the tangent modulus stiffness matrix, as given in Eqs. (35) or (36), must be integrated.

A further distinction among the various formulations is associated with the solution procedures used, which may be named the predictor and the direct substitution procedures. In the former, estimated values of plastic strain are used in the governing linear matrix equation. Thus plastic effects are treated in the linear matrix equation by a modification that is external to the stiffness influence coefficient matrix. In the direct substitution procedure, plasticity is accounted for by means of an "internal" modification of the stiffness matrix.

In the strain (or stress) method, represented by Eqs. (25) and (38) [or Eqs. (26) and (39)], the sole distinction among these equations is that associated with the solution procedure used.

The direct substitution or internal modification procedure, while it retains the errors associated with stepwise linearization, eliminates the propagation of error associated with the

24

predictor or external modification procedure. This improvement
in accuracy for a given magnitude of the load increment is, how-
ever, accompanied by an increase in the number of numerical
operations required to obtain a solution. These operations can
be computationally expensive, since the elements of the influence
coefficient matrices, $[k_p]$ of Eq. (30), $[k_T]$ of Eq. (34), or
$[Y]$ of Eq. (38), must be recomputed at each incremental step of
loading. The effect of this can be mitigated by increasing the
magnitude of the load increment, but at the cost of greater in-
accuracy. A choice between the two basic procedures thus in-
volves a trade off between smaller load increment but less compu-
tation per increment, in the case of the predictor procedure, and
larger load increment but more computation per increment, in the
case of the direct substitution procedure. This choice will not
be obvious in any given problem.

An approach that combines the two procedures might prove to
be the most effective. For example, the predictor procedure may
be sufficiently accurate in those regions of a structure where
plastic flow has begun but has not yet been substantially de-
veloped. In those regions where plastic effects are predominant,
the direct substitution procedure could be used. This hybrid
procedure is most easily implemented by using the governing
matrix equation in terms of total strain increments (or stress
increments), i.e., Eqs. (25) and (38) [or Eqs. (26) and 39)]. In
Refs. 9 and 11 this procedure is developed and applied to a num-
ber of sample structures.

3. MATERIAL NONLINEARITY — MEMBRANE STRESS BEHAVIOR

The methods discussed in the preceding section have been applied to numerous structures subjected to a variety of loading and boundary conditions. The sample structures were chosen so as to be consistent with the goals of the present study. For the case of structures subjected to membrane stress alone, these goals included an evaluation of the use of a triangular element in which total strain and plastic strain are assumed to vary linearly, and the further evaluation (supplementing the investigation of Refs. 9 and 11) of the use of the Prager-Ziegler kinematic hardening theory of plasticity in predicting the essential features of cyclic loading with stress reversals into the plastic range. For the most part, the sample structures were chosen from among those that were the subject of an independent experimental study conducted at NASA Langley Research Center (see Refs. 26-28) the purpose of which was to investigate the plastic behavior of membrane stressed specimens subjected to cyclic loading conditions. Results from the experiments on these structures, which exhibited regions of high stress gradients, provided a stringent test of the accuracy of the finite element, and provided some additional information for the further evaluation of the Prager-Ziegler kinematic hardening theory.

The methods of plastic analysis described in the preceding section have been applied by a number of authors to structures subjected to membrane stress states (Refs. 8, 9, 11, 19, and 20). For the most part, our results for membrane stress behavior were obtained by using the strain (or stress) method in conjunction with the direct substitution procedure, Eq. (38) [or Eq. (39)].

Before discussing the solutions obtained, a few comments are in order on the assumptions made in the development of particular finite elements used in modeling the entire structure. In developing the governing equations in the form of Eqs. (38) or (39), besides making a displacement assumption, an explicit assumption must be made concerning the distribution of plastic strain (or increments of plastic strain) within each element. Making such an assumption, as opposed to defining the constitutive relations at a single representative point in the element [Eq. (34)], is a concept fundamental to these methods and forms the basis of our analysis. Since much of the previous work in developing methods of membrane stress analysis has involved the use of uniform strain elements, with the associated uniform distribution of

27

plastic strain implied, this distinction has not often been ex-
plicitly stated. It becomes clear, however, when we make use of
a higher order element, the effectiveness of which assumes
greater importance in a plastic than in an elastic analysis.
Whereas a given level of error in the description of the stress
field may be acceptable in an elastic analysis, the same level of
error may not be acceptable in a plastic one, since the latter is
especially sensitive to the accuracy with which the stress is
predicted.

To demonstrate the use of a higher order element, calcula-
tions were performed using a 6-node, 12 degree-of-freedom tri-
angular element based on the following quadratic function repre-
sentation for in-plane displacement

$$u = \alpha_1 + \alpha_2 x + \alpha_3 y + a_4 xy + \alpha_5 x^2 + \alpha_6 y^2$$

$$v = \alpha_7 + \alpha_8 x + \alpha_9 y + \alpha_{10} xy + \alpha_{11} x^2 + \alpha_{12} y^2 .$$

(40)

Use of this element, shown in Fig. 1, satisfies the above cri-
terion of providing an accurate description of the state of
stress in a structure, particularly in regions of high stress
gradient. Although, for the purpose of demonstrating the plastic
analysis, we will use this element here, other accurate high
order elements can similarly be used.

The further assumption is made that the plastic strain (or
strain increments) varies linearly in the plane of the triangular
element, and can be written as

$$\Delta\epsilon = \Delta\epsilon_i \left(1 - \frac{x}{x_j} - \frac{y}{y_k} + \frac{x_k y}{x_j y_k} \right) + \Delta\epsilon_j \left(\frac{x}{x_j} - \frac{x_k y}{x_j y_k} \right) + \Delta\epsilon_k \left(\frac{y}{y_k} \right) \quad (41)$$

where i, j, k represent the vertex nodes of the triangle. This
assumed distribution is illustrated in Fig. 2 where it can be
seen that the linear distribution is assumed to apply between
vertices of the triangle and over the entire area of the element.
Thus, if only one of the vertices of the triangle is in the plas-
tic range, the value of the plastic strain (or strain increment)
decreases linearly to zero at the other two vertices. This

28

eliminates the necessity of locating an elastic-plastic boundary in the interior of the element, and enables one to describe the distribution of plastic strain increments in any element once the nodal values are known. This represents a distinct practical advantage over the alternative approach of assuming a plastic strain distribution that provides for the existence of an elastic-plastic boundary at some intermediate position in the element, although the latter approach constitutes a refinement that should provide greater accuracy.

The linear function of Eq. (41) is used to describe all three components of plastic strain present in a plane stress analysis. When the function is written for each of these components, we obtain the linear function matrix $[\overline{W}_p]$ of Eq. (8) that relates plastic strain increments in the element to strain quantities at the vertices. This relation can be written as

$$
\left\{ \begin{array}{c} \Delta\epsilon_x \\ \Delta\epsilon_y \\ \Delta\gamma^P_{xy} \end{array} \right\} = [\overline{W}_p] \left\{ \begin{array}{c} \Delta\epsilon_{xi} \\ \Delta\epsilon_{xj} \\ \Delta\epsilon_{xk} \\ \Delta\epsilon_{yi} \\ \Delta\epsilon_{yj} \\ \Delta\epsilon_{yk} \\ \Delta\gamma^P_{xyi} \\ \Delta\gamma^P_{xyj} \\ \Delta\gamma^P_{xyk} \end{array} \right\} = [\overline{W}_p] \left\{ \Delta\epsilon_o \right\}
\tag{42}
$$

where $[\overline{W}_p]$ is a diagonally partitioned matrix whose submatrices are composed of the functions shown in Eg. (41).

With the above assumptions for plastic strain distribution and displacement, the element stiffness matrix and initial strain stiffness matrix may be explicitly determined. The stiffness

29

matrix [k] for this linear strain element is given in Refs. 29 and 30, and the initial strain stiffness matrix [k̄] is given in Appendix C.

Results

The six-node linear-strain triangle (LST) was used to generate the [A] and [J] matrices of Eq. (25) [or alternatively the [B] and [H] matrices of Eq. (26)]. This element was then used in conjunction with the strain (or stress) method-direct substitution procedure described in Section 2 to perform a cyclic plastic analysis of four sample structures under cyclic loading. These are:

1) A uniformly loaded rectangular notched bar with a theoretical stress concentration factor of $K_T = 2$ (based on an approximation due to Neuber, Ref. 31).

2) A uniformly loaded rectangular notched bar with a theoretical stress concentration factor of $K_T = 4$.

3) A uniformly loaded rectangular sheet with a centrally located circular hole.

4) A thin annular disk subjected to a uniform internal pressure.

The first three of these structures were the subject of experimental studies conducted at NASA Langley Research Center by John Crews (Ref. 26). The data obtained from these studies are compared here with the analytical results obtained from the current investigation.

The Prager-Ziegler kinematic hardening theory was employed in each of the cases studied. The use of this theory requires the specification of a parameter, c, which appears in Eq. (A.5). This parameter characterizes the hardening behavior of the material and, in the case of uniaxial stress, can be interpreted as the instantaneous slope of the stress versus plastic strain curve.

30

In the present application of the kinematic hardening theory, a heuristic approach is used to obtain the multiaxial hardening coefficient, one that was previously used in Ref. 11. In this procedure, each stress component is treated as though it alone were present, and a corresponding value for c is determined on the basis of a uniaxial stress-strain curve from a tensile test or of a stress-strain curve for pure shear. These curves can be described by the Ramberg-Osgood parameters [cf. Eq. (A.24), Appendix A]. A single value of c for the multiaxial case is then computed as a weighted average of the individual components. This procedure has proved adequate for the class of problems represented by the notched bars and rectangular sheet with a circular hole here considered. However, it is not generally applicable, and its use must be reevaluated for each structure encountered. One of its most serious shortcomings is the lack of invariance with respect to a rotation of the coordinate axes. This shortcoming is minimized for the structures considered since the stress component in the direction of the applied loading predominates throughout the structure. Further study of this problem, including the generation of additional experimental data, particularly with respect to cyclic loadings, is required to place the determination of the hardening coefficient on a sounder basis.

Notched bar, $K_T = 2$. — The first structure treated is the uniformly loaded notched bar, shown in Fig. 3. In Ref. 11, a plastic analysis for cyclic loading was performed for this structure on the basis of a finite-element idealization consisting of constant-strain triangles. In the present study this analysis was repeated, using the linear-strain triangles (LST). The finite-element idealization of the upper right quadrant of the notched bar, shown in Fig. 4, is identical to that used in Ref. 11. Although the LST element can adequately represent the structure's behavior with a coarser network of triangles, this idealization was used here to provide a more accurate representation of the growth of regions of plasticity in the vicinity of the notch root. The resulting stress concentration factor, based on nominal net section stress, obtained from the current analysis is 2.08 and represents a slight improvement ($\approx 3\%$) over the result previously obtained by using constant-strain triangular (CST) elements. This result compares more closely with the value, 2.11, obtained experimentally in Ref. 26. It should be noted, however, that the magnitude of the computational effort to

arrive at this result was substantially increased by using the LST element. This is a consequence of introducing midside nodes in the development of the triangular element. These nodes are at most coincident with only a single adjacent element, as compared with the unlimited number of elements that can be coincident at vertex nodes. The number of degrees of freedom, and therefore the size of the matrix to be inverted to obtain the [B] and [H] matrices (see Appendix B), consequently increase manyfold. For example, use of the LST element leads to 542 unknowns, while constant-strain triangles for the same idealization require only 144 unknowns. The advantage of the LST element for this problem, which does not exhibit a very high stress concentration factor, is therefore minimal. However, for rather steep stress gradients, as represented by the second notched bar considered, the advantage of this element becomes more substantial.

As indicated in Fig. 3, the material used in the notched bar is 2024-T3 aluminum alloy. Stress-strain curves for this material for initial tensile loading differ greatly from those obtained for initial compressive loading. This type of material behavior poses some difficulties in the present analysis, since the Von Mises yield condition assumes an initially isotropic material, in which the yield stresses in the normal directions are not only equal to one another but are initially equal in tension and compression. Consequently, in order to compare present results with the experimental results of Ref. 26, the initial yield surface as defined by the Von Mises yield condition was replaced by a surface of similar shape but with the center displaced appropriately with respect to the origin of stress space (cf. Ref. 11, p. 134). Correspondingly, the hardening properties in tension and compression were treated as different. In addition, the hardening properties in subsequent cycles of loading differ from those in the first cycle, which was taken into account in an approximate manner on the basis of limited test data (Ref. 26). These properties are defined by Ramberg-Osgood parameters associated with Eq. (A.24) with E equal to 1×10^7 lb/in.^{2} throughout, as follows:

Initial Tension

$$\sigma_{0.7} = 0.53 \times 10^5 \text{ lb/in.}^2$$

$$n = 37$$

Initial Compression

$$\sigma_{0.7} = 0.45 \times 10^5 \ \text{lb/in.}^2$$

$$n = 8.1$$

Subsequent Tension

$$\sigma_{0.7} = 0.53 \times 10^5 \ \text{lb/in.}^2$$

$$n = 7.5$$

Subsequent Compression

$$\sigma_{0.7} = 0.49 \times 10^5 \ \text{lb/in.}^2$$

$$n = 8.1 \ .$$

These parameters were also used for the other notched bar and the sheet with a circular hole.

Local stress versus strain histories at the notch root, computed for a single cycle of loading for each of several load ranges, are presented in Fig. 5 and compared with the experimental data of Ref. 26. The amplitude of load is denoted by S_{max}, where S is the nominal net section stress across the notch root. The figure indicates good agreement for both stress and strain during the first half cycle of tensile loading and an overprediction of strain at the maximum compressive loading. The loci of the computed half-cycle and full-cycle residual stresses, as influenced by the nominal stress amplitude, are shown as dashed lines in the figure. Comparison with experiment is favorable, with the maximum differences occurring for the higher maximum loading during the first half cycle.

Figure 6 shows load versus local strain at the notch root for three cycles of load and a maximum loading range represented by S_{max} of ± 50 ksi. Good correlation is indicated during the

first half cycle of tensile load and for the first half cycle of residual strain. However, there is an overprediction of strain at the minimum load ($S_{min} = -50$ ksi) in each cycle, which can be attributed in part to: 1) the use of larger elements in the interior of the structure at some distance from the notch root, and 2) the possibly poor representation of the second and third cycle stress-strain behavior.

The variation of the plastic stress-concentration factor with the nominal stress range ΔS is shown in Fig. 7. A comparison of results obtained from experiment, in conjunction with an empirical equation, Ref. 26, and results of the present analysis is shown for monotonically increasing tensile loads, where the factor is denoted by K_p. For reversed loading from tension in the first cycle, the factor is denoted by K_p'. As indicated, the correlation of results is quite good, with a maximum underprediction of stress concentration factor occurring at the maximum tensile load, $S = 50$ ksi.

The contours of the longitudinal stress σ_y are shown in Fig. 8 at various stages of the first cycle of loading. Figure 8a shows the contours at the maximum elastic load. The close spacing of the contours in the vicinity of the notch root marks the region of rapid stress variation in the area of highest stress concentration. At the maximum load, $S_{max} = 50$ ksi, there is a redistribution of stress due to plastic flow, so that the region of rapid stress variation is shifted along the notch boundary, as shown in Fig. 8b. Although the region of maximum stress is larger, it is, however, still located in the vicinity of the notch root. Figure 8c shows the first half-cycle residual stresses. As is to be expected, the maximum residual stresses are localized in the area of the notch root. Figures 8d and 8e denote the stress contours at the minimum load and the full-cycle residual stresses. These figures maintain the general trend indicated in Figs. 8b and 8c.

The propagation of the elastic-plastic boundary is shown in Fig. 9 for a full cycle of loading to $S_{max} = 50$ ksi. It is of interest here that the region of plasticity is localized in the vicinity of the notch root during initial tensile loading but encompasses a much wider area during reversed loading. The boundary for $S = 0$ in Fig. 9b represents the elastic-plastic boundary after the initial tensile loading is removed. Thus the residual stresses are of sufficient magnitude to cause reversed

plastic flow to occur during unloading. In addition, this more pronounced growth of the plastic zone in reversed loading can be attributed to a Bauschinger effect and to the fact that the material of the notched bar exhibits a lower yield stress in compression than in initial tensile loading.

Notched bar II, $K_T = 4$. — In the second notched bar structure (shown in Fig. 10) the notch root has a radius of 0.3 in. compared with a total bar length of 35 in., so that the notch is fairly sharp. Again the material is 2024-T3 aluminum alloy. A quadrant of the finite-element idealization of the structure is shown in Fig. 11. The enlarged region of this figure, representing the area near the notch root, indicates the fine network of triangles necessary in the high stress gradient region. The stress concentration factor based on net section stress obtained by using this idealization is 4.49, which is in exact agreement with the experimental result of Ref. 27. An elastic analysis using constant strain triangles was also performed, as a means of evaluating the LST element for a structure exhibiting a steep stress gradient. In order to compare results on the basis of the same number of degrees of freedom, the analysis using the constant-strain triangle is based on the idealization in Fig. 11, with every triangle replaced by four constant-strain elements. The resulting idealization contains 576 elements and has 620 degrees of freedom. Figure 12 shows the distribution of the longitudinal stress along the notch net section obtained by using both elements. Agreement is good at points well removed from the notch, but the LST triangle yields a steeper stress gradient than the CST element and a 6 percent higher peak stress at the notch boundary. It should be noted that the peak stress shown for the CST element is the stress in the element adjacent to the notch root, whereas the peak stress for the LST element is the nodal stress at the notch boundary. A plastic analysis was performed for cyclic loadings represented by an average net section stress of ±25 ksi. The Ramberg-Osgood parameters used to describe the hardening coefficient in this analysis are the same as those used for notched bar I. The local stress versus strain history at the notch root for a single cycle of loading is shown in Fig. 13 and compared with experimental data of Ref. 27. Although the general shape of the curve in Fig. 13, as compared with experiment, is maintained, the stresses in the first half cycle of load and the minimum strain after reversed loading are overestimated. Figure 14 shows the three-cycle load versus strain curve at the notch root for the loading range of ±25 ksi. Good correlation

with experimental data was obtained during the first half cycle of load and for the first half-cycle residual strain. As in the case of notched bar I, an overprediction of strain is in evidence during reversed loading and in subsequent cycles of loading.

The stress concentration factors K_p and K_p' are shown in Fig. 15. Good correlation is indicated with the few available experimental points.

Figure 16 shows the distribution of the normalized longitudinal stress along the horizontal axis of symmetry for three values of initial tensile loading. The localized effect of plasticity is evidenced by the redistribution of stress in the vicinity of the notch boundary. Since this stress distribution must be in static equilibrium with the applied load, the validity of the distribution shown in the figure was checked by measuring the area under the curves and comparing it with the applied load. In each case, equilibrium was exactly satisfied.

The growth of the plastic zone for one cycle of load is shown in Fig. 17. Again, due to the material behavior and the prediction of a Bauschinger effect, we see that the region of plasticity is larger during reversed loading from tension than in the initial loading. Due to the rapid variation of stress, the notch affects only a localized region near the root.

Rectangular sheet with circular hole. — The uniformly loaded rectangular sheet with central hole is shown in Fig. 18. As seen from the figure it has the same over-all dimensions as the first two structures and is made of the same material. The idealization used for this structure, shown in Fig. 19, is identical to the one used for notch II, except for the enlarged region shown in the figure.

The distribution of longitudinal stress normalized with respect to the applied stress is shown in Fig. 20. The solid curve denotes the elastic stress distribution at initial yield and compares well with the analysis of Howland, Ref. 32. The other two curves show the stress distribution at an intermediate and maximum tensile load. Static equilibrium was checked on the basis of these curves and was found to be satisfied.

Representations of the distribution of stress near the hole can be seen in the next two figures. Figure 21 shows the dis-

tribution of effective stress, $\left(\sigma_x^2 + \sigma_y^2 - \sigma_y\sigma_x + 3\tau_{xy}^2\right)^{\frac{1}{2}}$, at initial yield. As is well known, the rapid variation of stress occurs in the vicinity of the hole boundary on the axis of symmetry perpendicular to the load. This is evidenced by the close spacing of contours in this region. Figure 22 shows the change in stress contours at successive stages in the first full cycle of loading. The upper left quadrant shows the contours at the maximum applied load of 33.4 ksi. The effect of plasticity is evidenced here by the shift of the region of rapid stress variation along the hole boundary and by the wide spacing between the contours of effective stress in the region away from the hole.

The upper right quadrant shows the residual effective stress after the tensile load is removed. Closely spaced contours near the hole boundary indicate a rapid decay of residual stress with distance from the hole. The lower quadrants show the contours at the minimum load and the full-cycle residual effective stresses. The patterns are similar to that shown for initial tension.

The propagation of the elastic-plastic boundary is shown in Fig. 23 for an initial tensile loading and for reversed loading. As seen in the two prior example structures, the different yield stress in tension and compression in concert with the predicted Bauschinger effect causes a substantially larger plastic region to form during reversed loading.

The next series of figures shows the longitudinal strain versus net section stress during cyclic loading. Results at the hole boundary are shown for three full cycles of load and at points in the interior for one full cycle. Results from an experimental study of the cyclic behavior of this structure performed at the NASA Langley Research Center by J. Crews, Ref. 28, are also shown. The experimental points in the interior were chosen to coincide with node points of the idealized structure. Figure 24a shows results at the hole boundary. Good correlation is obtained with the experimental data, especially during initial loading and subsequent unloading. However, as in the case of the notched bars, an overprediction of strain is evidenced in the reversed load part of the cycle and in subsequent cycles. Figures 24b-f show the results at the interior points, which are identified by their coordinates. Here correlation with the experimental data is good.

Figures 25 and 26 show the distribution of longitudinal strain along the horizontal axis of symmetry for various levels

of initial tensile load and reversed loading. Correlation with experiment is quite good.

The last figure for this structure (Fig. 27) shows the stress concentration factor during initial tensile loading. Comparison is made with experimental points given by Griffith, Ref. 33, obtained by using a structure of similar dimensions and stress-strain behavior. Correlation with experiment is again seen to be excellent.

Thin annular disk. — The annular disk and a quadrant of its finite-element idealization are shown in Fig. 28. The genesis of this problem is in the determination of the residual stresses and strains around a hole in a large sheet into which a rivet has been squeezed. Since this problem exhibits symmetry with respect to the circumferential coordinate, it is imperative that a hardening coefficient c that is invariant with respect to coordinate rotation be used in the plasticity analysis. Consequently, a method alternative to that presented in Ref. 11 is used for this problem. It is based on effective stress, as discussed in Appendix A. The material for this structure is 2024-T351 aluminum alloy, with the Ramberg-Osgood material parameters given as $E = 10^7$, $\sigma_{0.7} = 47.5$ ksi, and $n = 11$.

Figure 29 shows the redistribution of circumferential stress at the hole boundary with increasing load level. In this case, the only stress that can change at this point, due to plasticity effects, is the circumferential stress, since equilibrium considerations require that the radial stress be equal to the applied internal pressure. Consequently, at the highest load considered, the circumferential stress is seen to be negative. Unloading from various load levels is also shown. Of interest here is the discrepancy between residual stress obtained from the analysis and the results obtained by assuming completely elastic unloading (shown by the dashed lines). It can be seen that there is reversed plastic yielding during unloading and that the predicted residual stresses have about the same value for unloading from all tensile loads considered.

The radial distribution of circumferential and residual circumferential stresses is shown in Figs. 30 and 31 for a few values of loading. Plasticity effects are evidenced by the marked decrease in stress with increase in load, a decrease associated with the propagation of the plastic region into the

38

interior. Of interest in Fig. 31 is the fact that the residual stresses, which are compressive near the hole, become increasingly tensile in the interior and near the outer boundary with increasing load. A redistribution of this kind must occur for the circumferential residual stresses to be in static equilibrium.

A solution to the complete problem involving the interaction of the plate and the squeeze rivet is presented in Ref. 34.

4. MATERIAL NONLINEARITY — BENDING AND COMBINED BENDING AND MEMBRANE BEHAVIOR

The plastic analysis of structures with plate or shell components in which bending effects may be significant has been the subject of many investigations (Refs. 10, 12-15, and 35-39). With few exceptions, these investigations have been concerned with determining only the "collapse load" of these structures by means of two fundamental theorems of limit analysis. These theorems were proved for elastic, ideally-plastic bodies by Drucker, Prager, and Greenberg (Ref. 40), and are associated with a definition of the collapse load as that value of load at which a structure undergoes arbitrary plastic deformations and is no longer serviceable.

Approximate solutions for the collapse load are based mainly on the kinematic approach, which permits the estimation of an upper bound on the load-carrying capacity of the structure. In this approach, a displacement pattern associated with a failure mechanism of the plate is assumed. The work done by the external loads in this displacement is equated to the energy dissipation within the plate, and a corresponding collapse load is determined. The assumed collapse mechanism is subject to various conditions and is chosen on a trial basis in such a way as to seek a minimum for the upper bound values obtained for the collapse.

Limit analysis techniques have been applied extensively to determine the load-carrying capacities of a variety of plates on the basis of various yield conditions. Although these techniques provide valuable information concerning the collapse patterns and collapse loadings of various structures, a complete solution that can trace the load-deflection history in the plastic range is frequently desirable and necessary. For instance, the structure may become unusable because of the development of excessive deformation before the theoretical collapse load is reached.

Several authors have considered problems of plastic bending in which the entire load-deformation history is desired. The structures considered include beams (Refs. 15 and 36), plates (Refs. 12, 13, 15, 35, and 37-39), and shells (Ref. 10). Solution techniques range from an exact solution of the governing differential equation (Ref. 36) and a finite difference approach (Ref. 38), to a finite-element technique (Refs. 10, 12, 13, and 15).

In several of these previous investigations (Refs. 37-39), it was assumed that at any point on the plate the entire thickness is either fully elastic or fully plastic. This assumption greatly facilitates the solution of the problem and is practically fulfilled in the case of a plate of sandwich construction in which the core does not possess any bending stiffness. For a solid plate, however, this simplifying assumption requires that the curve expressing the relationship between bending moment and curvature be approximated by two straight lines corresponding to the fully elastic and fully plastic states. For many structural materials this idealized moment-curvature relationship represents a very crude approximation of the actual one, and is therefore unrealistic. Another approximation that has been used involves the replacement of the actual plate by a layered model in which individual layers are either fully elastic or fully plastic.

The plastic bending analysis discussed here (Ref. 15) makes use of the linear matrix equation, Eq. (22), constituting the displacement method in conjunction with the predictor procedure. This governing matrix equation relates the applied loading to the nodal displacements and initial strains. The use of the initial strain concept in this analysis requires the development of appropriate matrix relations based on assumptions concerning the distribution of both displacement and initial (plastic) strain within a finite element.

For the case of membrane stress states, as has been seen, the plastic strains are assumed to vary in a prescribed manner in the plane of the element. For out-of-plane bending, an assumption must be made concerning the distribution of plastic strain through the thickness as well as in the middle surface of the element. Specifically, the present analysis assumes the plastic strains to vary linearly along the edges of a finite element between adjacent nodes, and in addition assumes a linear variation of plastic strains from the upper or lower surface of the element to an elastic-plastic boundary (or boundaries) located within the cross section of the element. These assumptions require the determination of the position of an elastic-plastic boundary in each element on the basis of assumptions concerning its shape. Thus the analysis here presented utilizes the concept of a finite element in which there is a progressive development of a plastic region, instead of the layered approach or a sandwich idealization of the actual solid plate. To provide a better understanding of the implementation of these assumptions, their application to three bending elements will be discussed in detail.

42

Beam Element of Rectangular Cross Section

A typical beam element, for which pure bending has been assumed, is shown in Fig. 32. The function for the displacement in the z-direction is assumed to be of cubic order in the coordinate x, and is written in terms of the generalized nodal displacements as

$$
w(x) = \left(1 - 3\frac{x^2}{\ell^2} + 2\frac{x^3}{\ell^3}\right)w_i + \left(3\frac{x^2}{\ell^2} - 2\frac{x^3}{\ell^3}\right)w_j
$$

$$
+ \left(x - 2\frac{x^2}{\ell} + \frac{x^3}{\ell^2}\right)w_{,xi} + \left(\frac{x^3}{\ell^2} - \frac{x^2}{\ell}\right)w_{,xj} .
$$

(43)

In choosing a displacement function, it is important to include all fundamental strained states and all rigid body terms. Equation (43) satisfies these requirements for a beam element, and in the case of a uniform bending stiffness, EI, allows for a constant shear load and linearly varying moment along the length of the element. The plastic strain distribution is assumed to vary linearly in the x-direction from its value at the upper (or lower) surface at node i, represented in Fig. 32 as ϵ_{0i}, to its value at the upper (or lower) surface at node j, represented as ϵ_{0j}. This assumed distribution is written as

$$
\epsilon = \left(\frac{z - \bar{z}}{t - \bar{z}}\right)\left[\epsilon_{0i}\left(1 - \frac{x}{\ell}\right) + \epsilon_{0j}\left(\frac{x}{\ell}\right)\right]
$$

(44)

where $\bar{z}$ represents the depth of the elastic-plastic boundary. A linear function for the plastic strain distribution was chosen because it represents the simplest form that can, by using successively finer idealizations of the structure, approximate the more complex actual distribution. In addition, as seen from Eq. (44), it is assumed that at a node the plastic strain varies linearly from its value at the upper or lower surface to zero at an elastic-plastic boundary located within the cross section.

The depth of the elastic-plastic boundaries, which propagate from the upper and lower surface, is measured from the neutral axis for pure bending, as shown in Fig. 32. In general, the

43

depth of these boundaries cannot be directly related to the load. Hence the value of $\bar{z}$ must be determined from the total strain distribution, which is assumed to vary linearly through the thickness in accordance with Kirchoff's hypothesis. The functional form describing the shape of the elastic-plastic boundary is assumed to be a linear function of the coordinate x and may be written as

$$\bar{z} = (\bar{z}_j - \bar{z}_i) \left(\frac{x}{\ell}\right) + \bar{z}_i \,, \tag{45}$$

where $\bar{z}_i$ and $\bar{z}_j$ represent the depth of the elastic-plastic boundary at nodes i and j, respectively. The choice of a linear function to describe the shape of the elastic-plastic boundary is made on the same basis as the choice of a linear distribution for plastic strain; i.e., the linear function represents the simplest form that can approximate the more complex actual shape with successively finer idealizations of the structure. On the basis of the preceding assumptions, the elastic-plastic boundary consists of a surface in the interior of the element that extends over the entire area of the element and intersects the edges along straight lines joining nodes, as illustrated in Fig. 32. In addition, these assumptions eliminate the necessity of determining an elastic-plastic boundary on the faces of the element between nodes, but still require locating such a boundary through the thickness.

The present assumptions have been further extended to include the effects of bending in combination with a membrane stress state. As seen in Fig. 33, this extension necessitates the separate determination of the positions of the two elastic-plastic boundaries relative to both the upper and lower surface. The functional representation of the plastic strain distribution and the representation of the elastic-plastic boundary are taken to be similar to Eqs. (44) and (45), but now written separately for the upper and lower surfaces. A second matrix, in addition to the usual stiffness matrix, termed the initial stress stiffness matrix (discussed in Section 2), is introduced to account for the effects of the membrane load on the bending stiffness. This problem also requires the introduction of a second displacement component, u, acting in the axial direction,

$$u(x) = \left(1 - \frac{x}{\ell}\right)u_i + \left(\frac{x}{\ell}\right)u_j \,. \tag{46}$$

44

It should be noted that, although the functional form of the plastic strain distribution, as shown in Eq. (44), does assume the existence of a neutral axis located within the cross section of the beam element, the present analysis is capable of considering plastic sections in which the neutral axis is not located within the thickness of the beam, i.e., the strains at the upper and lower surfaces are of the same sign. This situation occurs when the membrane stresses are larger than the bending stresses. The treatment of this situation is accomplished by modifying the functional form of the plastic strain distribution given in Eq. (44). This modification is presented in Appendix D.

The present method has also been extended to treat the more complex problem of the plastic bending of a plate.

Rectangular Bending Element

A typical rectangular plate element is shown in Fig. 34. The displacement function chosen is the one originally used by Bogner, Fox, and Schmit (Ref. 41), and is in terms of products of first order Hermitian polynomials.

$$
w = \sum_{i=1}^{2} \sum_{j=1}^{2} \left(H_{0i}^{(1)}(\xi) H_{0j}^{(1)}(\eta) w_{ij} + H_{1i}^{(1)}(\xi) H_{0j}^{(1)}(\eta) aw,_{xij} \right.
$$

$$
\left. + H_{0i}^{(1)}(\xi) H_{1j}^{(1)}(\eta) bw,_{yij} + H_{1i}^{(1)}(\xi) H_{1j}^{(1)}(\eta) abw,_{xyij} \right)
$$

(47)

where $\xi = x/a$, $\eta = y/b$, a is the length of the rectangular element in the x-direction, and b is the length in the y-direction, and where

$$
H_{01}^{(1)}(v) = 2v^3 - 3v^2 + 1
$$

$$
H_{02}^{(1)}(v) = -2v^3 + 3v^2
$$

$$
H_{11}^{(1)}(v) = v^3 - 2v^2 + v
$$

$$
H_{12}^{(1)}(v) = v^3 - v^2
$$

(48)

and the quantities w_{ij}, $aw_{,xij}$, $bw_{,yij}$ and $abw_{,xyij}$ are nodal generalized displacements.

The components of plastic strain are assumed to vary as products of zero order Hermitian polynomials in the plane of the element and linearly through the cross section from their values at the upper (or lower) surface to zero at the elastic-plastic boundary. The functional representation for this distribution may be written as

$$\epsilon(x,y,z) = \left(\frac{z - \bar{z}}{t - \bar{z}}\right) \sum_{i=1}^{2} \sum_{j=1}^{2} H_{0i}^{(0)}(\xi) H_{0j}^{(0)}(\eta) \epsilon_{ij} \tag{49}$$

where

$$H_{01}^{(0)}(v) = 1 - v$$

$$\tag{50}$$

$$H_{02}^{(0)}(v) = v$$

t is the half-thickness of the element,

$\bar{z}$ represents the ordinate of the elastic-plastic boundary, and

ϵ_{ij} are the nodal values of the plastic strain.

The function defining the elastic-plastic boundary is also assumed to be in the form of products of zero order Hermitian polynomials as shown in Fig. 34 and written here in the following form:

$$\bar{z}(x,y) = \sum_{i=1}^{2} \sum_{j=1}^{2} H_{0i}^{(0)}(\xi) H_{0j}^{(0)}(\eta) \bar{z}_{ij} \tag{51}$$

where $\bar{z}_{ij}$ represents the depth of the elastic-plastic boundary through the thickness at node ij. The value of the depth, which

46

must be determined at each of the four nodes of the rectangular element, is computed from the total strains by means of a procedure outlined in Appendix E.

The foregoing assumptions associated with the plastic strain distribution and the representation of the elastic-plastic boundary ensure compatibility of these quantities along element boundaries.

The problem of combined bending and membrane loading requires the introduction of assumptions for the in-plane displacement components, u and v, in the x and y directions, respectively. For the rectangular element these displacements were chosen as products of zero order Hermitian polynomials.

$$u(x,y) = \sum_{i=1}^{2} \sum_{j=1}^{2} H_{0i}^{(0)}(\xi) H_{0j}^{(0)}(\eta) u_{ij} \tag{52a}$$

$$v(x,y) = \sum_{i=1}^{2} \sum_{j=1}^{2} H_{0i}^{(0)}(\xi) H_{0j}^{(0)}(\eta) v_{ij}. \tag{52b}$$

In addition, as previously stated for the beam element, the problem of combined loading requires investigating states of stress and strain on both the upper and lower surface. This extension also requires a separate determination of the position of the two different elastic-plastic boundaries. Therefore, the functional representation of the plastic strain distribution and the representation of the elastic-plastic boundaries are taken to be of similar form to Eqs. (49) and (51), written for both the upper and lower surface.

Triangular Bending Element

A typical triangular bending element is shown in Fig. 35. The displacement function chosen for the lateral displacement is the one presented in Refs. 42 through 44 and is a full 21-term quintic polynomial in terms of unknown coefficients a_i, as follows:

$$w(x,y) = a_1 + a_2 x + a_3 y + a_4 x^2 + a_5 xy + \ldots + a_{21} y^5 . \qquad (53)$$

The components of plastic strain are assumed to vary linearly in the plane of the element. This linear distribution can be written as

$$\epsilon(x,y,z) = \left(\frac{z - \bar{z}}{t - \bar{z}} \right) \sum_{i=1}^{3} \omega_i \epsilon_i \qquad (54)$$

where ω_i represents the area coordinates discussed in detail in Appendix F, and ϵ_i is the value of the plastic strain at node i.

The ordinate of the elastic-plastic boundary is also assumed to vary linearly in the plane of the element, and may be written as

$$\bar{z}(x,y) = \sum_{i=1}^{3} \omega_i \bar{z}_i . \qquad (55)$$

A linear variation was chosen for the in-plane displacement components, u and v, in the x and y directions, respectively, for the triangular element. These displacement components may be written in terms of the area coordinates ω_i in the following form,

$$u(x,y) = \sum_{i=1}^{3} \omega_i u_i \qquad (56a)$$

$$v(x,y) = \sum_{i=1}^{3} \omega_i v_i \qquad (56b)$$

48

Once again, the extension for the combined loading case requires writing the functional representation of the plastic strain distribution and the elastic-plastic boundary in a form similar to Eqs. (54) and (55), respectively, for the upper and lower portions of the element separately.

The above assumptions are made in the development of the governing linear matrix relation as formulated to include the effects of initial strain, and specifically affect the element initial strain stiffness matrix, $[k^*]$, of Eq. (15). Initial strain stiffness matrices for the beam element, the rectangular plate element, and the triangular plate element are given in Appendices D, G, and H, respectively. The initial stress stiffness matrix for the beam element is given in Ref. 45, for the rectangular plate element in Ref. 11, and for the triangular plate element in Appendix I.

In the expression for the initial strain stiffness matrix, which is dependent on the assumptions concerning the distribution of both total and plastic strains, the quantity V_p is the volume of the plastic region in each finite element as determined by the representation of the elastic-plastic boundary. Consequently, the elements of the initial strain stiffness matrix are a function of, among other quantities, the depth of the elastic-plastic boundary at each node and must therefore be recomputed at each step in the incremental loading process.

The use of a predictor procedure solution technique is necessary in these problems, because the depth of the elastic-plastic boundary (and the current value of plastic strain) at those nodes of the structure that are in the plastic range cannot be expressed explicitly in terms of total strain with sufficient ease to make feasible the application of the direct substitution procedure. The position of the elastic-plastic boundary is determined at the end of each load increment, and is assumed to remain fixed during the next increment.

The treatment of combined bending and stretching in the plastic range requires some additional development. Two types of problems may be encountered. In one, the membrane stresses are generated as a consequence of the changing geometry of the structure. The effects of the changing geometry on the response of the structure as it deforms must be accounted for in the elastic and plastic ranges. Application of the methods to this type of problem will be discussed in Section 5. The second type of

49

problem, considered now, is limited to cases in which a membrane load is applied to the structure and the effects of changing geometry are neglected.

Although the analysis for combined bending and membrane behavior is of sufficient generality to permit the treatment of any combination of membrane and bending loading, the applications presented here consist only of those cases in which the applied membrane load is restricted to values less than that necessary to initiate plastic deformation. The lateral loads are applied in finite increments while the membrane load is held constant.

As previously stated, the solution of these problems requires that an additional stiffness matrix, termed the initial stress stiffness matrix, be introduced to account for the effects of the membrane load on the bending stiffness. The elements of this matrix are functions of, among other quantities, the membrane state of stress that exists in the elements prior to the application of additional loading in the next step. Plastic deformation causes a redistribution of both bending and membrane states of stress existing in the structure. Thus, with the exception of statically determinate problems where the membrane stress resultants remain constant, the elements of the initial stress stiffness matrix change, in general, with increasing loads because of the changes in the values of the membrane stress resultants.

In addition to modification of the initial stress stiffness matrix, the combined loading problem also requires the determination of the states of stress and strain (elastic and plastic) at the upper and lower surface separately, at the nodes of each finite element. Consequently, these considerations require that the effective plastic load vector of Eq. (20b) be written in the form,

$$
\left\{ \begin{array}{c} q_b \\ \hline q_m \end{array} \right\}^i = \left[\begin{array}{c|c} k^*_{bu} & k^*_{bL} \\ \hline k^*_{mu} & k^*_{mL} \end{array} \right]^i \left\{ \begin{array}{c} \epsilon^U_o \\ \hline \epsilon^L_o \end{array} \right\}^i .
$$

(57)

50

where $\{q_b\}$ and $\{q_m\}$ represent the bending and membrane components of the effective plastic load, and $[k_{bu}^*]$ and $[k_{mu}^*]$ are the bending and membrane components, respectively, of the initial strain stiffness matrix for plastic strains developing from the upper surface. Corresponding definitions apply to $[k_{bL}^*]$ and $[k_{mL}^*]$ for plastic strains developing from the lower surface. $\{\epsilon_o^U\}$ and $\{\epsilon_o^L\}$ are the values of the nodal plastic strain on the upper and lower surface, respectively.

Thus, with attention restricted to thin flat plate elements in the presence of membrane stress states, Eq. (21) may be written for an individual element as follows,

$$\left[\begin{array}{c|c} [k_b^{(0)}] + [k_b^{(1)}] & 0 \\ \hline 0 & [k_m] \end{array}\right] \left\{\begin{array}{c} \Delta d_{ob} \\ \hline \Delta d_{om} \end{array}\right\}^i = \left\{\begin{array}{c} \Delta p_{ob} \\ \hline \Delta p_{om} \end{array}\right\}^i + \left\{\begin{array}{c} \Delta q_b \\ \hline \Delta q_m \end{array}\right\}^{i-1} \tag{58}$$

where the elastic stiffness matrix, $[k_e]$, of Eq. (21) now includes $[k_b^{(0)}]$, the usual bending stiffness matrix, $[k_b^{(1)}]$, the initial stress stiffness matrix, and $[k_m]$, the membrane stiffness matrix. The displacement vector $\{\Delta d_o\}$ is now separated into $\{\Delta d_{ob}\}$ and $\{\Delta d_{om}\}$, the increments of the generalized displacements associated with bending and membrane deformation, respectively; and the load vector $\{\Delta p_o\}$ is separated into $\{\Delta p_{ob}\}$ and $\{\Delta p_{om}\}$, the increments of lateral load and in-plane load, respectively. With these definitions, Eq. (58) can be expanded and written as two matrix equations,

$$\left[[k_b^{(0)}] + [k_b^{(1)}]\right]^i \{\Delta d_{ob}\}^i = \{\Delta p_{ob}\}^i + \{\Delta q_b\}^{i-1} \tag{59a}$$

and

$$\left[k_m\right]^i \{\Delta d_{om}\}^i = \{\Delta p_{om}\}^i + \{\Delta q_m\}^{i-1} . \tag{59b}$$

Each of these matrix equations may be solved separately to determine the increments of generalized displacement associated with bending and membrane deformations. The solutions follow for the increments of total strain, stress, and plastic strain. The new locations of the elastic-plastic boundaries at nodes are determined and used in forming the initial strain stiffness matrix. The redistribution of the membrane stresses is also determined (see Appendix J) and used to compute the elements of the initial stress stiffness matrix to be used in the next increment.

Finally, although Eqs. (59a) and (59b) are solved independently, this does not imply that bending and membrane behavior are uncoupled in the plastic range. The bending affects the membrane results through the plastic load vector, since plastic strains are computed from the combination of bending and membrane stresses. The membrane strains affect the bending results similarly through the bending plastic load vector and additionally through the redistribution of membrane stress resultants, which modifies the elements of the initial stress stiffness matrix.

Cyclic Loading

In order to develop a method capable of representing the cyclic behavior of plates in pure bending, the simpler case of cyclic loading of a beam is used first as a model. The procedure is then generalized to account for the more complex multiaxial stress state present in plate structures. A correspondence between uniaxial and "effective" stress (strain) concepts is used, with the procedure kept as consistent as possible with the chosen plasticity theory and finite-element and kinematic strain assumptions.

Various possible elastic, ideally-plastic stress (or strain) states for a beam during one complete cycle of pure bending are shown in Figs. 36a-k. The corresponding positions of the stress states at the extreme fiber on a representative cyclic stress-strain curve for a strain-hardening material are indicated in Fig. 36a. The points on this curve are merely meant to indicate their relative locations during the load cycles and naturally do not correspond to their actual positions, which would require an elastic, ideally-plastic stress-strain curve. The plastic strain and stress (elastic strain) distribution for the first cycle during initial loading is indicated in Fig. 36a. All distributions are based upon previous kinematic and finite element total

and plastic strain assumptions. From point "a", the structure is assumed to unload elastically. The stress distribution and plastic strain distribution at incipient plastic deformation on reversed loading are shown in Fig. 36b. Note that the stress distribution is bilinear while the cumulative plastic strain distribution is linear. Note also that the elastic range for unloading and reversed loading is twice the initial elastic range for loading (σ_o). This situation may not be true for multiaxial behavior because of a redistribution of stresses due to displacement of the stress state along the yield surface. As yielding during reversed loading progresses, the elastic strain distribution, total plastic strain distribution, and plastic strain generated during reversed loading are shown in Fig. 36c. Although the cumulative plastic strain has a bilinear distribution, the plastic strain developed during this phase of the cyclic loading is linear. In this figure, the current elastic-plastic boundary has not yet propagated through the depth as far as the previous boundary nor is the slope of the fictitious elastic distribution (line 1-2 in Fig. 36c) the same as that for loading. The fictitious elastic distribution referred to here is the stress distribution that would exist at the cross section if plastic deformation did not occur during the current half-cycle. Hence, because of the change in slope of the fictitious elastic distribution, the location of the elastic-plastic boundary through the depth cannot be calculated by using the total strain distribution, as outlined in Appendix E, and a different method must be developed. In this connection, it is interesting to note that the new slope of the fictitious distribution intersects the neutral axis not at the zero total strain location but at the yield strain (stress) during the loading cycle. This is also the case in Fig. 36b for the actual elastic distribution. If loading were to proceed further until the depth of the current elastic-plastic boundary, $\bar{z}$, is less than the previous one as measured from the neutral axis (see Fig. 36d), the cumulative plastic strain distribution would now be linear, but the plastic strain generated solely during reversed loading would have a bilinear distribution.

If, instead, one unloads and reloads from the situation depicted in Fig. 36c (the current value of $\bar{z}$ is greater than the previous one), Figs. 36e, f, g, and h indicate the total plastic and current cycle plastic strains occurring at incipient yielding, further yielding, and growth of the current plastic region beyond both previous regions. If unloading and reloading proceeded from the point illustrated in Fig. 36d, it would fol-

low the stages shown in Figs. 36b, c, and d (with the pictures revised to indicate the current sense of loading). In all cases (Figs. 36e, f, g, h or 36b, c, d), either the cumulative plastic strain or the plastic strain developed during the current cycling phase is linear. The only obstacle to describing cyclic behavior for an arbitrary number of cycles (using the current assumptions) appears if the second unloading and reloading occur from the state depicted in Fig. 36f [i.e., if the current value of $\bar{z} > \bar{z}^{(2)} > \bar{z}^{(1)}$]. What happens upon reversing from this load is shown in Figs. 36i, j, k. The difficulty arises for the situation depicted in Fig. 36k. For this state of stress the elastic-plastic boundary has propagated further toward the neutral axis than for the states of stress shown in Fig. 36c. In this situation neither the cumulative plastic nor current plastic strain is linear. Such linearity is essential for the analysis in its present state, since it is assumed that the plastic strain distribution varies linearly through the thickness from some value at the extreme fibers to zero at the elastic-plastic boundary. This assumption is employed in the formation of the initial strain stiffness matrix. Similar occurrences of even more multilinear distributions of plastic strain in subsequent cycles complicate the problem still further, and for this reason the current investigation is limited to one full cycle.

The generalization of the uniaxial case to the multiaxial problem is depicted in Fig. 37. Only the upper half of the plate is shown. The following definitions are made by analogy with the beam problem:

$$S_{yield}^{(1)} \equiv \sqrt{J_2(\sigma_{ij})} \ , \quad \text{with} \quad \sigma_{ij} \quad \text{computed, using the}$$

strain at initial yield during the first loading, where J_2 is the second invariant of the stress tensor σ_{ij};

$$S_e^{(1)} \equiv \sqrt{J_2(\sigma_{ij})} \ , \quad \text{with} \quad \sigma_{ij} \quad \text{computed, using the}$$

elastic strains at the end of loading;

$$S_T^{(1)} \equiv \sqrt{J_2(\sigma_{ij})} \ , \quad \text{with} \quad \sigma_{ij} \quad \text{computed from the elastic}$$

stress-strain relations, using the total strains as elastic strains, with S_T referred to as the fictitious effective elastic stress;

54

$\beta \equiv S_e^{(1)} - S_{yield}^{(1)}$, and is a measure of strain hardening;

$\tilde{\beta} = \dfrac{\bar{z}^{(1)}}{t - \bar{z}^{(1)}} \beta$ is the neutral axis intercept of the slope

of the fictitious effective elastic stress distribution during reversed loading, and is seen to be based on the assumption of linearity of the distribution of $S_e^{(1)}$ in the plastic range;

$\bar{S}^{(1)} \equiv S_T^{(1)} - S_e^{(1)}$, and may be considered as effective stress lost through plastic behavior upon loading;

$\bar{S}_{yield}^{(2)} \equiv \sqrt{J_2(\sigma_{ij})}$, with σ_{ij} computed, using the stresses (derived from elastic strains) at initial yield during unloading or reversed loading;

$S_f \equiv \sqrt{J_2(\sigma_{ij})}$, with σ_{ij} computed, using the individual components of elastic strain, $e_{ij}^T - \epsilon_{ij}^{(1)}$; i.e., it is the effective stress that would exist if the plate did not go plastic during reversed loading;

$\bar{S}^{(2)}$ may be considered as effective stress lost through plastic behavior during reversed loading.

Hence for loading, we have $\bar{z}^{(1)}$ calculated by the method of Appendix E. For reversed loading, $\bar{z}^{(2)}$, is determined from similar triangles, as follows,

$$\bar{z}^{(2)} = t \left[\frac{S_{yield}^{(1)} + S_{yield}^{(2)} - \tilde{\beta}}{S_{yield}^{(1)} + S_f - \tilde{\beta}} \right] \tag{60}$$

when $\bar{z}^{(2)} \geq \bar{z}^{(1)}$, and is determined from Eq. (E.9) of Appendix E, with σ_o replaced by $S_{yield}^{(2)}$, when $\bar{z}^{(2)} \leq z^{(1)}$. At

55

initial reversed yielding, $\bar{z}^{(2)} = t$, since $S_e = S^{(2)}_{yield}$, and its value then decreases toward zero as S_e increases, since all other quantities remain fixed.

In Fig. 37, the quantity $S^{(1)}_e$, i.e., the actual effective stress, is shown to vary linearly from the top (bottom) surface to the elastic-plastic boundary. This is not exactly true, even with the linear plastic strain assumptions made here. This variation is "almost" linear (the square root of a quadratic function), however. Stanton (Ref. 18), who makes no assumption on plastic strain or effective stress distribution through the thickness, shows results for thin plates that indicate that their departure from linearity is indeed small. This additional assumption was needed here to determine $\tilde{\beta}$ and $\bar{z}^{(2)}$ when $\bar{z}^{(2)} > \bar{z}^{(1)}$. The validity of this assumption is supported, in some measure, by the continuous variation of $\bar{z}^{(2)}$ when the transition takes place from one method of calculation, Eq. (60), to the other, Eq. (E.9) (see Fig. 36d).

The cycling procedure for one full cycle consists of loading up to a prescribed maximum value. The plate is then unloaded elastically and the new critical load for reversed yielding, P^*, is calculated by the method described in Appendix E of Ref. 11. Here, however,

$$\left\{\sigma\right\} = P^* [E][W] \left\{\bar{d}_o\right\} + \left\{\sigma_R\right\} \tag{61}$$

where $\{\bar{d}_o\}$ are the displacements for a unit load and $\{\sigma_R\}$ are the residual stresses. Thus $\{\bar{B}\}$ in Eq. (E.3) of Appendix E of Ref. 11 equals $[E][W]\{\bar{d}_o\}$ in the current analysis. In addition, the value of $\{\sigma_R\}$ is determined in the following manner. When the maximum desired load is reached, the final value of the "effective plastic load," $\{Q_f\}$, is stored and remains on the structure. The residual displacements, stresses, etc., are calculated in a manner similar to that presented in Appendix G of Ref. 11. First, the residual displacements are calculated by setting $\{P\} \equiv 0$ in Eq. (22b).

$$\left\{D_R\right\} = [K_e]^{-1} \left\{Q_f\right\} \tag{62}$$

56

where $\{Q_f\} = [K_f^*]\{\epsilon_{of}\}$. Now the residual total strains are obtained,

$$\left\{e_R^T\right\} = [W] \left\{d_R\right\} \tag{63}$$

and the residual elastic strains are calculated,

$$\left\{e_R^e\right\} = \left\{e_R^T\right\} - \left\{\epsilon\right\} . \tag{64}$$

Finally, the residual stresses are

$$\left\{\sigma_R\right\} = [E] \left\{e_R^e\right\} \tag{65}$$

The residual stresses and strains, as computed by means of the above procedures, are valid at the end of any cycle of loading only if the zero load state is reached without the occurrence of reversed yielding. Where this is not the case, incremental plasticity calculations must be performed from the point of initiation of reversed yielding, as determined by the procedure outlined in Appendix E of Ref. 11, until the zero load state is reached. At this point the above relations for residual stresses and strains can again be used.

Upon reversed yielding the plastic load vector generated in this portion of the cycle is added to that obtained at the end of the loading cycle. Thus, although the accumulated plastic strain distribution is not linear, it is the sum of two linear portions. This procedure continues until the load is reversed, or until the new $\bar{z}$ [i.e., $\bar{z}^{(2)}$ as previously defined] is smaller than the previous $\bar{z}$. For the latter case, the plastic load is calculated by using only the cumulative plastic strain, since this is now linear (see Fig. 36d), even though the current plastic strain distribution is not. For subsequent loading the total plastic "loads" obtained during both loading and reversed loading are saved and remain on the structure. The new critical load and residuals are calculated from the sum of these loads.

Results

The goals associated with the case of bending, alone or in combination with membrane loads, include verification of the assumptions employed in the analysis (plastic strain distribution through the thickness, location and shape of the elastic-plastic boundary within the element, etc.) and the feasibility of using the developed methods as analytical tools for plastic bending problems. To this end extensive computations were carried out for beams and plates under pure bending or combined bending and membrane loads. Our solutions are compared with previously published data, where such are available.

A discussion and tabulation of computation times for several representative problems are presented in Appendix K.

Beams. — To demonstrate the feasibility of the plastic bending analysis, the method is applied initially to two beams, a simply supported and a cantilever beam. Results for these structures from an exact solution of the governing differential equation assuming elastic, ideally-plastic material behavior are available for comparison. As a consequence of assuming elastic, ideally-plastic behavior and of the fact that both structures are statically determinate, an analytic expression can be written that relates the depth of the elastic-plastic boundary to the applied load. The finite element analysis is applied to the beam structures with the use of this relationship, thus providing a means of determining the validity of assumptions made in choosing such quantities as the displacement function, the form for the plastic strain distribution, and the representation of the elastic-plastic boundary.

Figure 38a shows a nondimensionalized load versus central deflection curve for a uniformly loaded simply supported beam. Six elements were used in the idealization of one-half of the beam. In this figure, w_0 is the center deflection, w_0^* is the center deflection at the maximum load for which the beam is entirely elastic, and ρ represents the nondimensional load parameter,

$$\rho = \frac{p}{p_0} \left(\frac{a}{t} \right)^2 ,$$

where p is the applied load intensity and $p_0 = 4b\sigma_0$. The re-
sults obtained from the finite element analysis compare quite
favorably with the corresponding results from the exact solution
(Ref. 36), as shown in Fig. 38a. The collapse load determined
from the near vertical slope of the load-deflection curve is ap-
proximately 3 percent higher than the exact collapse load, which
occurs at a value of $\rho = 1$.

The propagation of the elastic-plastic boundary through the
thickness and in the plane of the elements is shown in Fig. 38b.
From this figure it can be seen that although the depth of the
boundary at plastic nodes is exact, the assumption associated
with its shape between nodes (i.e., linear) may lead to irregu-
larities in its representation, as evidenced at the load values
of $\rho = 1.00$ and $\rho = 1.03$. These irregularities indicate that
the actual boundary lies between the nodes, $6x/a = 3$ and
$6x/a = 4$, on the upper and lower surface of the beam. The error
introduced by the assumption of a linear boundary between nodes
can be reduced by using more elements in the idealization of the
beam. Also noteworthy in Fig. 38b is the development of a fully
plastic cross section at the center of the beam at a load corre-
sponding to $\rho = 1$. In a continuum analysis, the development of
this fully plastic cross section is sufficient to cause collapse
of the structure. In the finite element analysis, however, col-
lapse is not indicated until both cross sections of the element
containing the center of the beam become fully plastic.

Results in the form of a nondimensionalized load versus tip-
deflection curve for a uniformly loaded cantilever beam are shown
in Fig. 39a. Elastic, ideally-plastic material behavior was as-
sumed. Comparison with results from an exact solution, shown as
the solid curve in the figure, indicates good correlation up to
the collapse load. For this problem, as for the simply supported
beam, the depth of the elastic-plastic boundary can be directly
related to the applied load. Once again, this relationship was
used to obtain the results shown in the figure.

The propagation of the elastic-plastic boundary through the
cross section and in the plane of the elements is shown in
Fig. 39b. As indicated in the figure, the development of the
plastic region is much more localized for this structure than for
the simply supported beam. Consistent with a continuum approach,
collapse of this structure is indicated in the finite element
analysis by the development of one fully plastic cross section at
the root of the beam.

For both the simply supported and the cantilever beam, as previously mentioned, an exact relationship was used between the depth of the elastic-plastic boundary at nodes in the plastic range and the applied load to obtain results from the finite element analysis. Use of this relationship, which admittedly does not exist for most structures of interest, was justified as a way to check the validity of the assumptions made in choosing such quantities as the displacement function, the plastic strain distribution, and the representation of the elastic-plastic boundary. As the results indicated, these assumptions appear to be justified for the finite element analysis.

Since the depth of the elastic-plastic boundary is not generally known at the current load step, a more generally applicable procedure was devised and applied to the cantilever beam. Results were recomputed and a load-deflection curve was obtained by using an approximate value for the depth of the elastic-plastic boundary (see Fig. 40). This value, for any increment of load, is based on the total strain distribution determined at the end of the preceding load increment. This procedure cannot lead to the development of a fully plastic cross section. Consequently, it is assumed that a fully plastic cross section exists at a node when plasticity has developed through a specified proportion of the thickness. The deflections and slope of the load-deflection curve for this structure increase quite rapidly beyond a value of load for which plasticity has developed through 80 percent of the end cross section. Thus in the analysis this value was chosen as the criterion to determine the development of a fully plastic cross section. The degree of approximation associated with the use of the approximate procedure for determining values of the depth of the elastic-plastic boundary is illustrated in the figure by a comparison with the exact solution. The results can be seen to compare favorably for most of the load range considered. The maximum divergence, which occurs in the vicinity of the collapse load, is about 7 percent.

Also shown in Fig. 40 are results for the cantilever beam for the case of strain-hardening material behavior. These results, shown as the dotted curve, are compared with the corresponding results obtained by assuming elastic, ideally-plastic behavior. The close agreement of results for strain-hardening and perfectly plastic behavior can be attributed to the use of Ramberg-Osgood strain hardening parameters chosen to approximate the elastic, ideally-plastic stress-strain curve. The slope of the load-deflection curve for strain-hardening behavior illus-

60

trates that the beam still possesses some stiffness beyond the theoretical collapse load predicted by assuming perfectly plastic behavior.

Figure 41 illustrates the application of the procedure to a simply supported beam subjected to combined bending and axial loads. As previously discussed, the analysis for this problem requires the introduction of an initial stress stiffness matrix to account for the effect of the axial load on the bending stiffness. Independent determination of the position of the two elastic-plastic boundaries relative to the upper and lower surfaces is also required for this analysis because the axial load has the effect of introducing asymmetry about the middle surface. Results have been obtained for cases in which a uniform lateral load acts in conjunction with a constant tensile or compressive axial load, indicated in the figure by $T = +1000$ and $T = -1000$, respectively. These results are compared with those for the case of pure bending, indicated as $T = 0$. As shown in the figure, the effect of the axial compressive load, compared to the case of pure bending, is to reduce the structure's stiffness while the tensile load increases it. No solution to this problem by using a continuum analysis similar to the one developed for pure bending in the plastic range appears to be available for comparison. For the case of compressive axial load, the lateral load was incremented to a value that resulted in failure of the structure. This failure is indicated in Fig. 41 by the near vertical slope of the load-deflection curve. It should be noted that in this problem it was not necessary to develop a completely plastic cross section for collapse to occur. The reduction of stiffness caused by the axial compressive load and the propagation of the elastic-plastic boundary through only a portion of the thickness was sufficient to cause failure. This type of failure is associated with plastic buckling rather than with the formation of a mechanism.

Of special interest in elastic and elastic-plastic structural analysis is the behavior of plates with various shapes and boundary conditions. In addition, the plastic analysis of structures with cutouts is extremely important, since the cutouts generally result in regions of high stress gradient that can initiate plastic flow. It was on this basis that the structures considered in this section were chosen to demonstrate the plastic pure bending analysis of plates. For these structures, at least an elastic solution and, for most, an elastic-plastic or limit analysis solution are available in the literature.

<u>Rectangular plates — bending alone</u>. — The procedure for pure bending was applied first to a simply supported uniformly loaded square plate. Using a 36-element idealization to represent the quarter panel, load versus central deflection curves for this structure, assuming elastic, ideally-plastic and elastic, strain-hardening material behavior, have been determined and are shown in Fig. 42a. Once again, as in the case of the beam, the close agreement of results for both types of material behavior is attributable to the choice of strain-hardening parameters that approximate elastic, ideally-plastic material behavior.

The Ramberg-Osgood parameters that were used in computing the hardening coefficient, as outlined in Appendix A, are:

$$E = 10^7 \text{ lb/in.}^2$$

$$\sigma_{0.7} = 35,400 \text{ lb/in.}^2$$

$$n = 19.5 .$$

These parameters were used together with a yield stress of $\sigma_{yield} = 30,000$ lb/in.^{2}, and Poisson's ratio $\nu = 0.30$.

Also shown in Fig. 42a is a comparison of results from the present analysis, with elastic, ideally-plastic material behavior being assumed, with those of Ref. 38. Agreement is good for most of the load range considered, with the greatest discrepancy occurring as the magnitude of the load approaches the collapse value for the structure.

The idealization and yield sequence for the square plate are shown in Fig. 42b for the upper left-hand quadrant of the structure. Yielding originates on the upper and lower surface at the corners of the plate at a load of $\rho = pa^2/6M_0 = 0.502$ and commences at the center of the plate at $\rho = 0.579$. Beyond this value of load, the plastic regions propagate from the vicinity of the corners and the center of the plate until a collapse mechanism forms.

The collapse load for this structure, determined by assuming elastic, ideally-plastic material behavior, is the value of the load at which the pattern of fully plastic elements is such that

62

the structure becomes a mechanism. The collapse load, as deter-
mined by the present analysis is $\rho = 1.137$ and compares favor-
ably with a value of 1.070 obtained from a limit analysis de-
scribed in Ref. 35. The pattern of development of the plastic
region in the plane of the plate and the propagation of the
elastic-plastic boundary through the thickness of the plate are
shown in Figs. 42c and 42d, respectively. The crosshatched area
in Fig. 42c represents those regions of the plate in which plas-
ticity has developed to some degree but extends through less than
80 percent of the thickness. The shaded area represents those
regions in which plasticity extends through more than 80 percent
of the thickness. Considering the latter region as fully plastic
leads to the development of plastic hinges along the diagonals of
the square plate, as shown in Fig. 42c. As in the case of the
beam, this criterion is necessary because determining the depth
of the elastic-plastic boundary on the basis of total strains
cannot lead to the development of a fully plastic section.

The pattern of development of the plastic region in a narrow
rectangular plate $(\eta = 0.3)$ is shown in Figs. 43a-43c. In
Fig. 43a the 80 percent criterion was again used to determine
the pattern of fully plastic sections in forming the collapse
mechanism. From this figure it is evident that the sections that
form the collapse pattern do not all lie on the diagonals of the
plate.

A comparison of available upper bound solutions for the load-
carrying capacities of rectangular plates of various aspect
ratios is shown in Fig. 44a. The solid curve represents the so-
lution (Ref. 46) obtained by using the von Mises yield criterion
in conjunction with assumed collapse pattern (1) shown in the
figure. The dotted curve, taken from Ref. 47, represents the
upper bound solution obtained by using the Tresca yield condition
in conjunction with assumed collapse pattern (2). Results from
the finite-element analysis, represented by the solid circles,
indicate that displacement pattern (2) provides a more accurate
representation of the collapse mechanism than does pattern (1).
An upper bound solution, obtained by the present authors, using
the second displacement pattern in conjunction with the von Mises
yield condition is shown as the dashed curve in Fig. 44a. The
results from the present analysis compare favorably with this
solution and are slightly below it except for extremely low as-
pect ratios. For such narrow plates, the use of the 80 percent
criterion in conjunction with the calculation of the depth of the
elastic-plastic boundary from the total strain distribution of

the preceding step is not adequate. A relaxation of the 80 per-
cent criterion based on a careful examination of the load-deflec-
tion history appears to be warranted. A possible alternative
might be to incorporate an iterative procedure in the method of
solution.

It should be noted that in Fig. 44a, the length of the plate,
2a, is kept fixed while the width, 2b, decreases to zero.
Thus the nondimensionalized collapse load $\rho = pa^2/6M_o$ increases
with decreasing aspect ratio, and approaches infinity as the as-
pect ratio approaches zero. In Fig. 44b the width is kept fixed
while the length increases to infinity. For this case the non-
dimensionalized collapse load $\rho = pb^2/6M_o$ decreases as the as-
pect ratio decreases, and appears to approach the collapse load
for a uniformly-loaded infinite strip. The collapse load for the
infinite strip is computed to be $\rho = 0.385$, and is determined
from a yield limit analysis by assuming that the collapse mecha-
nism consists of a "yield-hinge" formed along the entire length
of the plate.

The collapse pattern and the propagation of the elastic-
plastic boundary through the thickness along two axes of a uni-
formly-loaded square plate with three simply supported edges and
one free edge are shown in Figs. 45a-45c. The fully plastic
region appears first in the vicinity of the midpoint of the free
edge and propagates from this point and from the corners formed
by the simple supports to form the "Y" shaped collapse mecha-
nism. The load at which the mechanism forms is $\rho = 0.715$. This
compares fairly closely with a collapse load of $\rho = 0.654$, ob-
tained from a yield limit analysis in Ref. 35. The curve of load
versus deflection at the midpoint of the free edge is shown in
Fig. 45d. The slope of this curve is nearly vertical as the
magnitude of the load approaches the collapse value.

Results for the elastic, ideally-plastic behavior of a uni-
formly-loaded clamped square plate are shown in Fig. 46. The
collapse mechanism for this structure, as shown in Fig. 46a,
consists of a pattern of fully plastic elements formed along the
diagonals and the edges (with the exception of the corners) of
the plate. The value of the load at which this occurs, as deter-
mined from the present analysis, is $\rho = 2.59$, which is signifi-
cantly higher than those values determined from a yield limit
analysis. A value of 2.31 is predicted in Ref. 48, and a value
of 2.052 is given in Ref. 35. The inability of the present
analysis to predict the collapse load of the clamped plate

64

accurately may be attributed, in part, to the need for a much finer idealization of the structure, particularly along the edges where there is a rapid change in curvature.

The propagation of the elastic-plastic boundary through the depth along $y = 0$ is shown for three values of load in Fig. 46b. As indicated in the figure, two plastic regions exist: the first is localized in the vicinity of the clamped edges, and the second region originates at the center of the plate and propagates toward the edges. At a load of $\rho = 2.41$ the latter region is seen to be of irregular shape for $x/a > 0.5$.

Deflection profiles along $y = 0$ are shown for three values of load in Fig. 46c. The load of $\rho = 0.617$ represents the maximum elastic load. The deflection profile for $\rho = 2.41$ illustrates the diminishing effect of the clamped boundary in restraining displacements in the region near the edges. At this value of load the sections along the edges, with the exception of the corners, are nearly fully plastic.

The distribution of moments M_x and M_y along $y = 0$ and $y = a$ are shown for two values of load in Figs. 46d to 46g. The moments are nondimensionalized with respect to the fully plastic moment M_0 (i.e., the moment at a fully plastic section for the one-dimensional case of a beam). The redistribution of moments as a consequence of plastic flow is clearly evident in these figures. Similar redistributions are indicated in Refs. 38 and 39.

The collapse pattern of a uniformly-loaded simply supported square plate with a centrally located square hole is shown in Fig. 47a. A free edge is assumed along the perimeter of the hole, and the ratio of the width of the hole to the width of the plate is 1/3. The collapse pattern and the value of the nondimensionalized collapse load, $\rho = 1.01$, are very nearly the same as those obtained for the simply supported square plate without the hole. The magnitude of the collapse load obtained in the present analysis is approximately 3 percent greater than the value of $\rho = 0.977$ obtained from the upper-bound yield limit analysis of Ref. 35.

Distributions of bending moments in the x and y directions along the axis of symmetry $y = 0$ are shown for two values of load in Figs. 47b and 47c, respectively. At a load of $\rho = 0.222$, which represents the maximum elastic load for this

structure, the maximum value of M_x occurs in the vicinity of $6x/a = 4$ and the maximum value of M_y at the edge of the hole. In the case of M_y the redistribution that occurs at a load of $\rho = 0.950$ is pronounced. At this load the maximum moment is located at some distance from the edge of the hole. A similar redistribution is indicated in Fig. 47d for the case of the moments M_x and M_y along the diagonal.

The maximum twisting moment M_{xy} occurs at the corner of the square hole for purely elastic behavior, as shown in Fig. 47e. As a consequence of plastic deformation, the maximum value of M_{xy} shifts to the corners of the plate.

In Fig. 48, results obtained for the uniformly-loaded simply supported square plate by using the 16-degree-of-freedom rectangular element are compared with results obtained by using the 18-degree-of-freedom triangular element. The total number of degrees of freedom used in the representation of a quadrant of the structure is 144 for the rectangular and 150 for the triangular element. Load increments of $\Delta\rho = 0.0046$ are used for both idealizations. Results in the form of a deflection profile and moments M_x and M_y along $y = 0$ are in complete agreement at the maximum elastic load $\rho = 0.50$. Results for a load of $\rho = 0.95$ are virtually the same for both idealizations, with the triangular element solution predicting slightly smaller displacements and moments along $y = 0$.

The value of the collapse load obtained by using the triangular element is the same as that obtained by using the rectangular elements. In addition, the collapse pattern and the propagation of the elastic-plastic boundaries determined by using the triangular elements are the same as those shown in Figs. 42c and 42d.

The idealization and the collapse pattern of a uniformly-loaded simply supported square plate with a centrally located circular hole are shown in Fig. 49a. The idealization of a quadrant of the structure consists of a network of 81 triangular elements with 49 nodes, resulting in 266 degrees of freedom. A free edge is assumed around the circular hole, and the ratio of the diameter of the hole to the length of the plate is 1/3.

Collapse of this structure, as predicted by the present analysis, occurs at a load of $\rho = pa^2/6M_o = 1.07$. The collapse

mechanism consists of a region of fully plastic nodes formed along the edge of the free hole and extending along the diagonal to the corner of the plate.

The deflection and circumferential moment around the circular hole are shown for three values of load in Figs. 49b and 49c. At the maximum elastic load, $\rho = 0.402$, the results from the finite element analysis are compared with the results of a previous investigation, Ref. 49. The correlation of results for moment and deflection is quite good, with a maximum discrepancy of 3 percent occurring at $\theta = 0°$.

The variation of the deflections around the hole from $\theta = 0°$ to $\theta = 45°$ increases as the magnitude of the load increases into the plastic range. However, the effect of plasticity reduces the variation of the circumferential moment around the hole, and at $\rho = 1.02$ the circumferential moment distribution is nearly uniform at a value equal to the fully plastic moment, M_o.

Deflection profiles of the plate along the horizontal (or vertical) axis of symmetry, $\theta = 0°$, and along the diagonal, $\theta = 45°$, are shown for three values of load in Figs. 49d and 49e. The distribution of radial and circumferential moments along $\theta = 0°$ and $\theta = 45°$ are shown in Figs. 49f-49i. The redistribution of moments resulting from plastic deformation is very much in evidence in these figures. It is of interest to note in Fig. 49i that, in a limited region near the hole boundary, values of the circumferential moment along the diagonal are greater than that of the fully plastic moment. This can occur only for states of multiaxial stress where one stress component exceeds the ideally-plastic yield stress of the material.

Circular plates — bending alone. — Two idealizations used for the representation of circular plates and an annular plate are shown in Fig. 50. Idealization (a) consists of 50 elements and 36 nodes and results in 153 degrees of freedom in representing both a simply supported and a clamped plate. Idealization (b) represents a consistent refinement of idealization (a) and consists of 128 elements and 81 nodes and results in 387 degrees of freedom for both the simply supported and clamped plate. The unshaded triangles of idealization (b) are employed in the representation of an annular plate. The elimination of the shaded triangles results in a 110 element, 72 node idealization, and

320 degrees of freedom are required for the case of an annular plate simply supported along both the inner and outer circumference. For the annular plate clamped along the outer circumference and free along the inner boundary, 332 bending degrees of freedom are required.

Results for the case of a uniformly-loaded simply supported circular plate of radius a are shown in Fig. 51. Elastic, ideally-plastic material behavior is assumed, with the value of the fully plastic moment, M_o, equal to 4000 lb in/in. Both idealizations of Fig. 50 were used, and the results obtained from both sets of computations were virtually the same throughout the entire load range. Results in the form of deflection profiles, propagation of the elastic-plastic boundary, and the distribution of circumferential and radial moments are shown for three load values in Figs. 51a to 51d.

The deflection profiles shown in Fig. 51a indicate that the plate assumes a nearly conical shape, with the formation of a "yield hinge" at the center of the plate, as the load approaches the collapse value. The present analysis predicts a collapse load of $\rho = pa^2/M_o = 6.50$. It should be noted that the triangular elements used are conforming elements, and hence no slope discontinuities (kinks) can exist as they do in a limit analysis. This collapse load compares quite favorably with the value of $\rho = 6.51$ predicted from a yield limit analysis in Ref. 50. The limit analysis requires the entire plate to be fully plastic at collapse, whereas in the present analysis collapse is indicated when a "fully plastic" section forms at the center of the plate. Beyond this point the displacements increase quite rapidly. The elastic-plastic boundaries at various stages of loading are plotted in Fig. 51b. Consistent with our assumptions concerning the shape of the boundary, the actual boundary is represented by a series of straight line segments. This shape is approximated by the smooth curves shown in Fig. 51b. Figures 51c and 51d illustrate the redistribution of circumferential and radial moments that take place in the plastic range.

The results from the present analysis, obtained by using load increments of $\Delta\rho = pa^2/M_o = 0.025$, are compared with results from the layered finite-element approach of Ref. 12. In the latter investigation, the elements and layers used for the idealization of the structure numbered 20 and 40, respectively, and the load was increased in increments of $\Delta\rho = 0.100$ to

68

0.125. Results from both analyses correlate quite well for the entire range of loading.

The uniformly-loaded simply supported circular plate was chosen as a typical case for application of the plastic bending analysis procedure to demonstrate the variation of results obtained by using a range of load increments. Load versus central deflection curves are shown in Fig. 52 for load increments ranging from $\Delta\rho = 0.0125$ to 0.20. The results are necessarily identical up to the load at which the yield condition is satisfied at the center of the structure $(\rho = pa^2/M_o = 3.28)$. These curves show there is a wide divergence among computed results. This is to be expected, since the predictor procedure followed in the present analysis uses estimated values of plastic strain and depth of elastic-plastic boundary at nodes based on values of these quantities computed at the preceding load level. As the load level increases and as the loading progresses further into the plastic range, these estimated values of plastic strain and location of the elastic-plastic boundary become less accurate. At a load level of $\rho = 6$ the maximum difference in computed results is approximately 25 percent. The results for $\Delta\rho = 0.0125$ and $\Delta\rho = 0.025$, however, do indicate some convergence of the results for most of the load range.

Results for the elastic, strain-hardening behavior of the uniformly-loaded simply supported circular plate are shown in Fig. 53. The stress-strain curve of the material chosen for the structure is described by the following Ramberg-Osgood parameters: $E = 10^7$ lb/in.^{2}, $\sigma_{0.7} = 24,000$ lb/in.^{2}, and $n = 6.66$. In addition, a yield stress of $\sigma_o = 16,000$ lb/in.^{2} and Poisson's ratio, $\nu = 0.33$, are used. Figures 53a and 53b illustrate the deflection profiles and location of the elastic-plastic boundaries at various stages of the loading. As can be anticipated, the redistribution of moments that occurs for elastic strain-hardening behavior, shown in Figs. 53c and 53d, is less pronounced than the redistribution that occurs by assuming elastic, ideally-plastic material behavior, as shown in Figs. 51c and 51d.

Results for the elastic, ideally-plastic behavior of a uniformly-loaded clamped circular plate of radius a are shown in Fig. 54. A yield stress of $\sigma_o = 16,000$ lb/in.^{2} and Poisson's ratio of 0.24 were used in the analysis. Both idealizations of Fig. 50 were employed to determine the elastic behavior of

this structure. The value of the radial moment along the clamped edge using idealization (a) is 8 percent greater than the corresponding value computed from a continuum analysis, Ref. 51. It is conjectured that this discrepancy is due in part to the representation of the actual circular boundary by a polygon. Some support for this conjecture is provided by the results using idealization (b). Since the latter representation yielded somewhat better results for the radial moment (4 percent greater than the exact value) it was chosen to represent the structure.

A refined representation is also required for the plastic analysis of this structure. As indicated in Fig. 54b, two separate regions of plasticity develop. The first is along the clamped edge; the second starts at the center of the plate and propagates in the radial direction. Collapse of the structure is indicated with the formation of fully plastic sections along the clamped edge (a "hinge circle") and of a fully plastic section or hinge at the center of the plate. The present analysis predicts the formation of this collapse mechanism at a load of $\rho = pa^2/M_0 = 12.45$, which agrees very closely with the value of $\rho = 12.5$ predicted from the yield limit analysis of Ref. 50.

Once again the results of the present analysis using load increments of $\Delta\rho = 0.125$ have been compared with the results from the layered finite element approach of Ref. 12. In the latter investigation the load was increased in increments of $\Delta\rho = 0.250$ and the elements and layers used for the idealization of the clamped plate totaled 20 and 40, respectively. Results from both analyses for the deflection profiles, shown in Fig. 54a, are in agreement for loads of $\rho = 6.5$ and $\rho = 9.0$. However, at a load of $\rho = 11.5$ there is a substantial difference in the results, with the present analysis predicting larger displacements than those obtained in the layered approach. Consistent with the prediction of larger displacements, the present analysis indicates the development of a larger region of plasticity in the plane and through the depth of the plate than that indicated in Ref. 12, as shown in Fig. 54b.

The difference in results for the deflection profile at $\rho = 11.5$ is disturbing, in view of the excellent agreement obtained with the layered finite element analysis in the case of the simply supported plate. A possible explanation for this difference may be the fact that the deflections increase rapidly as the load approaches the collapse value for the structure. Thus at a load of $\rho = 11.5$, which represents 92 percent of the

theoretical collapse load, the deflections become arbitrarily large and a comparison of values of displacements at this load may be of no significance.

The redistribution of moments in the circumferential and radial directions is shown in Figs. 54c and 54d. Comparison with Ref. 12 is good, with the exception of the circumferential moment distribution at a load of $\rho = 11.5$. A maximum difference of results appears along the clamped edge, $r = a$. At this point the value of circumferential moment, as given by Ref. 12, is equal to the fully plastic moment M_o. This value for M_θ is, however, questionable. From Fig. 54d, the same analysis appears to predict a value of the radial moment along the clamped edge greater (in absolute magnitude) than the fully plastic moment. Since M_θ and M_r are the only components of moment along the clamped edge, the condition predicted by Ref. 12, viz., $|M_\theta| = M_o$ and $|M_r| > M_o$, is inadmissible for a perfectly plastic material obeying the von Mises yield condition.

Results for the uniformly-loaded clamped plate assuming elastic, strain-hardening material behavior are shown in Fig. 55. The Ramberg-Osgood parameters are identical to those used for the simply supported plate of Fig. 53. Comparison of results with the layered finite element approach of Ref. 13 is favorable for most of the load range except for the deflection profile at a load of $p = 560$ lb/in.^{2}. Once again, the results for this structure from the present analysis consistently predict larger displacements in the plastic range than those given in Ref. 13. The redistribution of moments shown in Figs. 55c and 55d is less pronounced for the strain-hardening behavior than for the ideally-plastic materials.

Figure 56 illustrates the results for the elastic, ideally-plastic behavior of a uniformly-loaded annular plate, simply supported along both the inner and outer edges. The ratio of the inner to outer radius is 0.375. The unshaded triangles of idealization (b) (Fig. 50) are used to represent a quadrant of the structure. Values for the yield stress, Young's modulus, and Poisson's ratio are identical to those used for the simply supported plate of Fig. 51.

The value of the collapse load obtained from the present analysis is $\rho = pa^2/M_o = 28.1$. The collapse loads for annular plates with various ratios of inner to outer radius are given in

Fig. 4.5 of Ref. 52. These loads were obtained from a limit analysis by using the Tresca yield condition. For a ratio of $b/a = 0.375$, the value of the collapse load as determined from Fig. 4.5 is $\rho = 25.2$. The associated collapse pattern of the limit analysis, consistent with the Tresca yield surface, is represented by two concentric "hinge circles." For $b/a = 0.375$ these hinge circles are closely spaced, and from Fig. 4.5 of Ref. 52 are located at $r/a = 0.625$ and 0.670. Collapse occurs in the present analysis with the formation of one hinge circle located along $r/a = 0.625$.

The deflection profiles, propagation of the elastic-plastic boundaries, and distribution of circumferential and radial moment are plotted in Figs. 56b to 56d for three values of load. The load $pa^2/M_0 = 16.3$ represents the maximum elastic load for this plate.

Triangular plate — bending. — The plastic bending analysis has also been used to obtain results for the elastic, ideally-plastic behavior of a uniformly-loaded equilateral triangular plate simply supported along the edges. The idealization and dimensions of the plate are shown in Fig. 57a. Material properties are the same as those chosen for the ideally-plastic simply supported circular plate of Fig. 51. An analytical solution for the elastic deflections is given in Ref. 51. Excellent agreement with these results was obtained at the maximum elastic load

$$\rho = pH^2/6M_0 = 4.65, \quad \text{as shown in Fig. 57c.}$$

The collapse pattern for the triangular plate is indicated by the shaded region of Fig. 57a. The value of the load at which this collapse mechanism forms is $\rho = 10.06$. The corresponding value of the collapse load obtained by a limit analysis is $\rho = 10.39$. The limit analysis procedure used to obtain the latter value of the collapse load follows that outlined in Ref. 46. The von Mises yield condition was used in conjunction with an assumed collapse pattern formed along the medians of the triangle. The propagation of the elastic-plastic boundary through the thickness along the median $y = 0$ is shown for three values of load in Fig. 57b. Deflection profiles and distributions of moments M_x and M_y acting along the medians are plotted for loads of $\rho = 4.65$ and $\rho = 9.31$ in Figs. 57c to 57e, respectively.

The plastic analysis procedure outlined in this section has also been applied to structures under combined bending and

72

membrane loading. As stated above, the cases considered are lim-
ited to those for which a constant membrane load is applied to
the structure. The magnitude of the applied membrane load is re-
stricted to values less than that necessary to initiate plastic
deformation. The lateral load necessary to cause initial yield-
ing is then applied and additional lateral loads are applied in
finite increments while the membrane load is held constant.

Simply supported rectangular plates — combined loading. —
Curves of lateral load versus center deflection of a simply sup-
ported square plate under combined loading are shown in Fig. 58a
for elastic, ideally-plastic material behavior. The magnitude
and sense of the applied membrane load is indicated by α, the
ratio of the applied membrane load to the buckling load, N_{crit}
(α is positive for compressive membrane load and is negative for
tensile membrane load). For positive values of α the lateral
load was incremented to values that resulted in the failure of
the structure. This failure, indicated by the near vertical
slope of the load-deflection curves is associated with plastic
buckling rather than with the formation of a collapse mechanism.
Results for applied tensile membrane loads and pure bending
($\alpha = 0$) are also shown in Fig. 58a.

Load versus central deflection curves for the simply sup-
ported square plate under combined loading are shown in Figs. 58b
and 58c for elastic, strain-hardening behavior, and are compared
with the curves obtained for elastic, ideally-plastic behavior.
The Ramberg-Osgood strain-hardening parameters are:
$E = 10^7$ lb/in.^{2}, $\sigma_{0.7} = 35,400$ lb/in.^{2}, and $n = 8.5$. In addi-
tion a yield stress of $\sigma_0 = 30,000$ lb/in.^{2} and Poisson's
ratio, $\nu = 0.3$, are used. Initial yielding occurs at a lower
value of applied lateral load for strain-hardening behavior than
for ideally-plastic behavior, as indicated in Figs. 58b and 58c.
For compressive membrane loading, Fig. 58b, this earlier initial
yielding for strain-hardening behavior results in an earlier
failure of the structure than that associated with ideally-
plastic behavior.

The lateral load-carrying capacities of the simply supported
square plate subjected to various magnitudes of uniform membrane
load in one direction are shown in Fig. 59. The magnitudes of
the applied membrane loads range from $-1 \leq \alpha \leq 1$. For tensile
membrane loads and for the case of pure bending the value of the

73

lateral collapse load, $\rho = pa^2/6M_o$, is that value of load at which a collapse mechanism is formed. For compressive membrane loads, as previously stated, the value of the collapse load is determined from load-deflection behavior. The smooth variation of the value of the lateral load-carrying capacity in transition from compressive to tensile membrane loading offers some verification that the choice of an 80 percent criterion is a reasonable one.

The lateral load-carrying capacities of simply supported rectangular plates under combined loading are shown in Fig. 60. Results are shown for tensile and compressive membrane loads of $\alpha = -\frac{1}{2}$ and $\alpha = \frac{1}{2}$, respectively. In addition, the case of pure bending, previously shown in Fig. 44a, is repeated in Fig. 60.

Results are shown in Fig. 61 for a simply supported square plate subjected to a uniform lateral load and an in-plane shear load. Load versus central deflection is shown in Fig. 61a. The value of the load at which collapse occurs is $\rho = pa^2/6M_o = 0.518$. The idealization, consisting of a grid of 8 x 8 square elements, and the yield sequence are shown in Fig. 61b. This figure shows that initial yielding occurs at two opposite corners of the plate and subsequently develops along the diagonal joining these corners. The propagation of the elastic-plastic boundary through the thickness is illustrated in Fig. 61c.

Circular plates — combined loading. — Lateral load versus center deflection curves for simply supported circular plates subjected to various combinations of uniform lateral and in-plane radial loads are presented in Fig. 62a. Results for tensile and compressive membrane radial loads equal in absolute magnitude to one-third of the elastic buckling load $(\alpha = \pm\frac{1}{3})$ are compared with results for the case of pure bending $(\alpha = 0)$, assuming elastic, ideally-plastic material behavior. Also shown in this figure is a load-deflection curve for the case of elastic, strain-hardening material behavior, with the compressive load equal to 30 percent of the elastic buckling load. The ideally-plastic and strain-hardening parameters chosen to describe the mechanical properties are identical to those used for the cases shown in Figs. 51 and 53. The idealization shown in Fig. 50a was used to obtain the results shown in Fig. 62.

74

An apparent distinction between the behavior of the circular and rectangular plates under combined loadings, as considered here, is that in the former there is a more pronounced asymmetry in the development of stresses, strains, and plastic regions with respect to the middle surface. For the rectangular plates of Figs. 58 through 60, because of the material and geometric properties chosen, the stresses at initial yield attributable to the membrane loads are less than 3 percent of the total value. The predominant effect of the membrane load therefore is to stiffen (or soften) the structure. For the circular plates of Fig. 62, on the other hand, because of the material and geometric properties used, almost 75 percent of the total value of maximum elastic stress is due to the membrane behavior. Thus, for the circular plates, the effect of the membrane loads on both the stiffness and the stress distribution has a significant influence on the value of the lateral load at which initial yielding occurs. This is evident in Fig. 62a where the circular plate loaded radially in tension (and consequently stiffer) yields at a considerably lower value of lateral load than the same plate subjected to pure bending.

Failure of the ideally-plastic circular plate subjected to a compressive radial membrane load occurs as a plastic buckling type of phenomenon at a value of the lateral load 2.6 times the maximum elastic load. The corresponding plate exhibiting strain-hardening behavior experiences failure of a plastic buckling type at a lateral load 6.61 times the maximum elastic load. The plate subjected to the radial tensile loading was not loaded to failure.

The growth of the plastic regions for the cases involving $\alpha = \pm\frac{1}{3}$ are shown in Figs. 62b and 62c, respectively. The extent of these regions is seen to be similar for the case, $\rho = 1.37$, $\alpha = +\frac{1}{3}$, and the case, $\rho = 7.91$, $\alpha = -\frac{1}{3}$. Collapse is imminent in the former case but not in the latter.

The final problem considered is that of an annular plate clamped along the outer edge and free along the inner edge. The inner to outer radius ratio is 0.375 and the thickness is 0.5 inch. Results for the plate subjected to a uniformly-distributed lateral load acting alone and also in combination with a uniform compressive radial load equal to 25 percent of the elastic buckling load are presented in Fig. 63.. Elastic, ideally-plastic material behavior is assumed, with the mechanical properties chosen as follows: a yield stress of 30,000 psi, Young's

modulus of 10^7 psi, and Poisson's ratio of 0.3. Curves of load versus the deflection along the inner edge are shown for the two cases in Fig. 63a. The extent of the plastic regions at various stages of loading are presented in Fig. 63b for bending alone and Fig. 63c for the combined loading case. For the latter case two plastic regions appear initially, one emanating from the upper surface at the free edge and the second originating at the lower surface along the clamped edge. Although the region at the free edge is the first to appear as a result of the stress concentration along the hole boundary, the plastic zones along the clamped edge become more extensive as the lateral bending load increases.

Square plate subjected to cyclic loading. — To demonstrate application of the cyclic loading procedure, as outlined for the plastic bending analysis of this section, this procedure has been applied to a simply supported square plate exhibiting strain-hardening material properties. The Ramberg-Osgood parameters for this problem are the same as those used for the plate of Fig. 42. A cyclic load versus center displacement curve is shown in Fig. 64a for a load range of $\rho = \pm 1.67$ ($\rho = pa^2/6M^*$ where M^* is the yield moment, $M^* = \frac{2}{3}\sigma_0 t^2$). Since there are no available experimental data or previous analytical results for this structure for unloading and reversed loading, the computed results could not be verified. However, this curve clearly indicates the effects of cyclic plastic deformation. The initial yield load in tension is $\rho = 0.75$; reversed yielding begins at $\rho = 0.16$, prior to the removal of all the positive load; and subsequent yielding commences at $\rho = -0.16$, prior to the removal of all the negative load. Because of the presence of residual stresses and strains and the Bauschinger effect at the end of the first half-cycle, the magnitude of the center displacement at $\rho = -1.67$ is greater than that at $\rho = 1.67$.

Deflection profiles along $y = 0$ are shown in Fig. 64b. The profiles are plotted at the maximum elastic load, the maximum and minimum loads, and the residual displacements upon unloading from $\rho = \pm 1.67$ are also presented.

The distribution of normal stress components σ_x and σ_y at the surface along $y = 0$ are shown in Figs. 64c and 64d, respectively, and the shear stress distributions at the surface along $y = \pm a$ are shown in Fig. 64e.

76

5. COMBINED MATERIAL AND GEOMETRIC NONLINEARITY

In the preceding sections, the treatment of elastic-plastic bending of beams and plates has been based on the assumption of zero or constant applied membrane forces. The methods developed are, consequently, applicable only in the case of relatively small deflections, since it is well known that the membrane force generated by the bending of plates into nondevelopable surfaces is significant even when the deflection is only of the same order as the thickness of the plate (Ref. 51). The same effect is encountered in the bending of restrained beams.

It is desirable, under these circumstances, that a general method of analysis of great power (such as the finite-element method) should be extended to include the treatment of small strains and large deflections, alone or in combination with plastic behavior. Several methods have been developed within the framework of the finite-element approach to account for geometrically nonlinear behavior. These methods are generally classified as incremental, iterative, direct search technique, etc.

In the present report, we are concerned with geometric nonlinearity occurring in combination with plastic deformation. Consequently, a primary consideration in choosing a method for the analysis of geometric nonlinearity from among the several currently available is the ease with which it can be combined with methods of plastic analysis. For this reason, our approach is based upon a linearized incremental formulation, i.e., one in which the nonlinear analysis is reduced to the solution of a sequence of linear incremental equations. In Refs. 4, 15, 45, 53, and 54 this approach was used to solve problems involving geometric nonlinearity. Since the plasticity relations are themselves incremental, and the methods developed for the treatment of plastic effects depend upon a revision of the governing matrix equation in each loading step, the modifications necessary to incorporate "large deflection" terms are minimal.

A limitation of the incremental procedure, however, is the necessity of taking relatively small increments if the solution obtained is to converge adequately to the "exact" solution of the nonlinear problem. This can be costly in terms of computer time, since the inclusion of geometric nonlinearity involves more extensive revisions at each loading step than does the treatment of plasticity. This limitation can be eased somewhat by using

larger steps in conjunction with an iterative technique. The iteration need not be introduced immediately but may be postponed until the nonlinearity becomes sufficiently pronounced to require it.

Martin (Ref. 45) discusses an incremental numerical method, based on the direct stiffness approach, that is generally applicable for the treatment of problems involving geometric nonlinearity. This procedure approximates the nonlinear behavior by a sequence of linear steps. Either loading or displacement may be applied incrementally. This procedure requires the introduction of the initial stress stiffness matrix, and additionally the updating of the geometry at the end of each incremental loading step. These considerations and the introduction of the initial strain stiffness matrix represent the basic modification for the development of an incremental procedure to account for both types of nonlinearity.

Thus, the method of solution of the general geometrically nonlinear problem discussed here involves the solution of a sequence of "beam-column" type problems, in which values of the membrane stress resultants and the geometry of the deformed structure are updated in each increment of loading. For sufficiently small loading increments, the increments of rotation in any finite element will be small when measured with respect to a local coordinate system which translates and rotates with the element in successive loading steps (but is assumed to remain fixed within any one loading step). Consequently, squares and products of the increments of rotation may be neglected in computing increments of membrane strain. Furthermore, with respect to this local coordinate system and within individual loading increments the in-plane problem in each element, for initially flat structures, is uncoupled from the lateral problem, as indicated in Eq. (58), where the effective plastic load vector is given in Eq. (57).

Because of the presence of geometric nonlinearity, the entire element stiffness matrix [k_e] in Eq. (21) must be reformed in each loading step, with current stress levels and geometry being used. In the discussion of the development of the elastic stiffness matrix, it was mentioned that the only component matrices required are the conventional stiffness matrices (those not dependent upon the presence of stress) and the initial stress stiffness matrix. The latter matrix accounts for the change in bending stiffness due to the presence of membrane loads. In the

78

development of the initial stress stiffness matrix, the membrane stresses taken into account are those present at the beginning of the loading step, any further changes in these stresses occurring during the loading step being neglected in that development. This constitutes the linearization of the procedure during an increment of loading.

Some investigators (see Refs. 55-57) have indicated the need for an additional matrix, termed "the initial displacement" matrix, for the treatment of geometric nonlinearity. Because the current analysis utilizes a "moving" local coordinate system, this additional stiffness matrix is not required. The expression for Δe^T as used here for a beam element is given as

$$\Delta e^T = \frac{d(\Delta u)}{dx} + \frac{1}{2} \left(\frac{d(\Delta w)}{dx}\right)^2 - z \frac{d^2(\Delta w)}{dx^2} \tag{66}$$

where Δu and Δw represent the increments in the axial and lateral displacements of the neutral axis of the beam. The usual Bernoulli-Euler kinematic beam theory assumptions were made to obtain Eq. (66). The first term on the right side of the above equation represents the extension of the centerline of the beam resulting from axial loads; the second term is the contribution to the extensional strain due to lateral deflection (the rotation term); and the last term is the conventional bending strain term arising from the condition that normals to the neutral axis should, after deformation, remain straight and normal to the centerline and unextended.

Marçal's expression for the membrane component of total strain is given as

$$e^T = \frac{\partial u}{\partial x} + \frac{1}{2} \left(\frac{\partial w}{\partial x}\right)^2 . \tag{67}$$

Now,

$$e^T + \Delta e^T = \frac{\partial(u + \Delta u)}{\partial x} + \frac{1}{2} \left(\frac{\partial(w + \Delta w)}{\partial x}\right)^2$$

$$= \frac{\partial u}{\partial x} + \frac{\partial(\Delta u)}{\partial x} + \frac{1}{2}\left[\left(\frac{\partial w}{\partial x}\right)^2 + 2\left(\frac{\partial w}{\partial x}\right)\frac{\partial(\Delta w)}{\partial x} + \left(\frac{\partial(\Delta w)}{\partial x}\right)^2\right] \tag{68}$$

79

Subtracting Eq. (67) from Eq. (68) we get

$$\Delta e^T = \frac{\partial(\Delta u)}{\partial x} + \frac{1}{2}\left(\frac{\partial(\Delta w)}{\partial x}\right)^2 + \left(\frac{\partial w}{\partial x}\right)\left(\frac{\partial(\Delta w)}{\partial x}\right) . \tag{69}$$

The increments of the membrane components of total strain in Eqs. (66) and (69) differ only by the last term. This term leads to the initial displacement matrix. Since, in the method used here, Δw is measured with respect to a local coordinate system that rotates with the element, $\partial w/\partial x$, the slope at the beginning of the load increment is necessarily zero. Thus the initial displacement matrix is zero. If the datum were the original configuration, then the initial displacement matrix would be needed and the value of $\partial w/\partial x$ used would be the total value of the slope calculated at the end of the preceding step.

Equation (58) applies to an individual element with displacements taken with respect to the local coordinate system. To obtain the over-all response of the structure, the contribution of each element must be transformed into a global system and then assembled to obtain the over-all load-deflection relationship.

Toward this end, we may write, for an individual element,

$$\left\{\Delta d_o\right\}_\ell = [T] \left\{\Delta d_o\right\}_g \tag{70}$$

where $[T]$ is an orthogonal transformation matrix relating the generalized incremental nodal displacements referred to the local coordinate axes to those referred to the global axes. The subscripts ℓ and g refer to local and global coordinate systems, respectively. We can also write

$$\left\{\Delta p_o\right\}_g = [T]' \left\{\Delta p_o\right\}_\ell \tag{71}$$

because of the orthogonality of the transformation. The resulting global equation for an individual element is

$$[T]'\left[[k^{(0)}] + [k^{(1)}]\right][T] \left\{\Delta d_o\right\}_g^i = \left\{\Delta p_o\right\}_g^i + [T]'\left\{\Delta q\right\}_\ell^{i-1} \tag{72}$$

80

where, as discussed above, $[k^{(0)}]$ and $[k^{(1)}]$ are calculated on the basis of the geometry and membrane stresses existing at the start of the loading step. The vector of increments in the fictitious forces, $\{\Delta q\}$, is calculated in the manner discussed above in connection with plastic analysis. An increment of load is then applied and the corresponding displacement increments calculated from the matrix equation for the whole structure. The displacements are then transformed back to local coordinate systems appropriate to the beginning of the loading step. New internal forces are calculated, and total stresses, strains, and displacements are obtained by summing incremental values. The geometry is then updated and new local coordinate systems are formed. This process is repeated until the maximum specified load level is reached or the structure fails.

A detailed discussion of coordinate transformations for a beam element and a triangular bending element is presented in Appendix L.

Results for Geometric Nonlinearity

To illustrate the procedure for geometric nonlinearity, a simply supported restrained beam subjected to a uniform vertical load is considered. A plot of the central deflection versus lateral load for this beam is shown in Fig. 65a. The exact results were obtained from Ref. 51. As may be seen in Fig. 65a, agreement between the present and exact results for the center displacement is quite good. The length of the beam is 60 in., the moment of inertia is 0.1 in.^{4}, and the area of the rectangular cross section is 1.2 in.^{2}. To take advantage of symmetry, 6 elements were used to represent half the structure. A plot of internal axial force versus total load for the same beam is given in Fig. 65b. Once again, agreement with the exact results of Ref. 51 is excellent. It should be noted that in beam problems, the membrane force generated is tensile and tends to stiffen the structure.

Because of the presence of compressive axial forces in arches, elastic instability can occur when the loading reaches a critical value. To determine the value of the critical load accurately and establish a basis for its prediction, the determinant of the over-all stiffness matrix and the eigenvalues and eigenvectors are calculated by means of a procedure developed in Ref. 58.

81

To illustrate the procedure, several circular arches were analyzed and the results compared with those of other authors. Geometric imperfections and eccentric loadings were introduced in several cases to study their influence on the behavior of the arches. Straight beam elements were used in all the following examples.

Figure 66 is a plot of load versus central deflection for a simply supported shallow arch with a symmetric buckling pattern. The results are compared with those of Ref. 4, where a finite-element approach was also used. There is a 6 percent difference between the buckling loads obtained in the two analyses. Also plotted is the scaled determinant versus load. The value of this determinant crosses zero at the buckling load.

Figure 67 is another plot of load versus central deflection. Here the simply supported arch is deep and the governing buckling criterion is the antisymmetric or transitional one. The case for which the concentrated load is applied with eccentricities of two and five inches is also shown. These latter results are compared with those of Ref. 4. Also included are plots of the scaled determinant versus load. For the symmetrically applied load (e = 0), we get transitional or "bifurcation" buckling. For the eccentrically applied loads, we get "top of the knee" buckling. It is also interesting to note the difference in behavior of the determinant for these cases. For zero-eccentricity loading, the determinant approaches zero, with a near vertical slope; while for "top of the knee" buckling, it crosses the zero axis at a pronounced angle, an effect similar to the results shown in Fig. 66 for symmetric "top of the knee" buckling.

Figure 68 is similar to the two previous figures. Here, however, a clamped uniformly loaded antisymmetrically buckling arch is considered. The results for zero imperfections are compared with the exact results of Ref. 59 and with the results of Ref. 60, where a finite-element approach was used in combination with an iterative procedure. Excellent agreement with both is achieved. For this arch antisymmetric imperfections in shape were also introduced in the form of the buckling shape obtained from the eigenvector analysis. The maximum magnitude of the deflection mode shapes introduced as imperfections was of the order of one-tenth of an inch.

With zero imperfection, bifurcation type buckling occurs. However, when imperfections are introduced the lowest eigenvalue

never reaches unity nor does the determinant reach zero. Thus there is no clearly defined buckling load, and, in fact, the lowest eigenvalue decreases after having attained a maximum value of less than one. At that same load, the determinant begins increasing after having decreased toward zero. It is this load that is indicated in the figure for the two cases where imperfections were introduced.

Figure 69 shows the same arch as Fig. 67, but with a uniform load applied. Geometric imperfections were also introduced here. The behavior of this simply supported arch is found to be similar to that of the clamped arch of Fig. 68.

Load versus central deflection curves for a clamped circular arch subjected to a central concentrated load are shown in Fig. 70. Results from the present analysis are compared with those obtained in Refs. 61 and 62. The results indicate that although Marçal (Ref. 56) proposes the need for an additional matrix (the "initial displacement matrix") in the analysis of problems involving geometric nonlinearity, the technique of the present analysis does not require it. The results obtained here without the use of the initial displacement matrix compare quite well with the theoretical results of Ref. 62 and with the experimental results of Ref. 61. Further, the scatter in Marçal's results obtained by using successively finer idealizations was not exhibited in the present analysis. Although only the results for 16 elements are shown here, the buckling load obtained by using 8 elements is less than 2 percent higher than that obtained by using 16.

Results — Combined Material and Geometric Nonlinearity

In the preceding applications it was assumed that the relationship between stress and strain is linear. Although this is a reasonable representation of the actual material behavior for many problems, the specimen's proportional limit is quite often exceeded. Plasticity effects must then be included to gain an accurate insight into the physical response of the structure to additional loading. Furthermore, such important phenomena as plastic collapse and plastic buckling cannot be predicted unless this behavior is properly accounted for.

The restrained beam was chosen to illustrate the procedure for combined geometric and material nonlinearity. A yield stress of 30,000 psi was assumed, and a uniform vertical load applied.

83

Load versus central deflection curves obtained for purely elastic and for elastic, ideally-plastic material behavior are shown in Fig. 71a. The curves for plastic behavior are presented for idealizations involving 6, 12, and 24 elements for one-half of the beam. Differences in the results for these idealizations appear only after the end sections at the supports become fully plastic. Beyond the value of load at which this occurs, deflections increase quite rapidly and collapse occurs shortly thereafter. The counterbalancing effect of geometric and material nonlinearity is vividly depicted in Fig. 71a, where it is seen that there is a region of the load-deflection curve that is very nearly linear.

Figure 71b illustrates the growth of the plastic regions of the restrained beam. The dotted line at P = 10.74 kips indicates a jump in the representation of the plastic region when the end section becomes fully plastic.

The load-deflection history of the shallow circular arch subjected to a concentrated load, previously considered in Fig. 66, is again shown in Fig. 72. Load versus center deflection curves obtained by assuming elastic, ideally-plastic material behavior are shown for two values of yield stress. The onset of collapse for this structure is appreciably hastened by the introduction of plasticity. This is attributable to the reduction of the structure's stiffness resulting from the effects of yielding. For this structure, the effects of both types of nonlinearity are complementary. As in the case of the uniformly loaded beam subjected to a constant axial compressive load, the development of a fully plastic cross section is not necessary for collapse to take place, and failure occurs as a plastic buckling phenomenon.

Figure 73a illustrates the symmetrically buckling arch under a uniform load. The load-deflection curves of the elastic arch and of an elastic, ideally-plastic arch with yield stress of 30,000 psi are shown. Once again, the buckling load is considerably reduced by the complementary effects of geometric and physical nonlinearity. The onset of buckling is appreciably hastened when plasticity is included, a result also obtained in Ref. 63, where strain-hardening behavior was considered. Figure 73b indicates the rapid growth of the plastic regions in the arch as the loading is increased to the failure load. Figure 74 shows the arch of Fig. 73a, but now with clamped ends. This arch does not buckle elastically but deflects continuously with increasing load into the inverted position. Plasticity accelerates this passage through the zero rise position of the center.

84

6. CONCLUDING REMARKS

The methodology resulting from the current investigation is capable of treating the nonlinear response of a broad spectrum of structures under a variety of loading and boundary conditions. There are two general types of problems for which the treatment of plastic effects has its greatest significance. The first is concerned with the determination of failure loads and failure mechanisms of large structural systems, e.g., an aircraft wing, and assessing the survivability of these systems when they are subjected to some unexpectedly large loading. To take full advantage of the present nonlinear methods for use in this type of analysis it is necessary that they be made available as practical tools for the structural designer and analyst. Much remains to be done, however, in the refinement of computational techniques and the organization of large generalized programs to permit such analysis on a convenient basis and at a cost that is not prohibitive. This is particularly true of the treatment of plasticity in combination with geometric nonlinearity.

The second type of analysis for which the treatment of plastic effects is most significant is that of localized regions of a larger structural system in which yielding may occur as a result of stress concentration. This might apply, for example, to the region surrounding a fastener or cutout, or at junctures between structural components. A failure in such a localized region may result in the structural inadequacy of a larger over-all system. The present methods are particularly well suited to such analysis. However, for an accurate description of the plastic behavior of a structural component the present methods, as developed, require a more thorough understanding of inelastic material behavior. The principal area in which deficiencies still remain is that of constitutive relations for material properties. Although a basic understanding of the macroscopic behavior of simple structures in the plastic range has been attained by the application of available plasticity theories, these theories are still rather crude and limited in their applicability. In addition to a need for the refinement of theories of time-independent plasticity for initially isotropic materials subjected to monotonic loading and small strains, there is a need for the further development of plasticity theories to take proper account of initial anisotropy, time-dependence, cyclic loading including stress reversals into the plastic range, and large strains.

85

While these deficiencies inevitably raise questions concerning the accuracy of results obtained by finite-element plastic analysis, we do not believe that this should inhibit the development of such methods and associated computer programs. As improved constitutive relations become available, it should be possible to incorporate them readily into existing methods and programs.

APPENDIX A

PLASTICITY RELATIONS

A discussion of some of the plasticity relations used in developing the methods presented in this report must begin by specifying the initial yield condition that defines the elastic limit of the material. In all cases of multiaxial stress, the von Mises yield function, which describes a smooth surface in stress space and can be represented by a simple mathematical function, is chosen as the initial yield condition. With consideration limited to plane stress situations $(\sigma_z = \tau_{xz} = \tau_{yz} = 0)$, the von Mises yield function is represented as an ellipsoid in stress space, given by

$$f(\sigma_{ij}) = \sigma_x^2 - \sigma_x\sigma_y + \sigma_y^2 + 3\tau_{xy}^2 - \sigma_o^2 = 0 \qquad (A.1)$$

where σ_o is the yield stress in tension.

Describing the plastic behavior of a material requires additional information in the form of a constitutive relation between increments of plastic strain on the one hand and stress and stress increments on the other. This constitutive relation, termed the flow rule, is based on Drucker's postulate for work-hardening materials (Ref. 64). (For a discussion of this postulate and the conditions necessary for its satisfaction, see Appendix A of Ref. 11.) The flow rule, represented in tensor form, is written here as

$$d\epsilon_{ij} = d\lambda \frac{\partial f(\sigma_{ij},\alpha_{ij})}{\partial \sigma_{ij}} \qquad (A.2)$$

where $d\epsilon_{ij}$ is the increment of plastic strain; $f(\sigma_{ij},\alpha_{ij})$ represents the loading function, used to determine subsequent yielding from some plastic state; α_{ij} is a measure of the degree of work hardening; and $d\lambda$ is a positive scalar quantity.

Having selected a yield condition and flow rule, we must now choose a function that will establish conditions for subsequent yielding from a plastic state. Choice of a hardening rule depends on the ease with which it can be applied in the chosen

method of analysis as well as on its capability of representing the actual hardening behavior of structural materials. Furthermore, for some cases of interest in this report, the hardening rule should be capable of treating the Bauschinger effect exhibited during reversed plastic deformation. These requirements, together with the necessity of maintaining mathematical consistency with the yield function, constitute the criteria for final choice of a hardening rule. An appraisal of some of the hardening rules available (Ref. 11) indicates that the kinematic hardening theory due to Prager (Refs. 21 and 22) and modified by Ziegler (Ref. 23) satisfies these criteria. The hardening behavior postulated in this theory assumes that during plastic deformation the loading surface translates as a rigid body in stress space, maintaining the size, shape, and orientation of the yield surface. As a consequence of assuming a rigid translation of the loading surface, kinematic hardening theory predicts an ideal Bauschinger effect for completely reversed loading conditions; i.e., the magnitude of the increase of yield stress in one direction results in a decrease of yield stress of the same magnitude in the reverse direction.

An ideal Bauschinger effect, as predicted by kinematic hardening, can be expected to give, at best, an admittedly simplified approximation of the actual behavior of structural metals under cyclic loading. Experiments have shown that subsequent yield surfaces are more complex to describe than as a mere translation of the original surface. In view of the current state of the art of plasticity theory, however, the authors believe that kinematic hardening represents the simplest theory capable of predicting the essential features of cyclic plastic behavior.

An illustration of kinematic hardening, as applied in conjunction with the von Mises yield curve in the σ_1, σ_2 plane, is provided in Fig. 75. The yield surface and loading surface are shown in this figure for a shift of the stress state from point 1 to point 2. Denoting the translation of the center of the yield surface by α_{ij}, we may represent the loading function f in the form $f(\sigma_{ij} - \alpha_{ij})$; the subsequent yield condition is given as

$$f(\sigma_{ij} - \alpha_{ij}) = 0 \ . \tag{A.3}$$

Thus the von Mises yield condition for plane stress can be written as follows, to represent the subsequent yield condition:

88

$$f(\sigma_{ij}, \alpha_{ij}) = \bar{\sigma}_x^2 - \bar{\sigma}_x \bar{\sigma}_y + \bar{\sigma}_y^2 + 3\bar{\tau}_{xy}^2 - \sigma_o^2 = 0 \qquad (A.4)$$

where

$$\bar{\sigma}_{ij} = \sigma_{ij} - \alpha_{ij} .$$

The increment of translation of the loading surface $d\alpha_{ij}$, as given by Ziegler in Ref. 23, is computed at each loading step and summed to determine the total translation. Ziegler's modification of Prager's hardening rule is concerned with the assumptions associated with determining the magnitude and direction of the increment of translation of the loading surface. Specifically, it is assumed that $d\alpha_{ij}$ is directed along the radius vector connecting the center of the loading surface to the instantaneous stress state in stress space. The magnitude of $d\alpha_{ij}$ is determined from the condition that the stress state must remain on the translated loading surface during plastic deformation. Additional details associated with determining the translation of the loading surface are given in Ref. 11.

An expression for the scalar factor $d\lambda$, appearing in the flow rule of Eq. (A.2), is given in Refs. 11 and 23 and is rewritten here as follows:

$$d\lambda = \frac{1}{c} \frac{\dfrac{\partial f}{\partial \sigma_{ij}} d\sigma_{ij}}{\dfrac{\partial f}{\partial \sigma_{mn}} \dfrac{\partial f}{\partial \sigma_{mn}}} \qquad (A.5)$$

where c is a parameter characterizing the hardening behavior of the material. A procedure for determining this parameter, different from the one presented in Ref. 11, is discussed below.

Substituting Eqs. (A.4) and (A.5) into Eq. (A.2) yields the following explicit expressions for the plastic strain increments:

$$d\epsilon_x = \frac{M_1^2 d\sigma_x + M_1 M_2 d\sigma_y + M_1 M_3 d\tau_{xy}}{D} \qquad (A.6a)$$

89

$$d\epsilon_y = \frac{M_2 M_1 d\sigma_x + M_2^2 d\sigma_y + M_2 M_3 d\tau_{xy}}{D} \qquad (A.6b)$$

$$d\gamma_{xy}^P = \frac{M_3 M_1 d\sigma_x + M_3 M_2 d\sigma_y + M_3^2 d\tau_{xy}}{D} \qquad (A.6c)$$

where

$$M_1 = \bar{\sigma}_x - \frac{1}{2}\bar{\sigma}_y$$

$$M_2 = \bar{\sigma}_y - \frac{1}{2}\bar{\sigma}_x$$

$$M_3 = 3\bar{\tau}_{xy}$$

and

$$D = \frac{c}{4}\left(5\bar{\sigma}_x^2 - 8\bar{\sigma}_x\bar{\sigma}_y + 5\bar{\sigma}_y^2 + 36\bar{\tau}_{xy}^2\right) .$$

If we replace $d\sigma_{ij}$ by $\Delta\sigma_{ij}$ and $d\epsilon_{ij}$ by $\Delta\epsilon_{ij}$, Eqs. (A.6) can be written in a linear incremental matrix form relating plastic strain and stress increment, as,

$$\left\{\begin{matrix} \Delta\epsilon_x \\ \Delta\epsilon_y \\ \Delta\gamma_{xy}^P \end{matrix}\right\} = \frac{1}{D}\begin{bmatrix} M_1^2 & M_1 M_2 & M_1 M_3 \\ M_2 M_1 & M_2^2 & M_2 M_3 \\ M_3 M_1 & M_3 M_2 & M_3^2 \end{bmatrix}\left\{\begin{matrix} \Delta\sigma_x \\ \Delta\sigma_y \\ \Delta\tau_{xy} \end{matrix}\right\} . \qquad (A.7)$$

Thus the above linear incremental relationship can be compactly written as

$$\left\{\Delta\epsilon\right\} = [C]\left\{\Delta\sigma\right\} . \qquad (A.8)$$

90

Equations (A.5) through (A.8) pertain to elastic, strain-hardening behavior. The treatment of elastic, ideally-plastic material behavior requires implementing the "tangency condition" associated with such behavior, i.e., that the incremental stress vector be tangent to the yield surface during ideally-plastic flow. This condition provides a linear relation among the various components of stress increment. It can be expressed as follows:

$$\frac{\partial f}{\partial \sigma_{ij}} \, d\sigma_{ij} = \left(\sigma_x - \frac{1}{2} \sigma_y \right) d\sigma_x + \left(\sigma_y - \frac{1}{2} \sigma_x \right) d\sigma_y + 3\tau_{xy} d\tau_{xy} = 0 \quad (A.9)$$

If we set $d\sigma_{ij} = \Delta\sigma_{ij}$ and express $\Delta\sigma_x$ in terms of $\Delta\sigma_y$ and $\Delta\tau_{xy}$, Eq. (A.9) can be represented in matrix form as

$$\left\{ \begin{array}{c} \Delta\sigma_x \\ \Delta\sigma_y \\ \Delta\tau_{xy} \end{array} \right\} = \left[\begin{array}{ccc} 0 & -m_1 & -m_2 \\ 0 & 1 & 0 \\ 0 & 0 & 1 \end{array} \right] \left\{ \begin{array}{c} \Delta\sigma_x \\ \Delta\sigma_y \\ \Delta\tau_{xy} \end{array} \right\} \quad (A.10)$$

where

$$m_1 = \left(\sigma_y - \frac{1}{2} \sigma_x \right) \Big/ \left(\sigma_x - \frac{1}{2} \sigma_y \right)$$

$$m_2 = 3\tau_{xy} \Big/ \left(\sigma_x - \frac{1}{2} \sigma_y \right) .$$

The coefficient matrix of Eq. (A.10) is represented by the matrix $[\bar{E}]$. Thus the above linear relationship among the components of stress increment can be written as

$$\left\{ \Delta\sigma \right\} = [\bar{E}] \left\{ \Delta\sigma \right\} \quad (A.11)$$

91

The treatment of elastic, ideally-plastic material behavior also requires implementing the normality condition on the strain increment vector, thus providing a linear relation among the various components of plastic strain increments. This condition is represented by the flow rule of Eq. (A.2) and can be expressed as follows:

$$d\lambda = \frac{d\epsilon_x}{(\sigma_x - \frac{1}{2}\sigma_y)} = \frac{d\epsilon_y}{(\sigma_y - \frac{1}{2}\sigma_x)} = \frac{d\gamma^P_{xy}}{3\tau_{xy}} .$$ (A.12)

If we set $d\epsilon_{ij} = \Delta\epsilon_{ij}$, Eq. (A.12) leads to the incremental matrix relation that exists among the components of plastic strain increment. If we express $\Delta\epsilon_y$ and $\Delta\gamma^P_{xy}$ in terms of $\Delta\epsilon_x$, this matrix relation is given by

$$\left\{ \begin{array}{c} \Delta\epsilon_x \\ \Delta\epsilon_y \\ \Delta\gamma^P_{xy} \end{array} \right\} = \left[\begin{array}{ccc} 1 & 0 & 0 \\ m_1 & 0 & 0 \\ m_2 & 0 & 0 \end{array} \right] \left\{ \begin{array}{c} \Delta\epsilon_x \\ \Delta\epsilon_y \\ \Delta\gamma^P_{xy} \end{array} \right\} .$$ (A.13)

The coefficient matrix of Eq. (A.13) is represented by the matrix $[\tilde{E}]$. Thus, the above relationship may be represented in the following form,

$$\left\{ \Delta\epsilon \right\} = [\tilde{E}] \left\{ \Delta\epsilon \right\} .$$ (A.14)

It is apparent from Eqs. (A.9) and (A.12) that only two of the three components of stress increment and only one of the three components of plastic strain increment are required to obtain the remaining components. Thus only three of the six quantities are independent variables. The increments of stress and plastic strain can now be written in terms of a vector, $\{\Delta\omega\}$, representing these independent quantities, arbitrarily chosen as $\Delta\epsilon_x$, $\Delta\sigma_y$, and $\Delta\tau_{xy}$:

$$\{\Delta\omega\} = \left\{ \begin{array}{c} \Delta\epsilon_x \\ \Delta\sigma_y \\ \Delta\tau_{xy} \end{array} \right\} . \tag{A.15}$$

Because of the structure of the matrices $[\bar{E}]$ and $[\tilde{E}]$, Eqs. (A.11) and (A.14) may now be rewritten in the following form,

$$\{\Delta\sigma\} = [\bar{E}] \{\Delta\omega\} \tag{A.16}$$

and

$$\{\Delta\epsilon\} = [\tilde{E}] \{\Delta\omega\} . \tag{A.17}$$

The strain-displacement relations that are a necessary ingredient in the analysis are based on kinematic considerations and are independent of material properties. However, since they involve total strain (elastic plus plastic), the solution procedure requires an incremental relation between stress and total strain.

For both elastic, strain-hardening and elastic, ideally-plastic material behavior, the increment in total strain at a node can be written as the sum of an elastic and a plastic component, represented as $\{\Delta e^e\}$ and $\{\Delta\epsilon\}$, respectively, as follows,

$$\{\Delta e^T\} = \{\Delta e^e\} + \{\Delta\epsilon\} . \tag{A.18}$$

The increment in elastic strain is related to the stress increment $\{\Delta\sigma\}$ by means of Hooke's law. For plane stress this relation may be written as

$$
\left\{
\begin{array}{c}
\Delta e_x^e \\
\Delta e_y^e \\
\Delta \gamma_{xy}^e
\end{array}
\right\}
= \frac{1}{E}
\left[
\begin{array}{ccc}
1 & -\nu & 0 \\
-\nu & 1 & 0 \\
0 & 0 & 2(1+\nu)
\end{array}
\right]
\left\{
\begin{array}{c}
\Delta \sigma_x \\
\Delta \sigma_y \\
\Delta \tau_{xy}
\end{array}
\right\} .
\qquad \text{(A.19)}
$$

If we represent Eq. (A.19) as

$$
\left\{ \Delta e^e \right\} = [E]^{-1} \left\{ \Delta \sigma \right\}
\qquad \text{(A.20)}
$$

then Eq. (A.18) may be written in the form

$$
\left\{ \Delta e^T \right\} = [E]^{-1} \left\{ \Delta \sigma \right\} + \left\{ \Delta \epsilon \right\} .
\qquad \text{(A.21)}
$$

For an elastic, strain-hardening material we make use of the linear incremental relation between plastic strain and stress, i.e., Eq. (A.8), to obtain the incremental relation between stress and total strain given in the following equation:

$$
\left\{ \Delta \sigma \right\} = [R]^{-1} \left\{ \Delta e^T \right\}
\qquad \text{(A.22)}
$$

where

$$
[R] = [E]^{-1} + [C]
$$

It should be noted that there is no unique stress increment corresponding to a given plastic strain increment vector. There-fore the matrix [C] is singular. However, the matrix [R], defined in Eq. (A.22) will possess an inverse, thereby providing the necessary coefficients relating the stress increment to the increment of total strain.

For an elastic, ideally-plastic material we require a rela-tion between the vector $\{\Delta\omega\}$ and the increment of total strain. This is obtained by substituting Eqs. (A.16) and (A.17) into Eq. (A.21) to yield

94

$$\{\Delta\omega\} = [E^*]^{-1} \{\Delta e^T\} \qquad\qquad (A.23)$$

where

$$[E^*] \equiv [E]^{-1}[\bar{E}] + [\tilde{E}] \; .$$

A Multiaxial-Hardening Coefficient

The incremental constitutive relation between plastic strains and stresses, shown in matrix form in Eq. (A.7), requires knowledge of the inelastic behavior of the material in a state of multiaxial stress. As stated above, for the case of kinematic hardening this behavior is characterized by the parameter c, appearing in Eq. (A.5).

Since sufficient experimental information is lacking on the hardening behavior of structural materials under multiaxial stress states, the material properties generally used in inelastic analysis are determined from simple tensile or compressive tests of samples of the material. If the structure is in a state of uniaxial stress, the stress-strain relation is identical to that obtained from tension or compression tests. The hardening coefficient c can then be taken simply as the slope of the stress-versus-plastic-strain curve at the current stress level. In the general case of multiaxial stress with nonlinear strain-hardening, determining the hardening coefficient is much more complicated. It can be expected that c will vary not only with stress level but also with the ratio of various stress components to one another, i.e., with the location of the stress state on the loading surface. A procedure to determine the multiaxial hardening coefficient c in the kinematic hardening law was presented in Ref. 11. This procedure has two shortcomings; viz., the value obtained for c is not invariant with respect to a rotation of the coordinate axes, and hydrostatic stress is not properly taken into account. An alternative method outlined here overcomes these shortcomings. This method is based on the Ramberg-Osgood representation of a uniaxial stress-strain curve (Ref. 65); i.e.,

$$e = \frac{\sigma}{E} + \frac{3\sigma}{7E} \left| \frac{\sigma}{\sigma_{0.7}} \right|^{n-1} \qquad\qquad (A.24)$$

where n is a shape parameter given by

$$n = 1 + \frac{\log(17/7)}{\log(\sigma_{0.7}/\sigma_{0.85})} \, , \qquad (A.25)$$

e is the total strain, E is the slope of the linear portion of the stress-strain curve, and $\sigma_{0.7}$ and $\sigma_{0.85}$ are the stresses at which the curve has secant moduli of $0.7\,E$ and $0.85\,E$, respectively.

We recognize the nonlinear term in Eq. (A.24) as the plastic strain and use it to determine the inverse of the hardening coefficient

$$\frac{1}{c} = \left(\frac{d\epsilon}{d\sigma}\right) = \frac{3n}{7E} \left|\frac{\sigma}{\sigma_{0.7}}\right|^{n-1} \qquad (A.26)$$

where ϵ, the plastic strain, is equal to

$$\frac{3\sigma}{7E} \left|\frac{\sigma}{\sigma_{0.7}}\right|^{n-1} \; .$$

The single value of c to be introduced into Eq. (A.5) for multiaxial stress is computed by assuming that there exists a Ramberg-Osgood representation relating effective stress to effective strain, i.e.,

$$\bar{e} = \frac{\bar{\sigma}}{E} + \frac{3\bar{\sigma}}{7E} \left|\frac{\bar{\sigma}}{\sigma_{0.7}}\right|^{n-1} \qquad (A.27a)$$

where

$$\bar{e} = \frac{2}{\sqrt{3}} \left(e_x^2 + e_x e_y + e_y^2 + \frac{\gamma_{xy}^2}{4}\right)^{\frac{1}{2}} \qquad (A.27b)$$

96

and

$$\bar{\sigma} = \left(\sigma_x^2 - \sigma_x \sigma_y + \sigma_y^2 + 3\tau_{xy}^2 \right)^{\frac{1}{2}} . \tag{A.27c}$$

The inverse of the hardening coefficient can now be written as

$$\frac{1}{c} = \left(\frac{d\bar{\epsilon}}{d\bar{\sigma}} \right) = \frac{3n}{7E} \left| \frac{\bar{\sigma}}{\sigma_{0.7}} \right|^{n-1} \tag{A.28}$$

where $\bar{\epsilon}$, the plastic component of the effective strain, is equal to

$$\frac{3\bar{\sigma}}{7E} \left| \frac{\bar{\sigma}}{\sigma_{0.7}} \right|^{n-1} .$$

It should be noted that use of an effective stress-effective strain relation is usually associated with the isotropic hardening theory of plasticity, in which the various components of strain increment are determined from an effective strain increment. In our analysis, however, the components of strain increment are related to the stress increments through constitutive relations determined from kinematic hardening theory. The effective stress-effective strain relation and the definitions of these quantities, presented in Eqs. (A.27), are used merely to define the hardening coefficient of Eq. (A.28).

The Ramberg-Osgood parameters E, $\sigma_{0.7}$, and n used in Eqs. (A.27) are obtained from a uniaxial stress-strain curve for the material; therefore initial isotropy of the material is assumed.

It can be seen that this approach takes into account the fact that the hardening coefficient varies with the location of the stress point on the loading surface and that it reduces to the correct value in the special case of a single nonzero stress component.

97

The value of the hardening coefficient given in Eq. (A.28) applies to loading situations for which the stress state remains in a fairly localized region on the yield surface. Further generalization of this equation is necessary to accommodate cases of elastic unloading and subsequent reloading into the plastic range in which the stress state shifts to a different region on the loading surface. This generalization is identical to that associated with the use of the previous hardening coefficient of Ref. 11. Basically, the assumption is that the shape of the inelastic portion of the stress-strain curve is the same on reversed yielding as on initial yielding. The value of the hardening coefficient is thus the same as that shown in Eq. (A.28), with $\bar{\sigma}$ now written as

$$\bar{\sigma} = \left((\sigma_x - \bar{\alpha}_x)^2 - (\sigma_x - \bar{\alpha}_x)(\sigma_y - \bar{\alpha}_y) \right.$$

$$\left. + (\sigma_y - \bar{\alpha}_y)^2 + 3(\tau_{xy} - \bar{\alpha}_{xy})^2 \right)^{\frac{1}{2}}$$

(A.29)

where $\bar{\alpha}$ is the last computed value of α prior to unloading and reversed loading in the plastic range.

98

APPENDIX B

FORMULATION OF [B] AND [H] MATRICES

This appendix presents a derivation of the [B] and [H] matrices for the six node (LST) triangle. The derivation makes use of Eq. (23), written here as

$$\{\Delta D\} = [K_e]^{-1} \{\Delta P\} + [K_e]^{-1} [\bar{K}] \{\Delta \epsilon_o\} \qquad (B.1)$$

where

$\{\Delta P\}$ is the vector of increments in applied nodal forces;

$[K_e]$ is the elastic stiffness matrix for the structure after proper boundary conditions have been taken into account;

$\{\Delta D\}$ is the nonzero nodal displacement vector;

$[\bar{K}]$ is the initial strain matrix for the entire structure; and

$\{\Delta \epsilon_o\}$ is the vector of nodal initial strain increments.

Equation (B.1) is used with the equation for stress increment at the ith node written as

$$\{\Delta \sigma\}_i = [E] \{\Delta \tilde{e}^e\}_i$$

$$= [E] \left(\{\Delta e^T\} - \{\Delta \epsilon_o\} \right)_i \qquad (B.2)$$

where the elements of the [E] matrix are the usual elastic co-efficients associated with the stress-strain relations for plane stress. The vector $\{\Delta \tilde{e}^e\}$ is the average elastic strain increment at the node. This vector is defined as the average total strain increment in the elastic range or the average total strain

99

increment minus the plastic strain increment in the plastic region as shown in Eq. (B.2). Average values were used in this case because the provision of displacement compatibility at nodes for the LST triangle does not ensure that strains and, therefore, stresses will be compatible at nodes. Hence, total strain or stress from each element adjacent to a node must be computed and then divided by the number of adjacent elements in order to determine the average stress or strain. Average total strain can be related to the nodal displacements of the entire structure by means of the matrix $[\tilde{W}_i]$ so that

$$\left\{\Delta\tilde{e}^T\right\}_i = [\tilde{W}_i] \left\{\Delta d_o\right\} . \tag{B.3}$$

Substitution of Eq. (B.3) into Eq. (B.2) yields the expression for stress increment in terms of the increments of nodal displacement and plastic strain as follows

$$\left\{\Delta\sigma\right\}_i = [E][\tilde{W}_i] \left\{\Delta d_o\right\} - [E] \left\{\Delta\epsilon_o\right\} . \tag{B.4}$$

Equation (B.4) is then assembled for all nodes at which stress values are desired, to yield,

$$\left\{\Delta\sigma\right\} = [S] \left\{\Delta D\right\} - [E_d] \left\{\Delta\epsilon_o\right\} \tag{B.5}$$

where $[S]$ is the assembled matrix of $[E][\tilde{W}_i]$, and $[E_d]$ is a diagonally partitioned matrix consisting of submatrices $[E]$. Substitution of Eq. (B.1) into Eq. (B.5) then yields the desired equation for stress increment,

$$\left\{\Delta\sigma\right\} = [B] \left\{\Delta P\right\} + [H] \left\{\Delta\epsilon_o\right\} \tag{B.6}$$

where

$$[B] = [S][K]^{-1}$$

100

and

$$[H] = - \left[[E_d] - [S][K]^{-1}[\bar{K}] \right] .$$

The corresponding definition for the matrices [A] and [J] shown in Eq. (24) of Section 2 are obtained from an equation for total strain increment. Their definitions can be written in terms of [B] and [H] as

$$[A] = [E_d]^{-1}[B]$$

$$\text{(B.7)}$$

$$[J] = [E_d]^{-1}[H] + [I]$$

where $[E_d]^{-1}$ is a diagonally partitioned matrix composed of submatrices $[E]^{-1}$.

It should be noted that the $[\bar{K}]$ and [H] (or [J]) matrices are formed in the present analysis as though a plastic (initial) strain increment existed at each node. If a node is in the elastic range, the plastic strain increment at that node is set equal to zero. In this manner all the necessary matrices from the elastic analysis are computed only once.

APPENDIX C

INITIAL STRAIN STIFFNESS MATRIX FOR LST ELEMENT

The stiffness matrix for the six node plane stress (LST) triangle has been derived in Refs. 29, 30, and 53. This appendix gives the initial strain stiffness matrix for the LST triangle used in the plasticity analysis of membrane stressed structures. The derivation of this matrix, given in integral form in Eq. (10), is based on the definitions of the element geometry and initial strain assumptions shown in Fig. 2. The integral form is rewritten here as follows:

$$[\bar{k}] = \iiint\limits_{V_p} [W]'[E][\bar{W}_p]dV \qquad (C.1)$$

where $[\bar{W}_p]$ represents the assumption made for a linear distribution of initial strain increment in Eq. (10), and $[W]$ relates nodal displacement to the element total strain.

This matrix is based on a quadratic distribution for the in-plane displacements and can be written as

$$[W] = \begin{bmatrix} 0 & 1 & 0 & y & 2x & 0 & 0 & 0 & 0 & 0 & 0 & 0 \\ 0 & 0 & 0 & 0 & 0 & 0 & 0 & 0 & 1 & x & 0 & 2y \\ 0 & 0 & 1 & x & 0 & 2y & 0 & 1 & 0 & y & 2x & 0 \end{bmatrix} \begin{bmatrix} [\alpha] & \vdots & 0 \\ -\!-\!- & + & -\!-\!- \\ 0 & \vdots & [\alpha] \end{bmatrix}^{-1} \qquad (C.2)$$

where the matrix $[\alpha]$ relates the coefficients of the polynomial form for displacement increments, Eq. (40), to the nodal displacements, and is written as

$$[\alpha] = \begin{bmatrix} 1 & 0 & 0 & 0 & 0 & 0 \\ 1 & x_j & 0 & 0 & x_j^2 & 0 \\ 1 & x_k & y_k & x_k y_k & x_k^2 & y_k^2 \\ 1 & x_{i'} & y_{i'} & x_{i'} y_{i'} & x_{i'}^2 & y_{i'}^2 \\ 1 & x_{j'} & y_{j'} & x_{j'} y_{j'} & x_{j'}^2 & y_{j'}^2 \\ 1 & x_{k'} & y_{k'} & x_{k'} y_{k'} & x_{k'}^2 & y_{k'}^2 \end{bmatrix} \qquad (C.3)$$

and the incremental nodal displacement vector is written as follows:

$$\{\Delta d_0\} = \begin{Bmatrix} \Delta u_i \\ \Delta u_j \\ \Delta u_k \\ \Delta u_{i'} \\ \Delta u_{j'} \\ \Delta u_{k'} \\ \hline \Delta v_i \\ \cdot \\ \cdot \\ \cdot \\ \Delta v_{k'} \end{Bmatrix} . \qquad (C.4)$$

Substituting Eqs. (C.2), (C.3), and (41) into Eq. (C.1) and performing the matrix multiplication yields

104

$$[\bar{k}] = \frac{E}{1 - v^2} \iiint_{V_p} \Big([C_0] + x[C_1] + y[C_2] + x^2[C_3]$$

(C.5)

$$+ y^2[C_4] + xy[C_5] \Big) dV$$

where the $[C_i]$ matrices in Eq. (C.5) are constant matrices of order (12 x 9). The integration of Eq. (C.5) yields the following final form for $[\bar{k}]$,

$$[\bar{k}] = \frac{AhE}{12(1 - v^2)} \Big[12[C_0] + 4[C_1](x_j + x_k) + 4[C_2]y_k$$

$$+ 2[C_4]y_k^2 + 2[C_3](x_j^2 + x_jx_k + x_k^2) \qquad (C.6)$$

$$+ [C_5](y_kx_j + 2y_kx_k) \Big]$$

where A is the area of the element $(x_jy_k/2)$, E is Young's modulus, and h is the thickness.

The nonzero elements of the $[C_i]$ (i = 0 - 5) are given below.

$[C_0]$:

2,1 = 1	2,4 = v
3,7 = μ	8,7 = μ
9,1 = v	9,4 = 1

$[C_1]$:

$2,1 = -1/x_j$	$2,2 = 1/x_j$
$2,4 = -\nu/x_j$	$2,5 = \nu/x_j$
$3,7 = -\mu/x_j$	$3,8 = \mu/x_j$
$4,7 = \mu$	$5,1 = 2$
$5,4 = 2\nu$	$9,1 = -\nu/x_j$
$9,2 = \nu/x_j$	$9,4 = -1/x_j$
$9,5 = 1/x_j$	$10,1 = \nu$
$10,4 = 1$	$11,7 = 2\mu$

$[C_2]$:

$2,1 = -x_{jk}/2A$	$2,2 = -x_k/2A$
$2,3 = 1/y_k$	$2,4 = -\nu x_{jk}/2A$
$2,5 = \nu x_k/2A$	$2,6 = \nu/y_k$
$3,7 = -\mu x_{jk}/2A$	$3,8 = \mu x_k/2A$
$3,9 = \mu/y_k$	$4,1 = 1$
$4,4 = \nu$	$6,7 = 2\mu$
$8,7 = -\mu x_{jk}/2A$	$8,8 = \mu x_k/2A$
$8,9 = \mu/y_k$	$9,1 = -\nu x_{jk}/2A$
$9,2 = -\nu x_k/2A$	$9,3 = \nu/y_k$
$9,4 = -x_{jk}/2A$	$9,5 = -x_k/2A$
$9,6 = 1/y_k$	$10,7 = \mu$
$12,1 = 2\nu$	$12,4 = 2$

$[C_3]$:

$4,7 = -\mu/x_j$	$4,8 = \mu/x_j$
$5,1 = -2/x_j$	$5,2 = 2/x_j$
$5,4 = -2\nu/x_j$	$5,6 = 2\nu/x_j$
$10,1 = -\nu/x_j$	$10,2 = \nu/x_j$
$10,4 = -1/x_j$	$10,5 = 1/x_j$
$11,7 = -2\mu/x_j$	$11,8 = 2\mu/x_j$

106

$[C_4]$:

$$4,1 = x_{jk}/2A \qquad 4,2 = -x_k/2A$$
$$4,3 = 1/y_k \qquad 4,4 = -vx_{jk}/2A$$
$$4,5 = -vx_k/2A \qquad 4,6 = v/y_k$$
$$6,7 = -\mu x_{jk}/A \qquad 6,8 = -\mu x_k/A$$
$$6,9 = 2\mu/y_k \qquad 10,7 = -\mu x_{jk}/2A$$
$$10,8 = -\mu x_k/2A \qquad 10,9 = \mu/y_k$$
$$12,1 = -2vx_{jk}/2A \qquad 12,2 = -vx_k/A$$
$$12,3 = 2v/y_k \qquad 12,4 = -x_{jk}/A$$
$$12,5 = x_k/A \qquad 12,6 = 2/y_k$$

$[C_5]$:

$$4,1 = -1/x_j \qquad 4,2 = 1/x_j$$
$$4,4 = -v/x_j \qquad 4,5 = v/x_j$$
$$4,7 = -\mu x_{jk}/2A \qquad 4,8 = -\mu x_{jk}/2A$$
$$4,9 = \mu/y_k \qquad 5,1 = -x_{jk}/A$$
$$5,2 = -x_k/A \qquad 5,3 = 2/y_k$$
$$5,4 = -vx_{jk}/A \qquad 5,5 = -vx_k/A$$
$$5,6 = 2v/y_k \qquad 6,7 = -2\mu/x_j$$
$$6,8 = 2\mu/x_j \qquad 10,1 = -vx_{jk}/2A$$
$$10,2 = -vx_k/2A \qquad 10,3 = v/y_k$$
$$10,4 = -x_{jk}/2A \qquad 10,5 = -x_k/2A$$
$$10,6 = 1/y_k \qquad 10,7 = -\mu/x_j$$
$$10,8 = \mu/x_j \qquad 11,7 = -\mu x_{jk}/A$$
$$11,8 = -\mu x_k/A \qquad 11,9 = 2\mu/y_k$$
$$12,1 = -2v/x_j \qquad 12,2 = 2v/x_j$$
$$12,4 = -2/x_j \qquad 12,5 = 2/x_j$$

where v is Poisson's ratio, $\mu = \dfrac{1-v}{2}$, and $x_{jk} = x_j - x_k$.

APPENDIX D

INITIAL STRAIN STIFFNESS MATRICES FOR BEAM FINITE ELEMENT

The initial strain stiffness matrices for a beam element in bending alone and for combined bending and membrane loading are derived from the assumptions shown in Figs. 32 and 33 and are given in integral form in Eq. (15).

The matrix equation defining the fictitious nodal restoring forces in terms of the initial strain stiffness matrix for the pure bending of a beam with a rectangular cross section is

$$
\begin{Bmatrix} P_{z_i} \\ M_i \\ P_{z_j} \\ M_j \end{Bmatrix} = \frac{EI}{t^3}
\begin{bmatrix} c_1/\ell & c_2/\ell \\ c_3 & c_4 \\ -c_1/\ell & -c_2/\ell \\ c_5 & c_6 \end{bmatrix}
\begin{Bmatrix} \epsilon_{0i} \\ \epsilon_{0j} \end{Bmatrix} = [k^*] \begin{Bmatrix} \epsilon_0 \end{Bmatrix}
\tag{D.1}
$$

where

$$
c_1 = \frac{(\bar{z}_j - \bar{z}_i)^2}{20} + t^2 - \frac{\bar{z}_i(t + \bar{z}_i)}{2}
$$

$$
c_2 = \frac{9(\bar{z}_j - \bar{z}_i)^2}{20} + \frac{(\bar{z}_j - \bar{z}_i)(2\bar{z}_i + t)}{2} - t^2 + \frac{\bar{z}_i(t + \bar{z}_i)}{2}
$$

$$
c_3 = -\frac{(\bar{z}_j - \bar{z}_i)^2}{60} - \frac{(\bar{z}_j - \bar{z}_i)(2\bar{z}_i + t)}{12} + t^2 - \frac{\bar{z}_i(t + \bar{z}_i)}{2}
$$

$$
c_4 = \frac{(\bar{z}_j - \bar{z}_i)^2}{10} + \frac{(\bar{z}_j - \bar{z}_i)(2\bar{z}_i + t)}{12}
$$

$$c_5 = \frac{(\bar{z}_j - \bar{z}_i)^2}{15} + \frac{(\bar{z}_j - \bar{z}_i)(2\bar{z}_i + t)}{12}$$

$$c_6 = \frac{7(\bar{z}_j - \bar{z}_i)^2}{20} + \frac{5(\bar{z}_j - \bar{z}_i)(2\bar{z}_i + t)}{12} - t^2 + \frac{\bar{z}_i(t + \bar{z}_i)}{2} \ ;$$

where P_z and M represent the fictitious restoring force in the lateral direction and moment, respectively; t is the half thickness of the beam element; and $\bar{z}$ represents the depth of the elastic-plastic boundary. For this element, all $\bar{z}$'s are determined with respect to the median surface. Other quantities appearing in Eq. (D.1) are defined in Fig. 32.

The corresponding relation for the case of combined bending and membrane stresses is shown as follows,

$$\begin{Bmatrix} P_{z_i} \\ M_i \\ P_{x_i} \\ P_{z_j} \\ M_j \\ P_{x_j} \end{Bmatrix} = \frac{EI}{\ell^2 t^3} \begin{bmatrix} k_{11}^* & k_{12}^* & k_{13}^* & k_{14}^* \\ k_{21}^* & k_{22}^* & k_{23}^* & k_{24}^* \\ k_{31}^* & k_{32}^* & k_{33}^* & k_{34}^* \\ -k_{11}^* & -k_{12}^* & -k_{13}^* & -k_{14}^* \\ k_{51}^* & k_{52}^* & k_{53}^* & k_{54}^* \\ -k_{31}^* & -k_{32}^* & -k_{33}^* & -k_{34}^* \end{bmatrix} \begin{Bmatrix} \epsilon_{0i}^U \\ \epsilon_{0j}^U \\ \epsilon_{0i}^L \\ \epsilon_{0j}^L \end{Bmatrix} \qquad (D.2)$$

where

$$k_{11}^* = - (\ell^3/40)c_1 + (\ell/4)c_3$$

$$k_{12}^* = - (9\ell^3/40)c_1 - (\ell^2/4)c_2 - (\ell/4)c_3$$

$$k_{13}^* = - (\ell^3/40)c_4 + (\ell/4)c_6$$

$$k_{14}^* = -(9\ell^3/40)c_4 - (\ell^2/4)c_5 - (\ell/4)c_6$$

$$k_{21}^* = (\ell^4/120)c_1 + (\ell^3/24)c_2 + (\ell^2/4)c_3$$

$$k_{22}^* = -(\ell^4/20)c_1 - (\ell^3/24)c_2$$

$$k_{23}^* = (\ell^4/120)c_4 + (\ell^3/24)c_5 + (\ell^2/4)c_6$$

$$k_{24}^* = -(\ell^4/20)c_4 - (\ell^3/24)c_5$$

$$k_{31}^* = -(\ell^3/8)c_7 - (3\ell^2/8)c_8$$

$$k_{32}^* = -(\ell^3/4)c_7 - (3\ell^2/8)c_8$$

$$k_{33}^* = (\ell^3/8)c_9 + (3\ell^2/8)c_{10}$$

$$k_{34}^* = (\ell^3/4)c_9 + (3\ell^2/8)c_{10}$$

$$k_{51}^* = -(\ell^4/30)c_1 - (\ell^3/24)c_2$$

$$k_{52}^* = -(7\ell^4/40)c_1 - (5\ell^3/24)c_2 - (\ell^2/4)c_3$$

$$k_{53}^* = -(\ell^4/30)c_4 - (\ell^3/24)c_5$$

$$k_{54}^* = -(7\ell^4/40)c_4 - (5\ell^3/24)c_5 - (\ell^2/4)c_6$$

and

$$c_1 = \left(\bar{z}_j^U - \bar{z}_i^U\right)^2 \Big/ \ell^2$$

$$c_2 = -\left(\bar{z}_j^U - \bar{z}_i^U\right)\left(3t - 2\bar{z}_i^U\right) \Big/ \ell$$

$$c_3 = -\bar{z}_i^U\left(3t - \bar{z}_i^U\right)$$

$$c_4 = - \left(\bar{z}_j^L - \bar{z}_i^L \right)^2 \Big/ \ell^2$$

$$c_5 = \left(\bar{z}_j^L - \bar{z}_i^L \right) \left(t - 2\bar{z}_i^L \right) \Big/ \ell$$

$$c_6 = 2t^2 + t\bar{z}_i^L - \bar{z}_i^{L^2}$$

$$c_7 = \left(\bar{z}_j^U - \bar{z}_i^U \right) \Big/ \ell$$

$$c_8 = \bar{z}_i^U$$

$$c_9 = \left(\bar{z}_j^L - \bar{z}_i^L \right) \Big/ \ell$$

$$c_{10} = \bar{z}_i^L - 2t \quad .$$

The quantities P_{x_i} and P_{x_j} represent the fictitious re‑
storing forces in the axial direction. Here all $\bar{z}$'s are mea‑
sured with respect to the upper surface of the beam. All other
quantities appearing in Eq. (D.2) are defined in Fig. 33.

The initial strain matrix in Eq. (D.2) must be modified for
the treatment of problems in which the membrane strain generated
is sufficiently large to cause the entire cross section of the
beam to go plastic, with strains at both the upper and lower
surface being of the same sign. For these cases there is no
point within the thickness at which the plastic strain is zero.
Consequently, the functional form of the plastic strain distribu‑
tion must be modified to account for this.

Choosing

$$\epsilon^U = \left[1 + \left(R_i^U - 1 \right) \frac{z}{\bar{z}^U} \right] \left(1 - \frac{x}{\ell} \right) \epsilon_i^U + \left[1 + \left(R_j^U - 1 \right) \frac{z}{\bar{z}^U} \right] \left(\frac{x}{\ell} \right) \epsilon_j^U \qquad \text{(D.3a)}$$

retains the assumption of a linear plastic strain distribution through the thickness, while allowing for a continuous development of the plastic region. Also

$$\epsilon^L = \left[\frac{(z - \bar{z}^L) + R_i^L(2t - z)}{2t - \bar{z}^L}\right]\left(1 - \frac{x}{\ell}\right)\epsilon_i^L$$

(D.3b)

$$+ \left[\frac{(z - \bar{z}^L) + R_j^L(2t - z)}{2t - \bar{z}^L}\right]\left(\frac{x}{\ell}\right)\epsilon_j^L \ .$$

In these assumed forms,

$$R_i^U = \begin{cases} \epsilon_i^L/\epsilon_i^U & \text{if} & \epsilon_i^L/\epsilon_i^U \geq 0 \\ \\ 0 & \text{if} & \epsilon_i^L/\epsilon_i^U < 0 \end{cases}$$

(D.4)

$$R_i^L = \begin{cases} \epsilon_i^U/\epsilon_i^L & \text{if} & \epsilon_i^U/\epsilon_i^L \geq 0 \\ \\ 0 & \text{if} & \epsilon_i^U/\epsilon_i^L < 0 \end{cases} \ .$$

The initial strain stiffness matrix $[k^*]$ retains the same form as that in Eq. (D.2), but the coefficients c_1, c_2, ..., c_{10} now contain the factors R_i^U, R_j^U, R_i^L, R_j^L. Indeed, when $R_i^U = R_j^U = R_i^L = R_j^U = 0$, the c_i's reduce to those given above.

113

APPENDIX E

CALCULATION OF YIELD LOAD AND LOCATION OF ELASTIC-PLASTIC BOUNDARIES AT NODES

In the current analysis of beam and plate structures under combined lateral and in-plane loading it is necessary to locate the depth of the elastic-plastic boundary at nodes and to calculate the value of lateral loads at which yielding begins. A procedure to determine these quantities is outlined below.

For plane stress, the von Mises yield condition reduces to

$$J_2 = \sigma_x^2 + \sigma_y^2 - \sigma_x\sigma_y + 3\tau_{xy}^2 = \sigma_o^2 . \tag{E.1}$$

Since the beam or plate is elastic through its thickness until the yield condition is satisfied, we can write, for combined bending and membrane stress in the elastic range,

$$\{\sigma\} = \{\bar{N}\} + \rho \{\bar{M}\} = [E] \{e^T\} . \tag{E.2}$$

where for a plate

$$e_x^T = \frac{\partial u}{\partial x} + \frac{1}{2}\left(\frac{\partial w}{\partial x}\right)^2 - z \frac{\partial^2 w}{\partial x^2}$$

$$e_y^T = \frac{\partial v}{\partial y} + \frac{1}{2}\left(\frac{\partial w}{\partial y}\right)^2 - z \frac{\partial^2 w}{\partial y^2} \tag{E.3}$$

$$\gamma_{xy}^T = \frac{\partial u}{\partial y} + \frac{\partial v}{\partial x} + \frac{\partial w}{\partial x}\frac{\partial w}{\partial y} - 2z \frac{\partial^2 w}{\partial x \partial y}$$

and z is measured with respect to the middle surface. Here {N̄} represents the membrane contribution to the stresses and {M̄} represents the bending contribution. The quantity ρ in

Eq. (E.2) is as yet undefined, but it represents the functional form of the variation of the bending strains through the thickness. Substituting Eq. (E.2) into Eq. (E.1) gives:

$$J_2 = \rho^2 \left[\overline{M}_x^2 + \overline{M}_y^2 + 3\overline{M}_{xy}^2 - \overline{M}_x \overline{M}_y \right]$$

$$+ 2\rho \left[\overline{N}_x \overline{M}_x + \overline{N}_y \overline{M}_y + 3\overline{N}_{xy} \overline{M}_{xy} - \frac{1}{2}(\overline{N}_y \overline{M}_x + \overline{N}_x \overline{M}_y) \right] \qquad \text{(E.4)}$$

$$+ \overline{N}_x^2 + \overline{N}_y^2 + 3\overline{N}_{xy}^2 - \overline{N}_x \overline{N}_y \; .$$

Let

$$A = \overline{M}_x^2 + \overline{M}_y^2 + 3\overline{M}_{xy}^2 - \overline{M}_x \overline{M}_y$$

$$B = \overline{N}_x \overline{M}_x + \overline{N}_y \overline{M}_y + 3\overline{N}_{xy} \overline{M}_{xy} - \frac{1}{2}(\overline{N}_y \overline{M}_x + \overline{N}_x \overline{M}_y) \qquad \text{(E.5)}$$

$$C = \overline{N}_x^2 + \overline{N}_y^2 + 3\overline{N}_{xy}^2 - \overline{N}_x \overline{N}_y \; .$$

For combined membrane and bending loads, let $\rho = t - z$, where z is measured with respect to the upper surface of the plate.

The location of the elastic-plastic boundary through the thickness occurs at that point, defined as $\overline{z}$, where $J_2 = \sigma_o^2$. That condition can be expressed by the following quadratic equation:

$$A\rho^2 + 2B\rho + C - \sigma_o^2 = 0 \; .$$

Solving for ρ, we obtain

$$\rho = t - \overline{z} = \frac{-B \pm \sqrt{B^2 - A\left(C - \sigma_o^2\right)}}{A} \qquad \text{(E.6a)}$$

116

or

$$\bar{z} = t + \frac{B \mp \sqrt{B^2 - A\left(C - \sigma_o^2\right)}}{A} .$$

(E.6b)

This gives two values of $\bar{z}$, correctly indicating the presence of two elastic-plastic boundaries, which must satisfy the inequality $0 \leq \bar{z}^U \leq \bar{z}^L \leq 2t$. (Recall that $\bar{z}$ is measured with respect to the upper surface for combined bending and stretching.)

To determine expressions for the $\bar{N}$'s and $\bar{M}$'s, we combine the stress-strain and strain-displacement (neglecting nonlinear terms in displacements) equations.

$$\sigma_x = \frac{E}{1 - \nu^2} \left[\frac{\partial u}{\partial x} + (t - z)w,_{xx} + \nu \left(\frac{\partial v}{\partial y} + (t - z)w,_{yy} \right) \right]$$

$$\sigma_y = \frac{E}{1 - \nu^2} \left[\frac{\partial v}{\partial y} + (t - z)w,_{yy} + \nu \left(\frac{\partial u}{\partial x} + (t - z)w,_{xx} \right) \right]$$

(E.7)

$$\tau_{xy} = \frac{E}{2(1 + \nu)} \left[\frac{\partial u}{\partial y} + \frac{\partial v}{\partial x} + 2(t - z)w,_{xy} \right] .$$

Therefore, comparing Eqs. (E.7) and (E.2), we see that

$$\bar{N}_x = \frac{E}{1 - \nu^2} \left(\frac{\partial u}{\partial x} + \nu \frac{\partial v}{\partial y} \right) \qquad \bar{M}_x = \frac{E}{1 - \nu^2} [w,_{xx} + \nu w,_{yy}]$$

$$\bar{N}_y = \frac{E}{1 - \nu^2} \left(\frac{\partial v}{\partial y} + \nu \frac{\partial u}{\partial x} \right) \qquad \bar{M}_y = \frac{E}{1 - \nu^2} [w,_{yy} + \nu w,_{xx}]$$

(E.8)

$$\bar{N}_{xy} = \frac{E}{2(1 + \nu)} \left(\frac{\partial u}{\partial y} + \frac{\partial v}{\partial x} \right) \qquad \bar{M}_{xy} = \frac{E}{1 + \nu} w,_{xy} .$$

Substitution of these quantities into Eqs. (E.5) yields the following expressions for A, B, and C.

$$A = \frac{E^2}{(1 + \nu)^2} \left\{ (w,_{xx} - w,_{yy})^2 + 3w^2,_{xy} \right.$$

$$\left. + w,_{xx}w,_{yy} + \frac{\nu}{(1 - \nu)^2}(w,_{xx} + w,_{yy})^2 \right\}$$

$$B = \frac{E^2}{(1 - \nu^2)^2} \left\{ \frac{\partial u}{\partial x}\left[(1 - \nu + \nu^2)w,_{xx} - \frac{1}{2}(1 - 4\nu + \nu^2)w,_{yy} \right] \right.$$

$$+ \frac{\partial v}{\partial y}\left[-\frac{1}{2}(1 - 4\nu + \nu^2)w,_{xx} + (1 - \nu + \nu^2)w,_{yy} \right] \quad (E.9)$$

$$\left. + \frac{3}{2}(1 - \nu)^2 \left(\frac{\partial u}{\partial y} + \frac{\partial v}{\partial x} \right)w,_{xy} \right\}$$

$$C = \frac{E^2}{(1 + \nu)^2} \left\{ \left(\frac{\partial u}{\partial x} - \frac{\partial v}{\partial y} \right)^2 + \frac{3}{4} \left(\frac{\partial u}{\partial y} + \frac{\partial v}{\partial x} \right)^2 \right.$$

$$\left. + \frac{\partial u}{\partial x} \frac{\partial v}{\partial y} + \frac{\nu}{(1 - \nu)^2} \left(\frac{\partial u}{\partial x} + \frac{\partial v}{\partial y} \right)^2 \right\} .$$

In the case of pure bending, $\overline{N}_x = \overline{N}_y = \overline{N}_{xy} \equiv 0$. Also, $\rho = -z$, with z measured from the middle surface. Therefore, $B = C \equiv 0$, and Eq. (E.6b) reduces to:

$$-\overline{z} = \frac{\pm \sqrt{A\sigma_o^2}}{A} = \pm \frac{\sigma_o}{\sqrt{A}}$$

(E.10)

$$z = \mp \frac{\sigma_o}{\sqrt{A}};$$

and so indeed we get two equal roots of opposite sign, indicating symmetry with respect to the median surface. Here $0 \leq |\overline{z}| \leq t$.

In any plasticity problem it is necessary to compute the load at which plastic behavior is initiated. For combined bending

118

and membrane problems, it is assumed that the membrane load is applied first (the plate may not go plastic in membrane loading alone) and then the lateral load is increased to the value that causes initial yielding of the plate. Consequently, the stresses at the upper and lower surface at initial yielding can be written as

$$\sigma_x = \frac{E}{1 - v^2} \left[\left(\frac{\partial u}{\partial x} + v \frac{\partial v}{\partial y} \right) \pm tk \left(w,_{xx}^{(1)} + vw,_{yy}^{(1)} \right) \right]$$

$$\sigma_y = \frac{E}{1 - v^2} \left[\left(\frac{\partial v}{\partial y} + v \frac{\partial u}{\partial x} \right) \pm tk \left(w,_{yy}^{(1)} + vw,_{yy}^{(1)} \right) \right] \qquad (E.11)$$

$$\tau_{xy} = \frac{E}{2(1 + v)} \left[\frac{\partial u}{\partial y} + \frac{\partial v}{\partial x} \pm 2ktw,_{xy}^{(1)} \right]$$

where k is the lateral load required to cause initial yielding, i.e., $J_2 = \sigma_0^2$; and the superscript (1) indicates curvatures due to a unit lateral load.

Thus, if we let $\rho = \pm kt$ in Eq. (E.6a), we get

$$\pm kt = \frac{- B \pm \sqrt{B^2 - A\left(C - \sigma_0^2 \right)}}{A} . \qquad (E.12)$$

Therefore, the critical lateral load necessary to cause initial yielding is

$$P_{crit} = k = \frac{- B \pm \sqrt{B^2 - A\left(C - \sigma_0^2 \right)}}{tA} \qquad (E.13a)$$

if, at the critical node, yielding occurs first at the upper surface, and

$$P_{crit} = k = \frac{B \pm \sqrt{B^2 - A\left(C - \sigma_0^2 \right)}}{tA} \qquad (E.13b)$$

119

if, at the critical node, yielding occurs first at the lower surface. Of the two roots for each situation we take the smallest positive value.

Sometimes it is more convenient to express the quantities A, B, C in Eq. (E.9) in terms of the membrane and bending strains at the lower surface. Multiplying and dividing appropriate terms in Eq. (E.9) by -t we get:

$$A = \frac{E^2}{t^2(1+v)^2}\left\{\left(e_{xb}^L - e_{yb}^L\right)^2 + \frac{3}{4}\gamma_{xyb}^{L\,2}\right.$$

$$\left. + e_{xb}^L e_{yb}^L + \frac{v}{(1-v)^2}\left(e_{xb}^L + e_{yb}^L\right)^2\right\}$$

$$B = -\frac{E^2}{t(1-v^2)^2}\left\{e_{xm}\left[(1-v+v^2)e_{xb}^L - \frac{1}{2}(1-4v+v^2)e_{yb}^L\right]\right.$$

(E.14)

$$\left. + e_{ym}\left[-\frac{1}{2}(1-4v+v^2)e_{xb}^L + (1-v+v^2)e_{yb}^L\right]\right.$$

$$\left. + \frac{3}{4}(1-v)^2\gamma_{xym}\gamma_{xyb}^L\right\}$$

$$C = \frac{E^2}{(1+v)^2}\left\{(e_{xm} - e_{ym})^2 + \frac{3}{4}\gamma_{xym}^2 + e_{xm}e_{ym}\right.$$

$$\left. + \frac{v}{(1-v)^2}(e_{xm} + e_{ym})^2\right\} ,$$

where the subscripts b and m refer to bending and membrane strains, respectively. In the case of bending alone, B = C ≡ 0 and

$$P_{crit} = \frac{\pm \sigma_o}{t\sqrt{A}} .$$

(E.15)

120

APPENDIX F

TRIANGULAR COORDINATES AND INTEGRATION FORMULAS

This appendix presents a summary of pertinent information on triangular coordinates and several manipulations performed with them. It is included to clarify several sections in the report and appendices and to define certain quantities used extensively in the text. The discussion follows closely that given in Ref. 42.

The coordinates of a plane triangle 1-2-3 (see Fig. 76) lying in the $\bar{x}$-$\bar{y}$ plane of a global Cartesian coordinate system $\bar{x}, \bar{y}, \bar{z}$ are $(\bar{x}_1, \bar{y}_1)$, $(\bar{x}_2, \bar{y}_2)$, and $(\bar{x}_3, \bar{y}_3)$. Define now a "local global" Cartesian system x, y, z with axes parallel to the global axes $\bar{x}, \bar{y}, \bar{z}$, respectively, and its origin located at the centroid "c" of the triangle. The global coordinates of the centroid are:

$$\bar{x}_c = \tfrac{1}{3}(\bar{x}_1 + \bar{x}_2 + \bar{x}_3)$$

$$(F.1)$$

$$y_c = \tfrac{1}{3}(\bar{y}_1 + \bar{y}_2 + \bar{y}_3) \ .$$

The local coordinates of the nodes of the triangle are:

$$x_i = \bar{x}_i - \bar{x}_c$$

$$i = 1, 2, 3 \ . \qquad (F.2)$$

$$y_i = \bar{y}_i - \bar{y}_c$$

Hence we see that

$$x_1 + x_2 + x_3 = 0$$

$$(F.3)$$

$$y_1 + y_2 + y_3 = 0$$

and the area of the triangle is

$$A = \frac{1}{2} \begin{vmatrix} 1 & x_1 & y_1 \\ 1 & x_2 & y_2 \\ 1 & x_3 & y_3 \end{vmatrix} \tag{F.4}$$

Any point $P(\bar{x}, \bar{y})$ within the triangle, when joined to the vertices by straight lines, divides it into three subtriangles (see Fig. 77). Now let A_1, A_2, A_3 be the areas of these sub-triangles, and define the three area coordinates of P as

$$\omega_i = \frac{A_i}{A} \qquad i = 1, 2, 3 , \tag{F.5}$$

where the subscript i refers to the vertex of the triangle opposite the subarea A_i. Now $A = A_1 + A_2 + A_3$ is the total area of the triangle, and as a result

$$\omega_1 + \omega_2 + \omega_3 = 1 . \tag{F.6}$$

The equation, ω_i = constant, represents a line parallel to the side opposite vertex i. The coordinates of vertex i are $\omega_i = 1$, $\omega_j = \omega_k = 0$ $(i \neq j \neq k)$.

The Cartesian coordinates x, y are related to the area coordinates by the matrix equation

$$\begin{Bmatrix} 1 \\ x \\ y \end{Bmatrix} = \begin{bmatrix} 1 & 1 & 1 \\ x_1 & x_2 & x_3 \\ y_1 & y_2 & y_3 \end{bmatrix} \begin{Bmatrix} \omega_1 \\ \omega_2 \\ \omega_3 \end{Bmatrix} . \tag{F.7}$$

122

The inverse relationship may be written as

$$
\begin{Bmatrix} \omega_1 \\ \omega_2 \\ \omega_3 \end{Bmatrix} = \frac{1}{2A} \begin{bmatrix} x_2 y_3 - x_3 y_2 & y_2 - y_3 & x_3 - x_2 \\ x_3 y_1 - x_1 y_3 & y_3 - y_1 & x_1 - x_3 \\ x_1 y_2 - x_2 y_1 & y_1 - y_2 & x_2 - x_1 \end{bmatrix} \begin{Bmatrix} 1 \\ x \\ y \end{Bmatrix}
$$

(F.8)

$$
= \frac{1}{2A} \begin{bmatrix} 2A_1 & b_1 & a_1 \\ 2A_2 & b_2 & a_2 \\ 2A_3 & b_3 & a_3 \end{bmatrix} \begin{Bmatrix} 1 \\ x \\ y \end{Bmatrix} .
$$

Note here that, from the definitions,

$$
a_1 + a_2 + a_3 = 0
$$

(F.9)

$$
b_1 + b_2 + b_3 = 0 .
$$

The definition of these area coordinates ω_i makes the integration of polynomial terms over the triangular region extremely simple. These integrations are necessary for the formation of the stiffness, initial strain stiffness, and initial stress stiffness matrices. The integration of polynomials expressed in area coordinates is independent of the shape of the triangle and can be written as a multiple of the area; i.e.,

$$
\int_A \omega_i^{M_i} \omega_j^{M_j} \omega_k^{M_k} dA = \rho A
$$

(F.10)

where i, j, k represent any permutation of 1, 2, 3. In Ref. 66, a general formula for ρ is given as

$$\rho = 2 \frac{(M_i)! (M_j)! (M_k)!}{(M_i + M_j + M_k + 2)!} \quad . \tag{F.11}$$

Using this relationship and considering the local Cartesian coordinate system located at the centroid of the triangle, we can define

$$P_{pq} = \int_A x^p y^q dA \quad . \tag{F.12}$$

But

$$x = x_1 \omega_1 + x_2 \omega_2 + x_3 \omega_3$$

$$\tag{F.13}$$

$$y = y_1 \omega_1 + y_2 \omega_2 + y_3 \omega_3 \quad .$$

Substituting Eq. (F.13) into Eq. (F.12) gives

$$P_{pq} = \int_A (x_1 \omega_1 + x_2 \omega_2 + x_3 \omega_3)^p (y_1 \omega_1 + y_2 \omega_2 + y_3 \omega_3)^q dA \quad . \tag{F.14}$$

Succinct forms for this expression, using Eqs. (F.3) and (F.11) for $n = p + q$, ranging from 0 through 6, are given in Ref. 42. A general formula for all orders is derived in Appendix I and is repeated here:

$$P_{pq} = 2A \frac{p! \, q!}{(p + q + 2)!} \cdot$$

$$\sum_{r=0}^{p} \sum_{s=0}^{r} \sum_{t=0}^{q} \sum_{u=0}^{t} \frac{[(p+q) - (r+t)]! [(r+t) - (s+u)]! [s+u]!}{(p-r)! (r-s)! (q-t)! (t-u)! s! u!} \cdot$$

$$\tag{F.15}$$

$$\left(x_1^{p-r} \, y_1^{q-t} \, x_2^{r-s} \, y_2^{t-u} \, x_3^{s} \, y_3^{u} \right) \quad .$$

124

INITIAL STRAIN STIFFNESS MATRICES
FOR RECTANGULAR PLATE ELEMENT

The initial strain stiffness matrices for a rectangular plate element in pure bending and in combined bending and membrane loading have been derived from the assumptions shown in Fig. 34 and defined in integral form in Eq. (15). For bending alone, the initial strain stiffness matrix can be written as:

$$
\begin{Bmatrix} P_{z11} \\ M_x 11/a \\ M_{y11}/b \\ M_{xy11}/ab \\ P_{z21} \\ \vdots \\ P_{z12} \\ \vdots \\ P_{z22} \\ M_{x22}/a \\ M_{y22}/b \\ M_{xy22}/ab \end{Bmatrix}
= \frac{E}{3(1 - \nu^2)}
\begin{bmatrix} L(i,j) \\ (16 \times 12) \end{bmatrix}
\begin{bmatrix} G_d \\ (12 \times 12) \end{bmatrix}
\begin{Bmatrix} \epsilon_{x11} \\ \epsilon_{y11} \\ \gamma^P_{xy11} \\ \epsilon_{x21} \\ \vdots \\ \epsilon_{x12} \\ \vdots \\ \epsilon_{x22} \\ \epsilon_{y22} \\ \gamma^P_{xy22} \end{Bmatrix}
= [k^*]\{\epsilon_0\} .
$$

$$(G.1)$$

Here P_z and the M's represent the fictitious restoring force in the lateral direction and fictitious moments, respectively. The matrix $[G_d]$ is a diagonally partitioned array with 3 x 3 submatrices given by:

$$[G] = \begin{bmatrix} \dfrac{b}{a} & v\,\dfrac{b}{a} & 0 \\[2ex] v\,\dfrac{a}{b} & \dfrac{a}{b} & 0 \\[2ex] 0 & 0 & 1 - v \end{bmatrix}.$$

The coefficients of the terms in $L(i,j)$ are given in Table 1; e.g.,

$$L(1,1) = (-7/20)(2t^2) + (4/15)t\bar{z}_{11} + (1/12)t\bar{z}_{12} + (0)t\bar{z}_{21}$$

$$+ (0)t\bar{z}_{22} + (27/140)\bar{z}_{11}^2 + (39/1400)\bar{z}_{12}^2 + (-3/140)\bar{z}_{21}^2$$

$$+ (-13/4200)\bar{z}_{22}^2 + (33/350)\bar{z}_{11}\bar{z}_{12} + (3/70)\bar{z}_{11}\bar{z}_{21}$$

$$+ (11/1050)\bar{z}_{11}\bar{z}_{22} + (11/1050)\bar{z}_{12}\bar{z}_{21}$$

$$+ (13/2100)\bar{z}_{12}\bar{z}_{22} + (-11/1050)\bar{z}_{21}\bar{z}_{22}.$$

As in the case of pure bending of a beam, all $\bar{z}$'s are measured with respect to the median surface. All other quantities appearing in Eq. (G.1) are defined in Fig. 34.

The corresponding relations for the case of a rectangular element under combined bending and membrane forces are as follows:

126

$$
\left\{
\begin{array}{c}
P_{z11} \\
M_{x11}/a \\
M_{y11}/b \\
M_{xy11}/ab \\
\vdots \\
M_{xy22}/ab \\
\text{-----} \\
P_{x11} \\
P_{y11} \\
P_{x21} \\
P_{y21} \\
P_{x12} \\
\vdots \\
P_{y22}
\end{array}
\right\}
=
\frac{E}{6(1 - \nu^2)}
\left[
\begin{array}{c:c}
k^*_{11} & k^*_{12} \\
\hdashline
k^*_{21} & k^*_{22}
\end{array}
\right]
\left\{
\begin{array}{c}
\epsilon^{U}_{x11} \\
\epsilon^{U}_{y11} \\
\gamma^{PU}_{xy11} \\
\epsilon^{U}_{x21} \\
\vdots \\
\epsilon^{U}_{x12} \\
\epsilon^{U}_{x22} \\
\gamma^{PU}_{xy22} \\
\text{-----} \\
\epsilon^{L}_{x11} \\
\epsilon^{L}_{y11} \\
\gamma^{PL}_{xy11} \\
\epsilon^{L}_{x21} \\
\vdots \\
\epsilon^{L}_{x12} \\
\vdots \\
\epsilon^{L}_{x22} \\
\vdots \\
\gamma^{PL}_{xy22}
\end{array}
\right\}
\qquad (G.2)
$$

where

$$[k_{11}^*] = \begin{bmatrix} L_b^U(i,j) \end{bmatrix} \begin{bmatrix} & G_d & \end{bmatrix}$$

$$[k_{12}^*] = \begin{bmatrix} L_b^L(i,j) \end{bmatrix} \begin{bmatrix} & G_d & \end{bmatrix}$$

$$[k_{21}^*] = ab \begin{bmatrix} L_M^U(i,j) \end{bmatrix}$$

$$[k_{22}^*] = ab \begin{bmatrix} L_M^L(i,j) \end{bmatrix} .$$

The numerical coefficients of the terms in $L_b^U(i,j)$ and $L_b^L(i,j)$ used in forming $[k_{11}^*]$ and $[k_{12}^*]$ are the same as those in the $L(i,j)$ for pure bending shown in Table 1. How-ever, the terms with which they are associated change as follows:

Pure Bending	Bending and Membrane Loading	
$L(i,j)$	$L_b^U(i,j)$	$L_b^L(i,j)$
$2t^2$	0	$-2t^2$
$t\bar{z}_{11}$	$-3t\bar{z}_{11}^U$	$t\bar{z}_{11}^L$
$t\bar{z}_{12}$	$-3t\bar{z}_{12}^U$	$t\bar{z}_{12}^L$
$t\bar{z}_{21}$	$-3t\bar{z}_{21}^U$	$t\bar{z}_{21}^L$
$t\bar{z}_{22}$	$-3t\bar{z}_{22}^U$	$t\bar{z}_{22}^L$
$\bar{z}_{11}^2$	$\bar{z}_{11}^{U^2}$	$-\bar{z}_{11}^{L^2}$
$\bar{z}_{12}^2$	$\bar{z}_{12}^{U^2}$	$-\bar{z}_{12}^{L^2}$
$\bar{z}_{21}^2$	$\bar{z}_{21}^{U^2}$	$-\bar{z}_{21}^{L^2}$
$\bar{z}_{22}^2$	$\bar{z}_{22}^{U^2}$	$-\bar{z}_{22}^{L^2}$
$\bar{z}_{11}\bar{z}_{12}$	$\bar{z}_{11}^U\bar{z}_{12}^U$	$-\bar{z}_{11}^L\bar{z}_{12}^L$
$\bar{z}_{11}\bar{z}_{21}$	$\bar{z}_{11}^U\bar{z}_{21}^U$	$-\bar{z}_{11}^L\bar{z}_{21}^L$
$\bar{z}_{11}\bar{z}_{22}$	$\bar{z}_{11}^U\bar{z}_{22}^U$	$-\bar{z}_{11}^L\bar{z}_{22}^L$
$\bar{z}_{12}\bar{z}_{21}$	$\bar{z}_{12}^U\bar{z}_{21}^U$	$-\bar{z}_{12}^L\bar{z}_{21}^L$
$\bar{z}_{12}\bar{z}_{22}$	$\bar{z}_{12}^U\bar{z}_{22}^U$	$-\bar{z}_{12}^L\bar{z}_{22}^L$
$\bar{z}_{21}\bar{z}_{22}$	$\bar{z}_{21}^U\bar{z}_{22}^U$	$-\bar{z}_{21}^L\bar{z}_{22}^L$

The membrane submatrices, $[k_{21}^*]$ and $[k_{22}^*]$, of the initial strain matrix may be determined by using the form:

$$\begin{bmatrix} L_M^U(i,j) \end{bmatrix} \text{ or } \begin{bmatrix} L_M^L(i,j) \end{bmatrix} = \begin{bmatrix} \dfrac{L_{11}}{a} & \dfrac{\nu L_{11}}{a} & \dfrac{\mu L_{13}}{b} & \dfrac{L_{14}}{a} & \dfrac{\nu L_{14}}{a} & \dfrac{L_{16}\mu}{b} & \dfrac{L_{17}}{a} & \dfrac{\nu L_{17}}{a} & \dfrac{L_{19}\mu}{b} & \dfrac{L_{110}}{a} & \dfrac{\nu L_{110}}{a} & \dfrac{L_{112}\mu}{b} \\[2mm] \dfrac{\nu L_{22}}{b} & \dfrac{L_{22}}{b} & \dfrac{L_{23}\mu}{a} & \dfrac{\nu L_{25}}{b} & \dfrac{L_{25}}{b} & \dfrac{L_{26}\mu}{a} & \dfrac{\nu L_{28}}{b} & \dfrac{L_{28}}{b} & \dfrac{L_{29}\mu}{a} & \dfrac{\nu L_{211}}{b} & \dfrac{L_{211}}{b} & \dfrac{L_{212}\mu}{a} \\[2mm] \dfrac{L_{31}}{a} & \dfrac{\nu L_{31}}{a} & \dfrac{L_{33}\mu}{b} & \dfrac{L_{34}}{a} & \dfrac{\nu L_{34}}{a} & \dfrac{L_{36}\mu}{b} & \dfrac{L_{37}}{a} & \dfrac{\nu L_{37}}{a} & \dfrac{L_{39}\mu}{b} & \dfrac{L_{310}}{a} & \dfrac{\nu L_{310}}{a} & \dfrac{L_{312}\mu}{b} \\[2mm] \dfrac{\nu L_{42}}{b} & \dfrac{L_{42}}{b} & \dfrac{L_{43}\mu}{a} & \dfrac{\nu L_{45}}{b} & \dfrac{L_{45}}{b} & \dfrac{L_{46}\mu}{a} & \dfrac{\nu L_{48}}{b} & \dfrac{L_{48}}{b} & \dfrac{L_{49}\mu}{a} & \dfrac{\nu L_{411}}{b} & \dfrac{L_{411}}{b} & \dfrac{L_{412}\mu}{a} \\[2mm] \dfrac{L_{51}}{a} & \dfrac{\nu L_{51}}{a} & \dfrac{L_{53}\mu}{b} & \dfrac{L_{54}}{a} & \dfrac{\nu L_{54}}{a} & \dfrac{L_{56}\mu}{b} & \dfrac{L_{57}}{a} & \dfrac{\nu L_{57}}{a} & \dfrac{L_{59}\mu}{b} & \dfrac{L_{510}}{a} & \dfrac{\nu L_{510}}{a} & \dfrac{L_{512}\mu}{b} \\[2mm] \dfrac{\nu L_{62}}{b} & \dfrac{L_{62}}{b} & \dfrac{L_{63}\mu}{a} & \dfrac{\nu L_{65}}{b} & \dfrac{L_{65}}{b} & \dfrac{L_{66}\mu}{a} & \dfrac{\nu L_{68}}{b} & \dfrac{L_{68}}{b} & \dfrac{L_{69}\mu}{a} & \dfrac{\nu L_{611}}{b} & \dfrac{L_{611}}{b} & \dfrac{L_{612}\mu}{a} \\[2mm] \dfrac{L_{71}}{a} & \dfrac{\nu L_{71}}{a} & \dfrac{L_{73}\mu}{b} & \dfrac{L_{74}}{a} & \dfrac{\nu L_{74}}{a} & \dfrac{L_{76}\mu}{b} & \dfrac{L_{77}}{a} & \dfrac{\nu L_{77}}{a} & \dfrac{L_{79}\mu}{b} & \dfrac{L_{710}}{a} & \dfrac{\nu L_{710}}{a} & \dfrac{L_{712}\mu}{b} \\[2mm] \dfrac{\nu L_{82}}{b} & \dfrac{L_{82}}{b} & \dfrac{L_{83}\mu}{a} & \dfrac{\nu L_{85}}{b} & \dfrac{L_{85}}{b} & \dfrac{L_{86}\mu}{a} & \dfrac{\nu L_{88}}{b} & \dfrac{L_{88}}{b} & \dfrac{L_{89}\mu}{a} & \dfrac{\nu L_{811}}{b} & \dfrac{L_{811}}{b} & \dfrac{L_{812}\mu}{a} \end{bmatrix}$$

where $\mu = \dfrac{1 - \nu}{2}$.

The coefficients in the expressions for $L_M^U(i,j)$ and $L_M^L(i,j)$ are given in Table 2. These should be multiplied by the appropriate quantities for the upper or lower surface; for example,

$$L_M^U(1,1) = 0(-1) + \bar{z}_{11}^U\left(-\frac{1}{4}\right) + \bar{z}_{12}^U\left(-\frac{1}{12}\right) + \bar{z}_{21}^U\left(-\frac{1}{8}\right) + \bar{z}_{22}^U\left(-\frac{1}{24}\right)$$

$$L_M^L(1,1) = t(-1) - \bar{z}_{11}^L\left(-\frac{1}{4}\right) - \bar{z}_{12}^L\left(-\frac{1}{12}\right) - \bar{z}_{21}^L\left(-\frac{1}{8}\right) - \bar{z}_{22}^L\left(-\frac{1}{24}\right).$$

All $\bar{z}$'s for combined bending and membrane loading are measured with respect to the upper surface. Other quantities are defined in Fig. 34.

APPENDIX H

INITIAL STRAIN STIFFNESS MATRICES
FOR TRIANGULAR PLATE ELEMENT

The initial strain stiffness matrices for a triangular plate element in pure bending and combined bending and membrane states are derived from the assumptions shown in Fig. 35 and defined in integral form in Eq. (15).

For bending alone, this matrix is defined by:

$$
\begin{Bmatrix}
P_{z1} \\
M_{x1} \\
M_{y1} \\
M_{xx1} \\
M_{xy1} \\
M_{yy1} \\
P_{z2} \\
\cdot \\
\cdot \\
\cdot \\
P_{z3} \\
M_{x3} \\
M_{y3} \\
M_{xx3} \\
M_{xy3} \\
M_{yy3}
\end{Bmatrix}
= [k^*]
\begin{Bmatrix}
\epsilon_{x1} \\
\epsilon_{y1} \\
\gamma^{P}_{xy1} \\
\epsilon_{x2} \\
\epsilon_{y2} \\
\gamma^{P}_{xy2} \\
\epsilon_{x3} \\
\epsilon_{y3} \\
\gamma^{P}_{xy3}
\end{Bmatrix}
.
\tag{H.1}
$$

The element initial strain stiffness matrix $[k^*]$ may be written as:

$$[k^*] = \iiint_{V_p} [W]'[E][W_p^*]dV \qquad (H.2)$$

where the matrix $[W]$ relates the total strains to the generalized displacements, $[E]$ is the matrix of coefficients associated with Hooke's law, and the matrix $[W_p^*]$ relates the plastic strains within the element to their nodal values. The last array is a function matrix whose elements are determined from the assumed distribution of plastic strain within the plane of the element. For the triangular bending element, it is assumed that the plastic strains vary linearly in the plane.

Integrating Eq. (H.2) through the thickness of the plastic region of the element and multiplying the triple product under the integral result in the following form for the element initial strain matrix:

$$[k^*] = -\frac{E}{3(1-\nu^2)}\iint_A (2t^2 - t\bar{z} - \bar{z}^2)\Big\{[Q_1] + x[Q_2]$$

$$+ y[Q_3] + \ldots y^4[Q_{15}]\Big\}dA \ . \qquad (H.3)$$

Substituting the functional variation of the elastic-plastic boundary, i.e., assuming that $\bar{z}$ varies linearly in the plane of the triangle, and integrating over the area, we obtain the final form for the element initial strain stiffness matrix

$$[k^*] = -\frac{E}{3(1-\nu^2)}[\bar{C}]'[A^{-1}]'\Big\{[Q_i]\Big\}'\left[\sum_{j=1}^{6} L_j\Big\{P_j\Big\}\right] \qquad (H.4)$$

132

Here, for notational brevity, $\{[Q_i]\}$ is a "vector" of 15 matrices of order (21×9), i.e.,

$$\left\{ \begin{array}{c} [Q_1] \\ [Q_2] \\ [Q_3] \\ \cdot \\ \cdot \\ \cdot \\ [Q_{15}] \end{array} \right\}$$

whose nonzero elements are given on succeeding pages. The $\{P_j\}$'s are vectors of 15 constants, defined below, and the L_j's are scalar functions, also defined below. The matrix $[\bar{C}]$ is the (21×18) condensation matrix, given in Ref. 42; it reduces the order of the stiffness matrix by imposing a cubic variation on the normal slopes. Finally, $[A]$ is a 21×21 matrix relating the 21 degrees of freedom to the independent parameters a_i of the fifth order displacement polynomial, also given in Ref. 42. The scalar quantities L_j are given by

$$L_1 = 2t^2 - \frac{t}{A}(\bar{z}_1 A_1 + \bar{z}_2 A_2 + \bar{z}_3 A_3) - \frac{1}{A^2}(\bar{z}_1 A_1 + \bar{z}_2 A_2 + \bar{z}_3 A_3)^2$$

$$L_2 = - \frac{t}{2A}(\bar{z}_1 b_1 + \bar{z}_2 b_2 + \bar{z}_3 b_3)$$

$$- \frac{1}{A^2}(\bar{z}_1 b_1 + \bar{z}_2 b_2 + \bar{z}_3 b_3)(\bar{z}_1 A_1 + \bar{z}_2 A_2 + \bar{z}_3 A_3)$$

$$L_3 = - \frac{t}{2A}(\bar{z}_1 a_1 + \bar{z}_2 a_2 + \bar{z}_3 a_3)$$

$$- \frac{1}{A^2}(\bar{z}_1 a_1 + \bar{z}_2 a_2 + \bar{z}_3 a_3)(\bar{z}_1 A_1 + \bar{z}_2 A_2 + \bar{z}_3 A_3)$$

$$L_4 = -\frac{1}{4A^2}(\bar{z}_1 b_1 + \bar{z}_2 b_2 + \bar{z}_3 b_3)^2$$

$$L_5 = -\frac{1}{2A^2}(\bar{z}_1 a_1 + \bar{z}_2 a_2 + \bar{z}_3 a_3)(\bar{z}_1 b_1 + \bar{z}_2 b_2 + \bar{z}_3 b_3)$$

$$L_6 = -\frac{1}{4A^2}(\bar{z}_1 a_1 + \bar{z}_2 a_2 + \bar{z}_3 a_3)^2 \ .$$

The vectors $\{P_j\}$ are given by

$$\{P_1\} = \begin{Bmatrix} P_{00} \\ 0 \\ 0 \\ P_{20} \\ P_{11} \\ P_{02} \\ P_{30} \\ P_{21} \\ P_{12} \\ P_{03} \\ P_{40} \\ P_{31} \\ P_{22} \\ P_{13} \\ P_{04} \end{Bmatrix}; \quad \{P_2\} = \begin{Bmatrix} 0 \\ P_{20} \\ P_{11} \\ P_{30} \\ P_{21} \\ P_{12} \\ P_{40} \\ P_{31} \\ P_{22} \\ P_{13} \\ P_{50} \\ P_{41} \\ P_{32} \\ P_{23} \\ P_{14} \end{Bmatrix}; \quad \{P_3\} = \begin{Bmatrix} 0 \\ P_{11} \\ P_{02} \\ P_{21} \\ P_{12} \\ P_{03} \\ P_{31} \\ P_{22} \\ P_{13} \\ P_{04} \\ P_{41} \\ P_{32} \\ P_{23} \\ P_{14} \\ P_{05} \end{Bmatrix}$$

$$
\{P_4\} = \begin{Bmatrix} P_{20} \\ P_{30} \\ P_{21} \\ P_{40} \\ P_{31} \\ P_{22} \\ P_{50} \\ P_{41} \\ P_{32} \\ P_{23} \\ P_{60} \\ P_{51} \\ P_{42} \\ P_{33} \\ P_{24} \end{Bmatrix} ; \quad
\{P_5\} = \begin{Bmatrix} P_{11} \\ P_{21} \\ P_{12} \\ P_{31} \\ P_{22} \\ P_{13} \\ P_{41} \\ P_{32} \\ P_{23} \\ P_{14} \\ P_{51} \\ P_{42} \\ P_{33} \\ P_{24} \\ P_{15} \end{Bmatrix} ; \quad
\{P_6\} = \begin{Bmatrix} P_{02} \\ P_{12} \\ P_{03} \\ P_{22} \\ P_{13} \\ P_{04} \\ P_{32} \\ P_{23} \\ P_{14} \\ P_{05} \\ P_{42} \\ P_{33} \\ P_{24} \\ P_{15} \\ P_{06} \end{Bmatrix} .
$$

The quantities A_i, a_i, b_i and P_{pq} are defined in Appendix F.

The nonzero elements of the $[Q_i]$ matrices are given below. Only the first three of nine columns are listed. To obtain the remaining six columns, let i, which is equal to 1 for columns 1-3, be 2 for columns 4-6 and 3 for columns 7-9.

$2AQ_1$:
$(4,3i-2) = 4A_i$ $(6,3i-2) = 4\nu A_i$

$(4,3i-1) = 4\nu A_i$ $(6,3i-1) = 4A_i$

$(5,3i) = 4\mu A_i$

$2AQ_2$:

$(4,3i-2) = 2b_i$	$(6,3i-2) = 2\nu b_i$	$(8,3i) = 8\mu A_i$
$(4,3i-1) = 2\nu b_i$	$(6,3i-1) = 2b_i$	$(9,3i-2) = 4\nu A_i$
$(5,3i) = 2\mu b_i$	$(7,3i-2) = 12A_i$	$(9,3i-1) = 4A_i$
	$(7,3i-1) = 12\nu A_i$	

$2AQ_3$:

$(4,3i-2) = 2a_i$	$(6,3i-2) = 2\nu a_i$	$(9,3i) = 8\mu A_i$
$(4,3i-1) = 2\nu a_i$	$(6,3i-1) = 2a_i$	$(10,3i-2) = 12\nu A_i$
$(5,3i) = 2\mu a_i$	$(8,3i-2) = 4A_i$	$(10,3i-1) = 12A_i$
	$(8,3i-1) = 4\nu A_i$	

$2AQ_4$:

$(7,3i-2) = 6b_i$	$(9,3i-2) = 2\nu b_i$	$(12,3i) = 12\mu A_i$
$(7,3i-1) = 6\nu b_i$	$(9,3i-1) = 2b_i$	$(13,3i-2) = 4\nu A_i$
$(8,3i) = 4\mu b_i$	$(11,3i-2) = 24A_i$	$(13,3i-1) = 4A_i$
	$(11,3i-1) = 24\nu A_i$	

$2AQ_5$:

$(7,3i-2) = 6a_i$	$(9,3i-2) = 2\nu a_i$	$(12,3i-2) = 12A_i$
$(7,3i-1) = 6\nu a_i$	$(9,3i-1) = 2a_i$	$(12,3i-1) = 12\nu A_i$
$(8,3i-2) = 2b_i$	$(9,3i) = 4\mu b_i$	$(13,3i) = 16\mu A_i$
$(8,3i-1) = 2\nu b_i$	$(10,3i-2) = 6\nu b_i$	$(14,3i-2) = 12\nu A_i$
$(8,3i) = 4\mu a_i$	$(10,3i-1) = 6b_i$	$(14,3i-1) = 12A_i$

$2AQ_6$:

$(8,3i-2) = 2a_i$	$(10,3i-2) = 6\nu a_i$	$(14,3i) = 12\mu A_i$
$(8,3i-1) = 2\nu a_i$	$(10,3i-1) = 6a_i$	$(15,3i-2) = 24\nu A_i$
$(9,3i) = 4\mu a_i$	$(13,3i-2) = 4A_i$	$(15,3i-1) = 24A_i$
	$(13,3i-1) = 4\nu A_i$	

136

$2AQ_7$:

$(11, 3i-2) = 12b_i$	$(13, 3i-2) = 2\nu b_i$	$(17, 3i) = 16\mu A_i$
$(11, 3i-1) = 12\nu b_i$	$(13, 3i-1) = 2b_i$	$(18, 3i-2) = 4\nu A_i$
$(12, 3i) = 6\mu b_i$	$(16, 3i-2) = 40A_i$	$(18, 3i-1) = 4A_i$
	$(16, 3i-1) = 40\nu A_i$	

$2AQ_8$:

$(11, 3i-2) = 12a_i$	$(13, 3i-2) = 2\nu a_i$	$(17, 3i-2) = 24A_i$
$(11, 3i-1) = 12\nu a_i$	$(13, 3i-1) = 2a_i$	$(17, 3i-1) = 24\nu A_i$
$(12, 3i-2) = 6b_i$	$(13, 3i) = 8\mu b_i$	$(18, 3i) = 24\mu A_i$
$(12, 3i-1) = 6\nu b_i$	$(14, 3i-2) = 6\nu b_i$	$(19, 3i-2) = 12\nu A_i$
$(12, 3i) = 6\mu a_i$	$(14, 3i-1) = 6b_i$	$(19, 3i-1) = 12A_i$

$2AQ_9$:

$(12, 3i-2) = 6a_i$	$(14, 3i-2) = 6\nu a_i$	$(18, 3i-2) = 12A_i$
$(12, 3i-1) = 6\nu a_i$	$(14, 3i-1) = 6a_i$	$(18, 3i-1) = 12\nu A_i$
$(13, 3i-2) = 2b_i$	$(14, 3i) = 6\mu b_i$	$(19, 3i) = 24\mu A_i$
$(13, 3i-1) = 2\nu b_i$	$(15, 3i-2) = 12\nu b_i$	$(20, 3i-2) = 24\nu A_i$
$(13, 3i) = 8\mu a_i$	$(15, 3i-1) = 12b_i$	$(20, 3i-1) = 24A_i$

$2AQ_{10}$:

$(13, 3i-2) = 2a_i$	$(15, 3i-2) = 12\nu a_i$	$(20, 3i) = 16\mu A_i$
$(13, 3i-1) = 2\nu a_i$	$(15, 3i-1) = 12a_i$	$(21, 3i-2) = 40\nu A_i$
$(14, 3i) = 6\mu a_i$	$(19, 3i-2) = 4A_i$	$(21, 3i-1) = 40A_i$
	$(19, 3i-1) = 4\nu A_i$	

$2AQ_{11}$:

$(16, 3i-2) = 20b_i$	$(18, 3i-2) = 2\nu b_i$
$(16, 3i-1) = 20\nu b_i$	$(18, 3i-1) = 2b_i$
$(17, 3i) = 8\mu b_i$	

$2AQ_{12}$:

$(16,3i-2) = 20a_i$ $(18,3i-2) = 2\nu a_i$ $(19,3i-2) = 6\nu b_i$

$(16,3i-1) = 20\nu a_i$ $(18,3i-1) = 2a_i$ $(19,3i-1) = 6b_i$

$(17,3i-2) = 12b_i$ $(18,3i)\quad = 12\mu b_i$

$(17,3i-1) = 12\nu b_i$

$(17,3i)\quad = 8\mu a_i$

$2AQ_{13}$:

$(17,3i-2) = 12a_i$ $(19,3i-2) = 6\nu a_i$ $(20,3i-2) = 12\nu b_i$

$(17,3i-1) = 12\nu a_i$ $(19,3i-1) = 6a_i$ $(20,3i-1) = 12b_i$

$(18,3i-2) = 6b_i$ $(19,3i)\quad = 12\mu b_i$

$(18,3i-1) = 6\nu b_i$

$(18,3i)\quad = 12\mu a_i$

$2AQ_{14}$:

$(18,3i-2) = 6a_i$ $(20,3i-2) = 12\nu a_i$ $(21,3i-2) = 20\nu b_i$

$(18,3i-1) = 6\nu a_i$ $(20,3i-1) = 12a_i$ $(21,3i-1) = 20b_i$

$(19,3i-2) = 2b_i$ $(20,3i)\quad = 8\mu b_i$

$(19,3i-1) = 2\nu b_i$

$(19,3i)\quad = 12\mu a_i$

$2AQ_{15}$:

$(19,3i-2) = 2a_i$ $(20,3i)\quad = 8\mu a_i$ $(21,3i-2) = 20\nu a_i$

$(19,3i-1) = 2\nu a_i$ $(21,3i-1) = 20a_i$

where $\mu = \dfrac{(1 - \nu)}{2}$ and once again, for bending alone, all $\bar{z}$'s
are measured with respect to the middle surface.

The initial strain stiffness matrix for this triangular element for the case of combined bending and stretching, and on the basis of the assumptions shown in Fig. 35, can be written as

138

$$
\begin{Bmatrix}
P_{z1} \\
M_{x1} \\
M_{y1} \\
M_{xx1} \\
M_{xy1} \\
M_{yy1} \\
\vdots \\
M_{yy3} \\
\hdashline
P_{x1} \\
P_{y1} \\
P_{x2} \\
P_{y2} \\
P_{x3} \\
P_{y3}
\end{Bmatrix}
=
\left[
\begin{array}{c:c}
k^*_{11} & k^*_{12} \\
(18 \times 9) & (18 \times 9) \\
\hdashline
k^*_{21} & k^*_{22} \\
(6 \times 9) & (6 \times 9)
\end{array}
\right]
\begin{Bmatrix}
\epsilon^U_{x1} \\
\epsilon^U_{y1} \\
\gamma^{PU}_{xy1} \\
\epsilon^U_{x2} \\
\epsilon^U_{y2} \\
\gamma^{PU}_{xy2} \\
\epsilon^U_{x3} \\
\epsilon^U_{y3} \\
\gamma^{PU}_{xy3} \\
\hdashline
\epsilon^L_{x1} \\
\epsilon^L_{y1} \\
\gamma^{PL}_{xy1} \\
\vdots \\
\gamma^{PL}_{xy3}
\end{Bmatrix}
= [k^*] \begin{Bmatrix} \epsilon \\ o \end{Bmatrix}
\qquad (H.5)
$$

where, in this case,

$$
[k^*_{11}] = - \frac{E}{6(1 - \nu^2)} [\bar{C}]' [A^{-1}]' \left\{ [Q_i] \right\}' \left[\sum_{j=1}^{6} L^U_j \left\{ P_j \right\} \right]
\qquad (H.6a)
$$

139

with

$$L_1^U = \frac{3t}{A}(\bar{z}_1^U A_1 + \bar{z}_2^U A_2 + \bar{z}_3^U A_3) - \frac{1}{A^2}(\bar{z}_1^U A_1 + \bar{z}_2^U A_2 + \bar{z}_3^U A_3)^2$$

$$L_2^U = \frac{3t}{2A}(\bar{z}_1^U b_1 + \bar{z}_2^U b_2 + \bar{z}_3^U b_3)$$
$$- \frac{1}{A^2}(\bar{z}_1^U b_1 + \bar{z}_2^U b_2 + \bar{z}_3^U b_3)(\bar{z}_1^U A_1 + \bar{z}_2^U A_2 + \bar{z}_3^U A_3)$$

$$L_3^U = \frac{3t}{2A}(\bar{z}_1^U a_1 + \bar{z}_2^U a_2 + \bar{z}_3^U a_3)$$
$$- \frac{1}{A^2}(\bar{z}_1^U A_1 + \bar{z}_2^U A_2 + \bar{z}_3^U A_3)(\bar{z}_1^U a_1 + \bar{z}_2^U a_2 + \bar{z}_3^U a_3)$$

$$L_4^U = - \frac{1}{4A^2}(\bar{z}_1^U b_1 + \bar{z}_2^U b_2 + \bar{z}_3^U b_3)^2$$

$$L_5^U = - \frac{1}{2A^2}(\bar{z}_1^U a_1 + \bar{z}_2^U a_2 + \bar{z}_3^U a_3)(\bar{z}_1^U b_1 + \bar{z}_2^U b_2 + \bar{z}_3^U b_3)$$

$$L_6^U = - \frac{1}{4A^2}(\bar{z}_1^U a_1 + \bar{z}_2^U a_2 + \bar{z}_3^U a_3)^2$$

and

$$[k_{12}^*] = \frac{E}{6(1 - \nu^2)}[\bar{C}]'[A^{-1}]' \left\{[Q_i]\right\}' \left[\sum_{j=1}^{6} L_j^L \left\{P_j\right\}\right] \qquad (H.6b)$$

140

with

$$L_1^L = 2t^2 + \frac{t}{A}(\bar{z}_1^L A_1 + \bar{z}_2^L A_2 + \bar{z}_3^L A_3) - \frac{1}{A^2}(\bar{z}_1^L A_1 + \bar{z}_2^L A_2 + \bar{z}_3^L A_3)^2$$

$$L_2^L = \frac{t}{2A}(\bar{z}_1^L b_1 + \bar{z}_2^L b_2 + \bar{z}_3^L b_3)$$

$$- \frac{1}{A^2}(\bar{z}_1^L b_1 + \bar{z}_2^L b_2 + \bar{z}_3^L b_3)(\bar{z}_1^L A_1 + \bar{z}_2^L A_2 + \bar{z}_3^L A_3)$$

$$L_3^L = \frac{t}{2A}(\bar{z}_1^L a_1 + \bar{z}_2^L a_2 + \bar{z}_3^L a_3)$$

$$- \frac{1}{A^2}(\bar{z}_1^L a_1 + \bar{z}_2^L a_2 + \bar{z}_3^L a_3)(\bar{z}_1^L A_1 + \bar{z}_2^L A_2 + \bar{z}_3^L A_3)$$

$$L_4^L = - \frac{1}{4A^2}(\bar{z}_1^L b_1 + \bar{z}_2^L b_2 + \bar{z}_3^L b_3)^2$$

$$L_5^L = - \frac{1}{2A^2}(\bar{z}_1^L a_1 + \bar{z}_2^L a_2 + \bar{z}_3^L a_3)(\bar{z}_1^L b_1 + \bar{z}_2^L b_2 + \bar{z}_3^L b_3)$$

$$L_6^L = - \frac{1}{4A^2}(\bar{z}_1^L a_1 + \bar{z}_2^L a_2 + \bar{z}_3^L a_3)^2 .$$

Note that all the matrices used in the construction of $[k_{11}^*]$ and $[k_{12}^*]$ are as previously defined for bending alone; only the L_j's are different.

The membrane portions of the initial strain matrix may now be written as

$$[k_{21}^*] = - \frac{E}{2(1-\nu^2)} \left\{ (\bar{z}_1^U A_1 + \bar{z}_2^U A_2 + \bar{z}_3^U A_3) [\tilde{Q}_1] \right.$$

$$+ \frac{1}{2A} \left[(\bar{z}_1^U b_1 + \bar{z}_2^U b_2 + \bar{z}_3^U b_3) P_{20} + (\bar{z}_1^U a_1 + \bar{z}_2^U a_2 + \bar{z}_3^U a_3) P_{11} \right] [\tilde{Q}_2]$$

$$\left. + \frac{1}{2A} \left[(\bar{z}_1^U b_1 + \bar{z}_2^U b_2 + \bar{z}_3^U b_3) P_{11} + (\bar{z}_1^U a_1 + \bar{z}_2^U a_2 + \bar{z}_3^U a_3) P_{02} \right] [\tilde{Q}_3] \right\}$$

$$\text{(H.6c)}$$

$$[k_{22}^*] = - \frac{E}{2(1-\nu^2)} \left\{ \left[2t - \frac{1}{A} (\bar{z}_1^L A_1 + \bar{z}_2^L A_2 + \bar{z}_3^L A_3) \right] A [\tilde{Q}_1] \right.$$

$$- \frac{1}{2A} \left[(\bar{z}_1^L b_1 + \bar{z}_2^L b_2 + \bar{z}_3^L b_3) P_{20} + (\bar{z}_1^L a_1 + \bar{z}_2^L a_2 + \bar{z}_3^L a_3) P_{11} \right] [\tilde{Q}_2]$$

$$\left. - \frac{1}{2A} \left[(\bar{z}_1^L b_1 + \bar{z}_2^L b_2 + \bar{z}_3^L b_3) P_{11} + (\bar{z}_1^L a_1 + \bar{z}_2^L a_2 + \bar{z}_3^L a_3) P_{02} \right] [\tilde{Q}_3] \right\}$$

$$\text{(H.6d)}$$

Here the $[\tilde{Q}_j]$ are 6 x 9 matrices, the first three columns of which are given below. To obtain the remaining six columns, let i which is equal to 1 for columns 1-3, be 2 for columns 4-6, and 3 for columns 7-9. In addition, the column indices must be increased by 3 to obtain columns 4-6 and by 6 to obtain columns 7-9.

$$[\tilde{Q}_1] = \frac{A_i}{2A^2} \begin{bmatrix} b_1 & \nu b_1 & \frac{1-\nu}{2} a_1 \\ \nu a_1 & a_1 & \frac{1-\nu}{2} b_1 \\ b_2 & \nu b_2 & \frac{1-\nu}{2} a_2 \\ \nu a_2 & a_2 & \frac{1-\nu}{2} b_2 \\ b_3 & \nu b_3 & \frac{1-\nu}{2} a_3 \\ \nu a_3 & a_3 & \frac{1-\nu}{2} b_3 \end{bmatrix} = \frac{A_i}{2A^2} [\hat{Q}] \qquad \text{(H.7a)}$$

$$[\tilde{Q}_2] = \frac{b_i}{4A^2} [\hat{Q}] \qquad \text{(H.7b)}$$

$$[\tilde{Q}_3] = \frac{a_i}{4A^2} [\hat{Q}] . \qquad \text{(H.7c)}$$

All $\bar{z}$'s are measured with respect to the upper surface for combined bending and membrane loadings.

As in the case of beams, the generated membrane strains may be sufficiently large to cause the entire cross section of the plate to go plastic without there being a point within the thickness at which the plastic strain is zero. The initial strain stiffness matrix must be modified in much the same manner as was done for the beam to accommodate this case. The functional form for the plastic strains used in deriving the initial strain stiffness matrix now becomes:

$$
\left\{ \begin{array}{c} \epsilon_x^U \\ \epsilon_y^U \\ \gamma_{xy}^{PU} \end{array} \right\} = \left[\; [C_1^U] \; \vdots \; [C_2^U] \; \vdots \; [C_3^U] \; \right] \left\{ \begin{array}{c} \epsilon_{x1}^U \\ \epsilon_{y1}^U \\ \gamma_{xy1}^{PU} \\ ---- \\ \epsilon_{x2}^U \\ \epsilon_{y2}^U \\ \gamma_{xy2}^{PU} \\ ---- \\ \epsilon_{x3}^U \\ \epsilon_{y3}^U \\ \gamma_{xy3}^{PU} \end{array} \right\}
$$

$$\text{(H.8a)}$$

where

$$
\left[C_i^U \right] = \left[1 + (K_i^U - 1) \frac{z}{z^U} \right] \left[\begin{array}{ccc} \omega_i & 0 & 0 \\ 0 & \omega_i & 0 \\ 0 & 0 & \omega_i \end{array} \right]
$$

where ω_i represents the area coordinates, defined in Appendix F, and

144

$$K_i^U = \begin{cases} \dfrac{\epsilon_i^L}{\epsilon_i^U} & \text{if} \quad \epsilon_i^L/\epsilon_i^U \geq 0 \\[3em] 0 & \text{if} \quad \epsilon_i^L/\epsilon_i^U < 0 \end{cases} \qquad .$$

For the lower surface, we have

$$\begin{Bmatrix} \epsilon_x^L \\ \epsilon_y^L \\ \gamma_{xy}^{PL} \end{Bmatrix} = \begin{bmatrix} [C_1^L] & \vdots & [C_2^L] & \vdots & [C_3^L] \end{bmatrix} \begin{Bmatrix} \epsilon_{x1}^L \\ \epsilon_{y1}^L \\ \gamma_{xy1}^{PL} \\ \hline \epsilon_{x2}^L \\ \epsilon_{y2}^L \\ \gamma_{xy2}^{PL} \\ \hline \epsilon_{x3}^L \\ \epsilon_{y3}^L \\ \gamma_{xy3}^{PL} \end{Bmatrix} \qquad \text{(H.8b)}$$

where

$$\left[c_i^L \right] = \left[\frac{(z - \bar{z}^L) + K_i^L(2t - z)}{2t - \bar{z}^L} \right] \begin{bmatrix} \omega_i & 0 & 0 \\ 0 & \omega_i & 0 \\ 0 & 0 & \omega_i \end{bmatrix}$$

with

$$K_i^L = \begin{cases} \epsilon_i^U/\epsilon_i^L & \text{if} & \epsilon_i^U/\epsilon_i^L \geq 0 \\ \\ 0 & \text{if} & \epsilon_i^U/\epsilon_i^L < 0 \end{cases} .$$

This form retains the assumption of a linear plastic strain distribution, and, as in the case of the beam (Appendix D), allows for a continuous development of the plastic region.

146

APPENDIX I

INITIAL STRESS STIFFNESS MATRIX
FOR TRIANGULAR PLATE ELEMENT

The stiffness matrix for the 18-degree-of-freedom triangular element was derived in Ref. 42. The displacement function used was a complete fifth order polynomial:

$$w(x,y) = \left\{ 1, x, y, \ldots, xy^4, y^5 \right\} \begin{Bmatrix} a_1 \\ \cdot \\ \cdot \\ \cdot \\ a_{21} \end{Bmatrix} .$$ (I.1)

The 21 degrees of freedom chosen were the displacements w_i, the slopes w_{x_i}, w_{y_i}, the curvatures $w,_{xx_i}$, $w,_{xy_i}$, and $w,_{yy_i}$ at each node, and the normal midpoint slopes $w,_{n_i}$ of each side. The latter were then eliminated by imposing a cubic variation on the edge normal slope $w,_n$ (see Ref. 42), yielding the 18-degree-of-freedom triangle.

The initial stress stiffness matrix is defined in Ref. 45, and for this triangular element may be written as

$$[k^{(1)}] = \iint_A [\bar{C}]'[A^{-1}]'[\hat{W}]'[N][\hat{W}][A^{-1}][\bar{C}]dA .$$ (I.2)

Here [A] is the 21 x 21 matrix relating the nodal degrees of freedom to the independent parameters a_i of Eq. (I.1), as follows

$$\{d_o\} = [A]\{a_i\} ;$$ (I.3)

$[\bar{C}]$ is the condensation matrix, which reduces the 21 x 21 stiffness matrix to 18 x 18 (i.e., it eliminates the midpoint normal slopes as independent degrees of freedom); $[\hat{W}]$ is the

function matrix relating the slopes $w,_x$, and $w,_y$ to the co-efficients a_i; and $[N]$ is the matrix of membrane stress re-sultants:

$$[N] = \begin{bmatrix} N_x & N_{xy} \\ \\ N_{xy} & N_y \end{bmatrix} \qquad (I.4)$$

Matrices $[A]$ and $[\bar{C}]$ are presented in Ref. 42. The elements of the product $\iint [\hat{W}]'[N][\hat{W}]dA$ are given below.

$1,i = 0$ $\qquad\qquad\qquad\qquad i = 1, 21$

$2,2 = (N_x)P_{00}$

$2,3 = (N_{xy})P_{00}$

$2,4 = 0$

$2,5 = 0$

$2,6 = 0$

$2,7 = 3P_{20}(N_x)$

$2,8 = 2P_{11}(N_x) + P_{20}(N_{xy})$

$2,9 = P_{02}(N_x) + 2P_{11}(N_{xy})$

$2,10 = 3P_{02}(N_{xy})$

$2,11 = 4P_{30}(N_x)$

$2,12 = 3P_{21}(N_x) + P_{30}(N_{xy})$

$2,13 = 2P_{12}(N_x) + 2P_{21}(N_{xy})$

$2,14 = P_{03}(N_x) + 3P_{12}(N_{xy})$

148

$2,15 = 4P_{03}(N_{xy})$

$2,16 = 5P_{40}(N_x)$

$2,17 = 4P_{31}(N_x) + P_{40}(N_{xy})$

$2,18 = 3P_{22}(N_x) + 2P_{31}(N_{xy})$

$2,19 = 2P_{13}(N_x) + 3P_{22}(N_{xy})$

$2,20 = P_{04}(N_x) + 4P_{13}(N_{xy})$

$2,21 = 5P_{04}(N_{xy})$

$3,3 = P_{00}(N_y)$

$3,4 = 0$

$3,5 = 0$

$3,6 = 0$

$3,7 = 3P_{20}(N_{xy})$

$3,8 = 2P_{11}(N_{xy}) + P_{20}(N_y)$

$3,9 = P_{02}(N_{xy}) + 2P_{11}(N_y)$

$3,10 = 3P_{02}(N_y)$

$3,11 = 4P_{30}(N_{xy})$

$3,12 = 3P_{21}(N_{xy}) + P_{30}(N_y)$

$3,13 = 2P_{12}(N_{xy}) + 2P_{21}(N_y)$

$3,14 = P_{03}(N_{xy}) + 3P_{12}(N_y)$

$3,15 = 4P_{03}(N_y)$

$3,16 = 5P_{40}(N_{xy})$

$3,17 = 4P_{31}(N_{xy}) + P_{40}(N_y)$

$$3,18 = 3P_{22}(N_{xy}) + 2P_{31}(N_y)$$

$$3,19 = 2P_{13}(N_{xy}) + 3P_{22}(N_y)$$

$$3,20 = P_{04}(N_{xy}) + 4P_{13}(N_y)$$

$$3,21 = 5P_{04}(N_y)$$

$$4,4 = 4P_{20}(N_x)$$

$$4,5 = 2P_{11}(N_x) + 2P_{20}(N_{xy})$$

$$4,6 = 4P_{11}(N_{xy})$$

$$4,7 = 6P_{30}(N_x)$$

$$4,8 = 4P_{21}(N_x) + 2P_{30}(N_{xy})$$

$$4,9 = 2P_{12}(N_x) + 4P_{21}(N_{xy})$$

$$4,10 = 6P_{12}(N_{xy})$$

$$4,11 = 8P_{40}(N_x)$$

$$4,12 = 6P_{31}(N_x) + 2P_{40}(N_{xy})$$

$$4,13 = 4P_{22}(N_x) + 4P_{31}(N_{xy})$$

$$4,14 = 2P_{13}(N_x) + 6P_{22}(N_{xy})$$

$$4,15 = 8P_{13}(N_{xy})$$

$$4,16 = 10P_{50}(N_x)$$

$$4,17 = 8P_{41}(N_x) + 2P_{50}(N_{xy})$$

$$4,18 = 6P_{32}(N_x) + 4P_{41}(N_{xy})$$

$$4,19 = 4P_{23}(N_x) + 6P_{32}(N_{xy})$$

$$4,20 = 2P_{14}(N_x) + 8P_{23}(N_{xy})$$

$$4,21 = 10P_{14}(N_{xy})$$

$$5,5 \quad = P_{02}(N_x) + 2P_{11}(N_{xy}) + P_{20}(N_y)$$

$$5,6 \quad = 2P_{02}(N_{xy}) + 2P_{11}(N_y)$$

$$5,7 \quad = 3P_{21}(N_x) + 3P_{30}(N_{xy})$$

$$5,8 \quad = 2P_{12}(N_x) + 3P_{21}(N_{xy}) + P_{30}(N_y)$$

$$5,9 \quad = P_{03}(N_x) + 3P_{12}(N_{xy}) + 2P_{21}(N_y)$$

$$5,10 = 3P_{03}(N_{xy}) + 3P_{12}(N_y)$$

$$5,11 = 4P_{31}(N_x) + 4P_{40}(N_{xy})$$

$$5,12 = 3P_{22}(N_x) + 4P_{31}(N_{xy}) + P_{40}(N_y)$$

$$5,13 = 2P_{13}(N_x) + 4P_{22}(N_{xy}) + 2P_{31}(N_y)$$

$$5,14 = P_{04}(N_x) + 4P_{13}(N_{xy}) + 3P_{22}(N_y)$$

$$5,15 = 4P_{04}(N_{xy}) + 4P_{13}(N_y)$$

$$5,16 = 5P_{41}(N_x) + 5P_{50}(N_{xy})$$

$$5,17 = 4P_{32}(N_x) + 5P_{41}(N_{xy}) + P_{50}(N_y)$$

$$5,18 = 3P_{23}(N_x) + 5P_{32}(N_{xy}) + 2P_{41}(N_y)$$

$$5,19 = 2P_{14}(N_x) + 5P_{23}(N_{xy}) + 3P_{32}(N_y)$$

$$5,20 = P_{05}(N_x) + 5P_{14}(N_{xy}) + 4P_{23}(N_y)$$

$$5,21 = 5P_{05}(N_{xy}) + 5P_{14}(N_y)$$

$$6,6 \quad = 4P_{02}(N_y)$$

$$6,7 \quad = 6P_{21}(N_{xy})$$

$$6,8 \quad = 4P_{12}(N_{xy}) + 2P_{21}(N_y)$$

$$6,9 \quad = 2P_{03}(N_{xy}) + 4P_{12}(N_y)$$

$$6,10 = 6P_{03}(N_y)$$

$$6,11 = 8P_{31}(N_{xy})$$

$$6,12 = 6P_{22}(N_{xy}) + 2P_{31}(N_y)$$

$$6,13 = 4P_{13}(N_{xy}) + 4P_{22}(N_y)$$

$$6,14 = 2P_{04}(N_{xy}) + 6P_{13}(N_y)$$

$$6,15 = 8P_{04}(N_y)$$

$$6,16 = 10P_{41}(N_{xy})$$

$$6,17 = 8P_{32}(N_{xy}) + 2P_{41}(N_y)$$

$$6,18 = 6P_{23}(N_{xy}) + 4P_{32}(N_y)$$

$$6,19 = 4P_{14}(N_{xy}) + 6P_{23}(N_y)$$

$$6,20 = 2P_{05}(N_{xy}) + 8P_{14}(N_y)$$

$$6,21 = 10P_{05}(N_y)$$

$$7,7 = 9P_{40}(N_x)$$

$$7,8 = 6P_{31}(N_x) + 3P_{40}(N_{xy})$$

$$7,9 = 3P_{22}(N_x) + 6P_{31}(N_{xy})$$

$$7,10 = 9P_{22}(N_{xy})$$

$$7,11 = 12P_{50}(N_x)$$

$$7,12 = 9P_{41}(N_x) + 3P_{50}(N_{xy})$$

$$7,13 = 6P_{32}(N_x) + 6P_{41}(N_{xy})$$

$$7,14 = 3P_{23}(N_x) + 9P_{32}(N_{xy})$$

$$7,15 = 12P_{23}(N_{xy})$$

$$7,16 = 15P_{60}(N_x)$$

$$7,17 = 12P_{51}(N_x) + 3P_{60}(N_{xy})$$

152

$$7,18 = 9P_{42}(N_x) + 6P_{51}(N_{xy})$$

$$7,19 = 6P_{33}(N_x) + 9P_{42}(N_{xy})$$

$$7,20 = 3P_{24}(N_x) + 12P_{33}(N_{xy})$$

$$7,21 = 15P_{24}(N_{xy})$$

$$8,8 = 4P_{22}(N_x) + 4P_{31}(N_{xy}) + P_{40}(N_y)$$

$$8,9 = 2P_{13}(N_x) + 5P_{22}(N_{xy}) + 2P_{31}(N_y)$$

$$8,10 = 0(N_x) + 6P_{13}(N_{xy}) + 3P_{22}(N_y)$$

$$8,11 = 8P_{41}(N_x) + 4P_{50}(N_{xy}) + 0(N_y)$$

$$8,12 = 6P_{32}(N_x) + 5P_{41}(N_{xy}) + P_{50}(N_y)$$

$$8,13 = 4P_{23}(N_x) + 6P_{32}(N_{xy}) + 2P_{41}(N_y)$$

$$8,14 = 2P_{14}(N_x) + 7P_{23}(N_{xy}) + 3P_{32}(N_y)$$

$$8,15 = 0(N_x) + 8P_{14}(N_{xy}) + 4P_{23}(N_y)$$

$$8,16 = 10P_{51}(N_x) + 5P_{60}(N_{xy}) + 0(N_y)$$

$$8,17 = 8P_{42}(N_x) + 6P_{51}(N_{xy}) + P_{60}(N_y)$$

$$8,18 = 6P_{33}(N_x) + 7P_{42}(N_{xy}) + 2P_{51}(N_y)$$

$$8,19 = 4P_{24}(N_x) + 8P_{33}(N_{xy}) + 3P_{42}(N_y)$$

$$8,20 = 2P_{15}(N_x) + 9P_{24}(N_{xy}) + 4P_{33}(N_y)$$

$$8,21 = 0(N_x) + 10P_{15}(N_{xy}) + 5P_{24}(N_y)$$

$$9,9 = P_{04}(N_x) + 4P_{13}(N_{xy}) + 4P_{22}(N_y)$$

$$9,10 = 0(N_x) + 3P_{04}(N_{xy}) + 6P_{13}(N_y)$$

$$9,11 = 4P_{32}(N_x) + 8P_{41}(N_{xy}) + 0(N_y)$$

$$9,12 = 3P_{23}(N_x) + 7P_{32}(N_{xy}) + 2P_{41}(N_y)$$

$$9,13 = 2P_{14}(N_x) + 6P_{23}(N_{xy}) + 4P_{32}(N_y)$$

$$9,14 = P_{05}(N_x) + 5P_{14}(N_{xy}) + 6P_{23}(N_y)$$

$$9,15 = 0(N_x) + 4P_{05}(N_{xy}) + 8P_{14}(N_y)$$

$$9,16 = 5P_{42}(N_x) + 10P_{51}(N_{xy}) + 0(N_y)$$

$$9,17 = 4P_{33}(N_x) + 9P_{42}(N_{xy}) + 2P_{51}(N_y)$$

$$9,18 = 3P_{24}(N_x) + 8P_{33}(N_{xy}) + 4P_{42}(N_y)$$

$$9,19 = 2P_{15}(N_x) + 7P_{24}(N_{xy}) + 6P_{33}(N_y)$$

$$9,20 = P_{06}(N_x) + 6P_{15}(N_{xy}) + 8P_{24}(N_y)$$

$$9,21 = 0(N_x) + 5P_{06}(N_{xy}) + 10P_{15}(N_y)$$

$$10,10 = 0(N_{xy}) + 9P_{04}(N_y)$$

$$10,11 = 12P_{32}(N_{xy}) + 0(N_y)$$

$$10,12 = 9P_{23}(N_{xy}) + 3P_{32}(N_y)$$

$$10,13 = 6P_{14}(N_{xy}) + 6P_{23}(N_y)$$

$$10,14 = 3P_{05}(N_{xy}) + 9P_{14}(N_y)$$

$$10,15 = 0(N_{xy}) + 12P_{05}(N_y)$$

$$10,16 = 15P_{42}(N_{xy}) + 0(N_y)$$

$$10,17 = 12P_{33}(N_{xy}) + 3P_{42}(N_y)$$

$$10,18 = 9P_{24}(N_{xy}) + 6P_{33}(N_y)$$

$$10,19 = 6P_{15}(N_{xy}) + 9P_{24}(N_y)$$

$$10,20 = 3P_{06}(N_{xy}) + 12P_{15}(N_y)$$

$$10,21 = 0(N_{xy}) + 15P_{06}(N_y)$$

$$11,11 = 16P_{60}(N_x) + 0(N_{xy})$$

$$11,12 = 12P_{51}(N_x) + 4P_{60}(N_{xy})$$

$$11,13 = 8P_{42}(N_x) + 8P_{51}(N_{xy})$$

$$11,14 = 4P_{33}(N_x) + 12P_{42}(N_{xy})$$

$$11,15 = 0(N_x) + 16P_{33}(N_{xy})$$

$$11,16 = 20P_{70}(N_x) + 0(N_{xy})$$

$$11,17 = 16P_{61}(N_x) + 4P_{70}(N_{xy})$$

$$11,18 = 12P_{52}(N_x) + 8P_{61}(N_{xy})$$

$$11,19 = 8P_{43}(N_x) + 12P_{52}(N_{xy})$$

$$11,20 = 4P_{34}(N_x) + 16P_{43}(N_{xy})$$

$$11,21 = 0(N_x) + 20P_{34}(N_{xy})$$

$$12,12 = 9P_{42}(N_x) + 6P_{51}(N_{xy}) + P_{60}(N_y)$$

$$12,13 = 6P_{33}(N_x) + 8P_{42}(N_{xy}) + 2P_{51}(N_y)$$

$$12,14 = 3P_{24}(N_x) + 10P_{33}(N_{xy}) + 3P_{42}(N_y)$$

$$12,15 = 0(N_x) + 12P_{24}(N_{xy}) + 4P_{33}(N_y)$$

$$12,16 = 15P_{61}(N_x) + 5P_{70}(N_{xy}) + 0(N_y)$$

$$12,17 = 12P_{52}(N_x) + 7P_{61}(N_{xy}) + P_{70}(N_y)$$

$$12,18 = 9P_{43}(N_x) + 9P_{52}(N_{xy}) + 2P_{61}(N_y)$$

$$12,19 = 6P_{34}(N_x) + 11P_{43}(N_{xy}) + 3P_{52}(N_y)$$

$$12,20 = 3P_{25}(N_x) + 13P_{34}(N_{xy}) + 4P_{43}(N_y)$$

$$12,21 = 0(N_x) + 15P_{25}(N_{xy}) + 5P_{34}(N_y)$$

$$13,13 = 4P_{24}(N_x) + 8P_{33}(N_{xy}) + 4P_{42}(N_y)$$

$$13,14 = 2P_{15}(N_x) + 8P_{24}(N_{xy}) + 6P_{33}(N_y)$$

$$13,15 = 0(N_x) + 8P_{15}(N_{xy}) + 8P_{24}(N_y)$$

$$13,16 = 10P_{52}(N_x) + 10P_{61}(N_{xy}) + 0(N_y)$$

$$13,17 = 8P_{43}(N_x) + 10P_{52}(N_{xy}) + 2P_{61}(N_y)$$

$$13,18 = 6P_{34}(N_x) + 10P_{43}(N_{xy}) + 4P_{52}(N_y)$$

$$13,19 = 4P_{25}(N_x) + 10P_{34}(N_{xy}) + 6P_{43}(N_y)$$

$$13,20 = 2P_{16}(N_x) + 10P_{25}(N_{xy}) + 8P_{34}(N_y)$$

$$13,21 = 0(N_x) + 10P_{16}(N_{xy}) + 10P_{25}(N_y)$$

$$14,14 = P_{06}(N_x) + 6P_{15}(N_{xy}) + 9P_{24}(N_y)$$

$$14,15 = 0(N_x) + 4P_{06}(N_{xy}) + 12P_{15}(N_y)$$

$$14,16 = 5P_{43}(N_x) + 15P_{52}(N_{xy}) + 0(N_y)$$

$$14,17 = 4P_{34}(N_x) + 13P_{43}(N_{xy}) + 3P_{52}(N_y)$$

$$14,18 = 3P_{25}(N_x) + 11P_{34}(N_{xy}) + 6P_{43}(N_y)$$

$$14,19 = 2P_{16}(N_x) + 9P_{25}(N_{xy}) + 9P_{34}(N_y)$$

$$14,20 = P_{07}(N_x) + 7P_{16}(N_{xy}) + 12P_{25}(N_y)$$

$$14,21 = 0(N_x) + 5P_{07}(N_{xy}) + 15P_{16}(N_y)$$

$$15,15 = 0(N_{xy}) + 16P_{06}(N_y)$$

$$15,16 = 20P_{43}(N_{xy}) + 0(N_y)$$

$$15,17 = 16P_{34}(N_{xy}) + 4P_{43}(N_y)$$

$$15,18 = 12P_{25}(N_{xy}) + 8P_{34}(N_y)$$

$$15,19 = 8P_{16}(N_{xy}) + 12P_{25}(N_y)$$

$15,20 = 4P_{07}(N_{xy}) + 16P_{16}(N_y)$

$15,21 = 0(N_{xy}) + 20P_{07}(N_y)$

$16,16 = 25P_{80}(N_x) + 0(N_{xy})$

$16,17 = 20P_{71}(N_x) + 5P_{80}(N_{xy})$

$16,18 = 15P_{62}(N_x) + 10P_{71}(N_{xy})$

$16,19 = 10P_{53}(N_x) + 15P_{62}(N_{xy})$

$16,20 = 5P_{44}(N_x) + 20P_{53}(N_{xy})$

$16,21 = 0(N_x) + 25P_{44}(N_{xy})$

$17,17 = 16P_{62}(N_x) + 8P_{71}(N_{xy}) + P_{80}(N_y)$

$17,18 = 12P_{53}(N_x) + 11P_{62}(N_{xy}) + 2P_{71}(N_y)$

$17,19 = 8P_{44}(N_x) + 14P_{53}(N_{xy}) + 3P_{62}(N_y)$

$17,20 = 4P_{35}(N_x) + 17P_{44}(N_{xy}) + 4P_{53}(N_y)$

$17,21 = 0(N_x) + 20P_{35}(N_{xy}) + 5P_{44}(N_y)$

$18,18 = 9P_{44}(N_x) + 12P_{53}(N_{xy}) + 4P_{62}(N_y)$

$18,19 = 6P_{35}(N_x) + 13P_{44}(N_{xy}) + 6P_{53}(N_y)$

$18,20 = 3P_{26}(N_x) + 14P_{35}(N_{xy}) + 8P_{44}(N_y)$

$18,21 = 0(N_x) + 15P_{26}(N_{xy}) + 10P_{35}(N_y)$

$19,19 = 4P_{26}(N_x) + 12P_{35}(N_{xy}) + 9P_{44}(N_y)$

$19,20 = 2P_{17}(N_x) + 11P_{26}(N_{xy}) + 12P_{35}(N_y)$

$19,21 = 0(N_x) + 10P_{17}(N_{xy}) + 15P_{26}(N_y)$

$$20,20 = P_{08}(N_x) + 8P_{17}(N_{xy}) + 16P_{26}(N_y)$$

$$20,21 = 0(N_x) + 5P_{08}(N_{xy}) + 20P_{17}(N_y)$$

$$21,21 = 25P_{08}(N_y)$$

After this matrix is formed, it must be pre- and postmultiplied by the product $[C]'[A^{-1}]'$ and its transpose, respectively, as shown in Eq. (I.2). It must also be transformed (if required) to satisfy the boundary conditions, just as the conventional stiffness matrix $[k^{(0)}]$ is transformed (see Ref. 42 for types of boundary transformations).

The quantities P_{pq} are defined as follows:

$$P_{pq} = \iint x^p y^q dA , \qquad (I.5)$$

where

$$x = \sum_{i=1}^{3} x_i \omega_i \qquad (I.6a)$$

$$y = \sum_{i=1}^{3} y_i \omega_i \qquad (I.6b)$$

are the local Cartesian coordinates; x_i, y_i are the local nodal coordinates; the ω_i are the triangular coordinates defined in Appendix F; and A is the area of the element.

Simple formulas for P_{pq} for orders up to $n = p + q = 6$ are given in Ref. 42. However, P_{pq}'s for $n = 7,8$ are needed for the initial stress stiffness matrix. Since obtaining succinct forms for these expressions is tedious, a general formula

158

(which includes the lower order terms) is used; this is developed as follows.

By definition,

$$P_{pq} = \iint (x_1\omega_1 + x_2\omega_2 + x_3\omega_3)^P (y_1\omega_1 + y_2\omega_2 + y_3\omega_3)^q dA \ . \qquad (I.7)$$

Now $(a + b + c)^P$ may be written as

$$(a + b + c)^P = \sum_{r=0}^{p} \sum_{s=0}^{r} \binom{p}{r}\binom{r}{s} a^{p-r} b^{r-s} c^s \qquad (I.8)$$

where

$$\binom{p}{r} = \frac{p!}{r! \, (p - r)!} \ , \qquad \text{etc.}$$

Therefore,

$$P_{pq} = \iint_A \sum_{r,s,t,u} \binom{p}{r}\binom{r}{s}\binom{q}{t}\binom{t}{u} \left[x_1^{p-r} y_1^{q-t} x_2^{r-s} y_2^{t-u} x_3^s y_3^u \right] \cdot$$

$$\left(\omega_1^{n-(r+t)} \omega_2^{(r+t)-(s+u)} \omega_3^{(s+u)} \right) dA \ . \qquad (I.9)$$

But

$$\iint_A \omega_i^{M_i} \omega_j^{M_j} \omega_k^{M_k} dA = 2A \, \frac{M_i! \, M_j! \, M_k!}{(M_i + M_j + M_k + 2)!} \qquad (I.10)$$

159

(see Appendix F). Thus the final form of the integral can be written as

$$P_{pq} = 2A \frac{p! \, q!}{(p + q + 2)!} \cdot$$

$$\sum_{r=0}^{p} \sum_{s=0}^{r} \sum_{t=0}^{q} \sum_{u=0}^{t} \frac{[(p+q) - (r+t)]! [(r+t) - (s+u)]! \, [s+u]!}{(p-r)! \, (r-s)! \, (q-t)! \, (t-u)! \, s! \, u!} \cdot$$

(I.11)

$$\left[x_1^{p-r} \, y_1^{q-t} \, x_2^{r-s} \, y_2^{t-u} \, x_3^{s} \, y_3^{u} \right] \cdot$$

APPENDIX J

CALCULATION OF MEMBRANE STRESS RESULTANTS

Values of membrane stress resultants, used in forming the elements of the initial stress stiffness matrices, are required in the solution of problems of geometric nonlinearity and in the combined bending and stretching plasticity analysis. For statically determinate bending and stretching problems, e.g., a rectangular plate with a uniformly applied membrane load in one direction, the values of the membrane stress resultants remain constant throughout the analysis. However, for statically indeterminate and geometrically nonlinear problems, these membrane stress resultants must be calculated from the elastic strain distribution through the thickness at nodes for each incremental step. Various possible distributions are shown in Fig. 78a-e.

The elastic stress-strain relation for an isotropic medium may be written as follows:

$$e_x^e = \frac{1}{E}(\sigma_x - \nu\sigma_y)$$

$$e_y^e = \frac{1}{E}(\sigma_y - \nu\sigma_x) \tag{J.1}$$

$$\gamma_{xy}^e = \frac{1}{G}\tau_{xy}$$

where $G = E/2(1 + \nu)$ is the shear modulus.

Equations (J.1) may be integrated through the thickness to obtain

$$\bar{e}_x = \int e_x^e dz = \frac{1}{E}\int (\sigma_x - \nu\sigma_y)dz = \frac{1}{E}(N_x - \nu N_y) . \tag{J.2a}$$

161

Similarly,

$$\bar{e}_y = \int e_y^e dz = \frac{1}{E}(N_y - \nu N_x) \tag{J.2b}$$

$$\bar{\gamma}_{xy} = \int \gamma_{xy}^e dz = \frac{1}{G} N_{xy} . \tag{J.2c}$$

The membrane stress resultants, N_x, N_y, and N_{xy}, may be written in terms of the $\bar{e}_{ij}$ quantities as

$$N_x = \frac{E}{(1 - \nu^2)}(\bar{e}_x + \nu \bar{e}_y) \tag{J.3a}$$

$$N_y = \frac{E}{(1 - \nu^2)}(\bar{e}_y + \nu \bar{e}_x) \tag{J.3b}$$

$$N_{xy} = G\bar{\gamma}_{xy} . \tag{J.3c}$$

Since a linear distribution through the thickness is assumed for both the total and plastic strain components, we can readily determine the values of $\bar{e}_{ij}$ from the elastic strain distribution through the thickness. For a generic strain $\bar{e}$, we have from Fig. 78a

$$\bar{e} = \frac{1}{2}\left(e_U^T(2\eta t) + e_L^T(2t - 2\eta t) - \epsilon^U \bar{z}^U - \epsilon^L(2t - \bar{z}^L)\right) \tag{J.4}$$

where

$$\eta = \frac{|e_U^T|}{|e_U^T| + |e_L^T|}$$

162

and ϵ^U, ϵ^L are the plastic strains at the upper and lower surfaces, e_U^T and e_L^T are the total strains at the upper and lower surfaces, $2t$ is the thickness of the element, and $\bar{z}^U$ and $\bar{z}^L$ represent the ordinates of the upper and lower elastic-plastic boundaries, respectively, measured from the upper surface.

At an elastic node, $(\epsilon^U = \epsilon^L = 0)$, Eq. (J.4) reduces to

$$\bar{e} = e_U^T(\eta t) + e_L^T(t - \eta t) . \tag{J.5}$$

Equations (J.4) and (J.5) apply at nodes where bending predominates over membrane behavior (where the total strains at the two surfaces are of opposite sign). A fully plastic node where the total strains are of the same sign is illustrated in Fig. 78b. In this case

$$\bar{e} = \frac{t}{2}(e_U^T + e_L^T - \epsilon^U - \epsilon^L) . \tag{J.6}$$

If the section is entirely elastic, we have

$$\bar{e} = \frac{t}{2}(e_U^T + e_L^T) . \tag{J.7}$$

If only the upper or the lower surface is plastic and the total strains are of the same sign (Figs. 78c and 78d), we have

$$\bar{e} = t(e_L^T + e_U^T) - \frac{1}{2} \epsilon^U \bar{z}^U \tag{J.8}$$

(for the upper surface only)

or

$$\bar{e} = t(e_L^T + e_U^T) - \frac{1}{2} \epsilon^L(2t - \bar{z}^L) \tag{J.9}$$

(for the lower surface only)

163

Equations (J.8) and (J.9) can be combined to treat the situation shown in Fig. 78e.

$$\bar{e} = t(e_L^T + e_U^T) - \frac{1}{2}\left[\epsilon^U \bar{z}^U + \epsilon^L(2t - \bar{z}^L)\right] .$$ (J.10)

The values of N_x, N_y, and N_{xy} determined in this way are nodal values. The actual value used in the initial stress stiff-ness matrix for the triangle is the average of the three nodal values. While it may be consistent to use values for the re-sultants at the centroid of the element, such values are more difficult to obtain and require much additional calculation. The difference between centroidal and average values decreases as the element size decreases.

APPENDIX K

COMPUTING TIMES FOR SOME PLATE BENDING PROBLEMS

All computations were carried out on the Grumman/IBM 360/75 system with a standard maximum available core storage of 307 K bytes. For several combined bending and membrane problems, however, up to 512 K bytes of core storage are required. Where possible, the computer programs were written in a manner that minimized the use of peripheral storage devices. Consequently, no tape units were used. However, random access disk units are required to store components of the element initial strain stiffness and initial stress stiffness matrices for the triangular bending element.

Some typical running times are presented below for several representative problems. The running times are influenced by the amount and number of requests for printed output data as well as by the number of degrees of freedom and number of increments required for a solution.

As can be seen from the table, there is a dramatic increase in required running times for problems involving combined bending and membrane stress using the triangular element [case (i), (j), (k)]. In these problems the increased time occurs as a consequence of reforming the initial stress stiffness matrix in each increment. Consequently, the total stiffness matrix for bending must be reformed in each increment of load and then the resulting system of equations solved. By contrast, the required times are considerably reduced for bending alone, [cases (a)-(f)] or for bending and membrane problems [cases (g) and (h)] where the stiffness matrix remains unchanged throughout the entire loading range. For these problems, a solution technique is used which performs an initial factorization of the stiffness matrix so that succeeding solutions require only matrix multiplication.

The increase in computer time necessary for those problems in which it is required to solve the system of equations in each increment becomes apparent when one compares case (b) with case (j). As seen from the tabulation given below, case (j) required more than triple the running time, although identical numbers of load increments were required for both cases and, in addition, case (b) had more degrees of freedom, members and nodes. This comparison suggests that reforming the stiffness

matrix and solving the resulting system of equations in each loading step should be avoided, if possible. In several instances, however, this may not be possible (e.g., geometric nonlinearity).

COMPUTATIONAL REQUIREMENTS FOR SOME REPRESENTATIVE PROBLEMS

Case	Problem Description	Presented in Figure	Members	Degrees of Freedom	Nodes	Increments Required for Solution	Time in Min.
				Idealization			
(a)	Clamped Square Plate	46	36	121	49	469	6.89
(b)	Square Plate-Square Hole	47	72	299	91	270	14.02
(c)	Square Plate- Circular Hole	49	84	266	56	200	14.49
(d)	Simply Supported Circular Plate	51	50	153	36	170	7.05
(e)	Clamped Circular Plate	54	50 128	153 387	36 81	206 196	27.70
(f)	Simply Supported Annular Plate	56	110	320	72	120	12.94
(g)	Simply Supported Rectangular Plate $\alpha = \frac{1}{2},\ \eta = \frac{1}{2}$	60	50	115 m[+] 200 b[±]	66	241	12.80
(h)	Simply Supported Rectangular Plate In-Plane Shear	61	64	152 m 256 b	81	72	2.61
(i)	Simply Supported Circular Plate $\alpha = \frac{1}{3}$	62	128	144 m 387 b	81	133	72.3
(j)	Simply Supported Circular Plate $\alpha = 0.3$	62	50	60 m 153 b	36	270	43.3
(k)	Annular Plate $\alpha = \frac{1}{4}$	63	110	132 m 332 b	72	121	59.6

[+] membrane

[±] bending

166

APPENDIX L

ESTABLISHMENT OF LOCAL COORDINATE SYSTEM
AND COORDINATE TRANSFORMATIONS

One of the major requirements of the incremental geometric nonlinearity analysis is the establishment of the current local coordinate system in which displacements in the next incremental step are to be determined. For a beam element this task is simple. The new local longitudinal axis is directed along the actual current axis of the beam element. The transverse axis is perpendicular to it and directed toward the bottom fibers of the beam (see Fig. 79).

The transformation matrix relating the displacements re-ferred to local and global axes may be written as

$$\{\Delta d\}_\ell = [T] \{\Delta d\}_g \tag{L.1}$$

where the subscripts ℓ and g refer to local and global co-ordinate axes, respectively. For the beam element, Eq. (L.1) is written as

$$
\begin{Bmatrix} \Delta w \\ \Delta\theta \\ \Delta u \end{Bmatrix} =
\begin{bmatrix} \cos\theta & 0 & -\sin\theta \\ 0 & 1 & 0 \\ \sin\theta & 0 & \cos\theta \end{bmatrix}
\begin{Bmatrix} \Delta\bar{w} \\ \Delta\bar{\theta} \\ \Delta\bar{u} \end{Bmatrix} \tag{L.2}
$$

where Δw, $\Delta\theta$, and Δu represent the increments of lateral dis-placement, rotation of the line element about the y-axis (slope), and the axial displacement in the local system, respectively. The barred quantities are the generalized nodal displacements in the global system. We can also write

$$\cos\theta = \frac{\bar{x}_2 - \bar{x}_1}{\ell} \qquad \sin\theta = \frac{\bar{z}_2 - \bar{z}_1}{\ell}$$

where ℓ is the current value of the element length. Values of the global coordinates are obtained by summing the increments of displacement Δu and Δw at the nodes and adding them to the coordinate values in the original configuration.

Since the transformation matrix $[T]$ of Eq. (L.2) is an orthogonal matrix, we can write the relationship between the increments of nodal generalized forces $\{\Delta P\}$ in the local and global axes as

$$\left\{\Delta P\right\}_g = [T]^{-1} \left\{\Delta P\right\}_\ell = [T]' \left\{ \begin{array}{c} \Delta F_z \\ \Delta M_y \\ \Delta F_x \end{array} \right\} \qquad (L.3)$$

where ΔF_z, ΔM_y, and ΔF_x represent the increments of lateral load, bending moment about the y-axis, and axial force in the local system, respectively.

The establishment of a local coordinate system for the triangular element is more complex than that for a beam element. In the solution of pure bending and combined bending and stretching problems, where geometry changes are neglected, the local system is always parallel to the global system. However, in large-deflection problems, due to the out-of-plane deformations (or because of the original configuration in the case of a shallow shell), no single coordinate system can be used to describe the local behavior of the elements. Consequently, a decision was made to keep the x-coordinate of each local coordinate system parallel to a side of the triangle (see Fig. 80a). In particular, the 1-2 side of each element was chosen. The y-coordinate is then selected to be perpendicular to the x-coordinate and in the plane of the triangle. The z-direction is perpendicular to the plane of the triangle and its direction is determined through the use of the right-hand rule. The location of the centroid of the triangle, with respect to the global system, may now be determined by using the relationships

$$\bar{x}_c = \frac{\bar{x}_1 + \bar{x}_2 + \bar{x}_3}{3}$$

$$\bar{y}_c = \frac{\bar{y}_1 + \bar{y}_2 + \bar{y}_3}{3} \tag{L.4}$$

$$\bar{z}_c = \frac{\bar{z}_1 + \bar{z}_2 + \bar{z}_3}{3}$$

The global coordinates with origin at the centroid of the element ("local-global" coordinates) are

$$\bar{x}_{i/c} = \bar{x}_i - \bar{x}_c$$

$$\bar{y}_{i/c} = \bar{y}_i - \bar{y}_c \qquad (i = 1, 2, 3) \tag{L.5}$$

$$\bar{z}_{i/c} = \bar{z}_i - \bar{z}_c$$

where the subscript i/c denotes the local-global coordinates. Vectors in the direction of sides 1-2 and 1-3 of the triangle may be obtained from

$$\bar{R}_{12} = (\bar{x}_2 - \bar{x}_1)\bar{i} + (\bar{y}_2 - \bar{y}_1)\bar{j} + (\bar{z}_2 - \bar{z}_1)\bar{k} = a\bar{i} + b\bar{j} + c\bar{k}$$

$$\tag{L.6}$$

$$\bar{R}_{13} = (\bar{x}_3 - \bar{x}_1)\bar{i} + (\bar{y}_3 - \bar{y}_1)\bar{j} + (\bar{z}_3 - \bar{z}_1)\bar{k} = d\bar{i} + e\bar{j} + f\bar{k}$$

where a, b, c, ..., etc., are the corresponding terms in parenthesis, and $\bar{i}$, $\bar{j}$, $\bar{k}$ are unit vectors in the direction of the global $\bar{x}$, $\bar{y}$, $\bar{z}$ axes. A unit vector in the local x-direction is then

$$\bar{u}_x = \frac{a\bar{i} + b\bar{j} + c\bar{k}}{\sqrt{a^2 + b^2 + c^2}} = \cos \alpha_1 \bar{i} + \cos \alpha_2 \bar{j} + \cos \alpha_3 \bar{k} \;. \tag{L.7}$$

Hence, angles α_i ($i = 1$, 2, 3) are defined to be the angles be-
tween the local x-axis and global axes, as shown in Fig. 80b.

A vector in the direction of the local z-axis may be ob-
tained from the vector cross product of $\bar{R}_{12}$ and $\bar{R}_{13}$. A unit
vector in this direction is

$$
u_z = \frac{(bf - ec)\bar{i} + (cd - af)\bar{j} + (ae - bd)\bar{k}}{\sqrt{(bf - ec)^2 + (cd - af)^2 + (ae - bd)^2}}
$$

$$
= \cos \gamma_1 \bar{i} + \cos \gamma_2 \bar{j} + \cos \gamma_3 \bar{k} .
$$

(L.8)

The angles γ_i are the angles between the local z and global
axes, as shown in Fig. 80c. A unit vector in the y-direction
may be obtained from the vector cross product of $\bar{u}_z$ and $\bar{u}_x$

$$
\bar{u}_y = \bar{u}_z \times \bar{u}_x
$$

$$
= \frac{N_1 \bar{i} + N_2 \bar{j} + N_3 \bar{k}}{\sqrt{a^2 + b^2 + c^2} \sqrt{(bf - ec)^2 + (cd - af)^2 + (ae - bd)^2}}
$$

(L.9)

$$
= \cos \beta_1 \bar{i} + \cos \beta_2 \bar{j} + \cos \beta_3 \bar{k}
$$

where

$$
N_1 = c(cd - af) - b(ae - bd)
$$

$$
N_2 = a(ae - bd) - c(bf - ec)
$$

$$
N_3 = b(bf - ec) - a(cd - af)
$$

and the angles β_i are the angles between the local y and the
global axes, as shown in Fig. 80d. All global coordinates may
now be transformed into the local system by using the known direc-
tion cosines

170

$$\left\{ \begin{array}{c} x \\ y \\ z \end{array} \right\} = \left[\begin{array}{ccc} \cos \alpha_1 & \cos \alpha_2 & \cos \alpha_3 \\ \cos \beta_1 & \cos \beta_2 & \cos \beta_3 \\ \cos \gamma_1 & \cos \gamma_2 & \cos \gamma_3 \end{array} \right] \left\{ \begin{array}{c} \bar{x} \\ \bar{y} \\ \bar{z} \end{array} \right\} . \qquad (L.10)$$

Thus the local-global nodal coordinates $\bar{x}_{i/c}$, $\bar{y}_{i/c}$, $\bar{z}_{i/c}$ may be transformed to the local coordinates with origin at the centroid of the triangular element. All local z coordinates will be zero, and the x and y coordinates are used to form the element stiffness matrices.

The inverse relationship to that given in Eq. (L.10) is written as

$$\left\{ \begin{array}{c} \bar{x} \\ \bar{y} \\ \bar{z} \end{array} \right\} = \left[\begin{array}{ccc} \cos \alpha_1 & \cos \beta_1 & \cos \gamma_1 \\ \cos \alpha_2 & \cos \beta_2 & \cos \gamma_2 \\ \cos \alpha_3 & \cos \beta_3 & \cos \gamma_3 \end{array} \right] \left\{ \begin{array}{c} x \\ y \\ z \end{array} \right\} . \qquad (L.11)$$

The transformation of the global incremental displacements to local coordinates is of the same form as Eq. (L.10). Thus,

$$\left\{ \begin{array}{c} \Delta u \\ \Delta v \\ \Delta w \end{array} \right\} = \left[\begin{array}{ccc} \cos \alpha_1 & \cos \alpha_2 & \cos \alpha_3 \\ \cos \beta_1 & \cos \beta_2 & \cos \beta_3 \\ \cos \gamma_1 & \cos \gamma_2 & \cos \gamma_3 \end{array} \right] \left\{ \begin{array}{c} \Delta \bar{u} \\ \Delta \bar{v} \\ \Delta \bar{w} \end{array} \right\} . \qquad (L.12)$$

The transformation matrix of Eq. (L.12), denoted as $[T_d]$, is an orthogonal matrix. Thus, $[T_d]'$ is used to relate the local to global components of the increments of the generalized forces corresponding to the displacements of Eq. (L.12).

Since the moments may be treated as vectors, they will transform in the same manner as the displacements. Therefore,

$$
\left\{ \begin{array}{c} \Delta M_x \\ \Delta M_y \\ \Delta M_z \end{array} \right\} = \left[\begin{array}{ccc} \cos \alpha_1 & \cos \alpha_2 & \cos \alpha_3 \\ \cos \beta_1 & \cos \beta_2 & \cos \beta_3 \\ \cos \gamma_1 & \cos \gamma_2 & \cos \gamma_3 \end{array} \right] \left\{ \begin{array}{c} \Delta M_{\bar{x}} \\ \Delta M_{\bar{y}} \\ \Delta M_{\bar{z}} \end{array} \right\} \qquad (L.13)
$$

Equation (L.13) represents a relationship between three force quantities. However, the displacement degrees of freedom associated with these physical forces are the two slopes $w_{,x}$ and $w_{,y}$. Since ΔM_z must be zero (from plate theory), we can eliminate the third of Eqs. (L.13). This last equation then gives

$$
\Delta M_{\bar{z}} = - \left(\frac{\Delta M_{\bar{x}} \cos \gamma_1 + \Delta M_{\bar{y}} \cos \gamma_2}{\cos \gamma_3} \right) \qquad (L.14)
$$

where $\cos \gamma_3 = 0$ only if $\gamma_3 = \pi/2$; i.e., $w_{,x}$ and $w_{,y}$ are very large compared to unity. Substituting for $\Delta M_{\bar{z}}$ in the remaining two equations of Eq. (L.13) gives:

$$
\left\{ \begin{array}{c} \Delta M_x \\ \Delta M_y \end{array} \right\} = \frac{1}{\cos \gamma_3} \left[\begin{array}{c|c} (\cos \alpha_1 \cos \gamma_3 & (\cos \alpha_2 \cos \gamma_3 \\ - \cos \alpha_3 \cos \gamma_1) & - \cos \alpha_3 \cos \gamma_2) \\ \hline (\cos \beta_1 \cos \gamma_3 & (\cos \beta_2 \cos \gamma_3 \\ - \cos \beta_3 \cos \gamma_1) & - \cos \beta_3 \cos \gamma_2) \end{array} \right] \left\{ \begin{array}{c} \Delta M_{\bar{x}} \\ \Delta M_{\bar{y}} \end{array} \right\} \qquad (L.15)
$$

or

$$
\left\{ \Delta M \right\}_\ell = [T_m] \left\{ \Delta M \right\}_g . \qquad (L.16)
$$

172

Using this as our guide, we write

$$
\left\{ \begin{array}{c} \Delta w,_x \\ \\ \Delta w,_y \end{array} \right\} = [T_m] \left\{ \begin{array}{c} \overline{\Delta w},_{\overline{x}} \\ \\ \overline{\Delta w},_{\overline{y}} \end{array} \right\} . \tag{L.17}
$$

Since we have eliminated ΔM_z from Eqs. (L.13), we do not have an orthogonal transformation, i.e.,

$$
[T_m]'[T_m] = [I] + 0(\theta^2) .
$$

where θ^2 is equivalent to the nonlinear terms (i.e., squares of rotations) in the strain-displacement relations of Eq. (6). To maintain a symmetric striffness matrix, we use the relationship

$$
\left\{ \Delta M \right\}_g = [T_m]' \left\{ \Delta M \right\}_\ell , \tag{L.18}
$$

fully realizing that the approximation involved requires the slopes (actually total slope of the surface) to be small compared to unity. Hence this analysis is limited to plates and shallow shells.

The derivation of a relationship between curvatures in the local and global systems is even more difficult. The three quantities $w,_{xx}$, $w,_{xy}$, $w,_{yy}$ in local coordinates must be expressed in terms of eighteen global quantities (i.e., $\overline{w},_{\overline{xx}}$, $\overline{w},_{\overline{xy}}$, $\overline{w},_{\overline{yy}}$, $\overline{w},_{\overline{xz}}$, $\overline{w},_{\overline{yz}}$, $\overline{w},_{\overline{zz}}$, $\overline{u},_{\overline{xx}}$, $\overline{u},_{\overline{xy}}$, ..., $\overline{v},_{\overline{xx}}$, ..., $\overline{v},_{\overline{zz}}$) if an exact transformation of derivatives is made. This leads to unwieldly stiffness matrices. Some approximations will be made in order to obtain a suitable transformation relation for the curvatures. These approximations are based on the nature of the theory used, the element properties, and the types of problems to be solved.

We have from Eq. (L.12), recalling that $[T_d]' = [T_d]^{-1}$,

$$
\overline{\Delta w} = \Delta u \cos \alpha_3 + \Delta v \cos \beta_3 + \Delta w \cos \gamma_3 . \tag{L.19}
$$

173

Then,

$$\Delta \bar{w},_{\bar{x}} = (\Delta u \cos \alpha_3 + \Delta v \cos \beta_3 + \Delta w \cos \gamma_3),_{\bar{x}} \qquad (L.20)$$

or, using the chain rule,

$$\Delta \bar{w},_{\bar{x}} = \Delta \bar{w},_x \frac{\partial x}{\partial \bar{x}} + \Delta \bar{w},_y \frac{\partial y}{\partial \bar{y}} + \Delta \bar{w},_z \frac{\partial z}{\partial \bar{z}} \qquad (L.21)$$

Since we are dealing with linear transformation relations between local and global coordinates, we have:

$$x,_{\bar{x}\bar{x}} = y,_{\bar{x}\bar{x}} = z,_{\bar{x}\bar{x}} = 0 \ . \qquad (L.22)$$

Thus

$$\Delta \bar{w},_{\bar{x}\bar{x}} = \Delta \bar{w},_{xx} \left(\frac{\partial x}{\partial \bar{x}}\right)^2 + \Delta \bar{w},_{yx} \left(\frac{\partial y}{\partial \bar{x}}\right)\left(\frac{\partial x}{\partial \bar{x}}\right) + \Delta \bar{w},_{zx} \left(\frac{\partial z}{\partial \bar{x}}\right)\left(\frac{\partial x}{\partial \bar{x}}\right)$$

$$+ \Delta \bar{w},_{xy} \left(\frac{\partial x}{\partial \bar{x}}\right)\left(\frac{\partial y}{\partial \bar{x}}\right) + \Delta \bar{w},_{yy} \left(\frac{\partial y}{\partial \bar{x}}\right)^2 + \Delta \bar{w},_{zy} \left(\frac{\partial z}{\partial \bar{x}}\right)\left(\frac{\partial y}{\partial \bar{x}}\right) \qquad (L.23)$$

$$+ \Delta \bar{w},_{xz} \left(\frac{\partial x}{\partial \bar{x}}\right)\left(\frac{\partial z}{\partial \bar{x}}\right) + \Delta \bar{w},_{yz} \left(\frac{\partial y}{\partial \bar{x}}\right)\left(\frac{\partial z}{\partial \bar{x}}\right) + \Delta \bar{w},_{zz} \left(\frac{\partial z}{\partial \bar{x}}\right)^2 \ .$$

The final form of the expression for $\Delta \bar{w},_{\bar{x}\bar{x}}$ is obtained by substituting for $\Delta \bar{w}$ from Eq. (L.19) and recalling from plate theory that Δu, Δv, and Δw are not functions of the z-coordinate. In addition, since Δu and Δv are chosen to be linear functions of x and y, all second and mixed derivatives of Δu and Δv with respect to x, y, and z are zero. Also,

$$\frac{\partial x}{\partial \bar{x}} = \cos \alpha_1 \quad , \quad \frac{\partial y}{\partial \bar{x}} = \cos \beta_1 \quad , \quad \ldots, \quad \text{etc.}$$

Therefore,

$$\Delta \bar{w},_{\bar{x}\bar{x}} = \cos \gamma_3 \Big[\Delta w,_{xx} \cos^2 \alpha_1 + \Delta w,_{xy} \cos \alpha_1 \cos \beta_1 +$$

$$\Delta w,_{yx} \cos \alpha_1 \cos \beta_1 + \Delta w,_{yy} \cos^2 \beta_1 \Big] \qquad \text{(L.24a)}$$

Following the same procedure, we find

$$\Delta \bar{w},_{\bar{x}\bar{y}} = \cos \gamma_3 \Big[\Delta w,_{xx} \cos \alpha_1 \cos \alpha_2 + \Delta w,_{xy} \cos \alpha_1 \cos \beta_2 +$$

$$\Delta w,_{yx} \cos \alpha_2 \cos \beta_1 + \Delta w,_{yy} \cos \beta_1 \cos \beta_2 \Big] \qquad \text{(L.24b)}$$

$$\Delta \bar{w},_{\bar{y}\bar{x}} = \cos \gamma_3 \Big[\Delta w,_{xx} \cos \alpha_1 \cos \alpha_2 + \Delta w,_{xy} \cos \alpha_2 \cos \beta_1 +$$

$$\Delta w,_{yx} \cos \alpha_1 \cos \beta_2 + \Delta w,_{yy} \cos \beta_1 \cos \beta_2 \Big] \qquad \text{(L.24c)}$$

$$\Delta \bar{w},_{\bar{y}\bar{y}} = \cos \gamma_3 \Big[\Delta w,_{xx} \cos^2 \alpha_2 + \Delta w,_{xy} \cos \alpha_2 \cos \beta_2 +$$

$$\Delta w,_{yx} \cos \alpha_2 \cos \beta_2 + \Delta w,_{yy} \cos^2 \beta_2 \Big] \qquad \text{(L.24d)}$$

Equations (L.24a) through (L.24d) represent the transformation of the in-plane curvature "tilted" by the angle γ_3. Thus the transformation relations between curvature may be written as

$$\Big\{ \Delta \kappa \Big\}_g = [T_\kappa]^{-1} \Big\{ \Delta \kappa \Big\}_\ell \qquad \text{(L.25)}$$

where

$$[T_K]^{-1} = \begin{bmatrix} \cos^2\alpha_1 & \cos\alpha_1\cos\beta_1 & \cos\alpha_1\cos\beta_1 & \cos^2\beta_1 \\ \cos\alpha_1\cos\alpha_2 & \cos\alpha_1\cos\beta_2 & \cos\alpha_2\cos\beta_1 & \cos\beta_1\cos\beta_2 \\ \cos\alpha_1\cos\alpha_2 & \cos\alpha_2\cos\beta_1 & \cos\alpha_1\cos\beta_2 & \cos\beta_1\cos\beta_2 \\ \cos^2\alpha_2 & \cos\alpha_2\cos\beta_2 & \cos\alpha_2\cos\beta_2 & \cos^2\beta_2 \end{bmatrix}$$

and

$$\{\Delta\kappa\}_g = \begin{Bmatrix} \Delta\bar{w},_{\bar{x}\bar{x}} \\ \Delta\bar{w},_{\bar{x}\bar{y}} \\ \Delta\bar{w},_{\bar{y}\bar{x}} \\ \Delta\bar{w},_{\bar{y}\bar{y}} \end{Bmatrix} \quad ; \quad \{\Delta\kappa\}_\ell = \begin{Bmatrix} \Delta w,_{xx} \\ \Delta w,_{xy} \\ \Delta w,_{yx} \\ \Delta w,_{yy} \end{Bmatrix}.$$

Once again $[T_K]'[T_K] = [I]$ only for flat configurations. For shallow configurations the error will be small. Thus, we use

$$\{\Delta\kappa\}_\ell = [T_K]\,\{\Delta\kappa\}_g \qquad\qquad (L.26)$$

and to maintain symmetry of the stiffness matrix,

$$\{\Delta P_K\}_g = [T_K]'\,\{\Delta P_K\}_\ell \qquad\qquad (L.27)$$

where $\{\Delta P_K\}$ represents the generalized nodal forces associated with the curvatures.

176

Finally, the over-all transformation matrix $[T]$ of Eq. (L.1) is written as

$$[T] = \begin{array}{c} \Delta u \\ \Delta v \\ \Delta w \\ \Delta w,_x \\ \Delta w,_y \\ \Delta w,_{xx} \\ \Delta w,_{xy} \\ \Delta w,_{yx} \\ \Delta w,_{yy} \end{array} \begin{matrix} \Delta \bar{u} \quad \Delta \bar{v} \quad \Delta \bar{w} & \Delta \bar{w},_{\bar{x}} \quad \Delta \bar{w},_{\bar{y}} & \Delta \bar{w},_{\bar{x}\bar{x}} \quad \Delta \bar{w},_{\bar{x}\bar{y}} \quad \Delta \bar{w},_{\bar{y}\bar{x}} \quad \Delta \bar{w},_{\bar{y}\bar{y}} \\ \left[\begin{array}{ccc|cc|cccc} & [T_d] & & & 0 & & & 0 & \\ \hline & 0 & & & [T_m] & & & 0 & \\ \hline & 0 & & & 0 & & & [T_K] & \end{array}\right] \end{matrix}$$

(L.28)

REFERENCES

1. Padlog, J., Huff, R. D., and Holloway, G. F., "The Unelastic Behavior of Structures Subjected to Cyclic, Thermal, and Mechanical Stressing Conditions," WADD-TR-60-271, 1960.

2. Percy, J. H., Loden, W. A., and Navaratna, D. R., "A Study of Matrix Analysis Methods for Inelastic Structures," RTD-TDR-63-4032, 1963.

3. Marçal, P. V., "A Stiffness Method for Elastic-Plastic Problems," Int. J. Mech. Sci., Vol. 7, 1965.

4. Argyris, J. H., "Continua and Discontinua," Proceedings of Conference on Matrix Methods in Structural Mechanics, Wright-Patterson AFB, Ohio, October 1965, AFFDL-TR-66-80.

5. Lansing, W., Jensen, W. R., and Falby, W., "Matrix Analysis Methods for Inelastic Structures," Proceedings of Conference on Matrix Methods in Structural Mechanics, Wright-Patterson AFB, Ohio, October 26-28, 1965, AFFDL-TR-66-80.

6. Pope, G. G., "The Application of the Matrix Displacement Method in Plane Elasto-Plastic Problems," Proceedings of Conference on Matrix Methods in Structural Mechanics, Wright-Patterson AFB, Ohio, October 26-28, 1965, AFFDL-TR-66-80.

7. Zienkiewicz, O. C., Valliappan, S., and King, I. P., "Elasto-Plastic Solutions of Engineering Problems: Initial Stress, Finite Element Approach," International Journal for Numerical Methods in Engineering, Vol. 1, No. 1, January-March 1969, pp. 75-100.

8. Marçal, P. V. and King, I. P., "Elastic-Plastic Analysis of Two-Dimensional Stress Systems by the Finite Element Method," Int. J. of Mech. Sci., Vol. 9, 1967, pp. 143-155.

9. Armen, H., Jr., Isakson, G., and Pifko, A., "Discrete Element Methods for the Plastic Analysis of Structures Subjected to Cyclic Loading," Proceedings of AIAA/ASME 8th Structures, Structural Dynamics, and Materials Conference, Palm Springs, California, March 1967, pp. 148-161 (to be published in International Journal for Numerical Methods in Engineering).

10. Khojasteh-Bakht, M., "Analysis of Elastic-Plastic Shells of Revolution under Axisymmetric Loading by the Finite Element Method," Structures and Materials Research, Department of Civil Engineering, University of California, Berkeley, SESM 67-8, April 1967.

11. Isakson, G., Armen, H., Jr., and Pifko, A., "Discrete-Element Methods for the Plastic Analysis of Structures," NASA Contractors Report, CR-803, October 1967.

12. Popov, E. P., Khojasteh-Bakht, M., and Yaghmai, S., "Analysis of Elastic-Plastic Circular Plates," ASCE J. Eng. Mech. Div., Vol. 93, No. EM6, December 1967, pp. 49-65.

13. Popov, E. P., Khojasteh-Bakht, M., and Yaghmai, S., "Bending of Circular Plates of Hardening Material," Int. J. Solids and Structures, Vol. 3, 1967, pp. 975-988.

14. Marçal, P. V., "A Comparative Study of Numerical Methods of Elastic-Plastic Analysis," AIAA Journal, Vol. 6, No. 1, January 1968, p. 157.

15. Armen, H., Jr., Pifko, A., and Levine, H. S., "A Finite Element Method for the Plastic Bending Analysis of Structures," Proceedings of Air Force Second Conference on Matrix Methods in Structural Mechanics, Wright-Patterson AFB, Ohio, October 15-17, 1968, AFFDL-TR-68-150.

16. Murray, D. W. and Wilson, E. L., "An Approximate Nonlinear Analysis of Thin Plates," Proceedings of Air Force Second Conference on Matrix Methods in Structural Mechanics, Wright-Patterson AFB, Ohio, October 15-17, 1968, AFFDL-TR-68-150.

17. Witmer, E. A. and Kotanchik, J. J., "Progress Report on Discrete-Element Elastic and Elastic-Plastic Analyses of Shells of Revolution Subjected to Axisymmetric and Asymmetric Loading," Proceedings of Air Force Second Conference on Matrix Methods in Structural Mechanics, Wright-Patterson AFB, Ohio, October 15-17, 1968, AFFDL-TR-68-150.

18. Stanton, E. L., "A Discrete Element Analysis of Elastoplastic Plates," Case Western Reserve University, Division of Solid Mechanics Structures and Mechanical Design, Report No. 27.

19. Yamada, T., Kawai, T., Yoshimura, N., and Sakurai, T., "Analysis of the Elastic-Plastic Problems by the Matrix Displacement Method," Proceedings of Air Force Second Conference on Matrix Methods in Structural Mechanics, Wright-Patterson AFB, Ohio, October 15-17, 1968, AFFDL-TR-68-150.

20. Yamada, T., Yoshimura, N., Sakurai, T., "Plastic Stress-Strain Matrix and Its Application for the Solution of Elastic-Plastic Problems by the Finite Element Method," Int. J. Mech. Sci., Vol. 10, 1968, pp. 343-354.

21. Prager, W., "The Theory of Plasticity: A Survey of Recent Achievements," (James Clayton Lecture) Proc. Instn. Mech. Engrs., Vol. 169, 1955, p. 41.

22. Prager, W., "A New Method of Analyzing Stress and Strains in Work-Hardening Plastic Solids," J. Appl. Mech., Vol. 23, 1956, p. 493.

23. Ziegler, H., "A Modification of Prager's Hardening Rule," Quart. Appl. Math., Vol. 17, No. 1, 1959, p. 55.

24. Mendelson, A. and Manson, S. S., "Practical Solution of Plastic Deformation Problems in the Elastic-Plastic Range," NASA TR-R-28, 1959.

25. Lin, T. H., Theory of Inelastic Structures, John Wiley and Sons, Inc., 1969.

26. Crews, J. H., Jr., "Local Plastic Stresses in Sheet Aluminum-Alloy Specimens with Stress-Concentration Factor of 2 Under Constant-Amplitude Loading," NASA TN-D-3152, December 1965.

27. Crews, J. H., Jr., Private Communication, NASA Langley Research Center, August 1967.

28. Crews, J. H., Jr., Private Communication, NASA Langley Research Center, February 1969.

29. Argyris, J. H., "Triangular Elements with Linearly Varying Strain for the Matrix Displacement Method," J. Royal Aero. Soc., Vol. 60, 1965, p. 711.

30. De Veubeke, B. F., "Displacement and Equilibrium Models in the Finite Element Method," in Stress Analysis, edited by Zienkiewicz and Hollister, John Wiley and Sons, Ltd., 1965, p. 145.

31. Neuber, H., "Theory of Notch Stresses: Principles for Exact Calculation of Strength with Reference to Structural Form and Material," AEC-TR-4547, U.S. Atomic Energy Comm., 1961.

32. Howland, R. C. J., "On the Stress in the Neighborhood of a Circular Hole in a Strip Under Tension," Trans. of the Royal Society, London, Series A, Vol. 229, 1929-1930, pp. 49-86.

33. Griffith, G. E., "Experimental Investigation of the Effects of Plastic Flow in a Tension Panel with a Circular Hole," NACA TN 1705, 1948.

34. Harris, H. G., Armen, H., Jr., and Pifko, A., "A Method for Determining the Stress Distribution in Plates with Squeeze Rivets," Grumman Aerospace Corporation A.D. Report No. 000-St. Mech. - 029, April 1969.

35. Hodge, P. G., Jr. and Belytschko, T., "Numerical Methods for the Limit Analysis of Plates," Journal of Applied Mechanics, Vol. 35, December 1968, pp. 796-802.

36. Prager, W. and Hodge, P. G., Jr., Theory of Perfectly Plastic Solids, J. Wiley and Sons, Inc., New York, 1951.

37. Haythornthwaite, R. M., "The Deflections of Plates in the Elastic-Plastic Range," Proceedings, 2nd U.S. National Congress of Applied Mechanics, Ann Arbor, Michigan, 1954, pp. 521-526.

38. Bhaumik, A. K. and Hanley, J. T., "Elasto-Plastic Plate Analysis by Finite Differences," Journal of the Structural Division, ASCE, October 1967, pp. 279-294.

39. Ang, A. H. S. and Lopez, L. A., "Discrete Model Analysis of Elastic-Plastic Plates," Journal of the Engineering Mechanics Division, ASCE, Vol. 94, No. EM1, February 1968, pp. 271-293.

182

40. Drucker, D. C., Prager, W., and Greenberg, H. J., "Extended Limit Design Theorems of Continuous Media," Quart. Appl. Math., Vol. 9, 1952, pp. 381-389.

41. Bogner, F. K., Fox, R. L., and Schmit, L. A., Jr., "The Generation of Interelement, Compatible Stiffness and Mass Matrices by the Use of Interpolation Formulas," Proceedings of Conference on Matrix Methods in Structural Mechanics, Wright-Patterson AFB, Ohio, October 26-28, 1965, AFFDL-TR-66-80.

42. Bell, K., "Analysis of Thin Plates in Bending Using Triangular Finite Elements," Institutt for Statikk, Norges Tekniske Hogskole, Trondheim, February 1968.

43. Argyris, J. H., Buck, K. E., Fried, I., Hilber, H. M., Mareczek, G., and Scharpf, D. W., "Some New Elements for the Matrix Displacement Method," Proceedings of Air Force Second Conference on Matrix Methods in Structural Mechanics, Wright-Patterson AFB, Ohio, October 15-17, 1968, AFFDL-TR-68-150.

44. Cowper, G. R., Kosko, E., Lindberg, G. M., and Olson, M. D., "A High Precision Triangular Plate-Bending Element," Aeronautical Report LR-514, National Research Council of Canada, Ottawa, December 1968.

45. Martin, H. C., "On the Derivation of Stiffness Matrices for the Analysis of Large Deflection and Stability Problems," Proceedings of Conference on Matrix Methods in Structural Mechanics, Wright-Patterson AFB, Ohio, October 26-28, 1965, AFFDL-TR-66-80.

46. Hodge, P. G., Jr., Plastic Analysis of Structures, McGraw-Hill Book Company, Inc., New York, 1959.

47. Shull, H. E. and Hu, L. W., "Load-Carrying Capacities of Simply Supported Rectangular Plates," Journal of Applied Mechanics, Vol. 30, No. 4, December 1963, pp. 617-621.

48. Sawczuk, A. and Jaeger, T., Grenztragfahigskeit - Theorie der Platten, Springer-Verlag, Berlin, 1963.

49. Lo, C. C. and Leissa, A. W., "Bending of Plates with Circular Holes," Acta Mechanica, Vol. IV, No. 1, 1967, pp. 64-78.

50. Hopkins, H. G. and Wang, A. J., "Load-Carrying Capacities for Circular Plates of Perfectly-Plastic Material with Arbitrary Yield Condition," Journal of the Mechanics and Physics of Solids, London, Vol. 3, 1954, pp. 117-129.

51. Timoshenko, S. and Woinowsky-Krieger, S., Theory of Plates and Shells, McGraw-Hill Book Co., New York, 1959.

52. Hodge, P. G., Limit Analysis of Rotationally Symmetric Plates and Shells, Prentice-Hall, Inc., New Jersey, 1963.

53. Felippa, C. A., "Refined Finite Element Analysis of Linear and Nonlinear Two Dimensional Structures," Structures and Materials Research Report, Department of Civil Engineering Report No. 66-22, University of California, Berkeley, October 1966.

54. Backus, W. E. and Mello, R. M., "Some Applications of Finite Element Analysis to Shell Buckling Prediction," Proceedings of Air Force Second Conference on Matrix Methods in Structural Mechanics, Wright-Patterson AFB, Ohio, October 15-17, 1968, AFFDL-TR-68-150.

55. Mallett, R. and Marçal, P., "Finite Element Analysis of Nonlinear Structures," Proceedings of ASCE, J. Struc. Div., Vol. 94, No. ST9, September 1968.

56. Marçal, P. V., "The Effect of Initial Displacement on Problems of Large Deflections and Stability," Division of Engineering, Brown University, Providence, R.I., November 1967.

57. Oden, J. T. and Kubitza, W. K., "Numerical Analysis of Nonlinear Pneumatic Structures," Proceedings, International Colloquium on Pneumatic Structures, Stuttgart, Germany, 1967.

58. Pifko, A. and Isakson, G., "A Finite Element Method for the Plastic Buckling Analysis of Plates," AIAA Journal, Vol. 7, No. 10, October 1969.

59. Wempner, G. and Kesti, N., "On the Buckling of Circular Arches and Rings," Proceedings of the Fourth U.S. National Congress of Applied Mechanics, (American Society of Mechanical Engineers, New York, 1962), Vol. 2.

60. Gallagher, R. H., Gellatly, R. A., Padlog, J., and Mallett, R. H., "A Discrete Element Procedure for Thin Shell Instability Analysis," AIAA Journal, Vol. 5, No. 1, January 1967.

61. Gjelsvik, A. and Bodner, S. R., "The Energy Criterion and Snap Buckling of Arches," Journal of the Engineering Mechanics Division, Proc. ASCE, Vol. 88, No. EM5, October 1962.

62. Mallett, R. H. and Berke, L., "Automated Method for the Large Deflection and Instability Analysis of Three-dimensional Truss and Frame Assemblies," AFFDL-TR-66-102, December 1966.

63. Lee, L. H. N. and Murphy, L. M., "Inelastic Buckling of Shallow Arches," Journal of the Engineering Mechanics Division, Proc. ASCE, Vol. 94, No. EM1, February 1968.

64. Drucker, D. C., "A More Fundamental Approach to Plastic Stress-Strain Relations," Proceedings, 1st U.S. National Congress of Applied Mechanics (Chicago, 1951), New York, 1952, p. 487.

65. Ramberg, W. and Osgood, W. R., "Description of Stress-Strain Curves by Three Parameters," NACA TN 902, 1943.

66. Bergan, P. G., "Plane Stress Analysis Using the Finite Element Method. Triangular Element with 6 Parameters in each Node," Report published at the Division of Structural Mechanics, the Technical University of Norway (NTH), Trondheim, October 1967.

185

TABLE I
COEFFICIENTS OF L(I,J) FOR USE IN FORMING INITIAL STRAIN MATRIX FOR RECTANGULAR ELEMENT.

	(1,1)	(1,2)	(1,3)	(1,4)	(1,5)	(1,6)
Z * T**2	-7/ 20	-7/ 20	1/ 4	7/ 20	-3/ 20	1/ 4
T * Z11	4/ 15	4/ 15	-9/ 100	0/ 1	1/ 12	-3/ 50
T * Z12	1/ 12	0/ 1	-3/ 50	0/ 1	0/ 1	-1/ 25
T * Z21	0/ 1	1/ 12	-3/ 50	-4/ 15	1/ 15	-9/ 100
T * Z22	0/ 1	0/ 1	-1/ 25	-1/ 12	0/ 1	-3/ 50
Z11**2	27/ 140	27/ 140	-1/ 25	3/ 140	33/ 700	-1/ 50
Z12**2	39/ 1400	-3/ 140	-1/ 50	13/ 4200	-11/ 2100	-1/ 100
Z21**2	-3/ 140	39/ 1400	-1/ 50	-27/ 140	9/ 280	-1/ 25
Z22**2	-13/ 4200	-13/ 4200	-1/ 100	-39/ 1400	-1/ 280	-1/ 50
Z11 * Z12	33/ 350	3/ 70	-1/ 25	11/ 1050	11/ 1050	-1/ 50
Z11 * Z21	3/ 70	33/ 350	-1/ 25	-3/ 70	39/ 700	-1/ 25
Z11 * Z22	11/ 1050	11/ 1050	-1/ 50	-11/ 1050	13/ 2100	-1/ 50
Z12 * Z21	11/ 1050	11/ 1050	-1/ 50	-11/ 1050	13/ 2100	-1/ 50
Z12 * Z22	13/ 2100	-11/ 1050	-1/ 50	-13/ 2100	-13/ 2100	-1/ 50
Z21 * Z22	-11/ 1050	13/ 2100	-1/ 50	-33/ 350	1/ 140	-1/ 25

	(1,7)	(1,8)	(1,9)	(1,10)	(1,11)	(1,12)
Z * T**2	-3/ 20	7/ 20	1/ 4	3/ 20	3/ 20	1/ 4
T * Z11	1/ 12	0/ 1	-3/ 50	0/ 1	0/ 1	-1/ 25
T * Z12	1/ 15	-4/ 15	-9/ 100	0/ 1	-1/ 12	-3/ 50
T * Z21	0/ 1	0/ 1	-1/ 25	-1/ 12	0/ 1	-3/ 50
T * Z22	0/ 1	-1/ 12	-3/ 50	-1/ 15	-1/ 15	-9/ 100
Z11**2	33/ 700	3/ 140	-1/ 50	11/ 2100	11/ 2100	-1/ 100
Z12**2	9/ 280	-27/ 140	-1/ 25	1/ 280	-33/ 700	-1/ 50
Z21**2	-11/ 2100	13/ 4200	-1/ 100	-33/ 700	1/ 280	-1/ 50
Z22**2	-1/ 280	-39/ 1400	-1/ 50	-9/ 280	-9/ 280	-1/ 25
Z11 * Z12	39/ 700	-3/ 70	-1/ 25	13/ 2100	-11/ 1050	-1/ 50
Z11 * Z21	11/ 1050	11/ 1050	-1/ 50	-11/ 1050	13/ 2100	-1/ 50
Z11 * Z22	13/ 2100	-11/ 1050	-1/ 50	-13/ 2100	-13/ 2100	-1/ 50
Z12 * Z21	13/ 2100	-11/ 1050	-1/ 50	-13/ 2100	-13/ 2100	-1/ 50
Z12 * Z22	1/ 140	-33/ 350	-1/ 25	-1/ 140	-39/ 700	-1/ 25
Z21 * Z22	-13/ 2100	-13/ 2100	-1/ 50	-39/ 700	-1/ 140	-1/ 25

	(2,1)	(2,2)	(2,3)	(2,4)	(2,5)	(2,6)
Z * T**2	-7/ 20	-1/ 20	-1/ 24	0/ 1	-1/ 30	1/ 24
T * Z11	2/ 9	1/ 30	3/ 100	2/ 45	1/ 60	-1/ 200
T * Z12	5/ 72	0/ 1	1/ 50	1/ 72	0/ 1	-1/ 300
T * Z21	2/ 45	1/ 60	-1/ 200	-2/ 45	1/ 60	-1/ 50
T * Z22	1/ 72	0/ 1	-1/ 300	-1/ 72	0/ 1	-1/ 75
Z11**2	3/ 20	3/ 140	1/ 50	1/ 35	3/ 350	0/ 1
Z12**2	13/ 600	-1/ 420	1/ 100	13/ 3150	-1/ 1050	0/ 1
Z21**2	1/ 140	9/ 1400	-1/ 300	-3/ 70	3/ 350	-1/ 100
Z22**2	13/ 12600	-1/ 1400	-1/ 600	-13/ 2100	-1/ 1050	-1/ 200
Z11 * Z12	11/ 150	1/ 210	1/ 50	22/ 1575	1/ 525	0/ 1
Z11 * Z21	2/ 35	3/ 175	0/ 1	1/ 70	9/ 700	-1/ 150
Z11 * Z22	22/ 1575	1/ 525	0/ 1	11/ 3150	1/ 700	-1/ 300
Z12 * Z21	22/ 1575	1/ 525	0/ 1	11/ 3150	1/ 700	-1/ 300
Z12 * Z22	13/ 1575	-1/ 525	0/ 1	13/ 6300	-1/ 700	-1/ 300
Z21 * Z22	11/ 3150	1/ 700	-1/ 300	-11/ 525	1/ 525	-1/ 100

	(2,7)	(2,8)	(2,9)	(2,10)	(2,11)	(2,12)
Z * T**2	-3/ 20	1/ 20	-1/ 24	0/ 1	1/ 30	1/ 24
T * Z11	5/ 72	0/ 1	1/ 50	1/ 72	0/ 1	-1/ 300
T * Z12	1/ 18	-1/ 30	3/ 100	1/ 90	-1/ 60	-1/ 200
T * Z21	1/ 72	0/ 1	-1/ 300	-1/ 72	0/ 1	-1/ 75
T * Z22	1/ 90	-1/ 60	-1/ 200	-1/ 90	-1/ 60	-1/ 50
Z11**2	11/ 300	1/ 420	1/ 100	11/ 1575	1/ 1050	0/ 1
Z12**2	1/ 40	-3/ 140	1/ 50	1/ 210	-3/ 350	0/ 1
Z21**2	11/ 6300	1/ 1400	-1/ 600	-11/ 1050	1/ 1050	-1/ 200
Z22**2	1/ 840	-9/ 1400	-1/ 300	-1/ 140	-3/ 350	-1/ 100
Z11 * Z12	13/ 300	-1/ 210	1/ 50	13/ 1575	-1/ 525	0/ 1
Z11 * Z21	22/ 1575	1/ 525	0/ 1	11/ 3150	1/ 700	-1/ 300
Z11 * Z22	13/ 1575	-1/ 525	0/ 1	13/ 6300	-1/ 700	-1/ 300
Z12 * Z21	13/ 1575	-1/ 525	0/ 1	13/ 6300	-1/ 700	-1/ 300
Z12 * Z22	1/ 105	-3/ 175	0/ 1	1/ 420	-9/ 700	-1/ 150
Z21 * Z22	13/ 6300	-1/ 700	-1/ 300	-13/ 1050	-1/ 525	-1/ 100

186

TABLE I
COEFFICIENTS OF L(I,J) FOR USE IN FORMING INITIAL STRAIN MATRIX FOR RECTANGULAR ELEMENT (Cont.)

	(3,1)	(3,2)	(3,3)	(3,4)	(3,5)	(3,6)
L * T**2	-1/ 20	-7/ 20	-1/ 24	1/ 20	-3/ 20	-1/ 24
T * L11	1/ 30	2/ 9	3/ 100	0/ 1	5/ 72	1/ 50
T * L12	1/ 60	2/ 45	-1/ 200	0/ 1	1/ 72	-1/ 300
T * L21	0/ 1	5/ 72	1/ 50	-1/ 30	1/ 18	3/ 100
T * L22	0/ 1	1/ 72	-1/ 300	-1/ 60	1/ 90	-1/ 200
L11**2	3/ 140	3/ 20	1/ 50	1/ 420	11/ 300	1/ 100
L12**2	9/ 1400	1/ 140	-1/ 300	1/ 1400	11/ 6300	-1/ 600
L21**2	-1/ 420	13/ 600	1/ 100	-3/ 140	1/ 40	1/ 50
L22**2	-1/ 1400	13/12600	-1/ 600	-9/ 1400	1/ 840	-1/ 300
L11 * L12	3/ 175	2/ 35	0/ 1	1/ 525	22/ 1575	0/ 1
L11 * L21	1/ 210	11/ 150	1/ 50	-1/ 210	13/ 300	1/ 50
L11 * L22	1/ 525	22/ 1575	0/ 1	-1/ 525	13/ 1575	0/ 1
L12 * L21	1/ 525	22/ 1575	0/ 1	-1/ 525	13/ 1575	0/ 1
L12 * L22	1/ 700	11/ 3150	-1/ 300	-1/ 700	13/ 6300	-1/ 300
L21 * L22	-1/ 525	13/ 1575	0/ 1	-3/ 175	1/ 105	0/ 1

	(3,7)	(3,8)	(3,9)	(3,10)	(3,11)	(3,12)
L * T**2	-1/ 30	0/ 1	1/ 24	1/ 30	0/ 1	1/ 24
T * L11	1/ 60	2/ 45	-1/ 200	0/ 1	1/ 72	-1/ 300
T * L12	1/ 60	-2/ 45	-1/ 50	0/ 1	-1/ 72	-1/ 75
T * L21	0/ 1	1/ 72	-1/ 300	-1/ 60	1/ 90	-1/ 200
T * L22	0/ 1	-1/ 72	-1/ 75	-1/ 60	-1/ 90	-1/ 50
L11**2	3/ 350	1/ 35	0/ 1	1/ 1050	11/ 1575	0/ 1
L12**2	3/ 350	-3/ 70	-1/ 100	1/ 1050	-11/ 1050	-1/ 200
L21**2	-1/ 1050	13/ 3150	0/ 1	-3/ 350	1/ 210	0/ 1
L22**2	-1/ 1050	-13/ 2100	-1/ 200	-3/ 350	-1/ 140	-1/ 100
L11 * L12	9/ 700	1/ 70	-1/ 150	1/ 700	11/ 3150	-1/ 300
L11 * L21	1/ 525	22/ 1575	0/ 1	-1/ 525	13/ 1575	0/ 1
L11 * L22	1/ 700	11/ 3150	-1/ 300	-1/ 700	13/ 6300	-1/ 300
L12 * L21	1/ 700	11/ 3150	-1/ 300	-1/ 700	13/ 6300	-1/ 300
L12 * L22	1/ 525	-11/ 525	-1/ 100	-1/ 525	-13/ 1050	-1/ 100
L21 * L22	-1/ 700	13/ 6300	-1/ 300	-9/ 700	1/ 420	-1/ 150

	(4,1)	(4,2)	(4,3)	(4,4)	(4,5)	(4,6)
L * T**2	-1/ 20	-1/ 20	1/ 144	0/ 1	-1/ 30	-1/ 144
T * L11	1/ 36	1/ 36	-1/ 100	1/ 180	1/ 72	1/ 600
T * L12	1/ 72	1/ 180	1/ 600	1/ 360	1/ 360	-1/ 3600
T * L21	1/ 180	1/ 72	1/ 600	-1/ 180	1/ 72	1/ 150
T * L22	1/ 360	1/ 360	-1/ 3600	-1/ 360	1/ 360	-1/ 900
L11**2	1/ 60	1/ 60	-1/ 100	1/ 315	1/ 150	0/ 1
L12**2	1/ 200	1/ 1260	1/ 600	1/ 1050	1/ 3150	0/ 1
L21**2	1/ 1260	1/ 200	1/ 600	-1/ 210	1/ 150	1/ 200
L22**2	1/ 4200	1/ 4200	-1/ 3600	-1/ 700	1/ 3150	-1/ 1200
L11 * L12	1/ 75	2/ 315	0/ 1	4/ 1575	4/ 1575	0/ 1
L11 * L21	2/ 315	1/ 75	0/ 1	1/ 630	1/ 100	1/ 300
L11 * L22	4/ 1575	4/ 1575	0/ 1	1/ 1575	1/ 525	0/ 1
L12 * L21	4/ 1575	4/ 1575	0/ 1	1/ 1575	1/ 525	0/ 1
L12 * L22	1/ 525	1/ 1575	0/ 1	1/ 2100	1/ 2100	-1/ 1800
L21 * L22	1/ 1575	1/ 525	0/ 1	-2/ 525	4/ 1575	0/ 1

	(4,7)	(4,8)	(4,9)	(4,10)	(4,11)	(4,12)
L * T**2	-1/ 30	0/ 1	-1/ 144	0/ 1	0/ 1	1/ 144
T * L11	1/ 72	1/ 180	1/ 600	1/ 360	1/ 360	-1/ 3600
T * L12	1/ 72	-1/ 180	1/ 150	1/ 360	-1/ 360	-1/ 900
T * L21	1/ 360	1/ 360	-1/ 3600	-1/ 360	1/ 360	-1/ 900
T * L22	1/ 360	-1/ 360	-1/ 900	-1/ 360	-1/ 360	-1/ 225
L11**2	1/ 150	1/ 315	0/ 1	2/ 1575	2/ 1575	0/ 1
L12**2	1/ 150	-1/ 210	1/ 200	2/ 1575	-1/ 525	0/ 1
L21**2	1/ 3150	1/ 1050	0/ 1	-1/ 525	2/ 1575	0/ 1
L22**2	1/ 3150	-1/ 700	-1/ 1200	-1/ 525	-1/ 525	-1/ 400
L11 * L12	1/ 100	1/ 630	1/ 300	1/ 525	1/ 1575	0/ 1
L11 * L21	4/ 1575	4/ 1575	0/ 1	1/ 1575	1/ 525	0/ 1
L11 * L22	1/ 525	1/ 1575	0/ 1	1/ 2100	1/ 2100	-1/ 1800
L12 * L21	1/ 525	1/ 1575	0/ 1	1/ 2100	1/ 2100	-1/ 1800
L12 * L22	4/ 1575	-2/ 525	0/ 1	1/ 1575	-1/ 350	-1/ 600
L21 * L22	1/ 2100	1/ 2100	-1/ 1800	-1/ 350	1/ 1575	-1/ 600

TABLE I
COEFFICIENTS OF L(I,J) FOR USE IN FORMING INITIAL STRAIN MATRIX FOR RECTANGULAR ELEMENT (Cont.)

	(5,1)	(5,2)	(5,3)	(5,4)	(5,5)	(5,6)
z * T**2	7/ 20	-3/ 20	-1/ 4	-7/ 20	-7/ 20	-1/ 4
T * ɛ11	-4/ 15	1/ 15	9/ 100	0/ 1	1/ 12	3/ 50
T * ɛ12	-1/ 12	0/ 1	3/ 50	0/ 1	0/ 1	1/ 25
T * ɛ21	0/ 1	1/ 12	3/ 50	4/ 15	4/ 15	9/ 100
T * ɛ22	0/ 1	0/ 1	1/ 25	1/ 12	0/ 1	3/ 50
ɛ11**2	-27/ 140	9/ 280	1/ 25	-3/ 140	39/ 1400	1/ 50
ɛ12**2	-39/ 1400	-1/ 280	1/ 50	-13/ 4200	-13/ 4200	1/ 100
ɛ21**2	3/ 140	33/ 700	1/ 50	27/ 140	27/ 140	1/ 25
ɛ22**2	13/ 4200	-11/ 2100	1/ 100	39/ 1400	-3/ 140	1/ 50
ɛ11 * ɛ12	-33/ 350	1/ 140	1/ 25	-11/ 1050	13/ 2100	1/ 50
ɛ11 * ɛ21	-3/ 70	39/ 700	1/ 25	3/ 70	33/ 350	1/ 25
ɛ11 * ɛ22	-11/ 1050	13/ 2100	1/ 50	11/ 1050	11/ 1050	1/ 50
ɛ12 * ɛ21	-11/ 1050	13/ 2100	1/ 50	11/ 1050	11/ 1050	1/ 50
ɛ12 * ɛ22	-13/ 2100	-13/ 2100	1/ 50	13/ 2100	-11/ 1050	1/ 50
ɛ21 * ɛ22	11/ 1050	11/ 1050	1/ 50	33/ 350	3/ 70	1/ 25

	(5,7)	(5,8)	(5,9)	(5,10)	(5,11)	(5,12)
z * T**2	3/ 20	3/ 20	-1/ 4	-3/ 20	7/ 20	-1/ 4
T * ɛ11	-1/ 12	0/ 1	3/ 50	0/ 1	0/ 1	1/ 25
T * ɛ12	-1/ 15	-1/ 15	9/ 100	0/ 1	-1/ 12	3/ 50
T * ɛ21	0/ 1	0/ 1	1/ 25	1/ 12	0/ 1	3/ 50
T * ɛ22	0/ 1	-1/ 12	3/ 50	1/ 15	-4/ 15	9/ 100
ɛ11**2	-33/ 700	1/ 280	1/ 50	-11/ 2100	13/ 4200	1/ 100
ɛ12**2	-9/ 280	-9/ 280	1/ 25	-1/ 280	-39/ 1400	1/ 50
ɛ21**2	11/ 2100	11/ 2100	1/ 100	33/ 700	3/ 140	1/ 50
ɛ22**2	1/ 280	-33/ 700	1/ 50	9/ 280	-27/ 140	1/ 25
ɛ11 * ɛ12	-39/ 700	-1/ 140	1/ 25	-13/ 2100	-13/ 2100	1/ 50
ɛ11 * ɛ21	-11/ 1050	13/ 2100	1/ 50	11/ 1050	11/ 1050	1/ 50
ɛ11 * ɛ22	-13/ 2100	-13/ 2100	1/ 50	13/ 2100	-11/ 1050	1/ 50
ɛ12 * ɛ21	-13/ 2100	-13/ 2100	1/ 50	13/ 2100	-11/ 1050	1/ 50
ɛ12 * ɛ22	-1/ 140	-39/ 700	1/ 25	1/ 140	-33/ 350	1/ 25
ɛ21 * ɛ22	13/ 2100	-11/ 1050	1/ 50	39/ 700	-3/ 70	1/ 25

	(6,1)	(6,2)	(6,3)	(6,4)	(6,5)	(6,6)
z * T**2	0/ 1	1/ 30	1/ 24	7/ 20	1/ 20	-1/ 24
T * ɛ11	2/ 45	-1/ 60	-1/ 50	-2/ 45	-1/ 60	-1/ 200
T * ɛ12	1/ 72	0/ 1	-1/ 75	-1/ 72	0/ 1	-1/ 300
T * ɛ21	-2/ 45	-1/ 60	-1/ 200	-2/ 9	-1/ 30	3/ 100
T * ɛ22	-1/ 72	0/ 1	-1/ 300	-5/ 72	0/ 1	1/ 50
ɛ11**2	3/ 70	-3/ 350	-1/ 100	-1/ 140	-9/ 1400	-1/ 300
ɛ12**2	13/ 2100	1/ 1050	-1/ 200	-13/ 12600	1/ 1400	-1/ 600
ɛ21**2	-1/ 35	-3/ 350	0/ 1	-3/ 20	-3/ 140	1/ 50
ɛ22**2	-13/ 3150	1/ 1050	0/ 1	-13/ 600	1/ 420	1/ 100
ɛ11 * ɛ12	11/ 525	-1/ 525	-1/ 100	-11/ 3150	-1/ 700	-1/ 300
ɛ11 * ɛ21	-1/ 70	-9/ 700	-1/ 150	-2/ 35	-3/ 175	0/ 1
ɛ11 * ɛ22	-11/ 3150	-1/ 700	-1/ 300	-22/ 1575	-1/ 525	0/ 1
ɛ12 * ɛ21	-11/ 3150	-1/ 700	-1/ 300	-22/ 1575	-1/ 525	0/ 1
ɛ12 * ɛ22	-13/ 6300	1/ 700	-1/ 300	-13/ 1575	1/ 525	0/ 1
ɛ21 * ɛ22	-22/ 1575	-1/ 525	0/ 1	-11/ 150	-1/ 210	1/ 50

	(6,7)	(6,8)	(6,9)	(6,10)	(6,11)	(6,12)
z * T**2	0/ 1	-1/ 30	1/ 24	3/ 20	-1/ 20	-1/ 24
T * ɛ11	1/ 72	0/ 1	-1/ 75	-1/ 72	0/ 1	-1/ 300
T * ɛ12	1/ 90	1/ 60	-1/ 50	-1/ 90	1/ 60	-1/ 200
T * ɛ21	-1/ 72	0/ 1	-1/ 300	-5/ 72	0/ 1	1/ 50
T * ɛ22	-1/ 90	1/ 60	-1/ 200	-1/ 18	1/ 30	3/ 100
ɛ11**2	11/ 1050	-1/ 1050	-1/ 200	-11/ 6300	-1/ 1400	-1/ 600
ɛ12**2	1/ 140	3/ 350	-1/ 100	-1/ 840	9/ 1400	-1/ 300
ɛ21**2	-11/ 1575	-1/ 1050	0/ 1	-11/ 300	-1/ 420	1/ 100
ɛ22**2	-1/ 210	3/ 350	0/ 1	-1/ 40	3/ 140	1/ 50
ɛ11 * ɛ12	13/ 1050	1/ 525	-1/ 100	-13/ 6300	1/ 700	-1/ 300
ɛ11 * ɛ21	-11/ 3150	-1/ 700	-1/ 300	-22/ 1575	-1/ 525	0/ 1
ɛ11 * ɛ22	-13/ 6300	1/ 700	-1/ 300	-13/ 1575	1/ 525	0/ 1
ɛ12 * ɛ21	-13/ 6300	1/ 700	-1/ 300	-13/ 1575	1/ 525	0/ 1
ɛ12 * ɛ22	-1/ 420	9/ 700	-1/ 150	-1/ 105	3/ 175	0/ 1
ɛ21 * ɛ22	-13/ 1575	1/ 525	0/ 1	-13/ 300	1/ 210	1/ 50

TABLE I

COEFFICIENTS OF L(I,J) FOR USE IN FORMING INITIAL STRAIN MATRIX FOR RECTANGULAR ELEMENT (Cont.)

	(7,1)	(7,2)	(7,3)	(7,4)	(7,5)	(7,6)
Z * T**2	1/20	-3/20	1/24	-1/20	-1/20	1/24
T * L11	-1/30	1/18	-3/100	0/1	5/72	-1/50
T * L12	-1/60	1/90	1/200	0/1	1/72	1/300
T * L21	0/1	5/72	-1/50	1/30	2/9	-3/100
T * L22	0/1	1/72	1/300	1/60	2/45	1/200
L11**2	-3/140	1/40	-1/50	-1/420	13/600	-1/100
L12**2	-9/1400	1/840	1/300	-1/1400	13/12600	1/600
L21**2	1/420	11/300	-1/100	3/140	3/20	-1/50
L22**2	1/1400	11/6300	1/600	9/1400	1/140	1/300
L11 * L12	-3/175	1/105	0/1	-1/525	13/1575	0/1
L11 * L21	-1/210	13/300	-1/50	1/210	11/150	-1/50
L11 * L22	-1/525	13/1575	0/1	1/525	22/1575	0/1
L12 * L21	-1/525	13/1575	0/1	1/525	22/1575	0/1
L12 * L22	-1/700	13/6300	1/300	1/700	11/3150	1/300
L21 * L22	1/525	22/1575	0/1	3/175	2/35	0/1

	(7,7)	(7,8)	(7,9)	(7,10)	(7,11)	(7,12)
Z * T**2	1/30	0/1	-1/24	-1/30	0/1	-1/24
T * L11	-1/60	1/90	1/200	0/1	1/72	1/300
T * L12	-1/60	-1/90	1/50	0/1	-1/72	1/75
T * L21	0/1	1/72	1/300	1/60	2/45	1/200
T * L22	0/1	-1/72	1/75	1/60	-2/45	1/50
L11**2	-3/350	1/210	0/1	-1/1050	13/3150	0/1
L12**2	-3/350	-1/140	1/100	-1/1050	-13/2100	1/200
L21**2	1/1050	11/1575	0/1	3/350	1/35	0/1
L22**2	1/1050	-11/1050	1/200	3/350	-3/70	1/100
L11 * L12	-9/700	1/420	1/150	-1/700	13/630	1/300
L11 * L21	-1/525	13/1575	0/1	1/525	22/1575	0/1
L11 * L22	-1/700	13/6300	1/300	1/700	11/3150	1/300
L12 * L21	-1/700	13/6300	1/300	1/700	11/3150	1/300
L12 * L22	-1/525	-13/1050	1/100	1/525	-11/525	1/100
L21 * L22	1/700	11/3150	1/300	9/700	1/70	1/150

	(8,1)	(8,2)	(8,3)	(8,4)	(8,5)	(8,6)
Z * T**2	0/1	1/30	-1/144	1/20	1/20	1/144
T * L11	1/180	-1/72	1/150	-1/180	-1/72	1/600
T * L12	1/360	-1/360	-1/900	-1/360	-1/360	-1/3600
T * L21	-1/180	-1/72	1/600	-1/36	-1/36	-1/100
T * L22	-1/360	-1/360	-1/3600	-1/72	-1/180	1/600
L11**2	1/210	-1/150	1/200	-1/1260	-1/200	1/600
L12**2	1/700	-1/3150	-1/1200	-1/4200	-1/4200	-1/3600
L21**2	-1/315	-1/150	0/1	-1/60	-1/60	-1/100
L22**2	-1/1050	-1/3150	0/1	-1/200	-1/1260	1/600
L11 * L12	2/525	-4/1575	0/1	-1/1575	-1/525	0/1
L11 * L21	-1/630	-1/100	1/300	-2/315	-1/75	0/1
L11 * L22	-1/1575	-1/525	0/1	-4/1575	-4/1575	0/1
L12 * L21	-1/1575	-1/525	0/1	-4/1575	-4/1575	0/1
L12 * L22	-1/2100	-1/2100	-1/1800	-1/525	-1/1575	0/1
L21 * L22	-4/1575	-4/1575	0/1	-1/75	-2/315	0/1

	(8,7)	(8,8)	(8,9)	(8,10)	(8,11)	(8,12)
Z * T**2	0/1	0/1	1/144	1/30	0/1	-1/144
T * L11	1/360	-1/360	-1/900	-1/360	-1/360	-1/3600
T * L12	1/360	-1/360	-1/225	-1/360	1/360	-1/900
T * L21	-1/360	-1/360	-1/3600	-1/72	-1/180	1/600
T * L22	-1/360	1/360	-1/900	-1/72	1/180	1/150
L11**2	1/525	-2/1575	0/1	-1/3150	-1/1050	0/1
L12**2	1/525	1/525	-1/400	-1/3150	1/700	-1/1200
L21**2	-2/1575	-2/1575	0/1	-1/150	-1/315	0/1
L22**2	-2/1575	1/525	0/1	-1/150	1/210	1/200
L11 * L12	1/350	-1/1575	-1/600	-1/2100	-1/2100	-1/1800
L11 * L21	-1/1575	-1/525	0/1	-4/1575	-4/1575	0/1
L11 * L22	-1/2100	-1/2100	-1/1800	-1/525	-1/1575	0/1
L12 * L21	-1/2100	-1/2100	-1/1800	-1/525	-1/1575	0/1
L12 * L22	-1/1575	1/350	-1/600	-4/1575	2/525	0/1
L21 * L22	-1/525	-1/1575	0/1	-1/100	-1/630	1/300

TABLE I

COEFFICIENTS OF L(I,J) FOR USE IN FORMING INITIAL STRAIN MATRIX FOR RECTANGULAR ELEMENT (Cont.)

	(9,1)	(9,2)	(9,3)	(9,4)	(9,5)	(9,6)
Z * T**2	-3/ 20	7/ 20	-1/ 4	3/ 20	3/ 20	-1/ 4
T * Z11	1/ 15	-4/ 15	9/ 100	0/ 1	-1/ 12	3/ 50
T * Z12	1/ 12	0/ 1	3/ 50	0/ 1	0/ 1	1/ 25
T * Z21	0/ 1	-1/ 12	3/ 50	-1/ 15	-1/ 15	9/ 100
T * Z22	0/ 1	0/ 1	1/ 25	-1/ 12	0/ 1	3/ 50
Z11**2	9/ 280	-27/ 140	1/ 25	1/ 280	-33/ 700	1/ 50
Z12**2	33/ 700	3/ 140	1/ 50	11/ 2100	11/ 2100	1/ 100
Z21**2	-1/ 280	-39/ 1400	1/ 50	-9/ 280	-9/ 280	1/ 25
Z22**2	-11/ 2100	13/ 4200	1/ 100	-33/ 700	1/ 280	1/ 50
Z11 * Z12	39/ 700	-3/ 70	1/ 25	13/ 2100	-11/ 1050	1/ 50
Z11 * Z21	1/ 140	-33/ 350	1/ 25	-1/ 140	-39/ 700	1/ 25
Z11 * Z22	13/ 2100	-11/ 1050	1/ 50	-13/ 2100	-13/ 2100	1/ 50
Z12 * Z21	13/ 2100	-11/ 1050	1/ 50	-13/ 2100	-13/ 2100	1/ 50
Z12 * Z22	11/ 1050	11/ 1050	1/ 50	-11/ 1050	13/ 2100	1/ 50
Z21 * Z22	-13/ 2100	-13/ 2100	1/ 50	-39/ 700	-1/ 140	1/ 25

	(9,7)	(9,8)	(9,9)	(9,10)	(9,11)	(9,12)
Z * T**2	-7/ 20	-7/ 20	-1/ 4	7/ 20	-3/ 20	-1/ 4
T * Z11	1/ 12	0/ 1	3/ 50	0/ 1	0/ 1	1/ 25
T * Z12	4/ 15	4/ 15	9/ 100	0/ 1	1/ 12	3/ 50
T * Z21	0/ 1	0/ 1	1/ 25	-1/ 12	0/ 1	3/ 50
T * Z22	0/ 1	1/ 12	3/ 50	-4/ 15	1/ 15	9/ 100
Z11**2	39/ 1400	-3/ 140	1/ 50	13/ 4200	-11/ 2100	1/ 100
Z12**2	27/ 140	27/ 140	1/ 25	3/ 140	33/ 700	1/ 50
Z21**2	-13/ 4200	-13/ 4200	1/ 100	-39/ 1400	-1/ 280	1/ 50
Z22**2	-3/ 140	39/ 1400	1/ 50	-27/ 140	9/ 280	1/ 25
Z11 * Z12	33/ 350	3/ 70	1/ 25	11/ 1050	11/ 1050	1/ 50
Z11 * Z21	13/ 2100	-11/ 1050	1/ 50	-13/ 2100	-13/ 2100	1/ 50
Z11 * Z22	11/ 1050	11/ 1050	1/ 50	-11/ 1050	13/ 2100	1/ 50
Z12 * Z21	11/ 1050	11/ 1050	1/ 50	-11/ 1050	13/ 2100	1/ 50
Z12 * Z22	3/ 70	33/ 350	1/ 25	-3/ 70	39/ 700	1/ 50
Z21 * Z22	-11/ 1050	13/ 2100	1/ 50	-33/ 350	1/ 140	1/ 25

	(10,1)	(10,2)	(10,3)	(10,4)	(10,5)	(10,6)
Z * T**2	-3/ 20	1/ 20	1/ 24	0/ 1	1/ 30	-1/ 24
T * Z11	1/ 18	-1/ 30	-3/ 100	1/ 90	-1/ 60	1/ 200
T * Z12	5/ 72	0/ 1	-1/ 50	1/ 72	0/ 1	1/ 300
T * Z21	1/ 90	-1/ 60	1/ 200	-1/ 90	-1/ 60	1/ 50
T * Z22	1/ 72	0/ 1	1/ 300	-1/ 72	0/ 1	1/ 75
Z11**2	1/ 40	-3/ 140	-1/ 50	1/ 210	-3/ 350	0/ 1
Z12**2	11/ 300	1/ 420	-1/ 100	11/ 1575	1/ 1050	0/ 1
Z21**2	1/ 840	-9/ 1400	1/ 300	-1/ 140	-3/ 350	1/ 100
Z22**2	11/ 6300	1/ 1400	1/ 600	-11/ 1050	1/ 1050	1/ 200
Z11 * Z12	13/ 300	-1/ 210	-1/ 50	13/ 1575	-1/ 525	0/ 1
Z11 * Z21	1/ 105	-3/ 175	0/ 1	1/ 420	-9/ 700	1/ 150
Z11 * Z22	13/ 1575	-1/ 525	0/ 1	13/ 6300	-1/ 700	1/ 300
Z12 * Z21	13/ 1575	-1/ 525	0/ 1	13/ 6300	-1/ 700	1/ 300
Z12 * Z22	22/ 1575	1/ 525	0/ 1	11/ 3150	1/ 700	1/ 300
Z21 * Z22	13/ 6300	-1/ 700	1/ 300	-13/ 1050	-1/ 525	1/ 100

	(10,7)	(10,8)	(10,9)	(10,10)	(10,11)	(10,12)
Z * T**2	-7/ 20	-1/ 20	1/ 24	0/ 1	-1/ 30	-1/ 24
T * Z11	5/ 72	0/ 1	-1/ 50	1/ 72	0/ 1	1/ 300
T * Z12	2/ 9	1/ 30	-3/ 100	2/ 45	1/ 60	1/ 200
T * Z21	1/ 72	0/ 1	1/ 300	-1/ 72	0/ 1	1/ 75
T * Z22	2/ 45	1/ 60	1/ 200	-2/ 45	1/ 60	1/ 50
Z11**2	13/ 600	-1/ 420	-1/ 100	13/ 3150	-1/ 1050	0/ 1
Z12**2	3/ 20	3/ 140	-1/ 50	1/ 35	3/ 350	0/ 1
Z21**2	13/12600	-1/ 1400	1/ 600	-13/ 2100	-1/ 1050	1/ 200
Z22**2	1/ 140	9/ 1400	1/ 300	-3/ 70	3/ 350	1/ 100
Z11 * Z12	11/ 150	1/ 210	-1/ 50	22/ 1575	1/ 525	0/ 1
Z11 * Z21	13/ 1575	-1/ 525	0/ 1	13/ 6300	-1/ 700	1/ 300
Z11 * Z22	22/ 1575	1/ 525	0/ 1	11/ 3150	1/ 700	1/ 300
Z12 * Z21	22/ 1575	1/ 525	0/ 1	11/ 3150	1/ 700	1/ 300
Z12 * Z22	2/ 35	3/ 175	0/ 1	1/ 70	9/ 700	1/ 150
Z21 * Z22	11/ 3150	1/ 700	1/ 300	-11/ 525	1/ 525	1/ 100

TABLE I
COEFFICIENTS OF L(I,J) FOR USE IN FORMING INITIAL STRAIN MATRIX FOR RECTANGULAR ELEMENT (Cont.)

	(11,1)	(11,2)	(11,3)	(11,4)	(11,5)	(11,6)
Z * T**2	1/ 30	0/ 1	1/ 24	-1/ 30	0/ 1	1/ 24
T * Z11	-1/ 60	2/ 45	-1/ 50	0/ 1	1/ 72	-1/ 75
T * Z12	-1/ 60	-2/ 45	-1/ 200	0/ 1	-1/ 72	-1/ 300
T * Z21	0/ 1	1/ 72	-1/ 75	1/ 60	1/ 90	-1/ 50
T * Z22	0/ 1	-1/ 72	-1/ 300	1/ 60	-1/ 90	-1/ 200
Z11**2	3/ 350	3/ 70	-1/ 100	-1/ 1050	11/ 1050	-1/ 200
Z12**2	-3/ 350	-1/ 35	0/ 1	-1/ 1050	-11/ 1575	0/ 1
Z21**2	1/ 1050	13/ 2100	-1/ 200	3/ 350	1/ 140	-1/ 100
Z22**2	1/ 1050	-13/ 3150	0/ 1	3/ 350	-1/ 210	0/ 1
Z11 * Z12	-9/ 700	-1/ 70	-1/ 150	-1/ 700	-11/ 3150	-1/ 300
Z11 * Z21	-1/ 525	11/ 525	-1/ 100	1/ 525	13/ 1050	-1/ 100
Z11 * Z22	-1/ 700	-11/ 3150	-1/ 300	1/ 700	-13/ 6300	-1/ 300
Z12 * Z21	-1/ 700	-11/ 3150	-1/ 300	1/ 700	-13/ 6300	-1/ 300
Z12 * Z22	-1/ 525	-22/ 1575	0/ 1	1/ 525	-13/ 1575	0/ 1
Z21 * Z22	1/ 700	-13/ 6300	-1/ 300	9/ 700	-1/ 420	-1/ 150

	(11,7)	(11,8)	(11,9)	(11,10)	(11,11)	(11,12)
Z * T**2	1/ 20	1/ 20	-1/ 24	-1/ 20	3/ 20	-1/ 24
T * Z11	-1/ 60	-2/ 45	-1/ 200	0/ 1	-1/ 72	-1/ 300
T * Z12	-1/ 30	-2/ 9	3/ 100	0/ 1	-5/ 72	1/ 50
T * Z21	0/ 1	-1/ 72	-1/ 300	1/ 60	-1/ 90	-1/ 200
T * Z22	0/ 1	-5/ 72	1/ 50	1/ 30	-1/ 18	3/ 100
Z11**2	-9/ 1400	-1/ 140	-1/ 300	-1/ 1400	-11/ 6300	-1/ 600
Z12**2	-3/ 140	-3/ 20	1/ 50	-1/ 420	-11/ 300	1/ 100
Z21**2	1/ 1400	-13/12600	-1/ 600	9/ 1400	-1/ 840	-1/ 300
Z22**2	1/ 420	-13/ 600	1/ 100	3/ 140	-1/ 40	1/ 50
Z11 * Z12	-3/ 175	-2/ 35	0/ 1	-1/ 525	-22/ 1575	0/ 1
Z11 * Z21	-1/ 700	-11/ 3150	-1/ 300	1/ 700	-13/ 6300	-1/ 300
Z11 * Z22	-1/ 525	-22/ 1575	0/ 1	1/ 525	-13/ 1575	0/ 1
Z12 * Z21	-1/ 525	-22/ 1575	0/ 1	1/ 525	-13/ 1575	0/ 1
Z12 * Z22	-1/ 210	-11/ 150	1/ 50	1/ 210	-13/ 300	1/ 50
Z21 * Z22	1/ 525	-13/ 1575	0/ 1	3/ 175	-1/ 105	0/ 1

	(12,1)	(12,2)	(12,3)	(12,4)	(12,5)	(12,6)
Z * T**2	1/ 30	0/ 1	-1/ 144	0/ 1	0/ 1	1/ 144
T * Z11	-1/ 72	1/ 180	1/ 150	-1/ 360	1/ 360	-1/ 900
T * Z12	-1/ 72	-1/ 180	1/ 600	-1/ 360	1/ 360	-1/ 3600
T * Z21	-1/ 360	1/ 360	-1/ 900	1/ 360	-1/ 360	-1/ 225
T * Z22	-1/ 360	-1/ 360	-1/ 3600	1/ 360	-1/ 360	-1/ 900
Z11**2	-1/ 150	1/ 210	1/ 200	-2/ 1575	1/ 525	0/ 1
Z12**2	-1/ 150	-1/ 315	0/ 1	-2/ 1575	-2/ 1575	0/ 1
Z21**2	-1/ 3150	1/ 700	-1/ 1200	1/ 525	1/ 525	-1/ 400
Z22**2	-1/ 3150	-1/ 1050	0/ 1	1/ 525	-2/ 1575	0/ 1
Z11 * Z12	-1/ 100	-1/ 630	1/ 300	-1/ 525	-1/ 1575	0/ 1
Z11 * Z21	-4/ 1575	2/ 525	0/ 1	-1/ 1575	1/ 350	-1/ 600
Z11 * Z22	-1/ 525	-1/ 1575	0/ 1	-1/ 2100	-1/ 2100	-1/ 1800
Z12 * Z21	-1/ 525	-1/ 1575	0/ 1	-1/ 2100	-1/ 2100	-1/ 1800
Z12 * Z22	-4/ 1575	-4/ 1575	0/ 1	-1/ 1575	-1/ 525	0/ 1
Z21 * Z22	-1/ 2100	-1/ 2100	-1/ 1800	1/ 350	-1/ 1575	-1/ 600

	(12,7)	(12,8)	(12,9)	(12,10)	(12,11)	(12,12)
Z * T**2	1/ 20	1/ 20	1/ 144	0/ 1	1/ 30	-1/ 144
T * Z11	-1/ 72	-1/ 180	1/ 600	-1/ 360	1/ 360	-1/ 3600
T * Z12	-1/ 36	-1/ 36	-1/ 100	-1/ 180	-1/ 72	1/ 600
T * Z21	-1/ 360	-1/ 360	-1/ 3600	1/ 360	-1/ 360	-1/ 900
T * Z22	-1/ 180	-1/ 72	1/ 600	1/ 180	-1/ 72	1/ 150
Z11**2	-1/ 200	-1/ 1260	1/ 600	-1/ 1050	-1/ 3150	0/ 1
Z12**2	-1/ 60	-1/ 60	-1/ 100	-1/ 315	-1/ 150	0/ 1
Z21**2	-1/ 4200	-1/ 4200	-1/ 3600	1/ 700	-1/ 3150	-1/ 1200
Z22**2	-1/ 1260	-1/ 200	1/ 600	1/ 210	-1/ 150	1/ 200
Z11 * Z12	-1/ 75	-2/ 315	0/ 1	-4/ 1575	-4/ 1575	0/ 1
Z11 * Z21	-1/ 525	-1/ 1575	0/ 1	-1/ 2100	-1/ 2100	-1/ 1800
Z11 * Z22	-4/ 1575	-4/ 1575	0/ 1	-1/ 1575	-1/ 525	0/ 1
Z12 * Z21	-4/ 1575	-4/ 1575	0/ 1	-1/ 1575	-1/ 525	0/ 1
Z12 * Z22	-2/ 315	-1/ 75	0/ 1	-1/ 630	-1/ 100	1/ 300
Z21 * Z22	-1/ 1575	-1/ 525	0/ 1	2/ 525	-4/ 1575	0/ 1

191

TABLE I
COEFFICIENTS OF L(I,J) FOR USE IN FORMING INITIAL STRAIN MATRIX FOR RECTANGULAR ELEMENT (Cont.)

	(13,1)	(13,2)	(13,3)	(13,4)	(13,5)	(13,6)
2 * T**2	3/ 20	3/ 20	1/ 4	-3/ 20	7/ 20	1/ 4
T * L11	-1/ 15	-1/ 15	-9/ 100	0/ 1	-1/ 12	-3/ 50
T * L12	-1/ 12	0/ 1	-3/ 50	0/ 1	0/ 1	-1/ 25
T * L21	0/ 1	-1/ 12	-3/ 50	1/ 15	-4/ 15	-9/ 100
T * L22	0/ 1	0/ 1	-1/ 25	1/ 12	0/ 1	-3/ 50
L11**2	-9/ 280	-9/ 280	-1/ 25	-1/ 280	-39/ 1400	-1/ 50
L12**2	-33/ 700	1/ 280	-1/ 50	-11/ 2100	13/ 4200	-1/ 100
L21**2	1/ 280	-33/ 700	-1/ 50	9/ 280	-27/ 140	-1/ 25
L22**2	11/ 2100	11/ 2100	-1/ 100	33/ 700	3/ 140	-1/ 50
L11 * L12	-39/ 700	-1/ 140	-1/ 25	-13/ 2100	-13/ 2100	-1/ 50
L11 * L21	-1/ 140	-39/ 700	-1/ 25	1/ 140	-33/ 350	-1/ 25
L11 * L22	-13/ 2100	-13/ 2100	-1/ 50	13/ 2100	-11/ 1050	-1/ 50
L12 * L21	-13/ 2100	-13/ 2100	-1/ 50	13/ 2100	-11/ 1050	-1/ 50
L12 * L22	-11/ 1050	13/ 2100	-1/ 50	11/ 1050	11/ 1050	-1/ 50
L21 * L22	13/ 2100	-11/ 1050	-1/ 50	39/ 700	-3/ 70	-1/ 25

	(13,7)	(13,8)	(13,9)	(13,10)	(13,11)	(13,12)
2 * T**2	7/ 20	-3/ 20	1/ 4	-7/ 20	-7/ 20	1/ 4
T * L11	-1/ 12	0/ 1	-3/ 50	0/ 1	0/ 1	-1/ 25
T * L12	-4/ 15	1/ 15	-9/ 100	0/ 1	1/ 12	-3/ 50
T * L21	0/ 1	0/ 1	-1/ 25	1/ 12	0/ 1	-3/ 50
T * L22	0/ 1	1/ 12	-3/ 50	4/ 15	4/ 15	-9/ 100
L11**2	-39/ 1400	-1/ 280	-1/ 50	-13/ 4200	-13/ 4200	-1/ 100
L12**2	-27/ 140	9/ 280	-1/ 25	-3/ 140	39/ 1400	-1/ 50
L21**2	13/ 4200	-11/ 2100	-1/ 100	39/ 1400	-3/ 140	-1/ 50
L22**2	3/ 140	33/ 700	-1/ 50	27/ 140	27/ 140	-1/ 25
L11 * L12	-33/ 350	1/ 140	-1/ 25	-11/ 1050	13/ 2100	-1/ 50
L11 * L21	-13/ 2100	-13/ 2100	-1/ 50	13/ 2100	-11/ 1050	-1/ 50
L11 * L22	-11/ 1050	13/ 2100	-1/ 50	11/ 1050	11/ 1050	-1/ 50
L12 * L21	-11/ 1050	13/ 2100	-1/ 50	11/ 1050	11/ 1050	-1/ 50
L12 * L22	-3/ 70	39/ 700	-1/ 25	3/ 70	33/ 350	-1/ 25
L21 * L22	11/ 1050	11/ 1050	-1/ 50	33/ 350	3/ 70	-1/ 25

	(14,1)	(14,2)	(14,3)	(14,4)	(14,5)	(14,6)
2 * T**2	0/ 1	-1/ 30	-1/ 24	3/ 20	-1/ 20	1/ 24
T * L11	1/ 90	1/ 60	1/ 50	-1/ 90	1/ 60	1/ 200
T * L12	1/ 72	0/ 1	1/ 75	-1/ 72	0/ 1	1/ 300
T * L21	-1/ 90	1/ 60	1/ 200	-1/ 18	1/ 30	-3/ 100
T * L22	-1/ 72	0/ 1	1/ 300	-5/ 72	0/ 1	-1/ 50
L11**2	1/ 140	3/ 350	1/ 100	-1/ 840	9/ 1400	1/ 300
L12**2	11/ 1050	-1/ 1050	1/ 200	-11/ 6300	-1/ 1400	1/ 600
L21**2	-1/ 210	3/ 350	0/ 1	-1/ 40	3/ 140	-1/ 50
L22**2	-11/ 1575	-1/ 1050	0/ 1	-11/ 300	-1/ 420	-1/ 100
L11 * L12	13/ 1050	1/ 525	1/ 100	-13/ 6300	1/ 700	1/ 300
L11 * L21	-1/ 420	9/ 700	1/ 150	-1/ 105	3/ 175	0/ 1
L11 * L22	-13/ 6300	1/ 700	1/ 300	-13/ 1575	1/ 525	0/ 1
L12 * L21	-13/ 6300	1/ 700	1/ 300	-13/ 1575	1/ 525	0/ 1
L12 * L22	-11/ 3150	-1/ 700	1/ 300	-22/ 1575	-1/ 525	0/ 1
L21 * L22	-13/ 1575	1/ 525	0/ 1	-13/ 300	1/ 210	-1/ 50

	(14,7)	(14,8)	(14,9)	(14,10)	(14,11)	(14,12)
2 * T**2	0/ 1	1/ 30	-1/ 24	7/ 20	1/ 20	1/ 24
T * L11	1/ 72	0/ 1	1/ 75	-1/ 72	0/ 1	1/ 300
T * L12	2/ 45	-1/ 60	1/ 50	-2/ 45	-1/ 60	1/ 200
T * L21	-1/ 72	0/ 1	1/ 300	-5/ 72	0/ 1	-1/ 50
T * L22	-2/ 45	-1/ 60	1/ 200	-2/ 9	-1/ 30	-3/ 100
L11**2	13/ 2100	1/ 1050	1/ 200	-13/ 12600	1/ 1400	1/ 600
L12**2	3/ 70	-3/ 350	1/ 100	-1/ 140	-9/ 1400	1/ 300
L21**2	-13/ 3150	1/ 1050	0/ 1	-13/ 600	1/ 420	-1/ 100
L22**2	-1/ 35	-3/ 350	0/ 1	-3/ 20	-1/ 140	-1/ 50
L11 * L12	11/ 525	-1/ 525	1/ 100	-11/ 3150	-1/ 700	1/ 300
L11 * L21	-13/ 6300	1/ 700	1/ 300	-13/ 1575	1/ 525	0/ 1
L11 * L22	-11/ 3150	-1/ 700	1/ 300	-22/ 1575	-1/ 525	0/ 1
L12 * L21	-11/ 3150	-1/ 700	1/ 300	-22/ 1575	-1/ 525	0/ 1
L12 * L22	-1/ 70	-9/ 700	1/ 150	-2/ 35	-3/ 175	0/ 1
L21 * L22	-22/ 1575	-1/ 525	0/ 1	-11/ 150	-1/ 210	-1/ 50

TABLE I
COEFFICIENTS OF L(I,J) FOR USE IN FORMING INITIAL STRAIN MATRIX FOR RECTANGULAR ELEMENT (Cont.)

	(15,1)	(15,2)	(15,3)	(15,4)	(15,5)	(15,6)
∠ * I**2	-1/ 30	0/ 1	-1/ 24	1/ 30	0/ 1	-1/ 24
T * ∠11	1/ 60	1/ 90	1/ 50	0/ 1	1/ 72	1/ 75
T * ∠12	1/ 60	-1/ 90	1/ 200	0/ 1	-1/ 72	1/ 300
T * ∠21	0/ 1	1/ 72	1/ 75	-1/ 60	2/ 45	1/ 50
T * ∠22	0/ 1	-1/ 72	1/ 300	-1/ 60	-2/ 45	1/ 200
∠11**2	3/ 350	1/ 140	1/ 100	1/ 1050	13/ 2100	1/ 200
∠12**2	3/ 350	-1/ 210	0/ 1	1/ 1050	-13/ 3150	0/ 1
∠21**2	-1/ 1050	11/ 1050	1/ 200	-3/ 350	3/ 70	1/ 100
∠22**2	-1/ 1050	-11/ 1575	0/ 1	-3/ 350	-1/ 35	0/ 1
∠11 * ∠12	9/ 700	-1/ 420	1/ 150	1/ 700	-13/ 6300	1/ 300
∠11 * ∠21	1/ 525	13/ 1050	1/ 100	-1/ 525	11/ 525	1/ 100
∠11 * ∠22	1/ 700	-13/ 6300	1/ 300	-1/ 700	-11/ 3150	1/ 300
∠12 * ∠21	1/ 700	-13/ 6300	1/ 300	-1/ 700	-11/ 3150	1/ 300
∠12 * ∠22	1/ 525	-13/ 1575	0/ 1	-1/ 525	-22/ 1575	0/ 1
∠21 * ∠22	-1/ 700	-11/ 3150	1/ 300	-9/ 700	-1/ 70	1/ 150

	(15,7)	(15,8)	(15,9)	(15,10)	(15,11)	(15,12)
∠ * I**2	-1/ 20	3/ 20	1/ 24	1/ 20	7/ 20	1/ 24
T * ∠11	1/ 60	-1/ 90	1/ 200	0/ 1	-1/ 72	1/ 300
T * ∠12	1/ 30	-1/ 18	-3/ 100	0/ 1	-5/ 72	-1/ 50
T * ∠21	0/ 1	-1/ 72	1/ 300	-1/ 60	-2/ 45	1/ 200
T * ∠22	0/ 1	-5/ 72	-1/ 50	-1/ 30	-2/ 9	-3/ 100
∠11**2	9/ 1400	-1/ 840	1/ 300	1/ 1400	-13/12600	1/ 600
∠12**2	3/ 140	-1/ 40	-1/ 50	1/ 420	-13/ 600	-1/ 100
∠21**2	-1/ 1400	-11/ 6300	1/ 600	-9/ 1400	-1/ 140	1/ 300
∠22**2	-1/ 420	-11/ 300	-1/ 100	-3/ 140	-3/ 20	-1/ 50
∠11 * ∠12	3/ 175	-1/ 105	0/ 1	1/ 525	-13/ 1575	0/ 1
∠11 * ∠21	1/ 700	-13/ 6300	1/ 300	-1/ 700	-11/ 3150	1/ 300
∠11 * ∠22	1/ 525	-13/ 1575	0/ 1	-1/ 525	-22/ 1575	0/ 1
∠12 * ∠21	1/ 525	-13/ 1575	0/ 1	-1/ 525	-22/ 1575	0/ 1
∠12 * ∠22	1/ 210	-13/ 300	-1/ 50	-1/ 210	-11/ 150	-1/ 50
∠21 * ∠22	-1/ 525	-22/ 1575	0/ 1	-3/ 175	-2/ 35	0/ 1

	(16,1)	(16,2)	(16,3)	(16,4)	(16,5)	(16,6)
∠ * I**2	0/ 1	0/ 1	1/ 144	-1/ 30	0/ 1	-1/ 144
T * ∠11	-1/ 360	-1/ 360	-1/ 225	1/ 360	-1/ 360	-1/ 900
T * ∠12	-1/ 360	1/ 360	-1/ 900	1/ 360	1/ 360	-1/ 3600
T * ∠21	1/ 360	-1/ 360	-1/ 900	1/ 72	-1/ 180	1/ 150
T * ∠22	1/ 360	1/ 360	-1/ 3600	1/ 72	1/ 180	1/ 600
∠11**2	-1/ 525	-1/ 525	-1/ 400	1/ 3150	-1/ 700	-1/ 1200
∠12**2	-1/ 525	2/ 1575	0/ 1	1/ 3150	1/ 1050	0/ 1
∠21**2	2/ 1575	-1/ 525	0/ 1	1/ 150	1/ 210	1/ 200
∠22**2	2/ 1575	2/ 1575	0/ 1	1/ 150	1/ 315	0/ 1
∠11 * ∠12	-1/ 350	1/ 1575	-1/ 600	1/ 2100	1/ 2100	0/ 1
∠11 * ∠21	1/ 1575	-1/ 350	-1/ 600	4/ 1575	-2/ 525	0/ 1
∠11 * ∠22	1/ 2100	1/ 2100	-1/ 1800	1/ 525	1/ 1575	0/ 1
∠12 * ∠21	1/ 2100	1/ 2100	-1/ 1800	1/ 525	1/ 1575	0/ 1
∠12 * ∠22	1/ 1575	1/ 525	0/ 1	4/ 1575	4/ 1575	0/ 1
∠21 * ∠22	1/ 525	1/ 1575	0/ 1	1/ 100	1/ 630	1/ 300

	(16,7)	(16,8)	(16,9)	(16,10)	(16,11)	(16,12)
∠ * I**2	0/ 1	-1/ 30	-1/ 144	-1/ 20	-1/ 20	1/ 144
T * ∠11	-1/ 360	1/ 360	-1/ 900	1/ 360	1/ 360	-1/ 3600
T * ∠12	-1/ 180	1/ 72	1/ 150	1/ 180	1/ 72	1/ 600
T * ∠21	1/ 360	1/ 360	-1/ 3600	1/ 72	1/ 180	1/ 600
T * ∠22	1/ 180	1/ 72	1/ 600	1/ 36	1/ 36	-1/ 100
∠11**2	-1/ 700	1/ 3150	-1/ 1200	1/ 4200	1/ 4200	-1/ 3600
∠12**2	-1/ 210	1/ 150	1/ 200	1/ 1260	1/ 200	1/ 600
∠21**2	1/ 1050	1/ 3150	0/ 1	1/ 200	1/ 1260	1/ 600
∠22**2	1/ 315	1/ 150	0/ 1	1/ 60	1/ 60	-1/ 100
∠11 * ∠12	-2/ 525	4/ 1575	0/ 1	1/ 1575	1/ 525	0/ 1
∠11 * ∠21	1/ 2100	1/ 2100	-1/ 1800	1/ 525	1/ 1575	0/ 1
∠11 * ∠22	1/ 1575	1/ 525	0/ 1	4/ 1575	4/ 1575	0/ 1
∠12 * ∠21	1/ 1575	1/ 525	0/ 1	4/ 1575	4/ 1575	0/ 1
∠12 * ∠22	1/ 630	1/ 100	1/ 300	2/ 315	1/ 75	0/ 1
∠21 * ∠22	4/ 1575	4/ 1575	0/ 1	1/ 75	2/ 315	0/ 1

193

TABLE 2

COEFFICIENTS OF $L_M^U(I,J)$ AND $L_M^L(I,J)$ FOR USE IN FORMING INITIAL STRAIN MATRIX FOR RECTANGULAR ELEMENT,

L_M^U	L_M^L	(1,1)	(1,2)	(1,3)	(1,4)	(1,5)	(1,6)
0	T	-1/ 1	0/ 1	-1/ 1	-1/ 1	0/ 1	-1/ 2
ZU11	-ZL11	-1/ 4	0/ 1	-1/ 4	-1/ 8	0/ 1	-1/12
ZU12	-ZL12	-1/12	0/ 1	-1/ 8	-1/24	0/ 1	-1/24
ZU21	-ZL21	-1/ 8	0/ 1	-1/12	-1/ 4	0/. 1	-1/12
ZU22	-ZL22	-1/24	0/ 1	-1/24	-1/12	0/ 1	-1/24
		(1,7)	(1,8)	(1,9)	(1,10)	(1,11)	(1,12)
0	T	-1/ 2	0/ 1	-1/ 1	-1/ 2	0/ 1	-1/ 2
ZU11	-ZL11	-1/12	0/ 1	-1/ 8	-1/24	0/ 1	-1/24
ZU12	-ZL12	-1/12	0/ 1	-1/ 4	-1/24	0/ 1	-1/12
ZU21	-ZL21	-1/24	0/ 1	-1/24	-1/12	0/ 1	-1/24
ZU22	-ZL22	-1/24	0/ 1	-1/12	-1/12	0/ 1	-1/12

L_M^U	L_M^L	(2,1)	(2,2)	(2,3)	(2,4)	(2,5)	(2,6)
0	T	0/ 1	-1/ 1	-1/ 1	0/ 1	-1/ 2	-1/ 1
ZU11	-ZL11	0/ 1	-1/ 4	-1/ 4	0/ 1	-1/12	-1/ 8
ZU12	-ZL12	0/ 1	-1/ 8	-1/12	0/ 1	-1/24	-1/24
ZU21	-ZL21	0/ 1	-1/12	-1/ 8	0/ 1	-1/12	-1/ 4
ZU22	-ZL22	0/ 1	-1/24	-1/24	0/ 1	-1/24	-1/12
		(2,7)	(2,8)	(2,9)	(2,10)	(2,11)	(2,12)
0	T	0/ 1	-1/ 1	-1/ 2	0/ 1	-1/ 2	-1/ 2
ZU11	-ZL11	0/ 1	-1/ 8	-1/12	0/ 1	-1/24	-1/24
ZU12	-ZL12	0/ 1	-1/ 4	-1/12	0/ 1	-1/12	-1/24
ZU21	-ZL21	0/ 1	-1/24	-1/24	0/ 1	-1/24	-1/12
ZU22	-ZL22	0/ 1	-1/12	-1/24	0/ 1	-1/12	-1/12

TABLE 2

COEFFICIENTS OF $L^U_M(I,J)$ AND $L^L_M(I,J)$ FOR USE IN FORMING INITIAL STRAIN MATRIX FOR RECTANGULAR ELEMENT (Cont.)

L^U_M	L^L_M	(3,1)	(3,2)	(3,3)	(3,4)	(3,5)	(3,6)
0	T	1/ 1	0/ 1	-1/ 2	1/ 1	0/ 1	-1/ 1
ZU11	-ZL11	1/ 4	0/ 1	-1/12	1/ 8	0/ 1	-1/12
ZU12	-ZL12	1/12	0/ 1	-1/24	1/24	0/ 1	-1/24
ZU21	-ZL21	1/ 8	0/ 1	-1/12	1/ 4	0/ 1	-1/ 4
ZU22	-ZL22	1/24	0/ 1	-1/24	1/12	0/ 1	-1/ 8

L^U_M	L^L_M	(3,7)	(3,8)	(3,9)	(3,10)	(3,11)	(3,12)
0	T	1/ 2	0/ 1	-1/ 2	1/ 2	0/ 1	-1/ 1
ZU11	-ZL11	1/12	0/ 1	-1/24	1/24	0/ 1	-1/24
ZU12	-ZL12	1/12	0/ 1	-1/12	1/24	0/ 1	-1/12
ZU21	-ZL21	1/24	0/ 1	-1/24	1/12	0/ 1	-1/ 8
ZU22	-ZL22	1/24	0/ 1	-1/12	1/24	0/ 1	-1/ 4

L^U_M	L^L_M	(4,1)	(4,2)	(4,3)	(4,4)	(4,5)	(4,6)
0	T	0/ 1	-1/ 2	1/ 1	0/ 1	-1/ 1	1/ 1
ZU11	-ZL11	0/ 1	-1/12	1/ 4	0/ 1	-1/12	1/ 8
ZU12	-ZL12	0/ 1	-1/24	1/12	0/ 1	-1/24	1/24
ZU21	-ZL21	0/ 1	-1/12	1/ 8	0/ 1	-1/ 4	1/12
ZU22	-ZL22	0/ 1	-1/24	1/24	0/ 1	-1/ 8	1/12

L^U_M	L^L_M	(4,7)	(4,8)	(4,9)	(4,10)	(4,11)	(4,12)
0	T	0/ 1	-1/ 2	1/ 2	0/ 1	-1/ 1	1/ 2
ZU11	-ZL11	0/ 1	-1/24	1/12	0/ 1	-1/24	1/24
ZU12	-ZL12	0/ 1	-1/12	1/12	0/ 1	-1/12	1/24
ZU21	-ZL21	0/ 1	-1/24	1/24	0/ 1	-1/ 8	1/12
ZU22	-ZL22	0/ 1	-1/12	1/24	0/ 1	-1/ 4	1/12

TABLE 2

COEFFICIENTS OF $L_M^U(I,J)$ AND $L_M^L(I,J)$ FOR USE IN FORMING INITIAL STRAIN MATRIX FOR RECTANGULAR ELEMENT (Cont.)

L_M^U	L_M^L	(5,1)	(5,2)	(5,3)	(5,4)	(5,5)	(5,6)
0	T	-1/2	0/1	1/2	-1/2	0/1	1/2
ZU11	-ZL11	-1/12	0/1	1/4	-1/24	0/1	1/12
ZU12	-ZL12	-1/12	0/1	1/8	-1/24	0/1	1/24
ZU21	-ZL21	-1/24	0/1	1/12	-1/12	0/1	1/12
ZU22	-ZL22	-1/24	0/1	1/24	-1/12	0/1	1/24
		(5,7)	(5,8)	(5,9)	(5,10)	(5,11)	(5,12)
0	T	-1/1	0/1	1/1	-1/1	0/1	1/2
ZU11	-ZL11	-1/12	0/1	1/8	-1/24	0/1	1/24
ZU12	-ZL12	-1/4	0/1	1/4	-1/8	0/1	1/12
ZU21	-ZL21	-1/24	0/1	1/24	-1/12	0/1	1/24
ZU22	-ZL22	-1/8	0/1	1/12	-1/4	0/1	1/12

L_M^U	L_M^L	(6,1)	(6,2)	(6,3)	(6,4)	(6,5)	(6,6)
0	T	0/1	1/1	-1/2	0/1	1/2	-1/2
ZU11	-ZL11	0/1	1/4	-1/12	0/1	1/12	-1/24
ZU12	-ZL12	0/1	1/8	-1/12	0/1	1/24	-1/24
ZU21	-ZL21	0/1	1/12	-1/24	0/1	1/12	-1/12
ZU22	-ZL22	0/1	1/24	-1/24	0/1	1/24	-1/12
		(6,7)	(6,8)	(6,9)	(6,10)	(6,11)	(6,12)
0	T	0/1	1/1	-1/1	0/1	1/2	-1/1
ZU11	-ZL11	0/1	1/8	-1/12	0/1	1/24	-1/24
ZU12	-ZL12	0/1	1/4	-1/4	0/1	1/12	-1/8
ZU21	-ZL21	0/1	1/24	-1/24	0/1	1/24	-1/12
ZU22	-ZL22	0/1	1/12	-1/8	0/1	1/12	-1/4

TABLE 2

COEFFICIENTS OF $L_M^U(I,J)$ AND $L_M^L(I,J)$ FOR USE IN FORMING INITIAL STRAIN MATRIX FOR RECTANGULAR ELEMENT (Cont.)

L_M^U	L_M^L	(7,1)	(7,2)	(7,3)	(7,4)	(7,5)	(7,6)
0	T	1/2	0/1	1/2	1/2	0/1	1/1
ZU11	-ZL11	1/12	0/1	1/12	1/24	0/1	1/12
ZU12	-ZL12	1/12	0/1	1/24	1/24	0/1	1/24
ZU21	-ZL21	1/24	0/1	1/12	1/12	0/1	1/4
ZU22	-ZL22	1/24	0/1	1/24	1/12	0/1	1/8
		(7,7)	(7,8)	(7,9)	(7,10)	(7,11)	(7,12)
0	T	1/1	0/1	1/2	1/1	0/1	1/1
ZU11	-ZL11	1/12	0/1	1/24	1/24	0/1	1/24
ZU12	-ZL12	1/4	0/1	1/12	1/8	0/1	1/12
ZU21	-ZL21	1/24	0/1	1/24	1/12	0/1	1/8
ZU22	-ZL22	1/8	0/1	1/12	1/4	0/1	1/4

L_M^U	L_M^L	(8,1)	(8,2)	(8,3)	(8,4)	(8,5)	(8,6)
0	T	0/1	1/2	1/2	0/1	1/1	1/2
ZU11	-ZL11	0/1	1/12	1/12	0/1	1/12	1/24
ZU12	-ZL12	0/1	1/24	1/12	0/1	1/24	1/24
ZU21	-ZL21	0/1	1/12	1/24	0/1	1/4	1/12
ZU22	-ZL22	0/1	1/24	1/24	0/1	1/8	1/12
		(8,7)	(8,8)	(8,9)	(8,10)	(8,11)	(8,12)
0	T	0/1	1/2	1/1	0/1	1/1	1/1
ZU11	-ZL11	0/1	1/24	1/12	0/1	1/24	1/24
ZU12	-ZL12	0/1	1/12	1/4	0/1	1/12	1/24
ZU21	-ZL21	0/1	1/24	1/24	0/1	1/8	1/12
ZU22	-ZL22	0/1	1/12	1/8	0/1	1/4	1/4
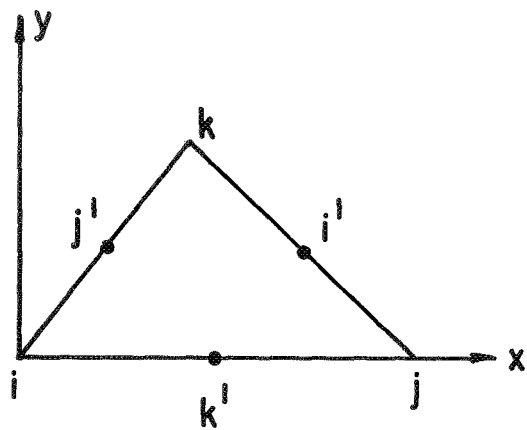
Fig. I.   SIX NODE TRIANGULAR FINITE ELEMENT
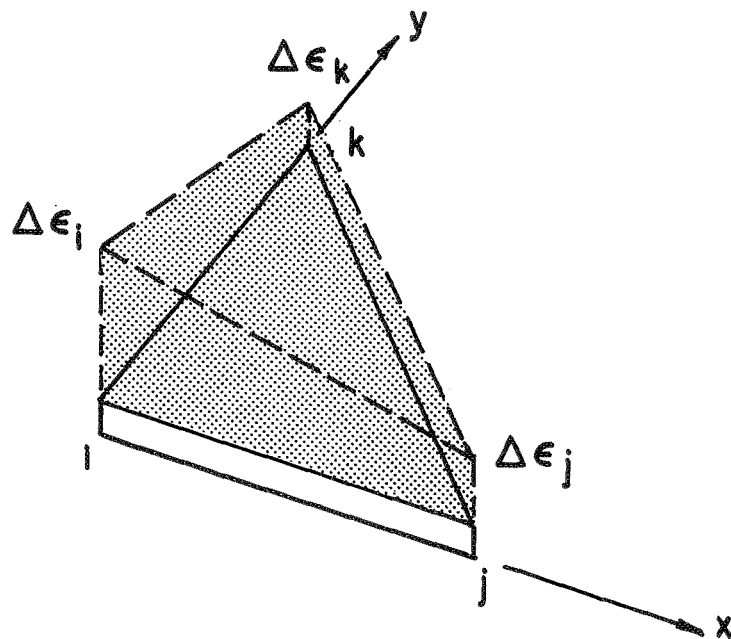
Fig. 2. DISTRIBUTION OF PLASTIC STRAIN INCREMENTS

Fig. 3   NOTCHED BAR I

127   Elements
284   Nodes
542   Degrees of freedom
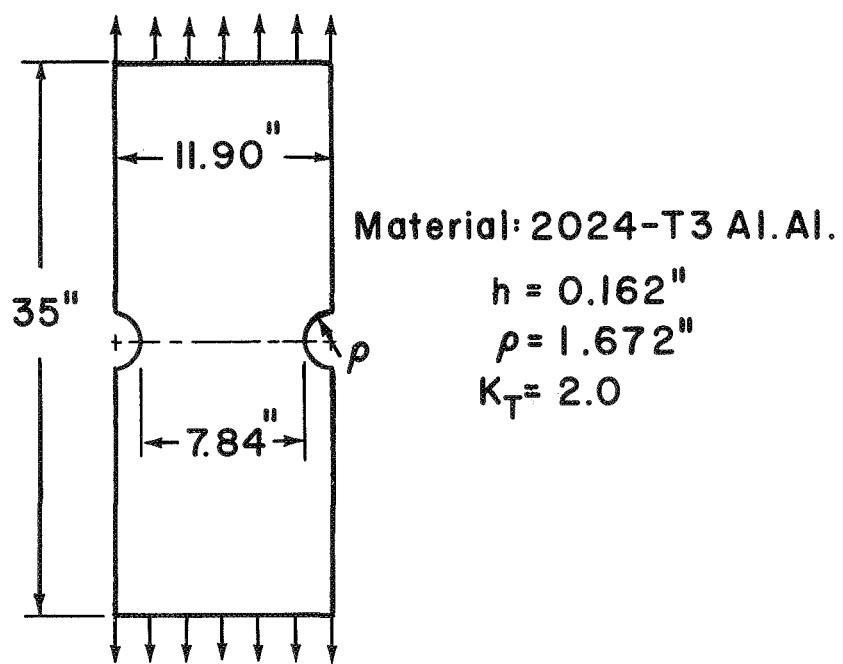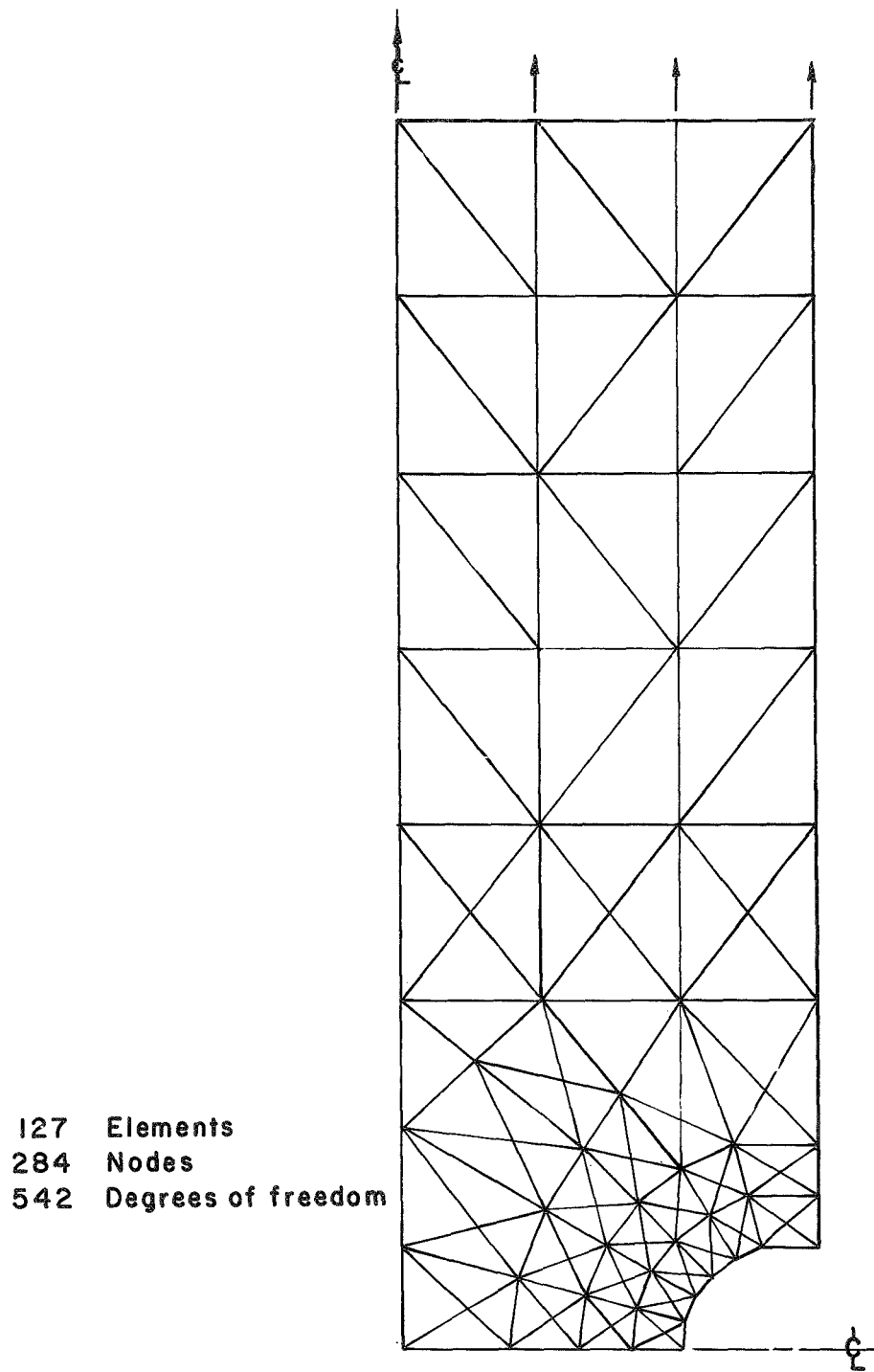
Fig. 4   FINITE ELEMENT IDEALIZATION OF QUADRANT
FOR NOTCH BAR I
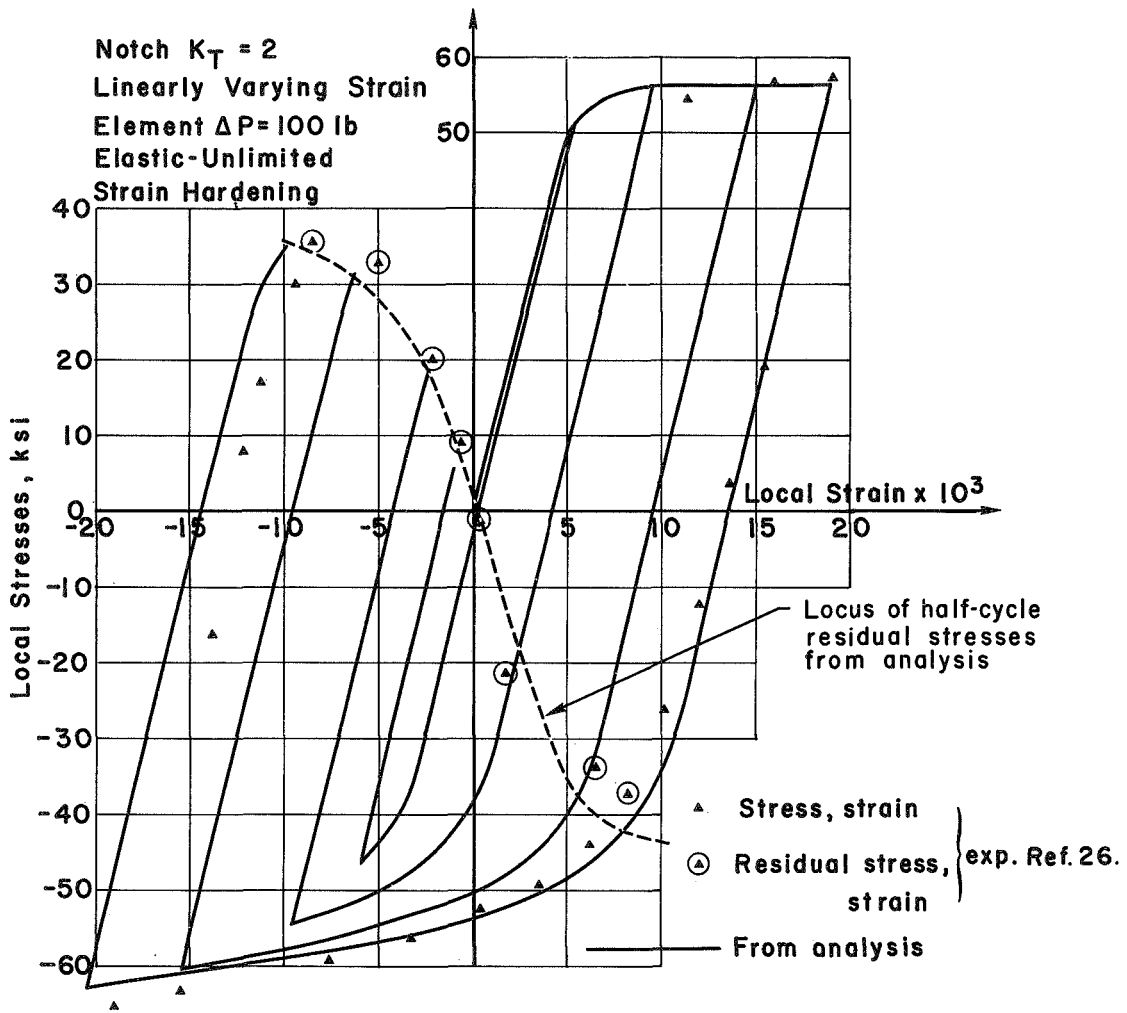
Fig. 5 NOTCHED BAR I· LOCAL STRESS-STRAIN CURVE AT NOTCH
ROOT FOR FIRST CYCLE OF REVERSED LOADING

201

Notch $K_T = 2$

Linearly Varying Strain
Element

$\Delta P = 100$ lb.

Elastic Unlimited Strain
Hardening

Local Strain $\times 10^3$

Load, kips

▲ 1st cycle
▲ 2nd cycle
□ 3rd cycle
} from experiment Ref. 26.

———— 1st cycle
·········· 2nd cycle
— — — — 3rd cycle
} from analysis
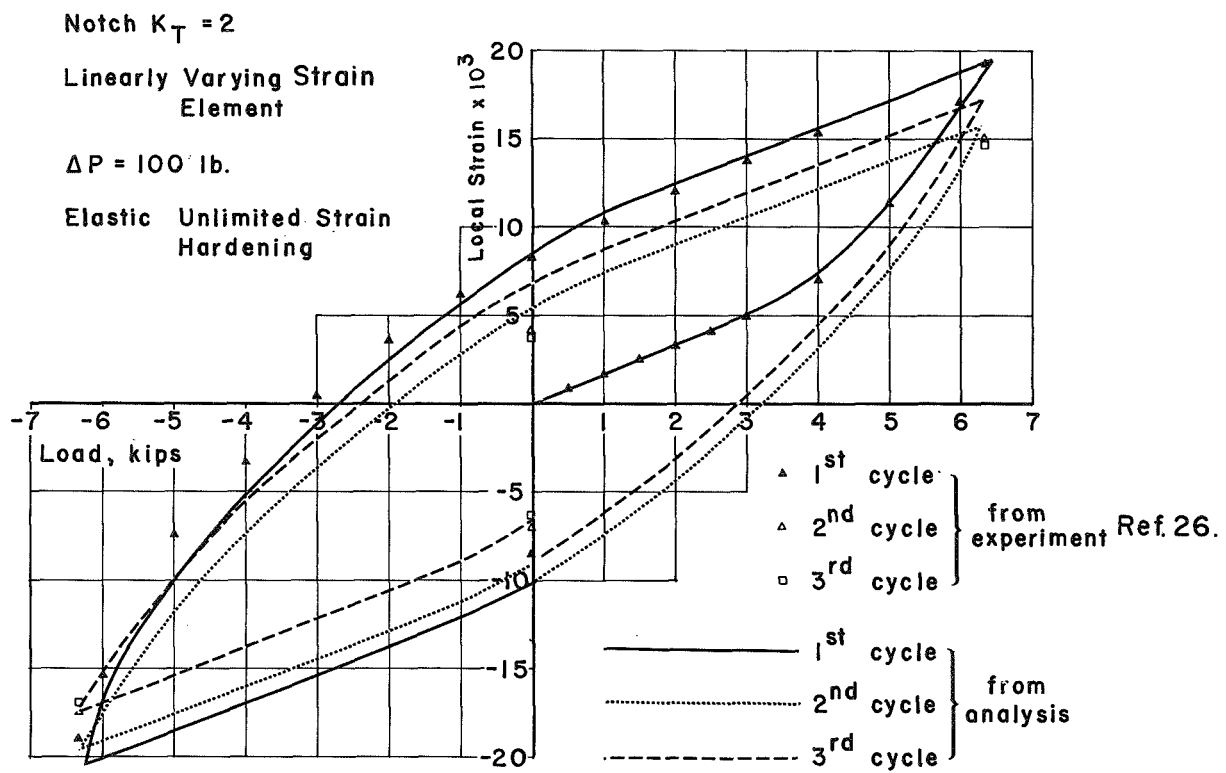
Fig. 6   NOTCHED BAR I: THREE CYCLE LOAD vs. STRAIN CURVE
AT NOTCH ROOT $S_{max} = 50$ ksi
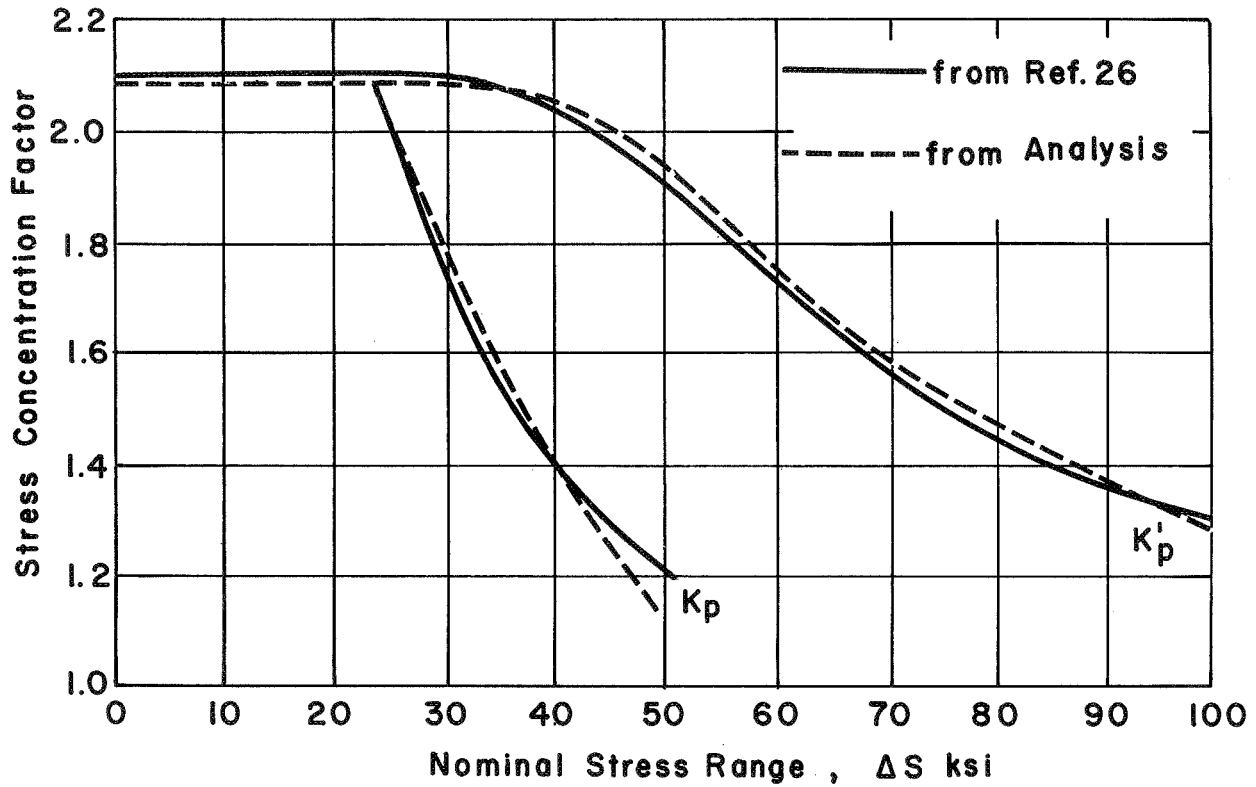
Fig. 7. NOTCH BAR I : PLASTIC STRESS CONCENTRATION FACTOR
AT NOTCH ROOT vs. NET SECTION STRESS RANGE.

(b) $S_{max} = 50.0$ ksi

(a) Maximum Elastic Load

(d) $S_{min} = -50.0$ ksi

(e) Residual Stress Distribution
$S = 0.0$ ksi

(c) Residual Stress Distribution
$S = 0.0$ ksi
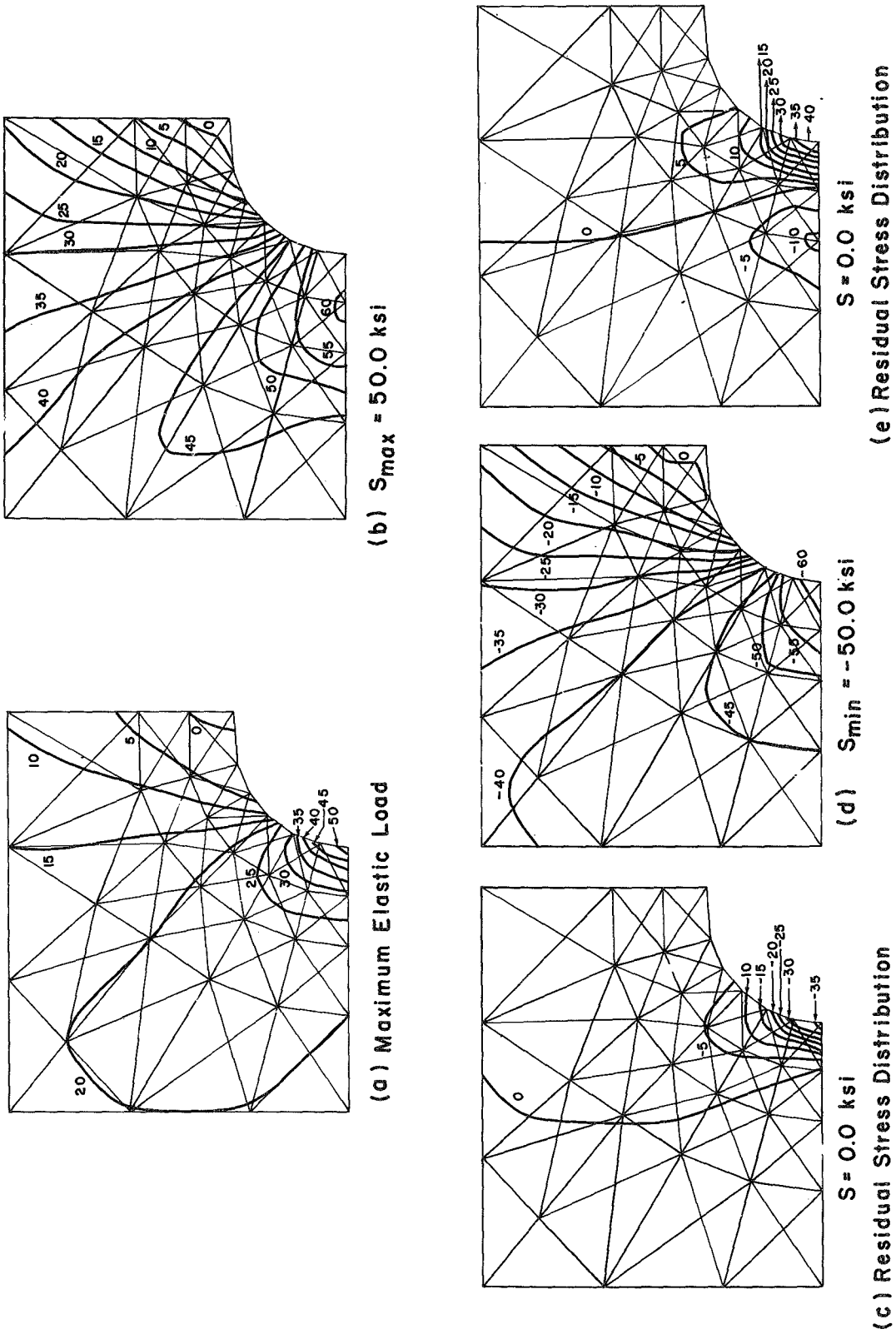
Fig. 8   NOTCHED BAR I: STRESS CONTOURS, σ_y
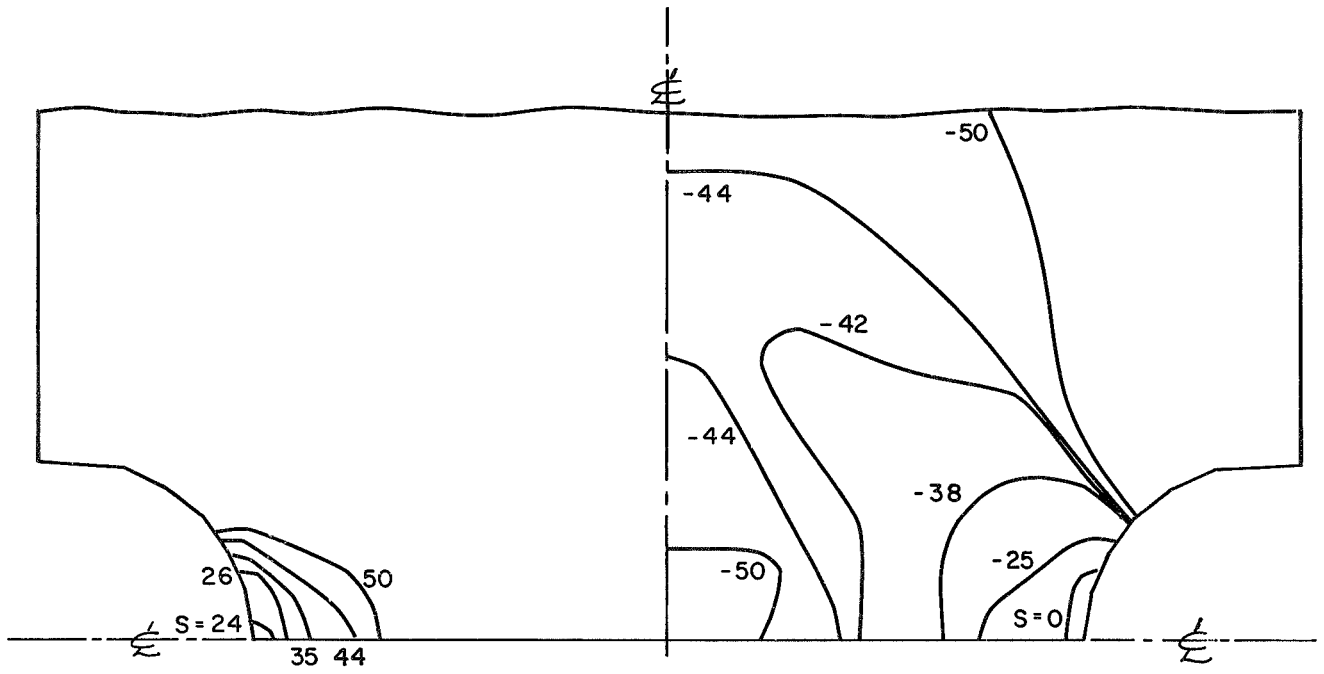
(a) First cycle of loading   (b) First cycle of unloading and reversed   loading

Fig. 9   NOTCHED BAR I· GROWTH OF ELASTIC - PLASTIC BOUNDARY

Material
2024-T3 Al. Al.
$h = 0.155"$
$\rho = 0.300"$
$K_T = 4.0$

ρ, radius

8.00"

35.0"

11.90"
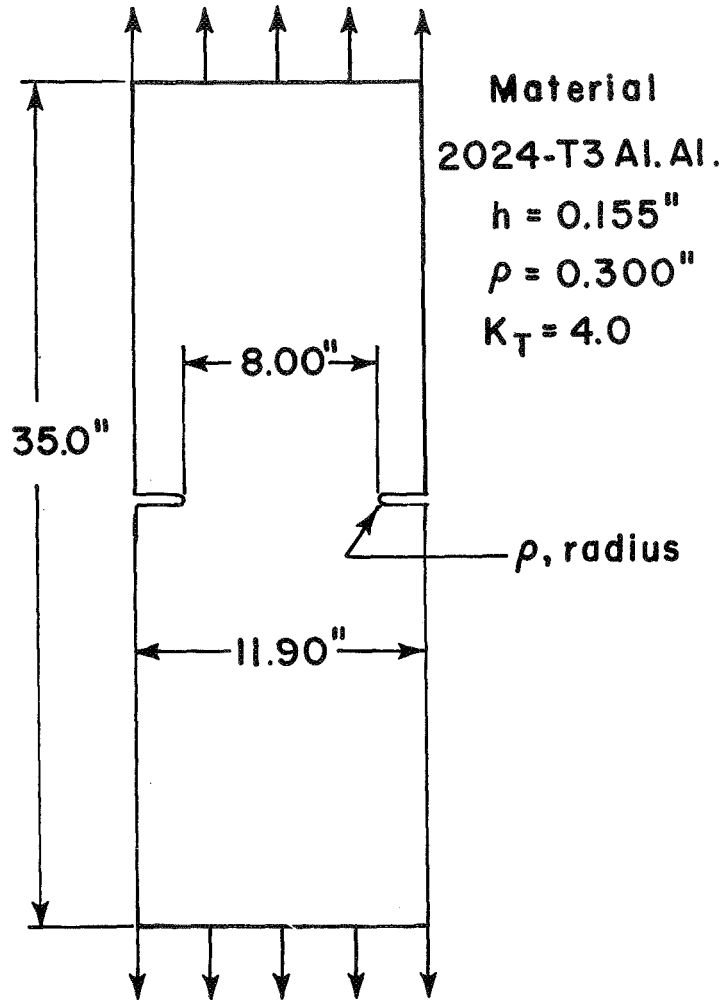
Fig. 10   NOTCHED BAR II
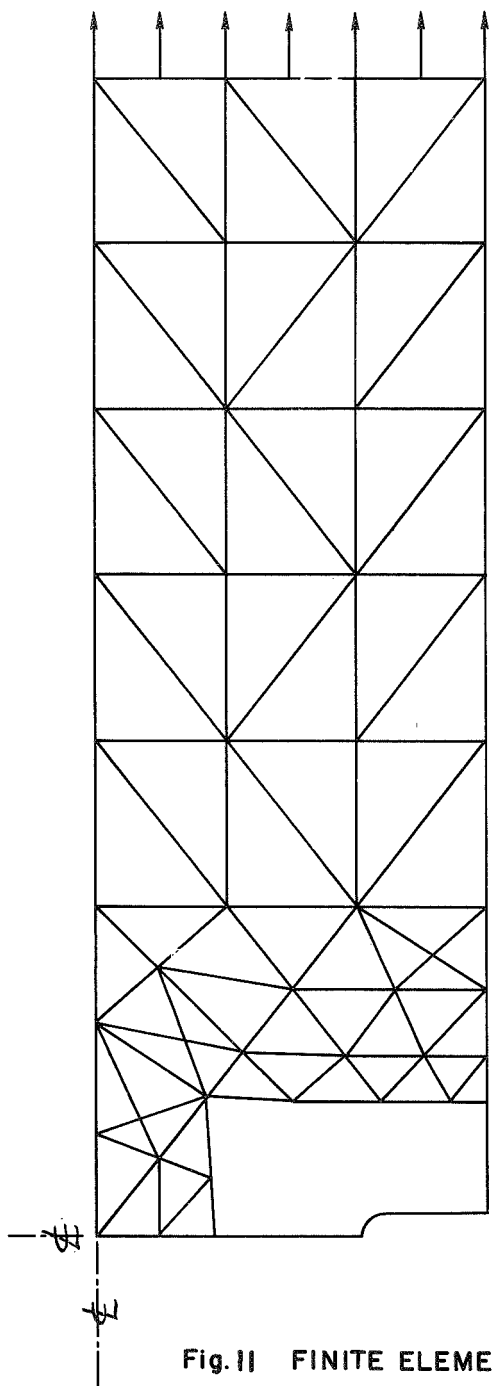
144 elements
327 nodes
620 degrees of freedom
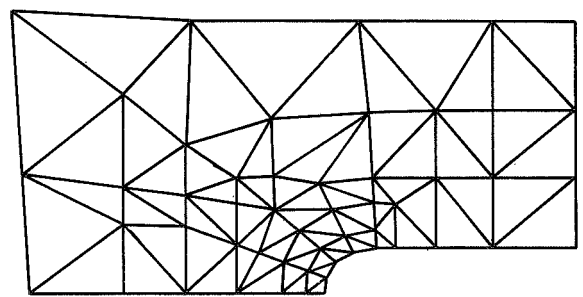
Fig. II   FINITE ELEMENT IDEALIZATION OF QUADRANT OF NOTCHED BAR II

207
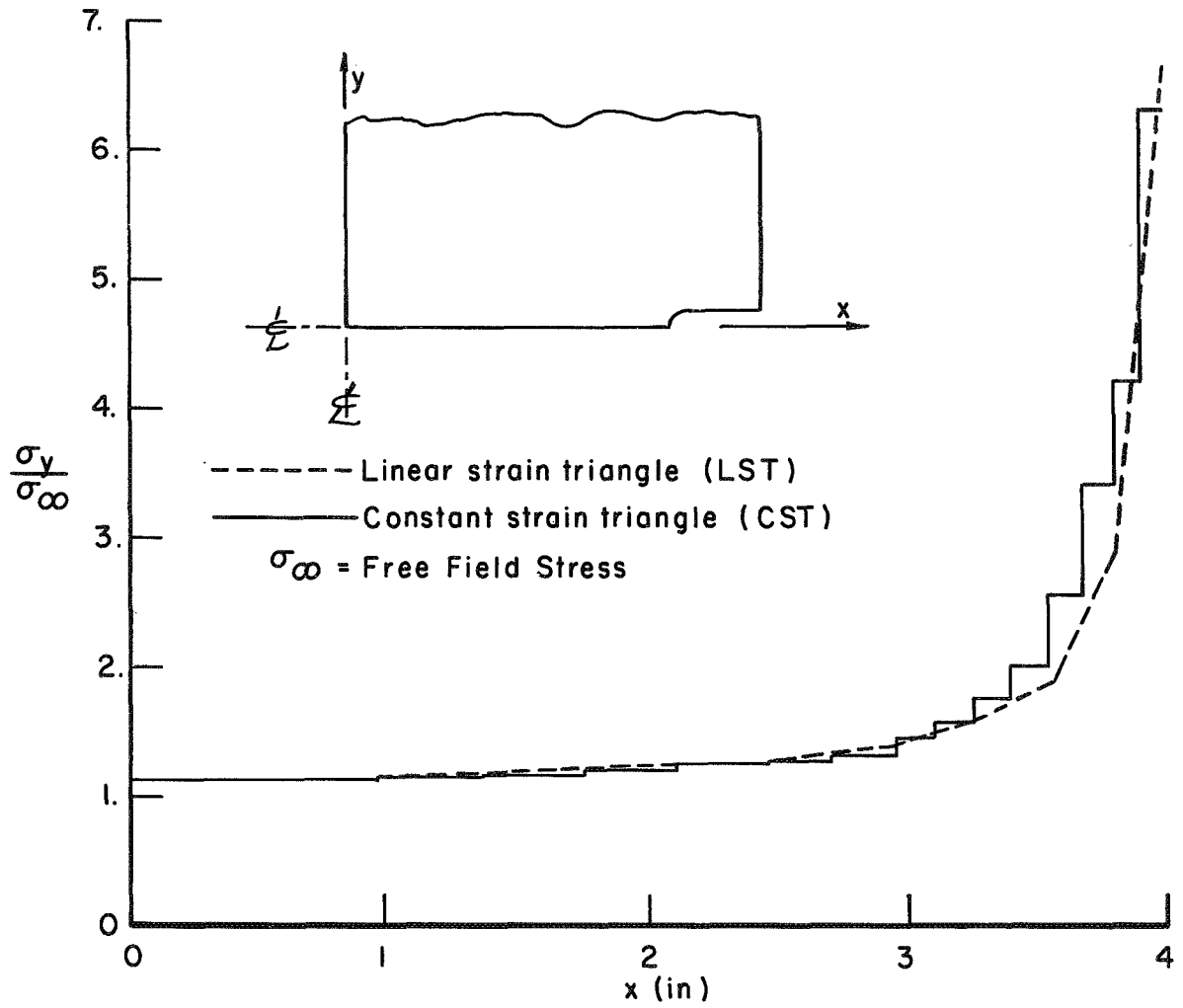
Fig. 12   NOTCHED BAR II, COMPARISON OF DISTRIBUTION OF NORMAL STRESS RATIO FOR CST AND LST TRIANGLES
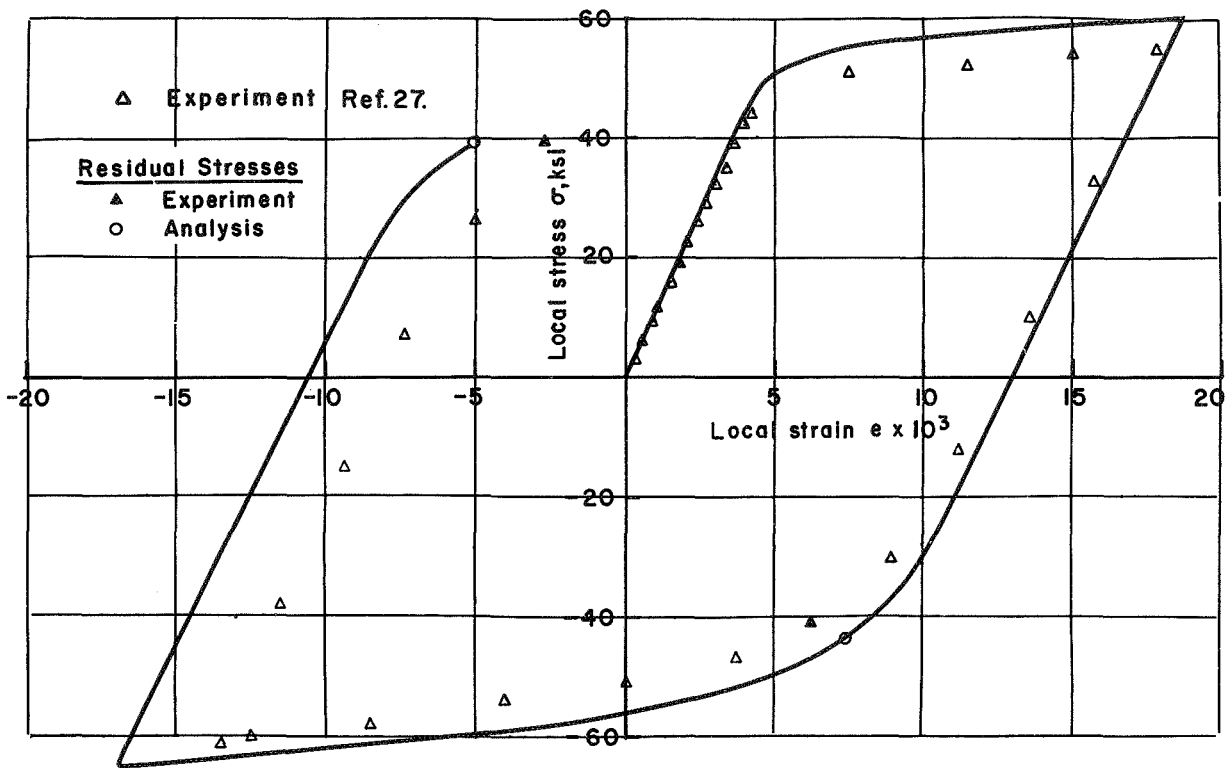
Fig.13   NOTCHED BAR II: LOCAL STRESS vs STRAIN AT NOTCH ROOT FOR FIRST CYCLE
OF REVERSED LOADING

Fig.14 NOTCHED BAR II - THREE CYCLE LOAD vs STRAIN CURVE AT NOTCH ROOT

S_{max}= 25 ksi
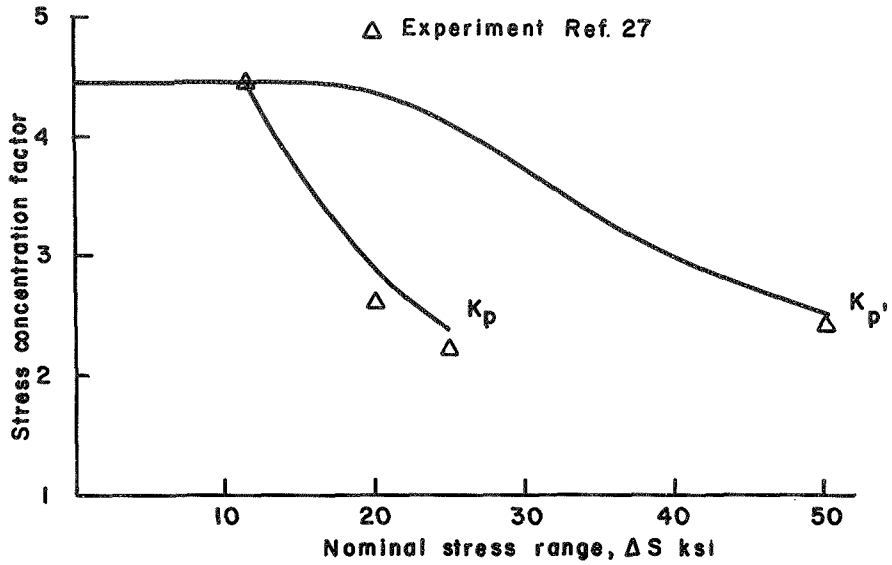
Fig. 15 NOTCHED BAR II: PLASTIC STRESS CONCENTRATION FACTORS AT NOTCH ROOT vs NET SECTION STRESS RANGE
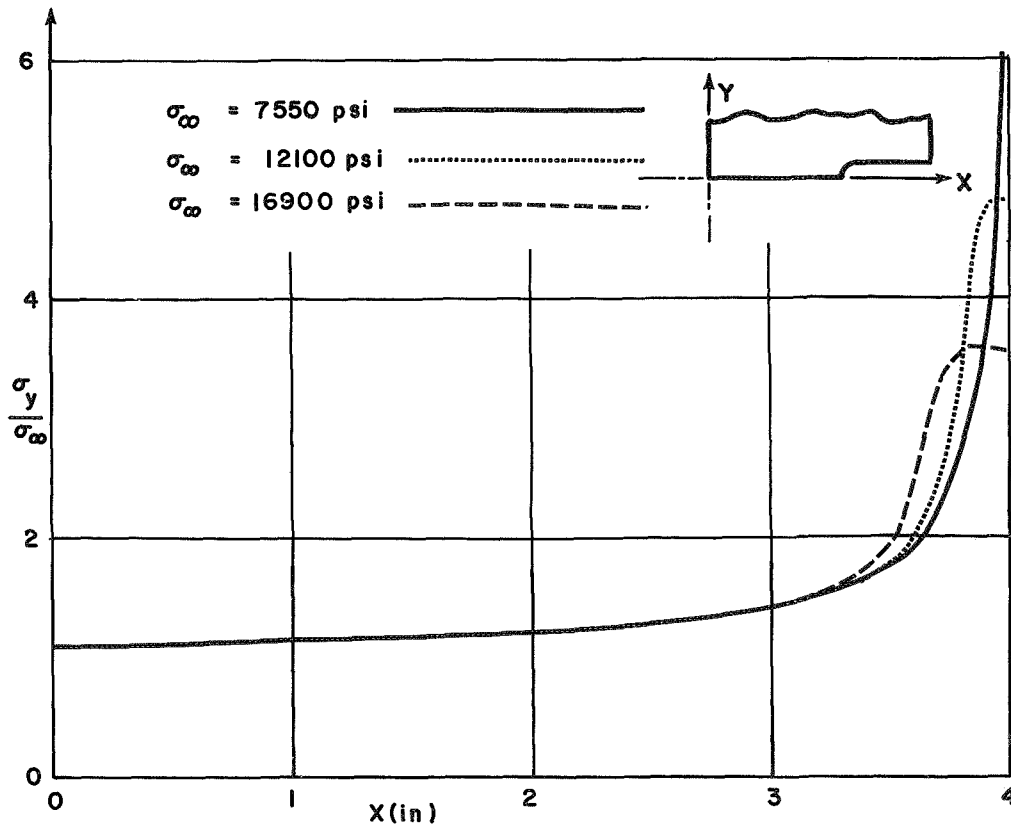
Fig. 16 NOTCHED BAR II – DISTRIBUTION OF NORMAL STRESS RATIO σ_y / σ_∞ ALONG AXIS OF SYMMETRY, y = 0
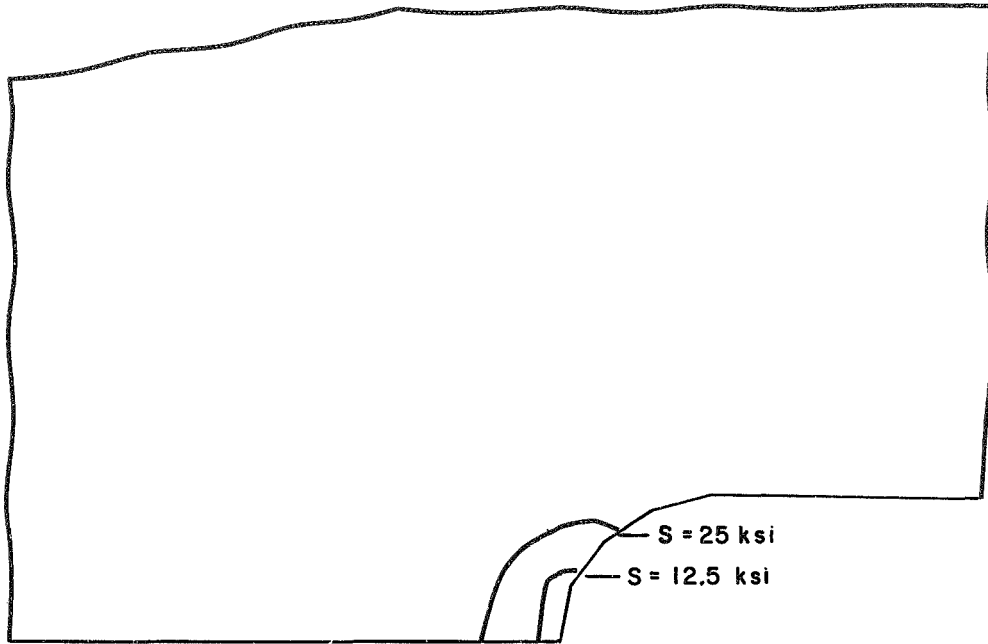
(a) First cycle of loading
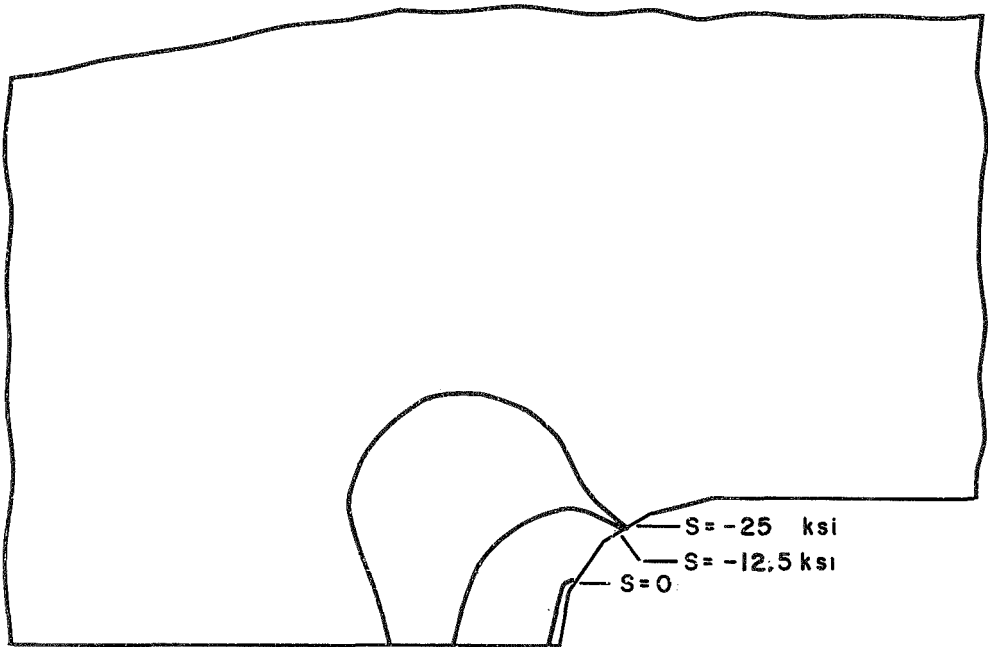
(b) First cycle of unloading and reversed loading

Fig. 17 NOTCHED BAR II: GROWTH OF ELASTIC-PLASTIC BOUNDARY

212
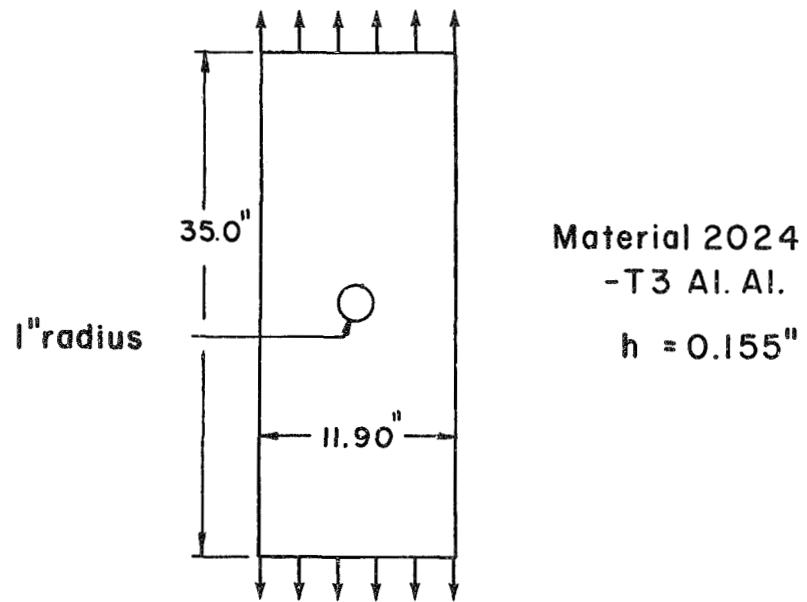
Fig. 18   RECTANGULAR SHEET WITH A
CENTRALLY LOCATED HOLE
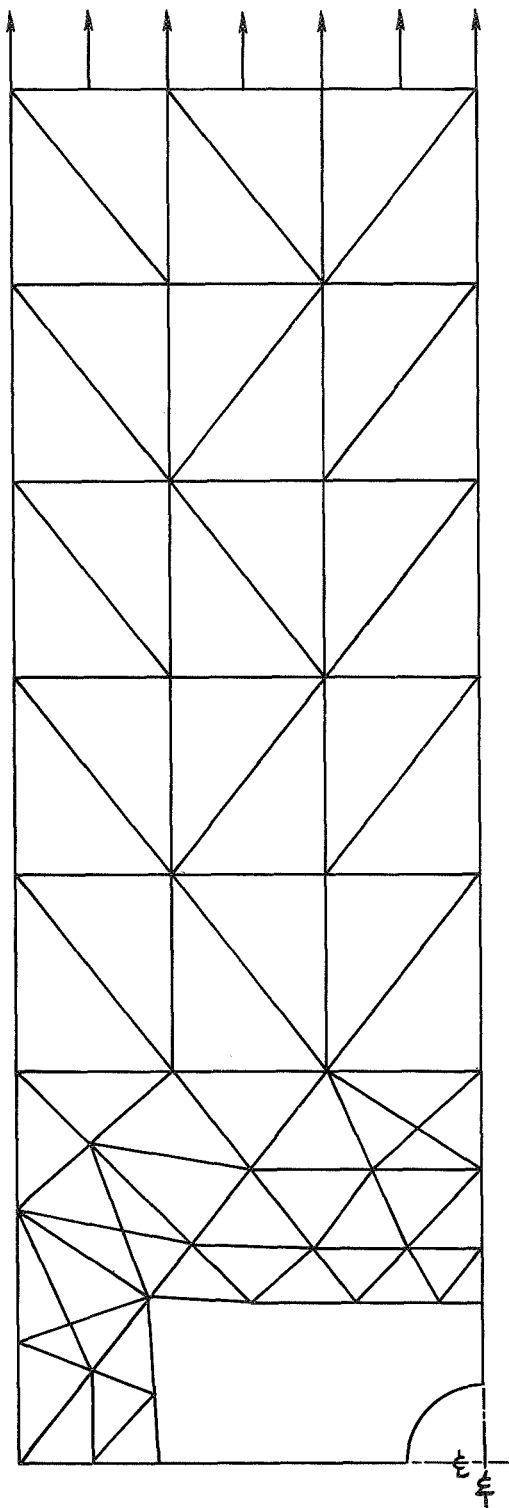
134 elements
301 nodes
566 degrees of freedom
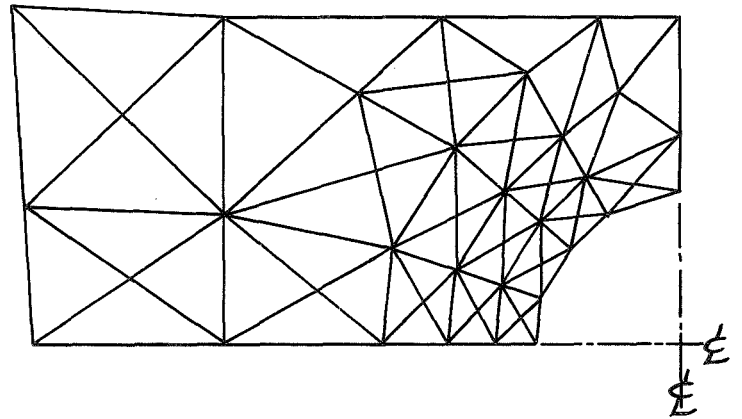
Fig. 19 FINITE ELEMENT IDEALIZATION OF QUADRANT OF RECTANGULAR
SHEET WITH CENTRALLY LOCATED HOLE
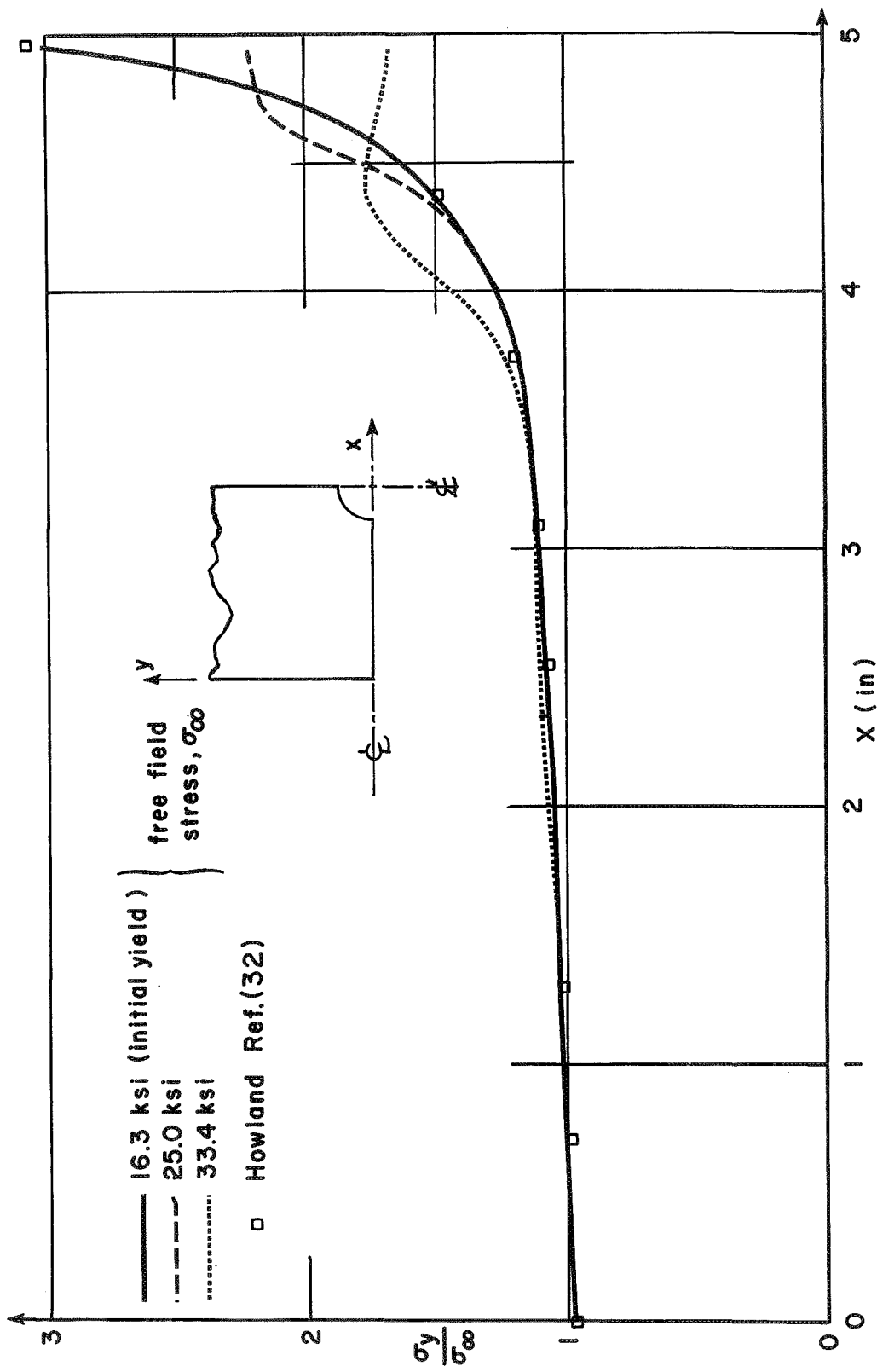
Fig. 20   RECTANGULAR SHEET WITH A CENTRALLY LOCATED HOLE : DISTRIBUTION OF
NORMAL STRESS RATIO, σ_y / σ_∞, ALONG HORIZONTAL AXIS OF SYMMETRY,
$y = 0$

215

EFFECTIVE STRESSES, IN ksi,
AT MAXIMUM ELASTIC LOAD
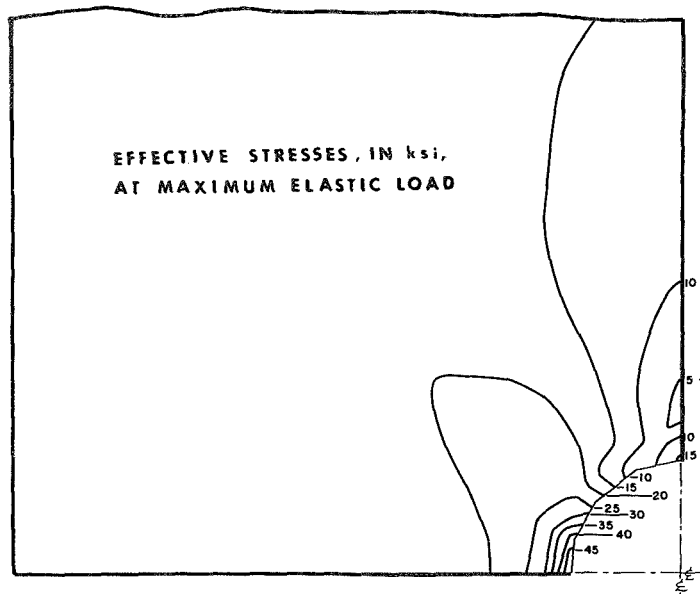
Fig. 21 RECTANGULAR SHEET WITH A CENTRALLY LOCATED HOLE:
CONTOURS OF EFFECTIVE STRESS AT MAXIMUM LOAD.

FIRST HALF CYCLE
EFFECTIVE STRESSES
AT MAXIMUM LOAD in ksi

FIRST HALF CYCLE RESIDUAL
EFFECTIVE STRESSES
In ksi

FULL CYCLE RESIDUAL EFFECTIVE STRESSES

FULL CYCLE EFFECTIVE
STRESSES AT MINIMUM
LOAD
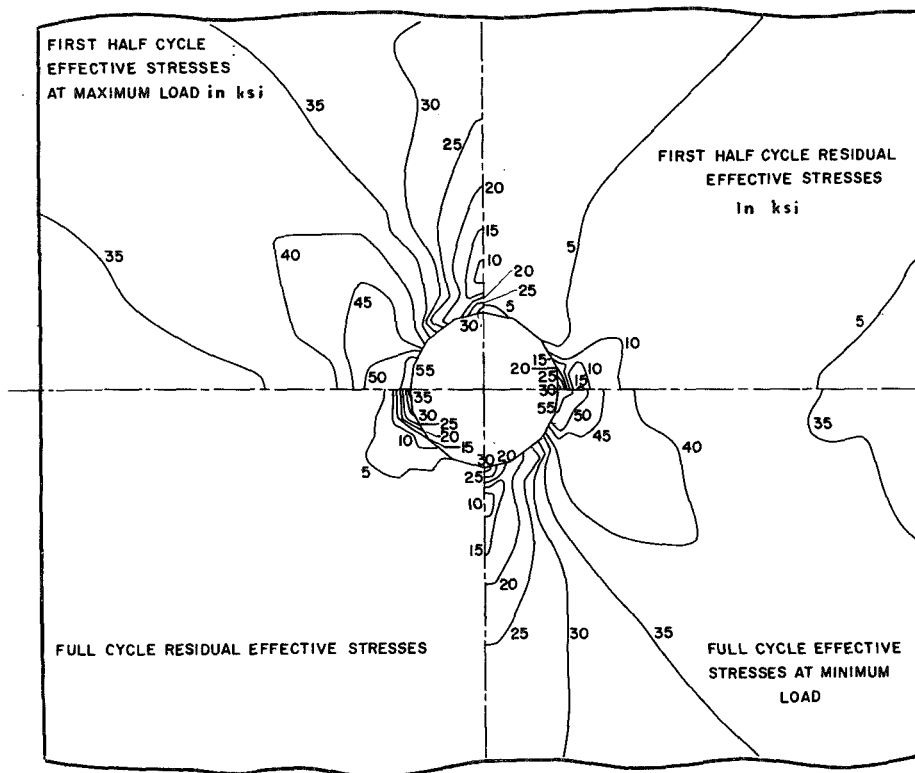
Fig. 22. COUNTOURS OF EFFECTIVE STRESS DURING FIRST
CYCLE OF LOADING
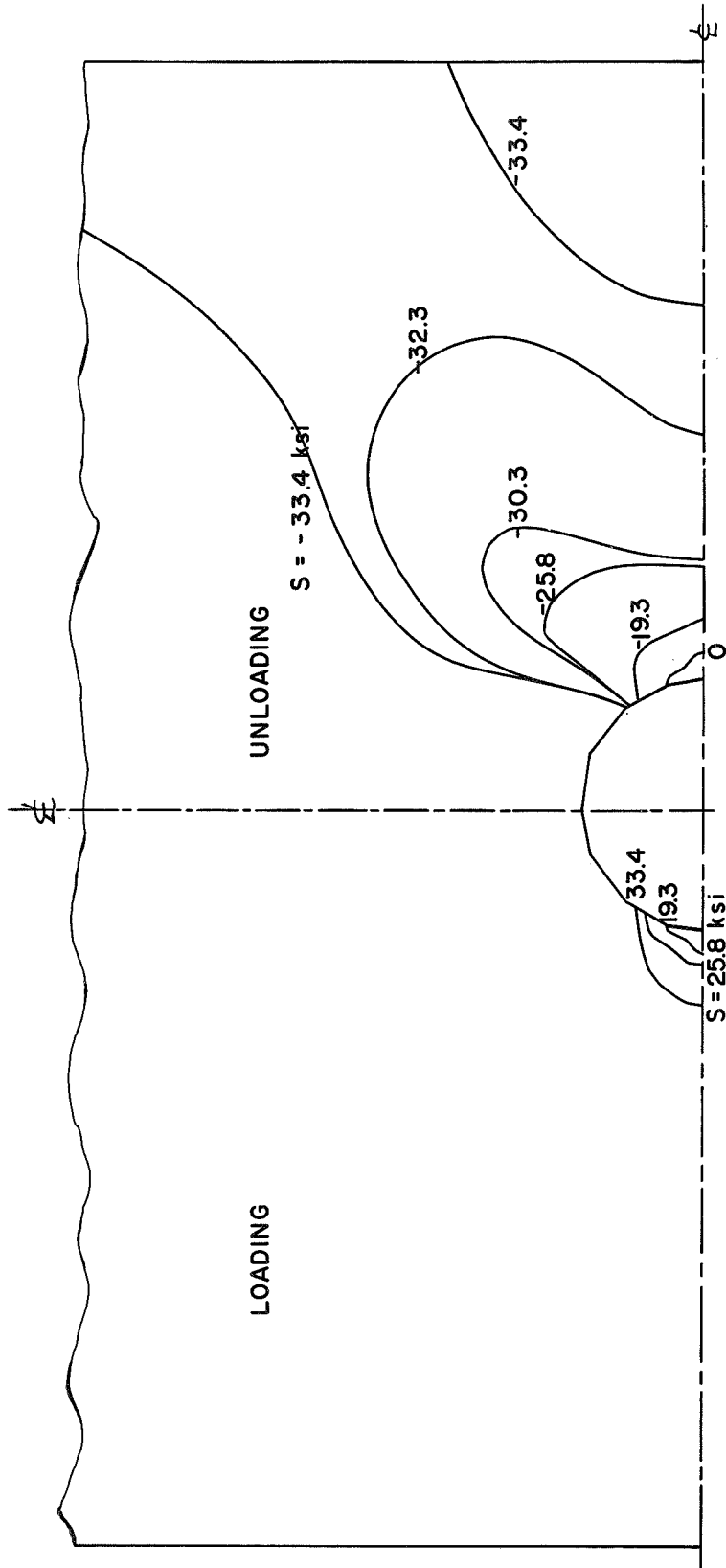
Fig.23 RECTANGULAR SHEET WITH A CENTRALLY LOCATED HOLE: GROWTH OF ELASTIC PLASTIC BOUNDARY

217
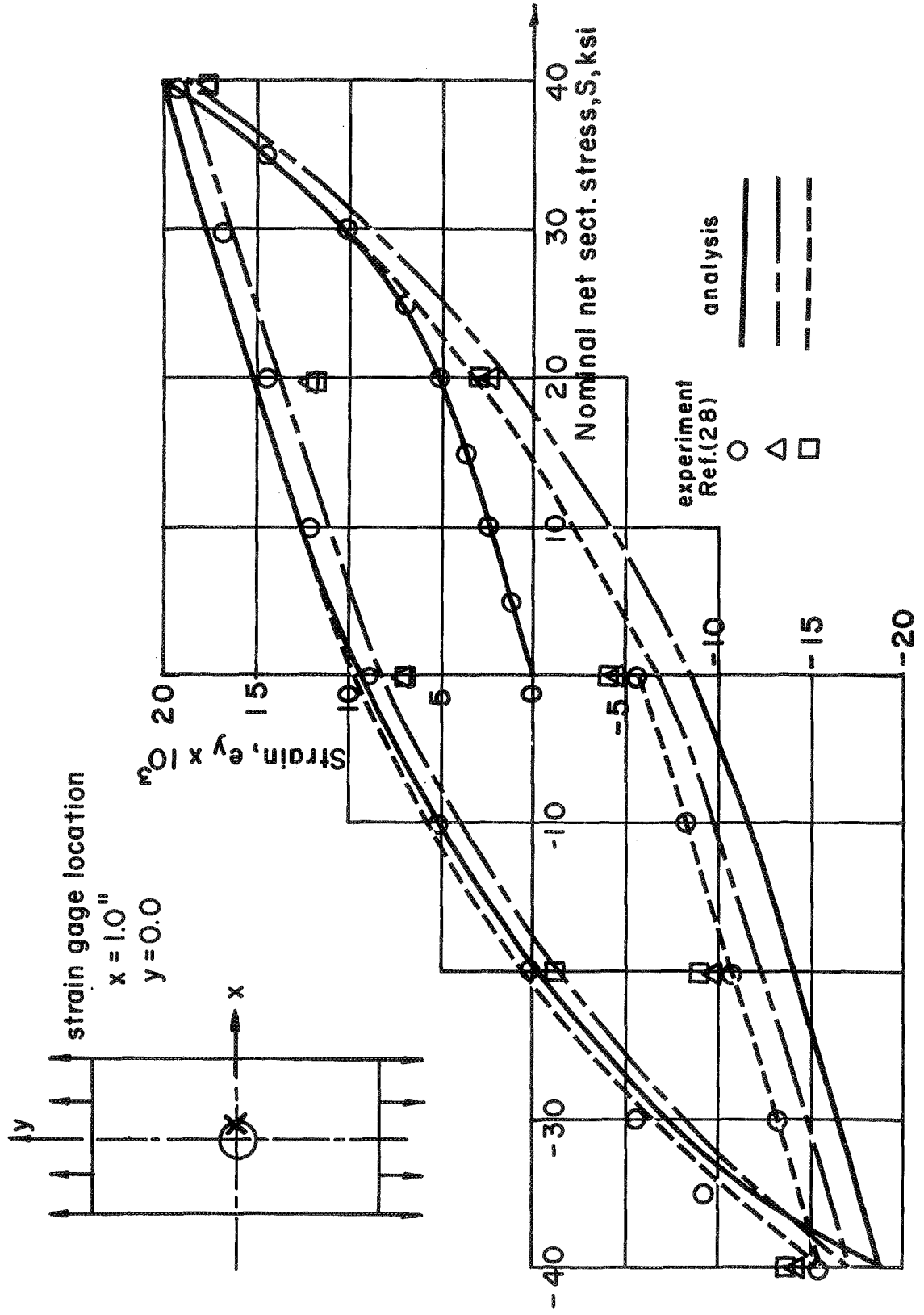
(a) Three cycle net section stress vs. strain at hole boundary

Fig. 24   RECTANGULAR SHEET WITH A CENTRALLY LOCATED HOLE

218
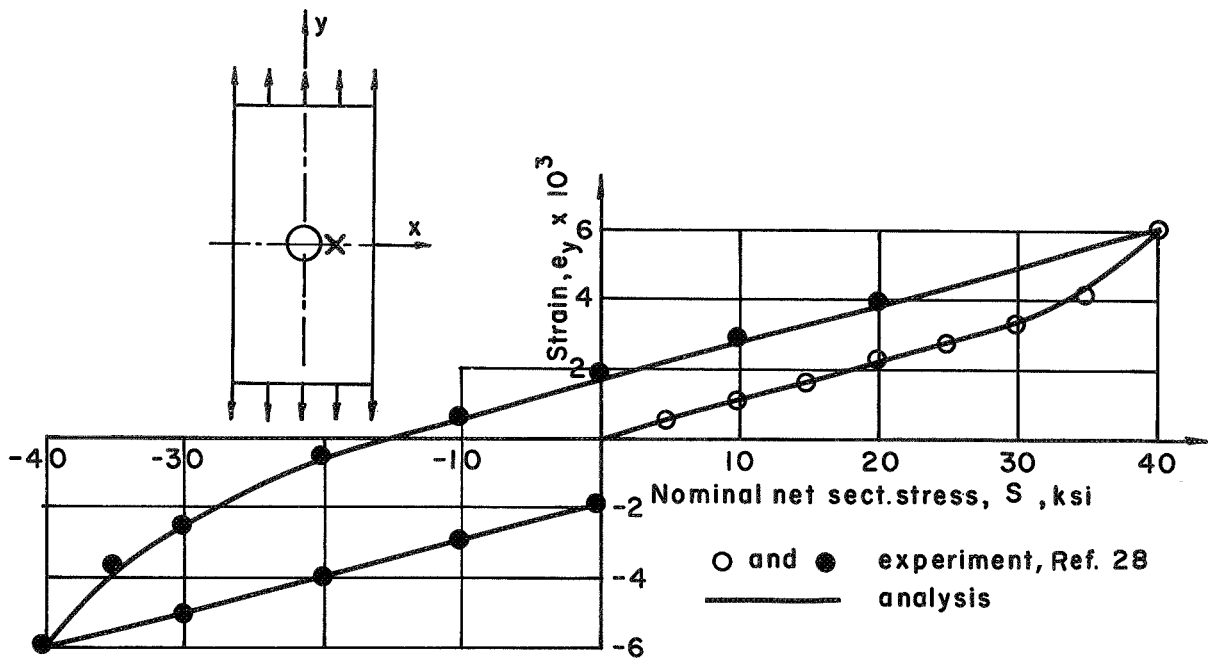
(b) One cycle net section stress vs. strain curve at x = 1.606", y = 0.0"
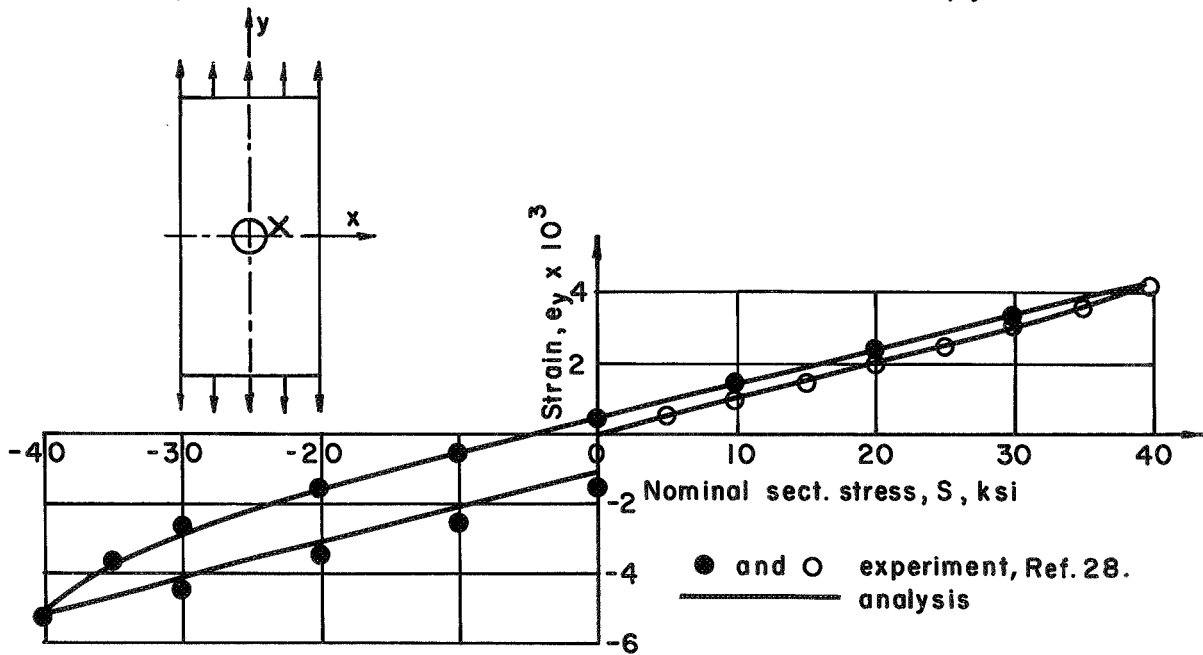
(c) One cycle net section vs. strain curve at x = 1.952", y = .561

Fig. 24 (cont.)   RECTANGULAR SHEET WITH A CENTRALLY
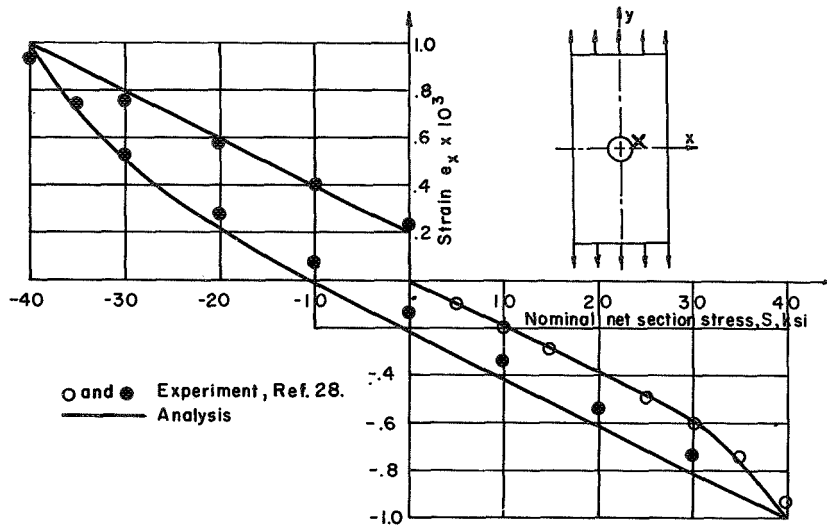
LOCATED HOLE

(d) One cycle net section stress vs. strain curve at x = 1.952", y = .561"
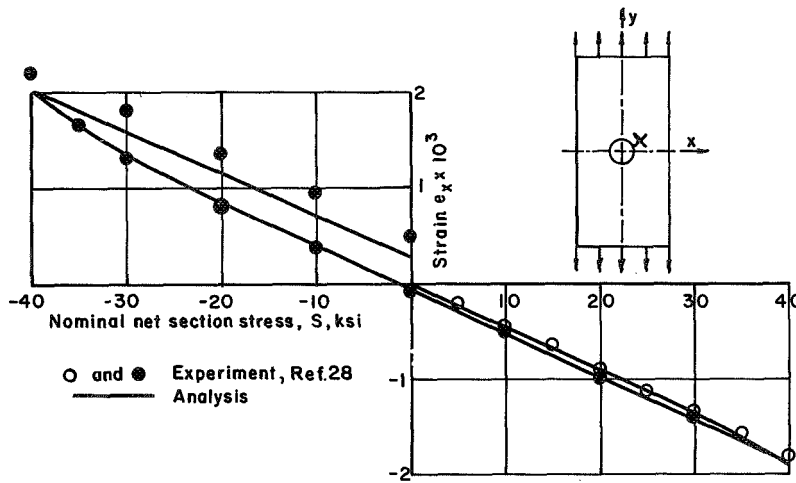
(e) One cycle net section stress vs strain curve at x = 1.585", y = 1.229"
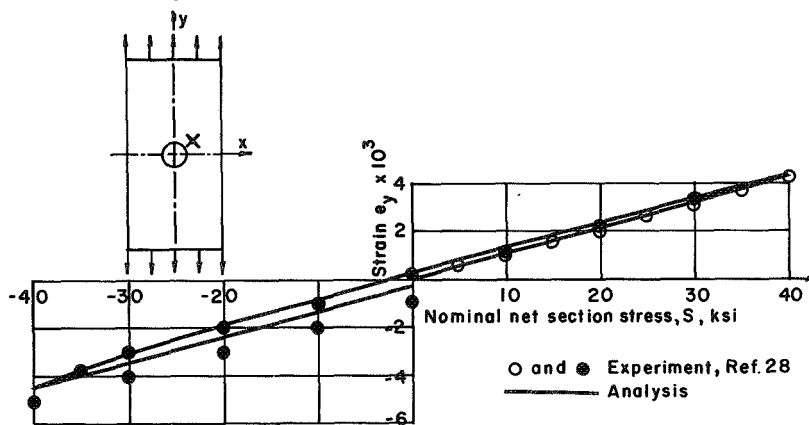
(f) One cycle net section stress vs. strain curve at x = 1.585" y = 1.229"

Fig. 24 (cont.) RECTANGULAR SHEET WITH A CENTRALLY LOCATED HOLE
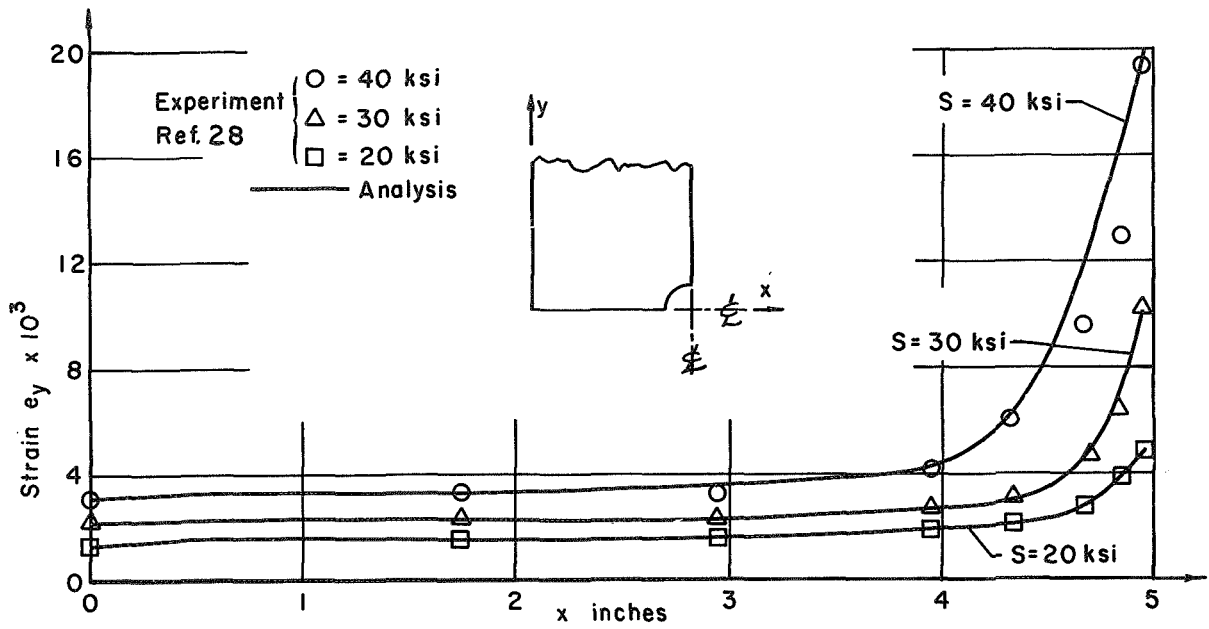
Fig. 25 RECTANGULAR SHEET WITH A CENTRALLY LOCATED HOLE: DISTRIBUTION OF
NORMAL STRAIN, e_y , ALONG HORIZONTAL AXIS OF SYMMETRY FOR FIRST
CYCLE OF LOADING
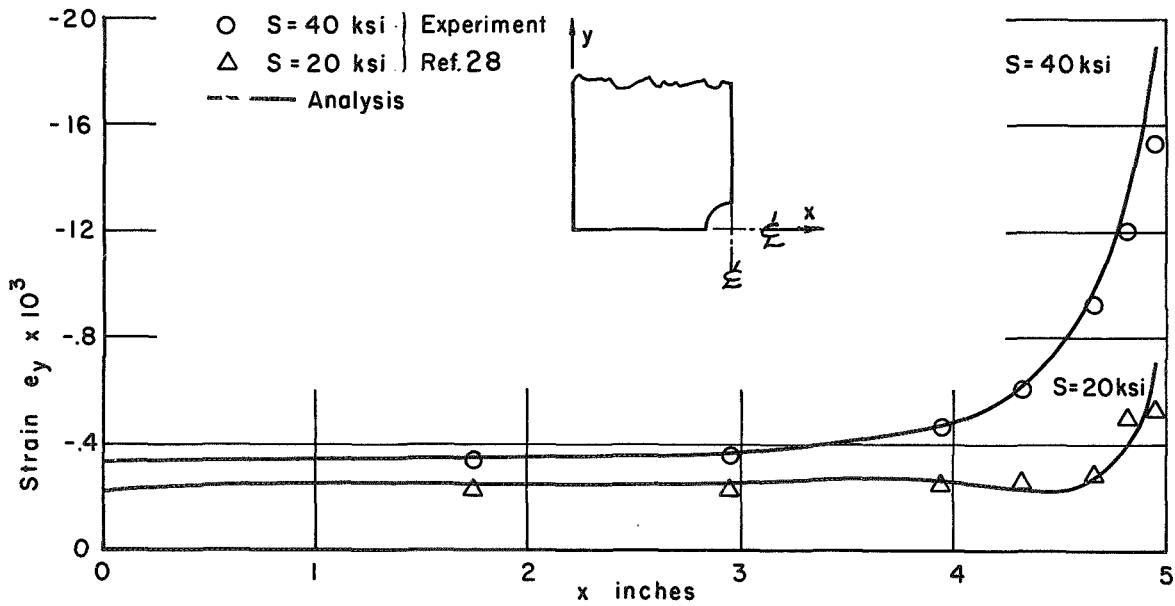
Fig. 26 RECTANGULAR SHEET WITH A CENTRALLY LOCATED HOLE : DISTRIBUTION OF
NORMAL STRAIN, e_y , ALONG HORIZONTAL AXIS OF SYMMETRY FOR FIRST
CYCLE OF REVERSED LOADING.
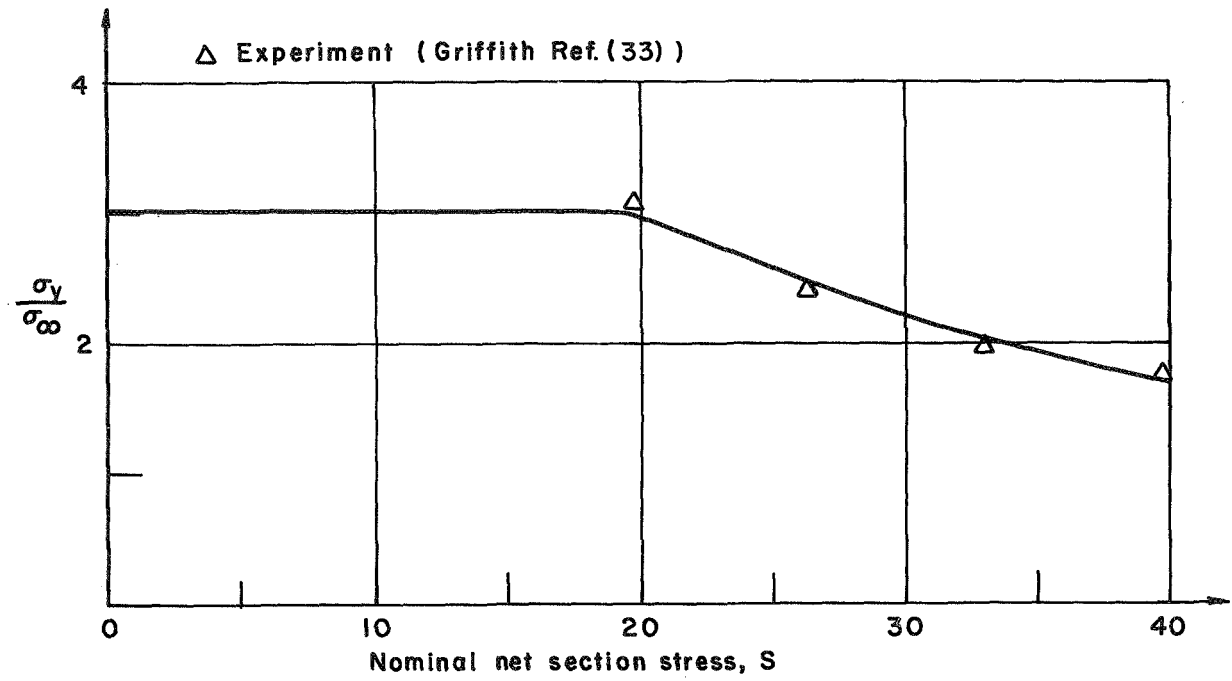
Fig. 27. RECTANGULAR SHEET WITH CENTRALLY LOCATED HOLE: PLASTIC STRESS
CONCENTRATION FACTOR, σ/σ_{∞}

222

144 Elements
313 Nodes
600 Degrees of freedom

$e/D = 2$

P_i
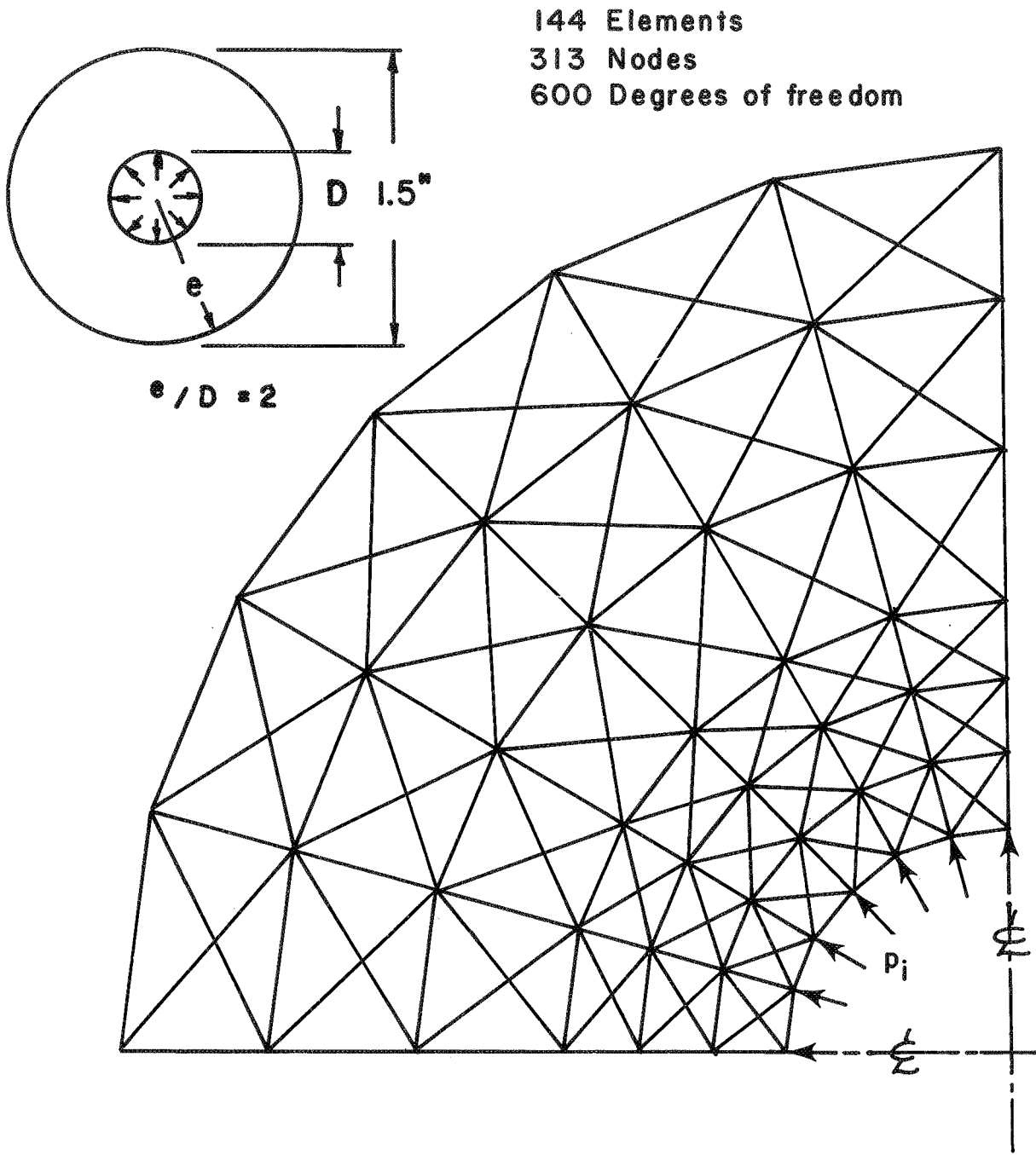
Fig. 28   ANNULAR DISC AND QUADRANT OF IDEALIZATION

223
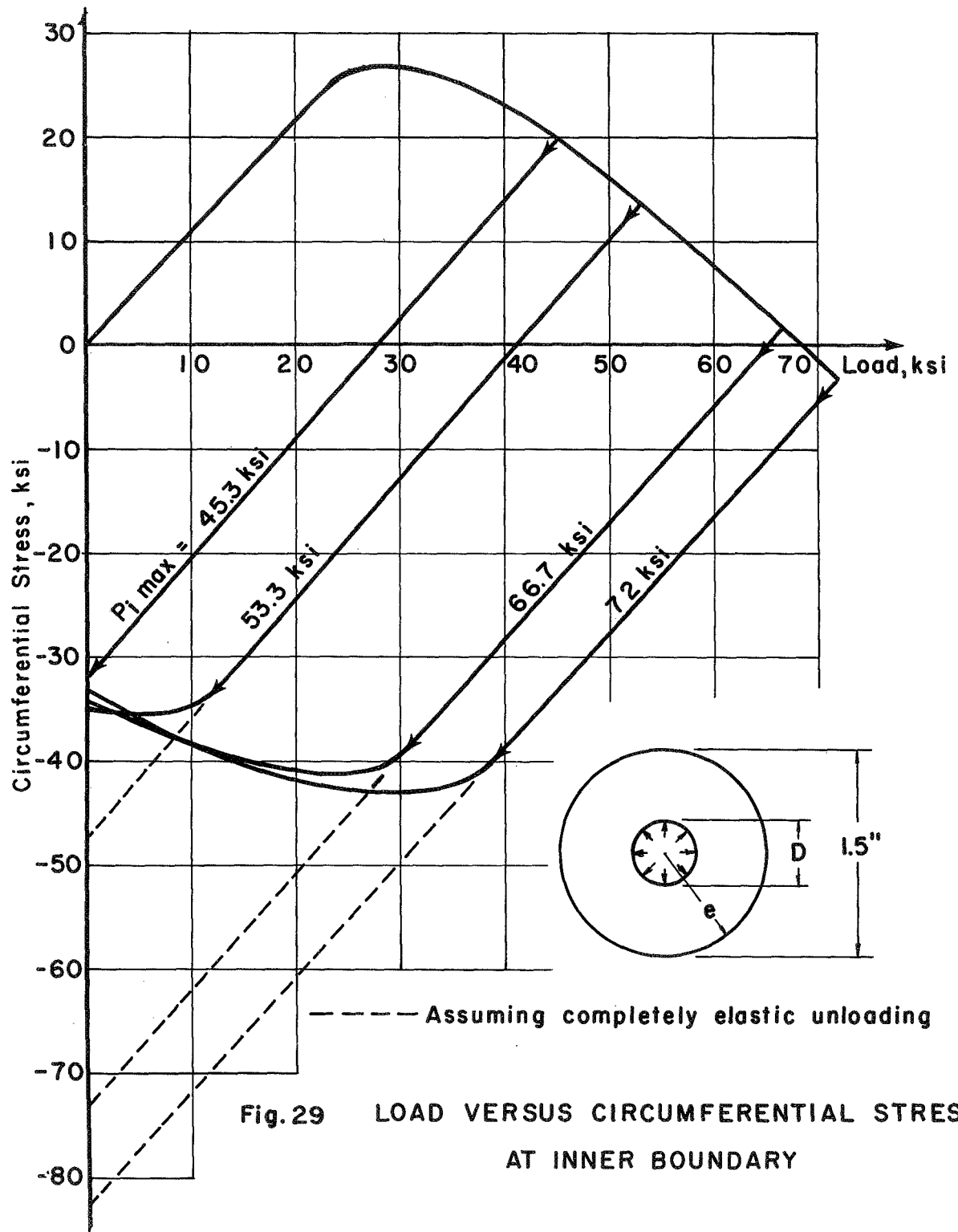
Fig. 29   LOAD VERSUS CIRCUMFERENTIAL STRESS
AT INNER BOUNDARY

– – – – – Assuming completely elastic unloading

224
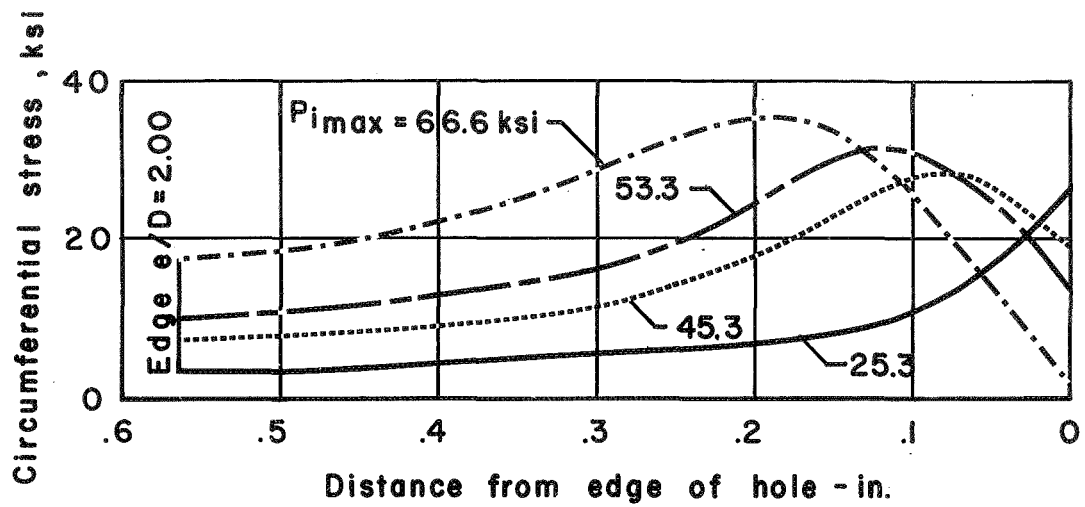
Fig.30   RADIAL DISTRIBUTION OF CIRCUMFERENTIAL STRESS
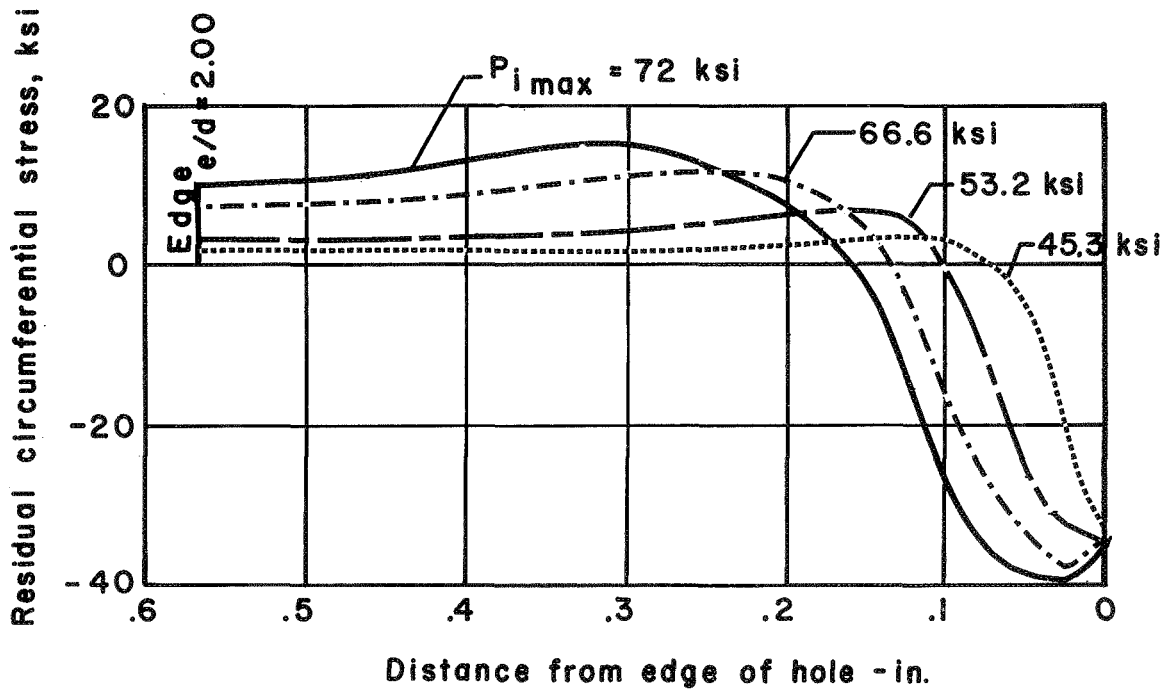
Fig. 31   RADIAL DISTRIBUTION OF RESIDUAL
CIRCUMFERENTIAL STRESS

225

Displacement Assumption:

$$w = \alpha_1 + \alpha_2 x + \alpha_3 x^2 + \alpha_4 x^3$$

Initial Strain Distribution

$$\epsilon = \left(\frac{z-\bar{z}}{t-\bar{z}}\right)\left[\epsilon_{oi}\left(1-\frac{x}{\ell}\right) + \epsilon_{oj}\left(\frac{x}{\ell}\right)\right]$$

Elastic-Plastic Boundary

$$\bar{z} = \left(\bar{z}_j - \bar{z}_i\right)\left(\frac{x}{\ell}\right) + \bar{z}_i$$
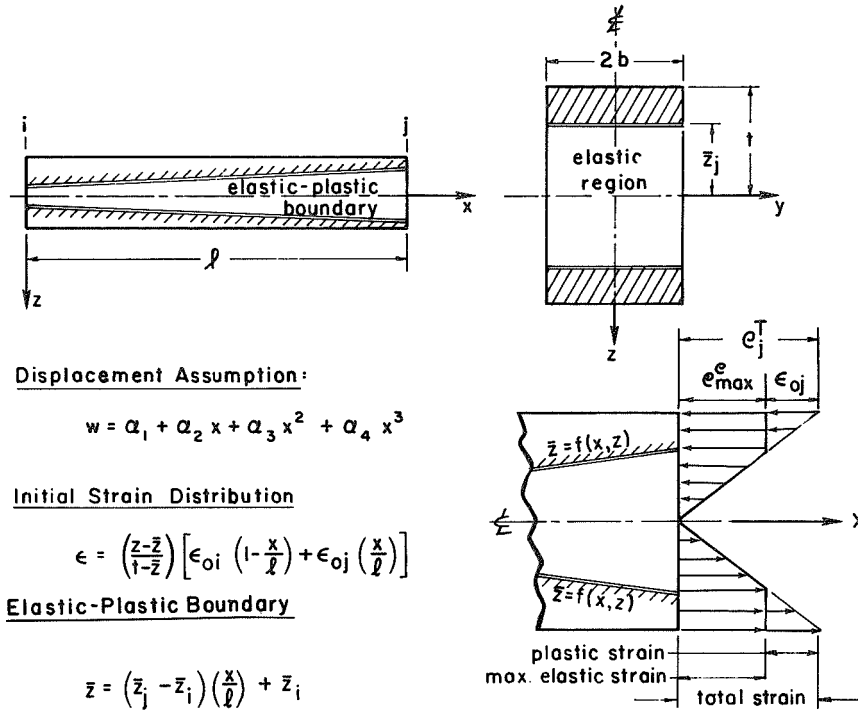
Fig. 32 TYPICAL ELASTIC-PLASTIC BEAM ELEMENT
(PURE BENDING)

Displacement Assumptions:

$$w = \alpha_1 + \alpha_2 x + \alpha_3 x^2 + \alpha_4 x^3$$

$$u = \alpha_5 + \alpha_6 x$$

Initial Strain Distribution:

$$\epsilon^u = \left(\frac{\bar{z}^u - z}{\bar{z}^u}\right)\left[\epsilon_i^u\left(1-\frac{x}{\ell}\right) + \epsilon_j^u\left(\frac{x}{\ell}\right)\right]$$

$$\epsilon^L = \left(\frac{z-\bar{z}^L}{2t-\bar{z}^L}\right)\left[\epsilon_i^L\left(1-\frac{x}{\ell}\right) + \epsilon_j^L\left(\frac{x}{\ell}\right)\right]$$

Elastic-Plastic Boundary

$$\bar{z}^u = \left(\bar{z}_j^u - \bar{z}_i^u\right)\left(\frac{x}{\ell}\right) + \bar{z}_i^u$$

and

$$\bar{z}^L = \left(\bar{z}_j^L - \bar{z}_i^L\right)\left(\frac{x}{\ell}\right) + \bar{z}_i^L$$
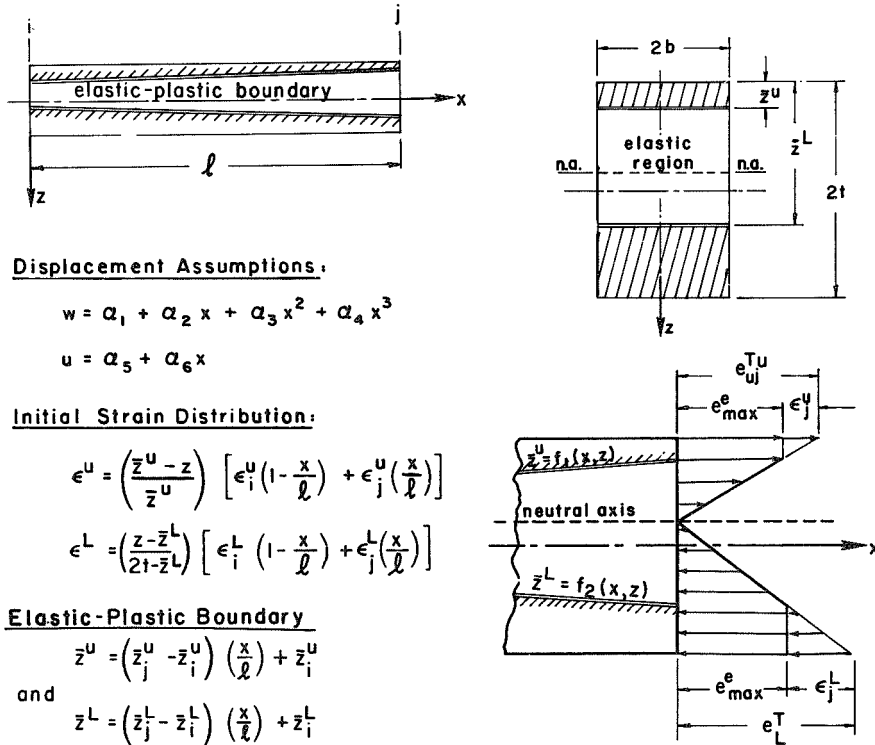
Fig. 33 TYPICAL ELASTIC-PLASTIC BEAM ELEMENT
(BENDING AND AXIAL LOADS)

226
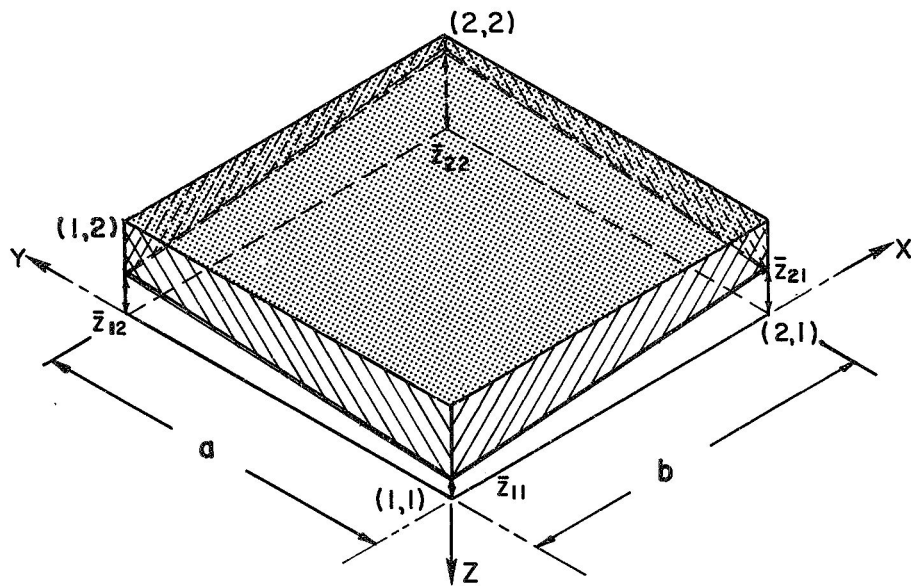
Displacement Assumption:

$$w = \sum_{i=1}^{2} \sum_{j=1}^{2} \left[H_{oi}^{(1)}(x) H_{oj}^{(1)}(y) W_{ij} + H_{1i}^{(1)}(x) H_{oj}^{(1)}(y) W_{,xij} + H_{oi}^{(1)}(x) H_{1j}^{(1)}(y) W_{,yij} + H_{1i}^{(1)}(x) H_{1j}^{(1)}(y) W_{,xyij} \right]$$

Initial Strain Distribution:

$$\epsilon(x,y,z) = \left(\frac{z-\bar{z}}{t-\bar{z}} \right) \sum_{i=1}^{2} \sum_{j=1}^{2} H_{oi}^{(0)}(x) H_{oj}^{(0)}(y) \epsilon_{ij}$$

Elastic-Plastic Boundary:

$$\bar{z}(x,y) = \sum_{i=1}^{2} \sum_{j=1}^{2} H_{oi}^{(0)}(x) H_{oj}^{(0)}(y) \bar{z}_{ij}$$

Fig. 34. TYPICAL ELASTIC-PLASTIC RECTANGULAR PLATE ELEMENT (PURE BENDING)

227
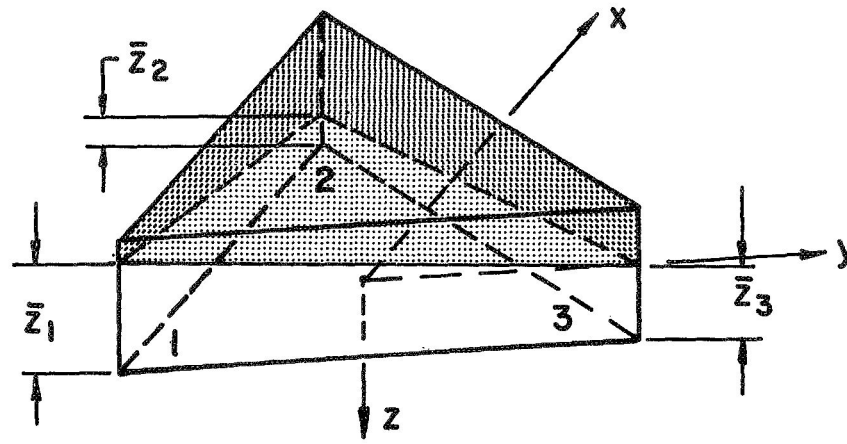
Displacement Assumption:

$$w = a_1 + a_2 x + a_3 y + a_4 x^2 + a_5 xy + \cdots\cdots\cdots\cdots + a_{21} y^5$$

Initial Strain Distribution:

$$\epsilon(x, y, z) = \left(\frac{z - \bar{z}}{t - \bar{z}}\right) \sum_{i=1}^{3} \omega_i \, \epsilon_i$$

Elastic-Plastic Boundary:

$$\bar{z}(x, y) = \sum_{i=1}^{3} \omega_i \, \bar{z}_i$$

Fig. 35. TYPICAL TRIANGULAR ELASTIC-PLASTIC
PLATE ELEMENT (PURE BENDING)

228
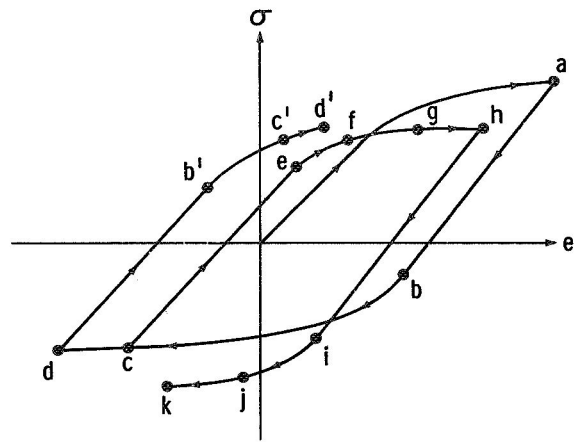
Typical Stress – Strain Curve
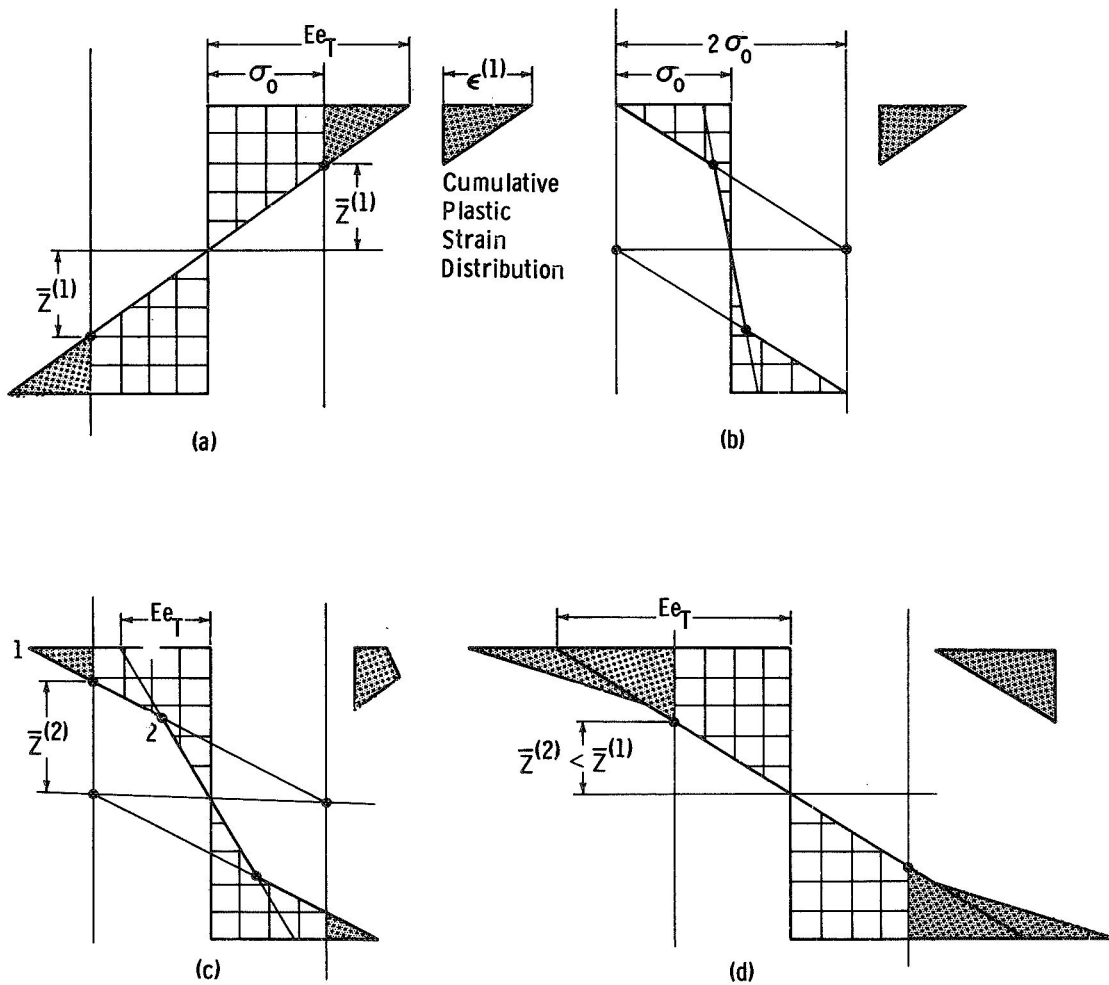
Fig. 36 Stress and Plastic Strain Distributions
For Cyclic Bending of a Beam
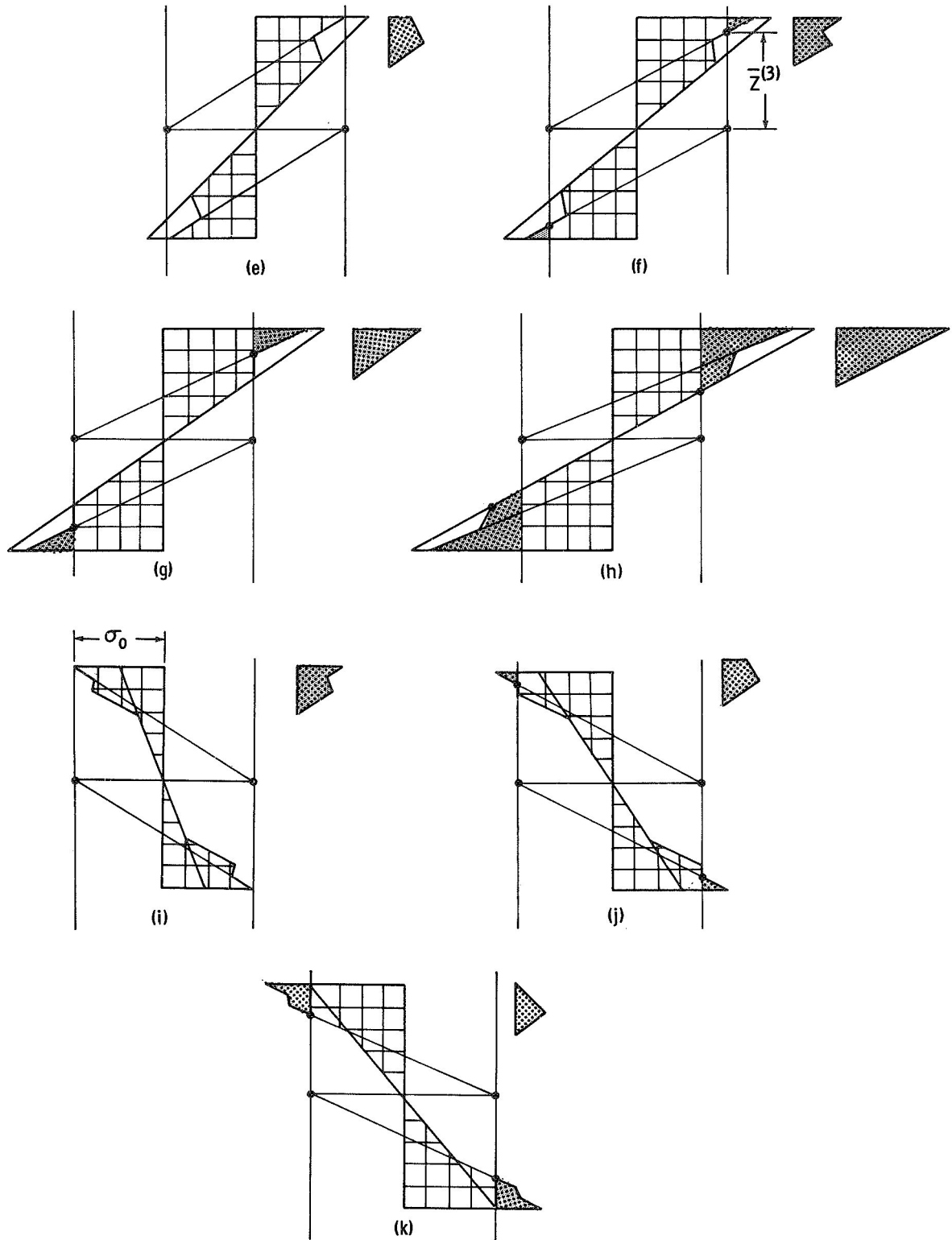
Fig. 36 (Cont) Stress and Plastic Strain Distributions
For Cyclic Bending of a Beam

230
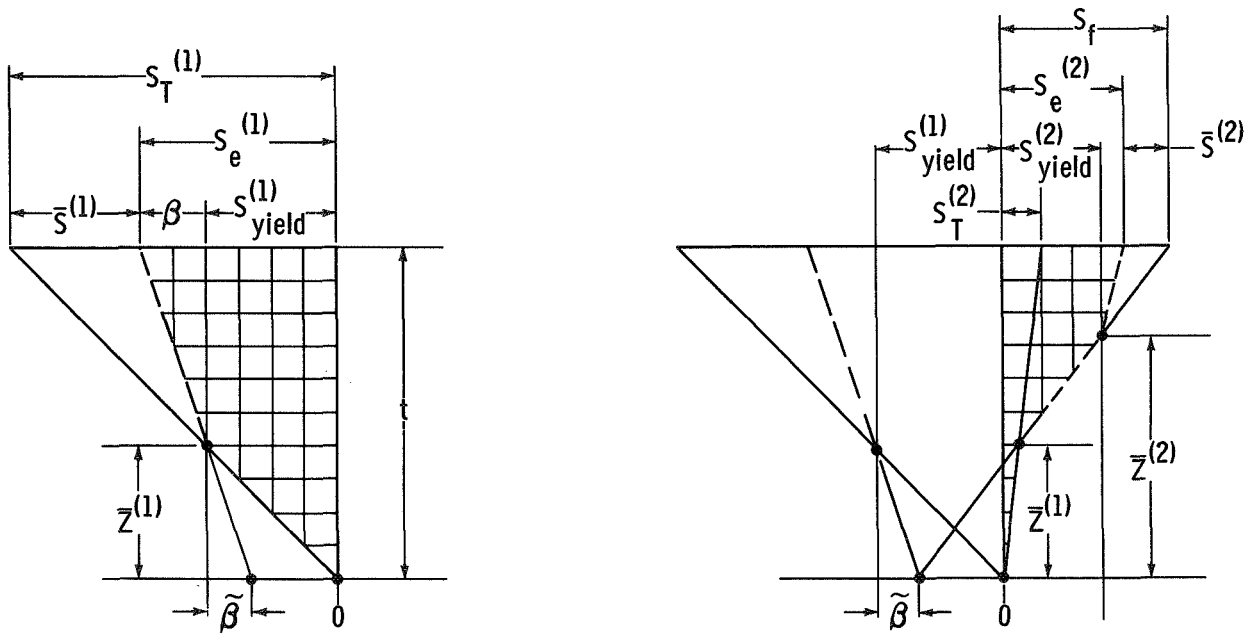
(a) Initial Loading

(b) Reversed Loading

$$\bar{Z}^{(1)} = t \left[\frac{S_{yield}^{(1)}}{S_T^{(1)}} \right]$$

$$\bar{\bar{Z}}^{(2)} = t \left[\frac{S_{yield}^{(1)} + S_{yield}^{(2)} - \widetilde{\beta}}{S_{yield}^{(1)} + S_f - \widetilde{\beta}} \right]$$

Fig. 37 Depth of Elastic-Plastic Boundary For Multiaxial Cyclic Loading

231
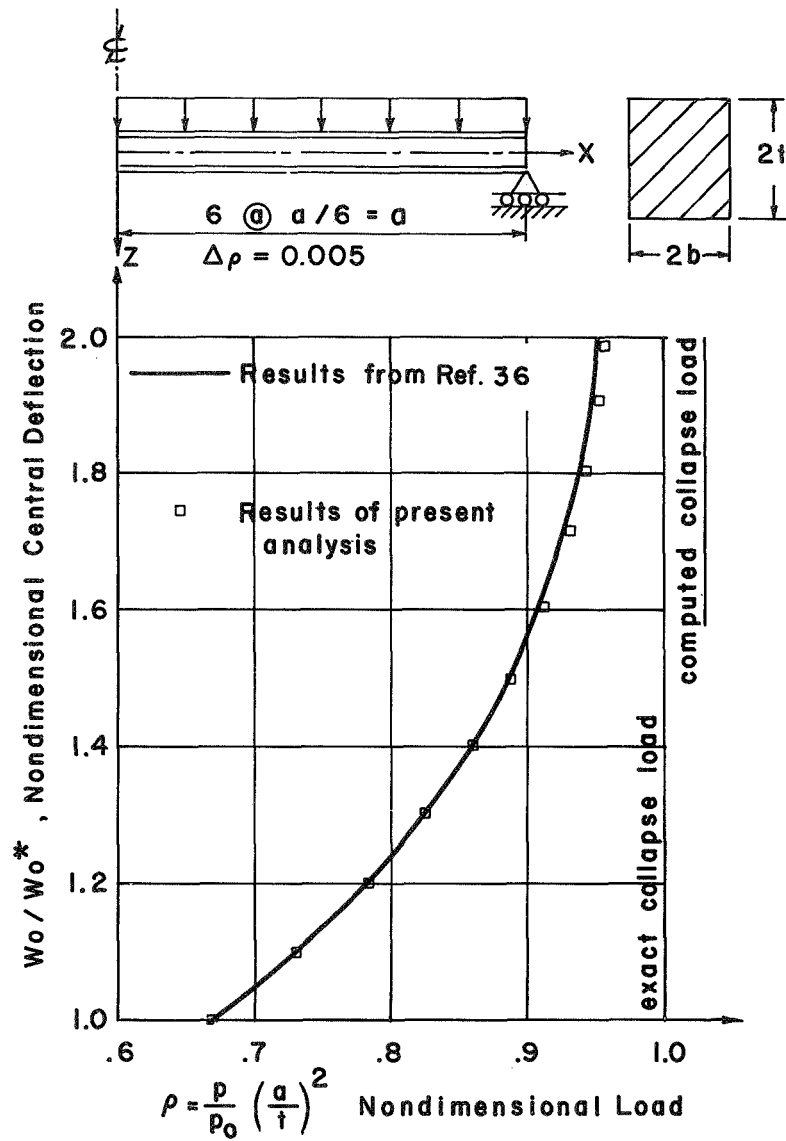
(a) Load versus center deflection
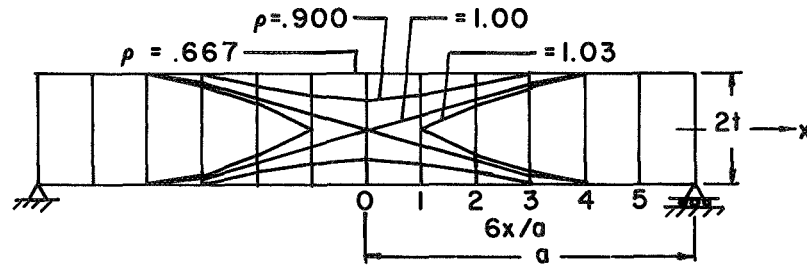
(b) Progression of elastic-plastic boundary.

Fig. 38 UNIFORMLY LOADED SIMPLY SUPPORTED BEAM
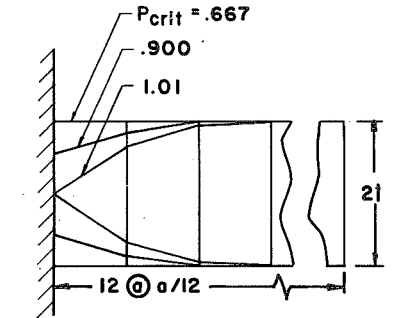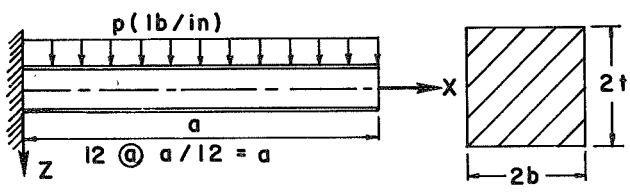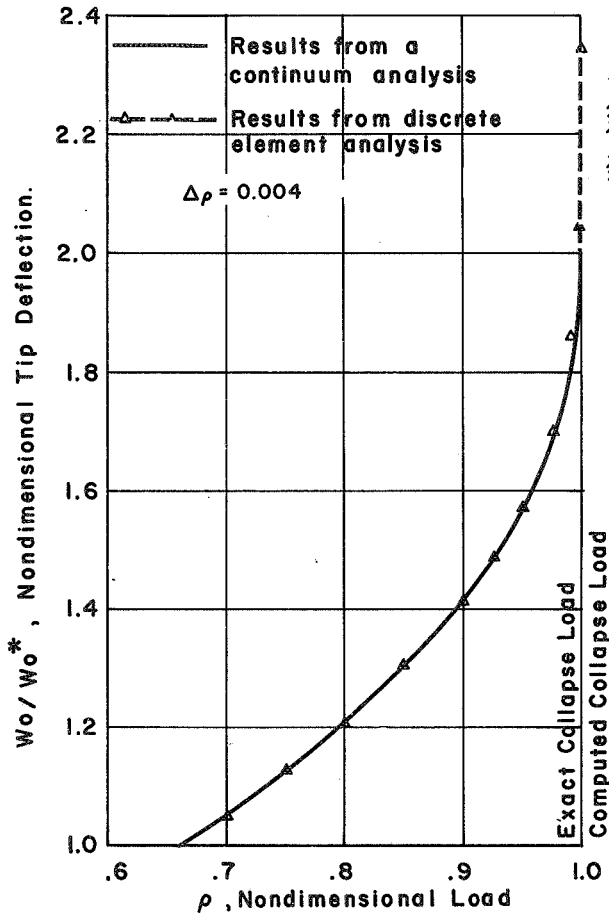
(a) Load vs. center deflection

(b) Progression of elastic-plastic boundary

Fig. 39 UNIFORMLY LOADED CANTILEVERED BEAM

233
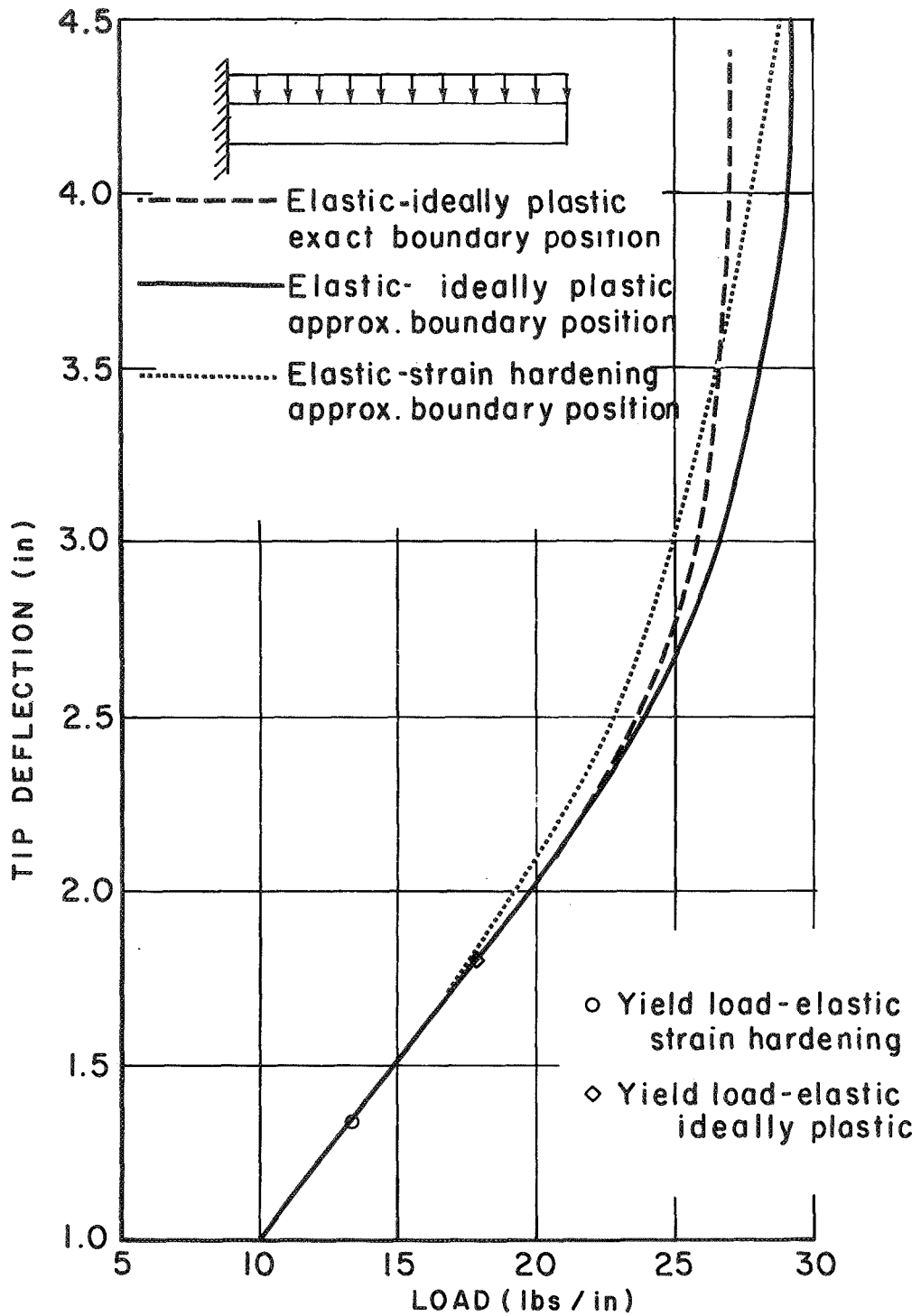
Fig. 40 LOAD VERSUS TIP DEFLECTION OF
CANTILEVER BEAM

234
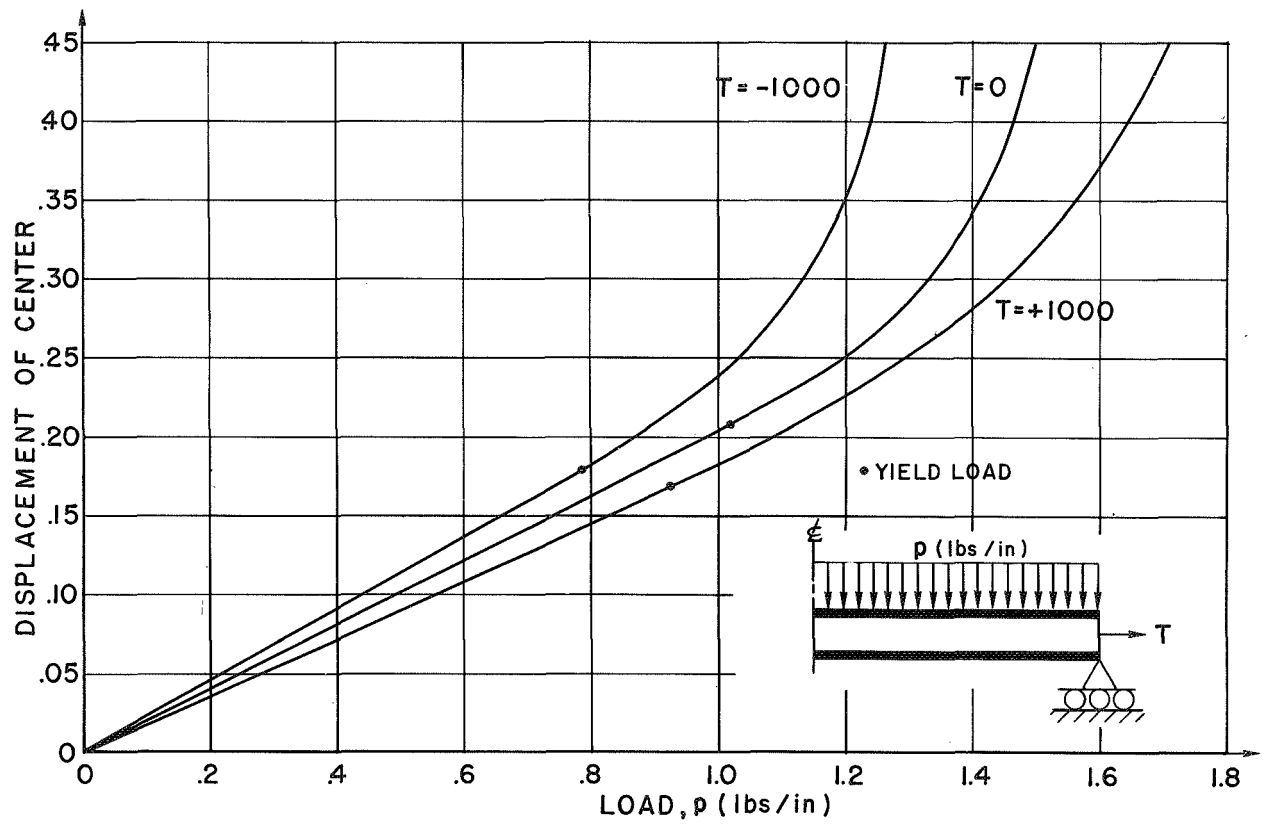
Fig. 41. SIMPLY SUPPORTED BEAM SUBJECTED TO COMBINED BENDING
AND AXIAL LOADS

235
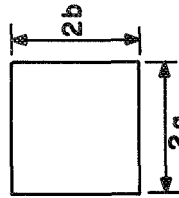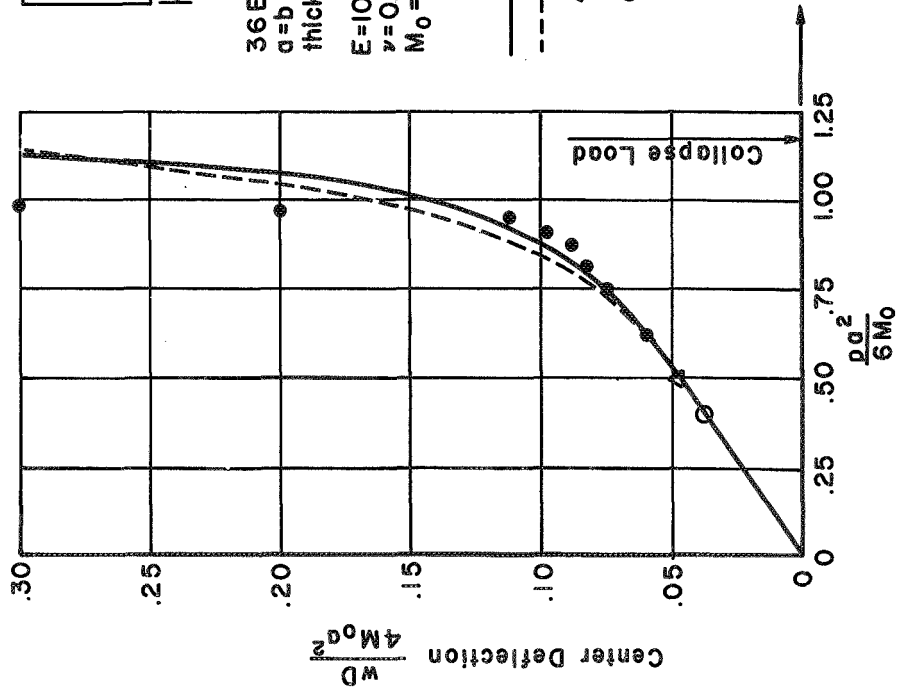
36 Element Idealization (6×6)
a=b=10 in.
thickness 2t=0.10 in.
$E=10^7$ lbs/in.^{2}
$\nu=0.3$
$M_0=\sigma_0 \times t^2 =90$ lb-in/in.

—— Elastic–ideally plastic
– – – Elastic–strain hardening
△— Yield load, elastic–ideally plastic
○— Yield load, elastic–strain hardening
● Reference 38

$\eta=\dfrac{b}{a}=1$
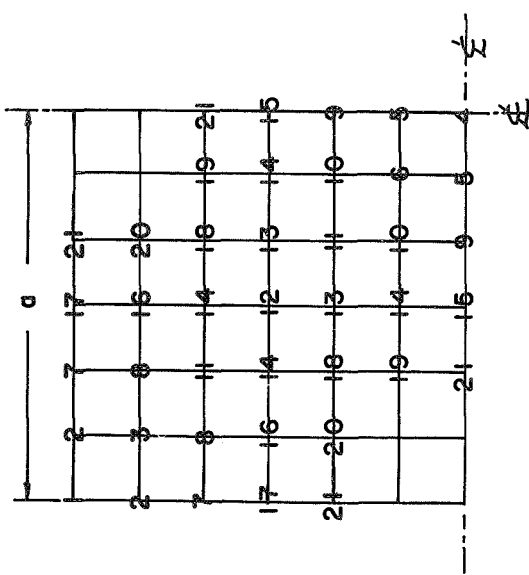
Sequence	Load $\dfrac{pa^2}{6M_0}$	Sequence	Load $\dfrac{pa^2}{6M_0}$
1	.502	12	.733
2	.539	13	.737
3	.566	14	.741
4	.579	15	.765
5	.598	16	.793
6	.613	17	.811
7	.632	18	.894
8	.641	19	.922
9	.644	20	.941
10	.654	21	.983
11	.728		

(a) Load vs. central deflection.

(b) Yield sequence

Fig. 42.   UNIFORMLY LOADED SIMPLY SUPPORTED SQUARE PLATE

— Partially yielded sections

— Fully plastic sections
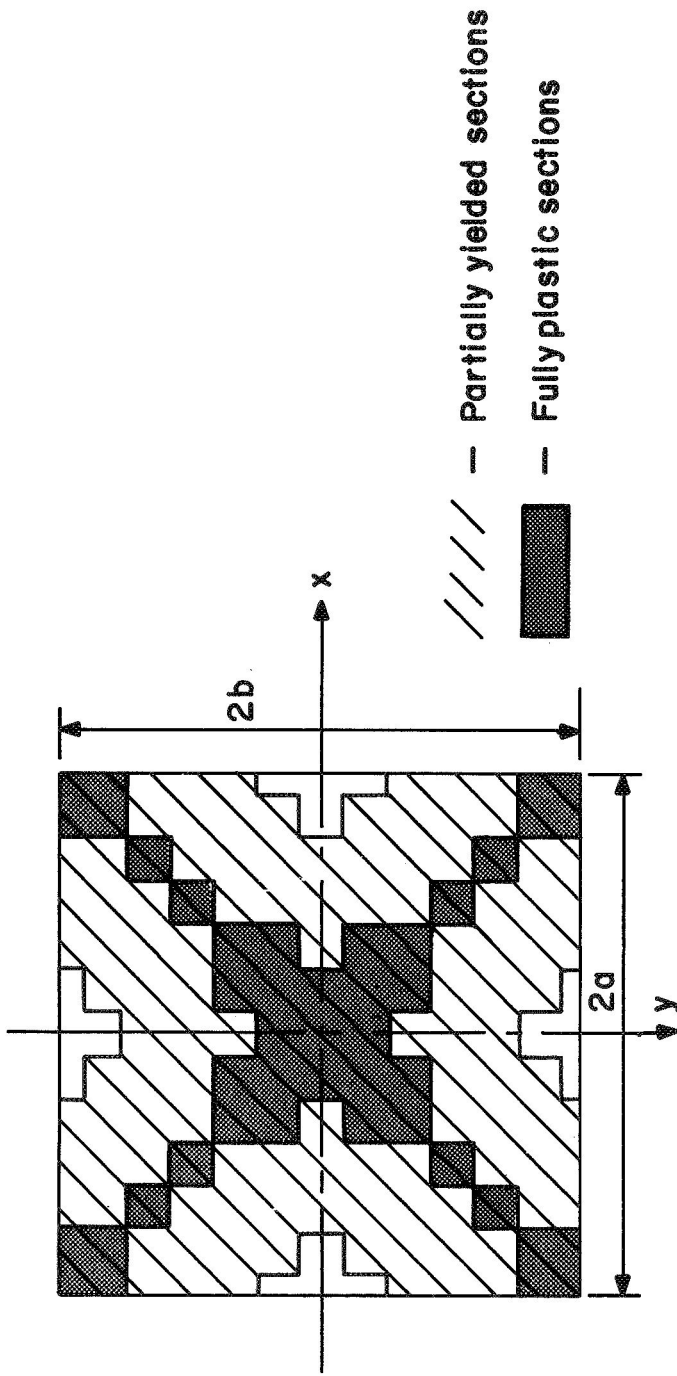
(c) Development of plastic region on the upper and lower surface at collapse load, $\rho = \dfrac{pa^2}{6M_0} = 1.14$.
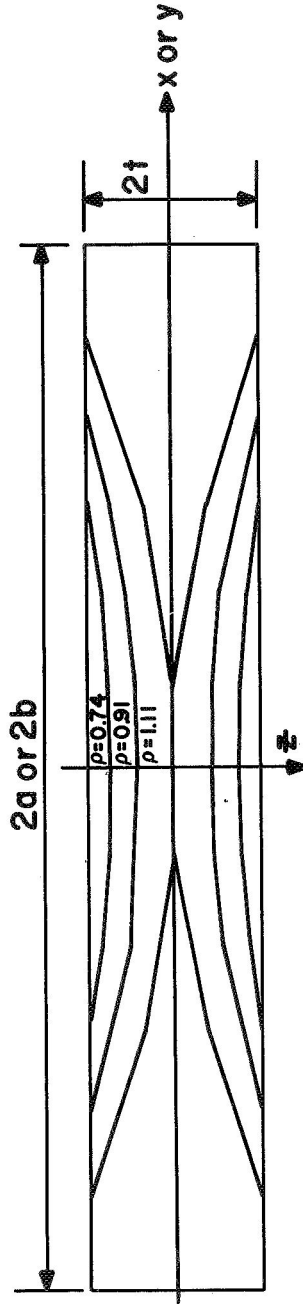
(d) Progression of boundary through the thickness along x=0, or y=0

Fig. 42. (cont) UNIFORMLY LOADED SIMPLY SUPPORTED SQUARE PLATE

237

$\eta = \frac{b}{a} = 0.3$

36 Element Idealization (9×4)

a = 10 in.
b = 3 in.
2t = 0.10 in.
E = 10^7 lbs/in^2
$\bar{\nu}$ = 0.3
M$_o$ = 90 lb-in./in.

///// – Partially yielded sections

▨ – Fully plastic sections

(a) Development of plastic region on the upper and lower surface at collapse load, $\rho = pa^2/6 M_o = 6.20$

$\rho = 3.95$
$\rho = 5.70$
$\rho = 6.20$

(b) Progression of boundary through the thickness along y=O   (c) Progression of boundary through the thickness along x=O

Fig. 43   UNIFORMLY LOADED SIMPLY SUPPORTED RECTANGULAR PLATE

Load Carrying Capacity, $p = \dfrac{p a^2}{6 M_0}$

Ratio, η, of Sides of Rectangular Plate

$\eta = \dfrac{b}{a}$

$a \geqq b$

2b

2a

(1) Hodge, Ref.(46) (2) Shull & Hu. Ref.(47)
Assumed Displacement Patterns

——— Pattern (1) – von Mises, Ref. (46)

— — — Pattern (2) – von Mises

·········· Pattern (2) – Tresca, Ref. (47)

Finite Element Solution – von Mises
36 Element Idealizations

(a) Comparison of yield limit solutions for rectangular plates.

Fig. 44.   COMPARISON OF UPPER BOUNDS ON LOAD CARRYING CAPACITIES OF UNIFORMLY
LOADED SIMPLY SUPPORTED RECTANGULAR PLATES

239
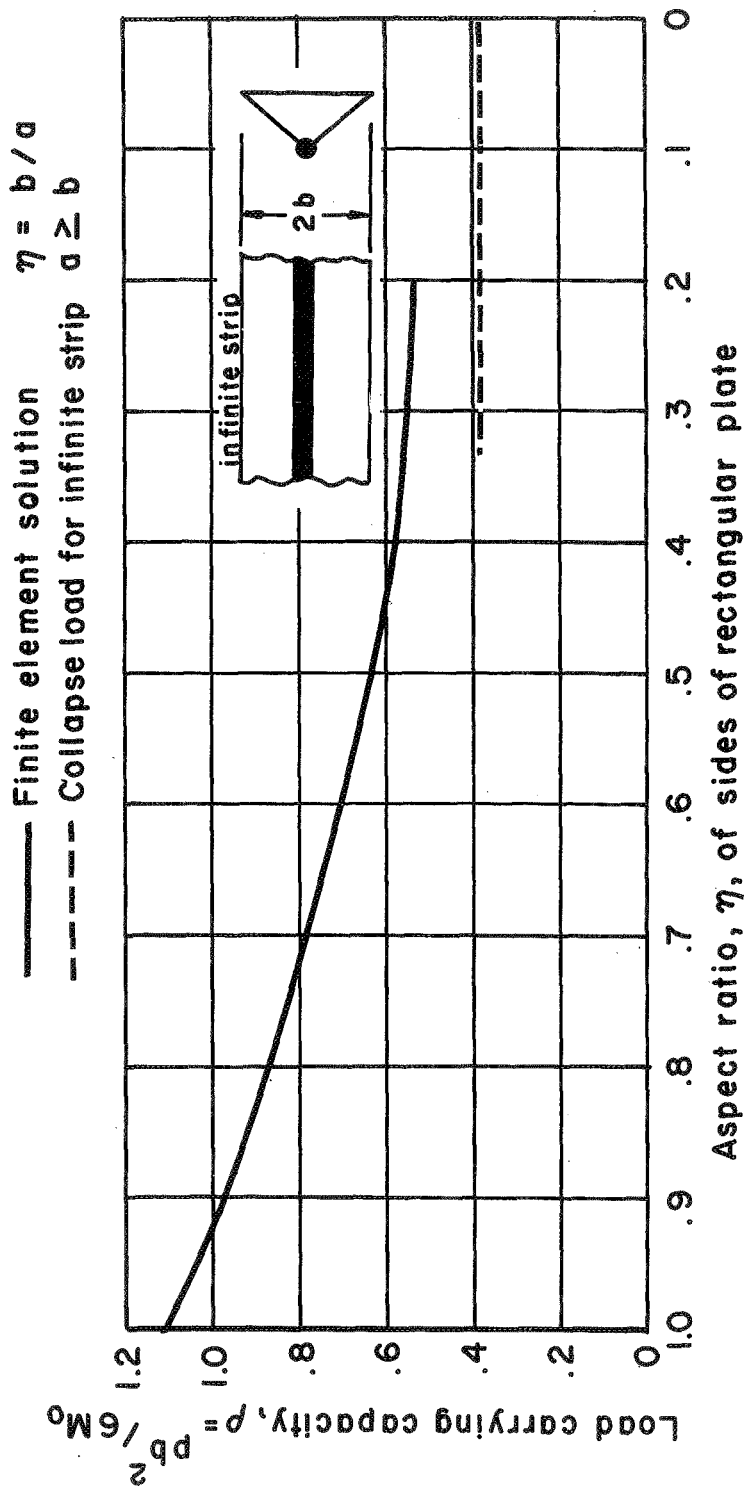
(b) Comparison with yield limit solution for an infinite strip

Fig. 44 (cont.) COMPARISON OF UPPER BOUNDS OF LOAD CARRYING CAPACITIES OF UNIFORMLY LOADED SIMPLY SUPPORTED RECTANGULAR PLATES.

(d) Load vs. deflection at midpoint of free edge.

(c) Progression of boundary through the thickness along x = 0

Partially yielded sections

Fully plastic sections
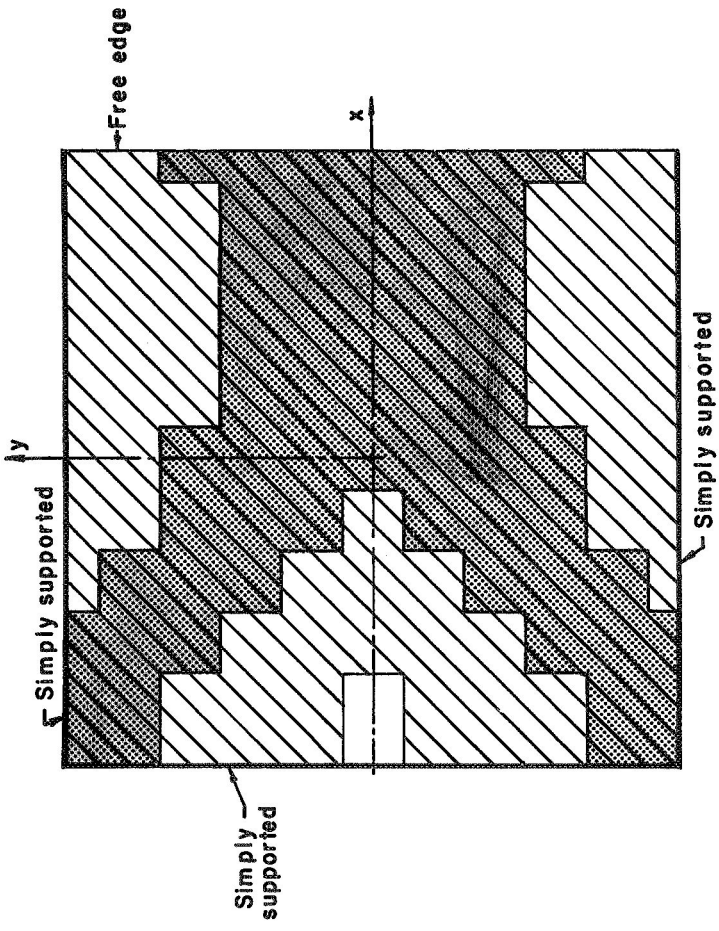
(a) Development of plastic region on the upper (lower) surface at the collapse load $\rho = .715$

(b) Progression of boundary through the thickness along y = 0

Fig. 45 UNIFORMLY LOADED SQUARE PLATE WITH THREE SIMPLE SUPPORTS AND ONE FREE EDGE

241
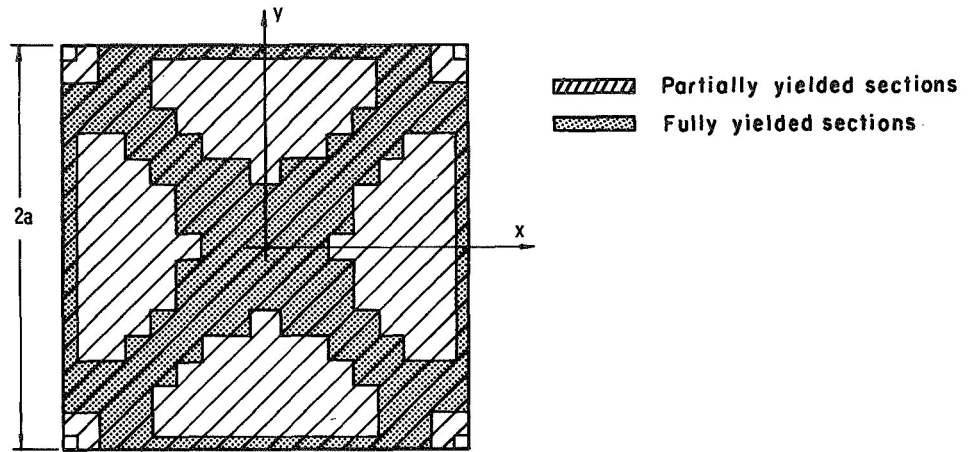
(a) Development of plastic region on the upper and lower surface
at the collapse load $\rho = pa^2/6\,M_0 = 2.59$
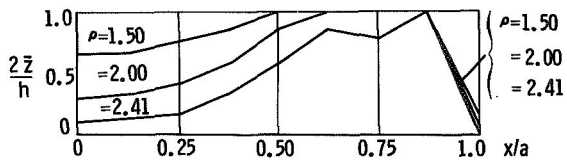
(b) Propagation of Elastic-Plastic Boundary Along y = 0
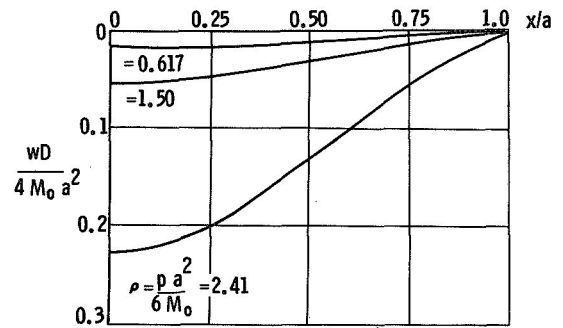
(c) Deflection Profiles Along y = 0

Fig. 46 Uniformly Loaded Clamped Square Plate
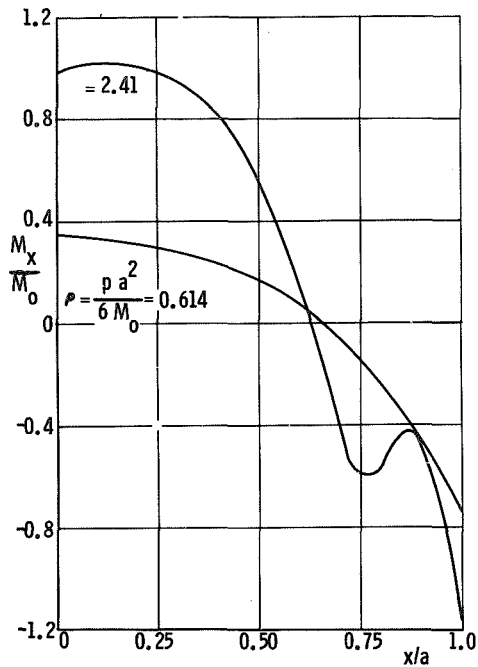
(d) Distribution of Moment in x-Direction Along y = 0
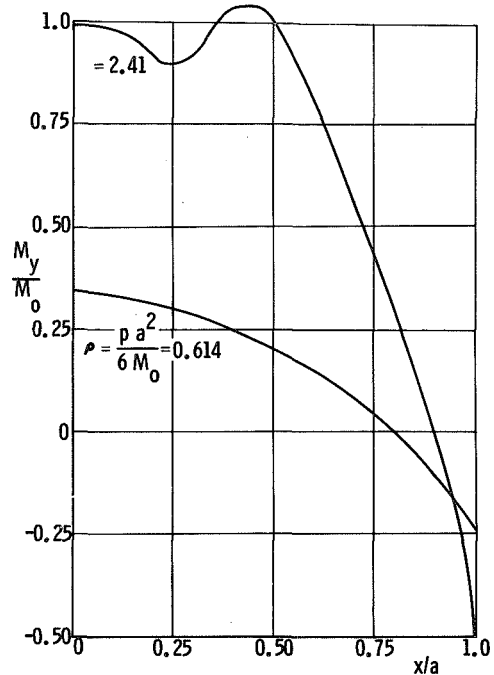
(e) Distribution of Moment in y-Direction Along y=0
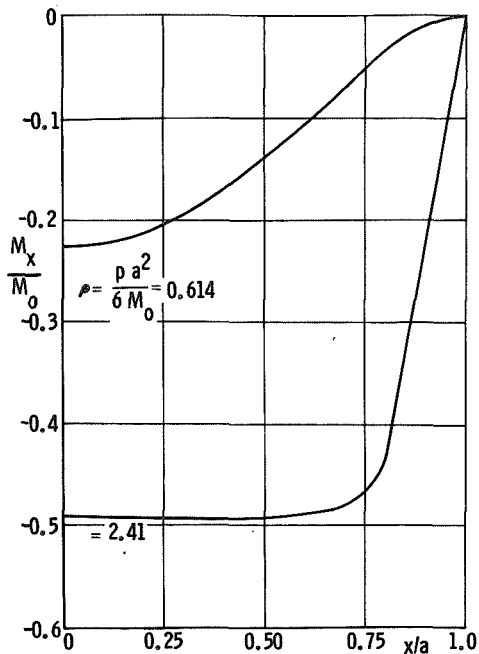
(f) Distribution of Moment in x-Direction Along y = a
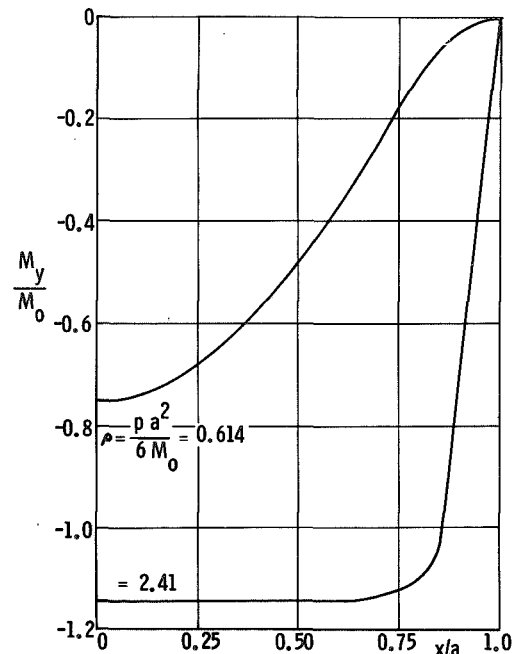
(g) Distribution of Moment in y-Direction Along y = a

Fig. 46 (Cont) Uniformly Loaded Clamped Square Plate

243
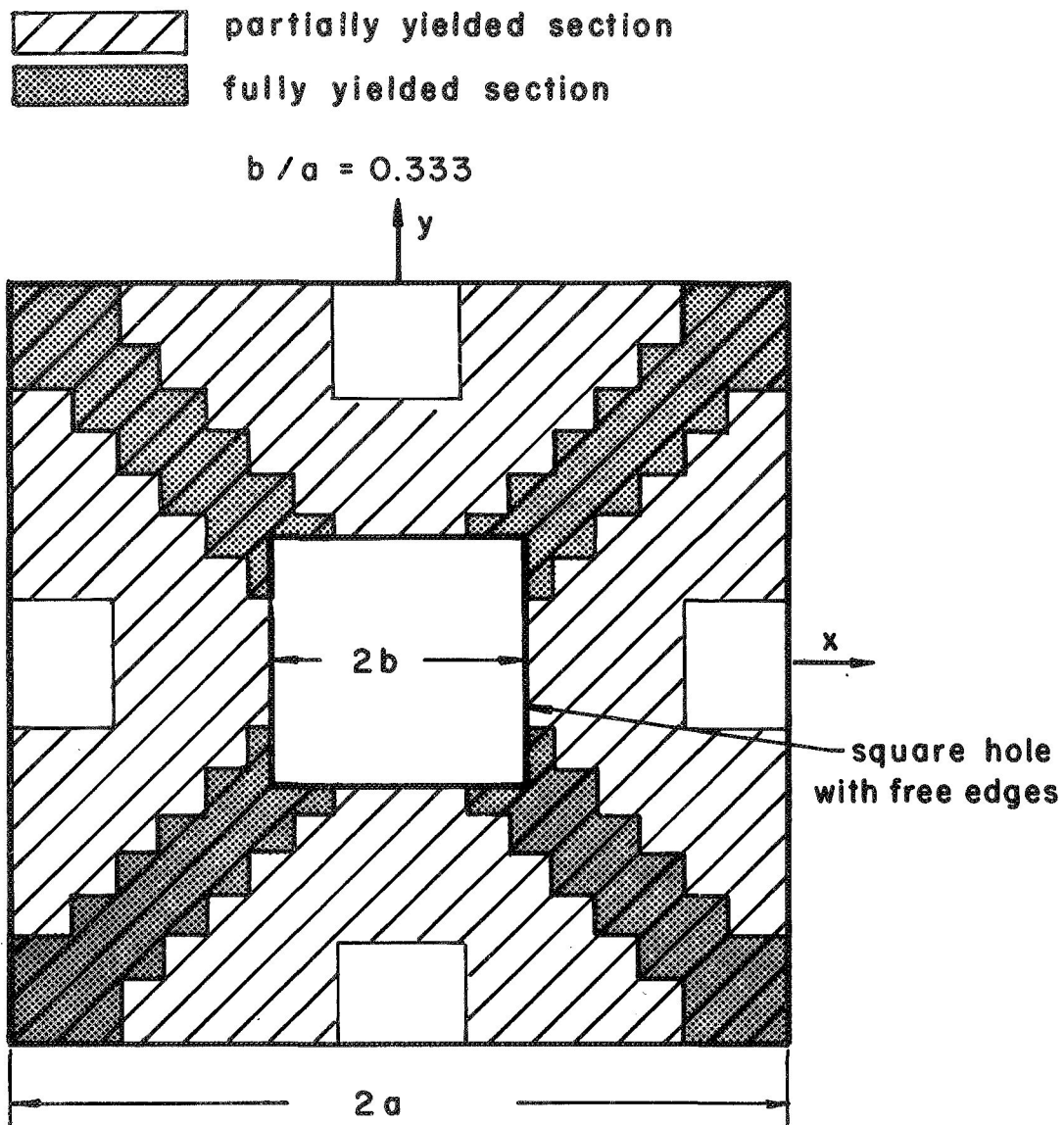
(a) Development of plastic region on the upper and lower surfaces at collapse load, $\rho = pa^2 /6M_0 = 1.01$

Fig. 47 UNIFORMLY LOADED SIMPLY SUPPORTED SQUARE PLATE WITH SQUARE HOLE.

244
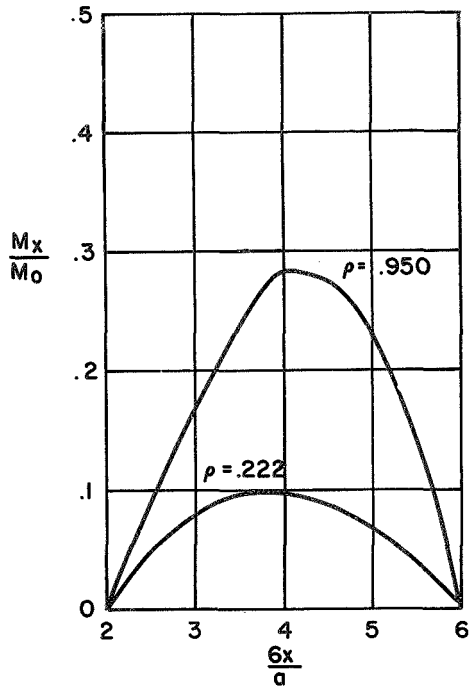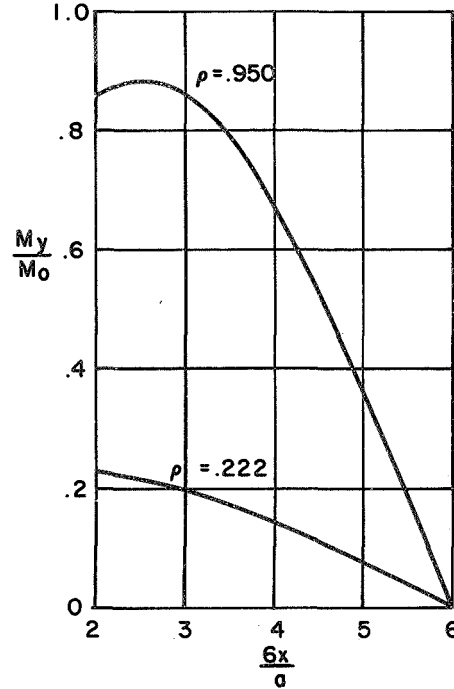
(b) Moment in x-direction along y=0   (c) Moment in y-direction along y=0
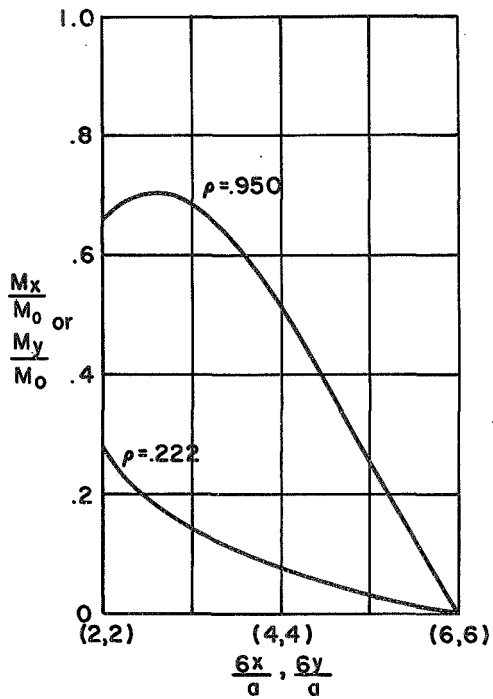
(d) Moment in x and y direction along
diagonal x=y
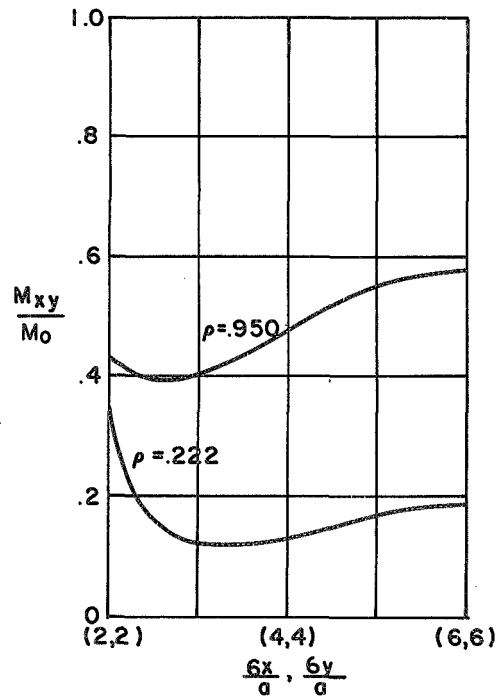
(e) Twist moment along diagonal x=y

Fig. 47 (cont.) UNIFORMLY LOADED SIMPLY SUPPORTED SQUARE PLATE
WITH SQUARE HOLE

245
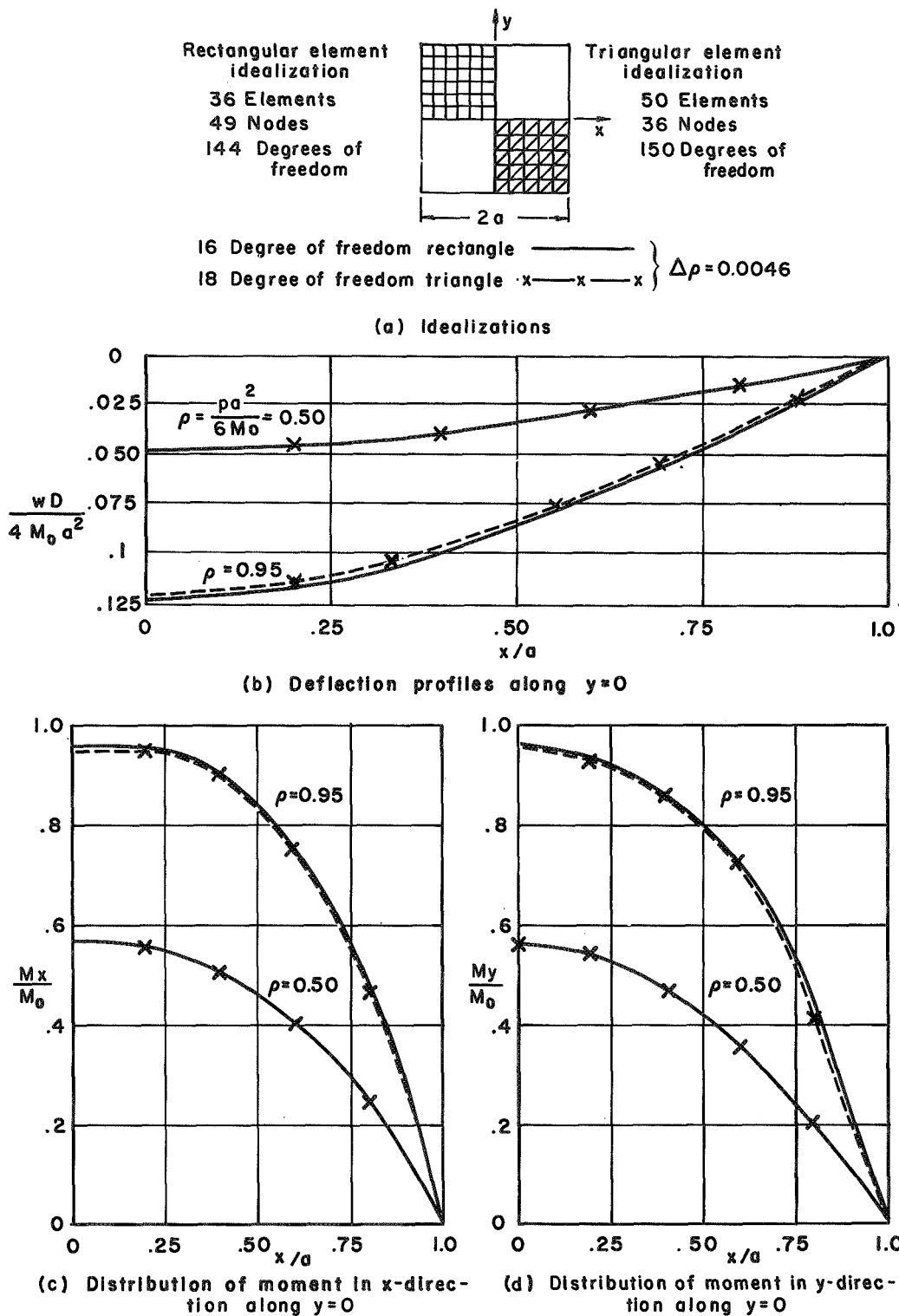
Fig. 48   COMPARISON OF RESULTS FOR UNIFORMLY LOADED SIMPLY
SUPPORTED SQUARE PLATE

246

81 Elements
49 Nodes
266 Degrees of
   freedom
b/a = 1/3

Partially yielded sections
Fully plastic sections
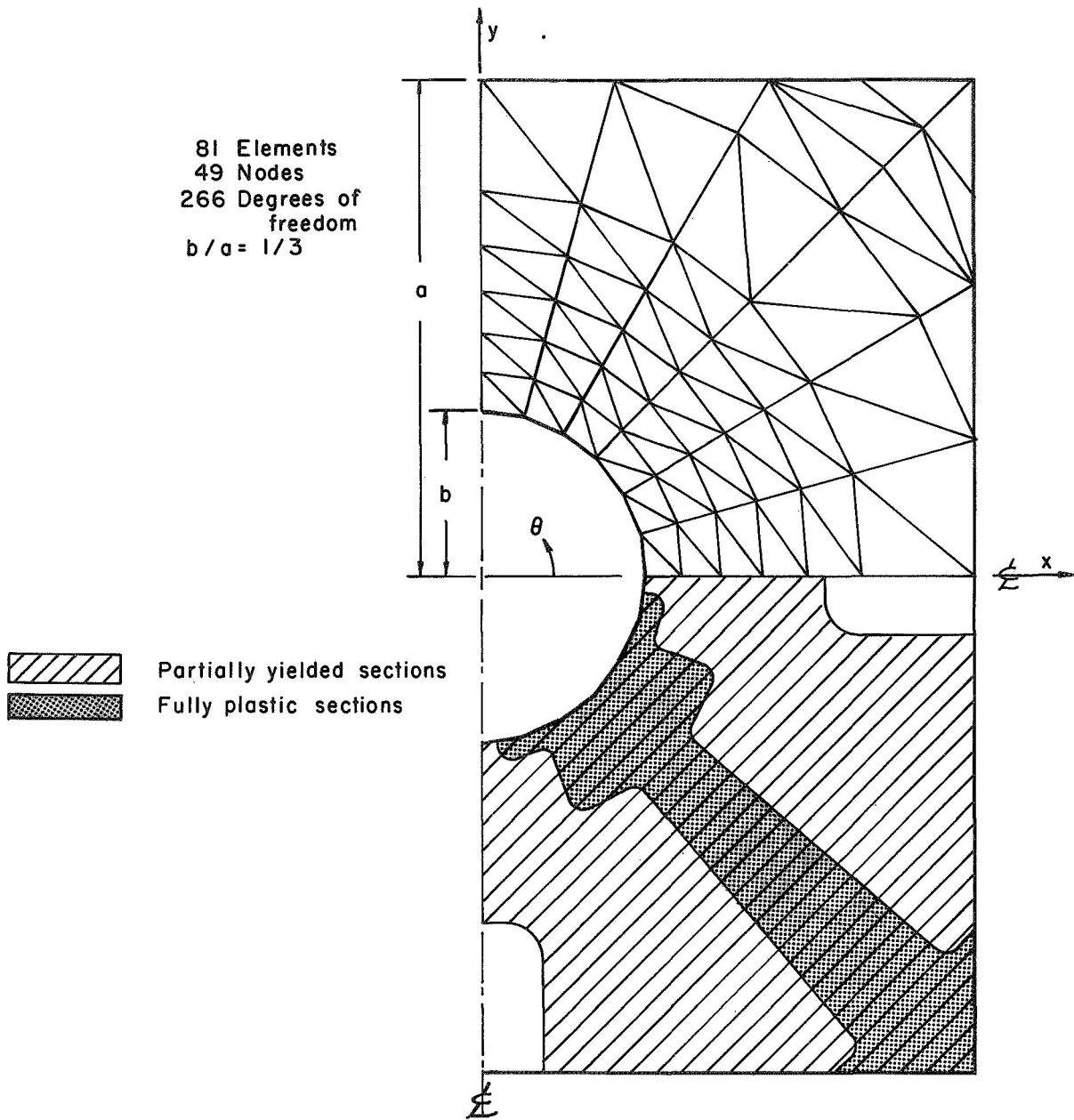
(a) Idealization and collapse pattern at $\rho = \dfrac{pa^2}{6M_0} = 1.07$

Fig. 49   UNIFORMLY LOADED SIMPLY SUPPORTED SQUARE PLATE WITH CENTRAL HOLE

247

$\rho = 1.02$

.20

.15

$\dfrac{wD}{4M_0a^2}$

.10

.706

.05

.402

0

0   15   30   45

θ, degrees
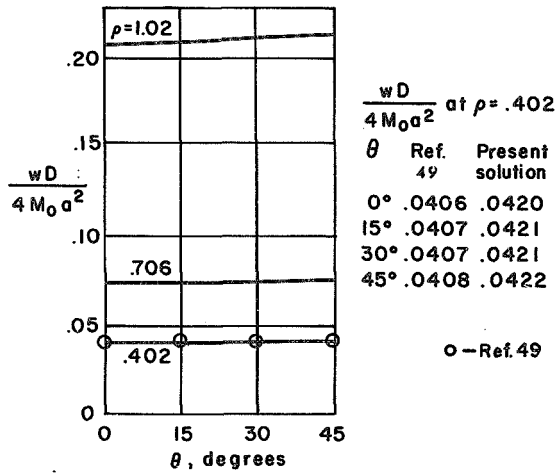
(b) Deflection along circular hole

$\dfrac{wD}{4M_0a^2}$ at $\rho = .402$

θ	Ref. 49	Present solution
0°	.0406	.0420
15°	.0407	.0421
30°	.0407	.0421
45°	.0408	.0422

O — Ref. 49

1.2

1.1

$\rho = 1.02$ 1.0

.9

.706

$\dfrac{M_\theta}{M_0}$ .8

.7

.6

.402   .5

0   15   30   45

θ, degrees
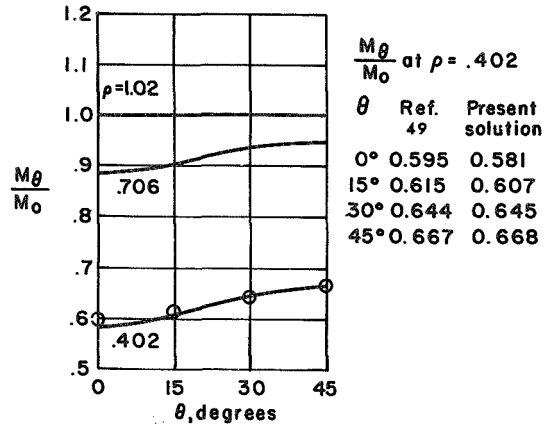
(c) Circumferential moment along circular hole

$\dfrac{M_\theta}{M_0}$ at $\rho = .402$

θ	Ref. 49	Present solution
0°	0.595	0.581
15°	0.615	0.607
30°	0.644	0.645
45°	0.667	0.668

$\rho = .402$

.05   .706

.10

$\dfrac{wD}{4M_0a^2}$

.15

1.02

.20

.25

.333   .500 $\dfrac{r}{a}$ .750   1.00

(d) Deflection profiles along $\theta = 0$

$\rho = .402$

.706

.05

.10

$\dfrac{wD}{4M_0a^2}$

.15   1.02

.20

.25

.333   .500   .750 $\dfrac{r}{a}$ 1.00   1.25   1.414
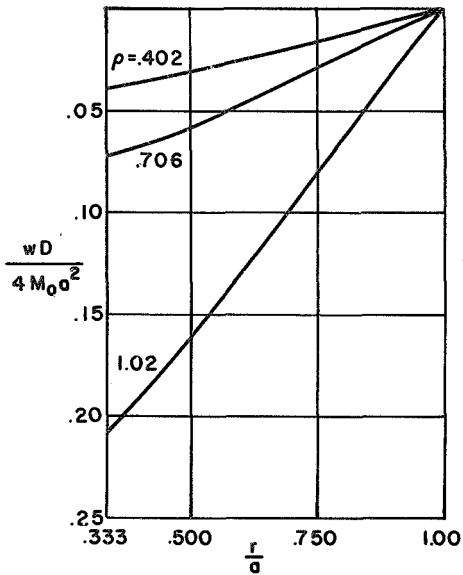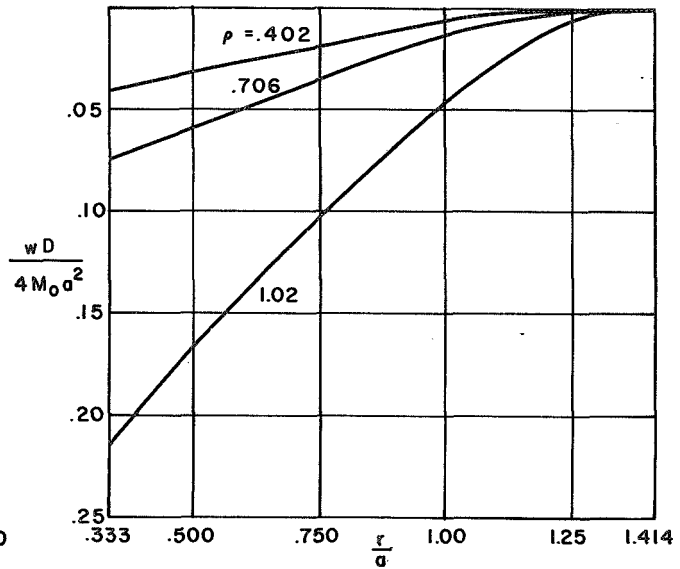
(e) Deflection profiles along $\theta = 45°$

Fig. 49 (cont.) UNIFORMLY LOADED SIMPLY SUPPORTED SQUARE PLATE WITH CENTRAL HOLE

248
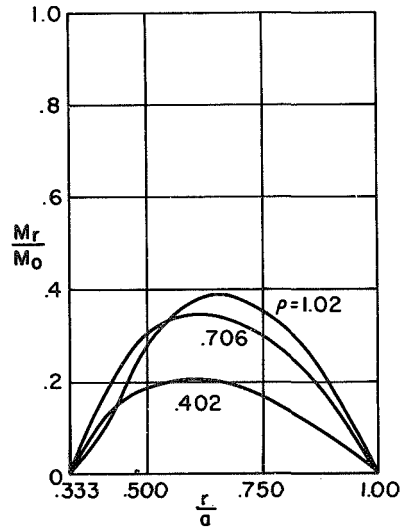
(f) Distribution of radial moment along $\theta = 0°$
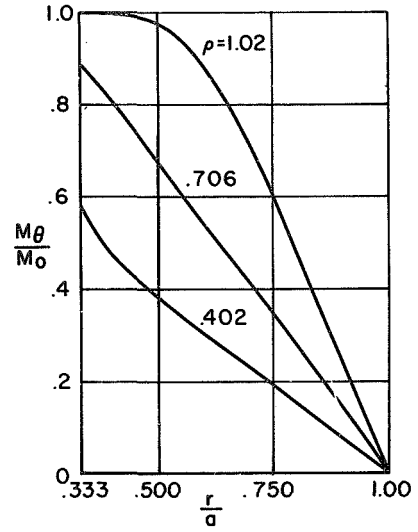
(g) Distribution of circumferential moment along $\theta = 0°$
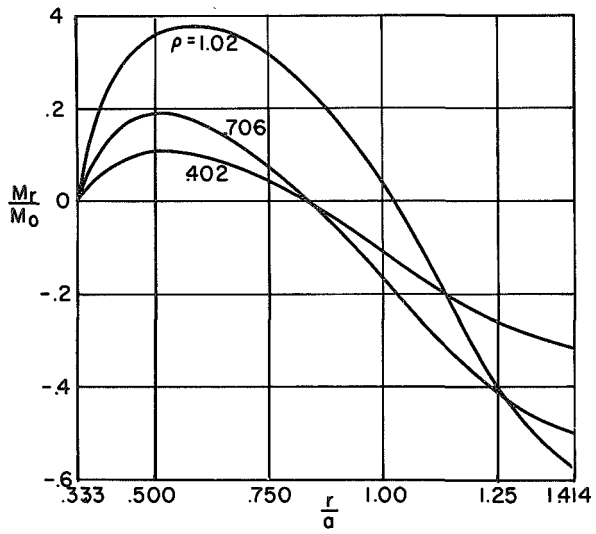
(h) Distribution of radial moment along $\theta = 45°$
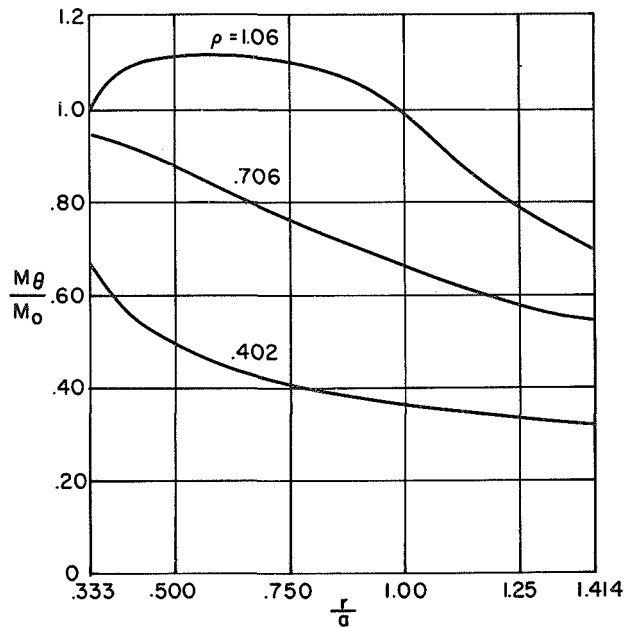
(i) Distribution of circumferential moment along $\theta = 45°$

Fig. 49 (cont.) UNIFORMLY LOADED SIMPLY SUPPORTED SQUARE PLATE WITH CENTRAL HOLE

249

250
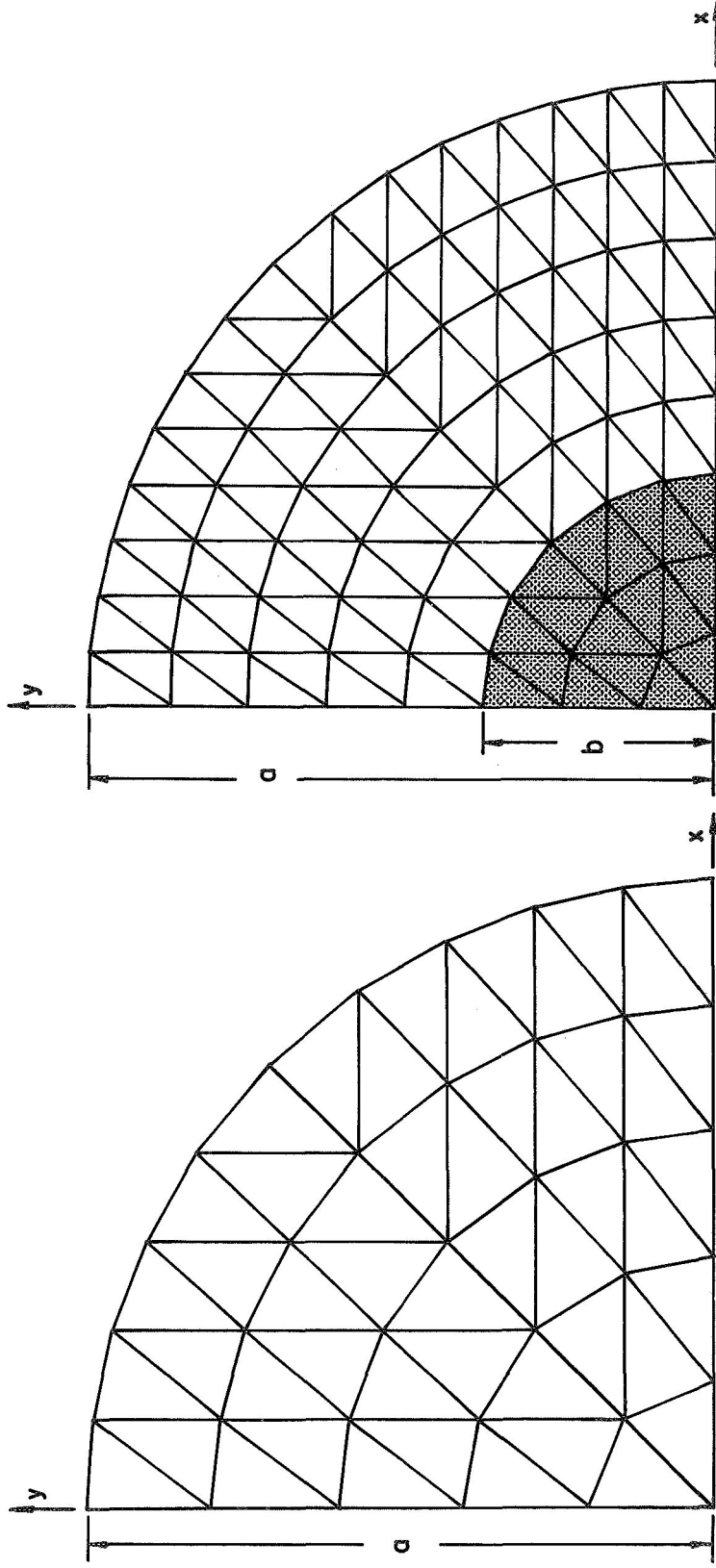
(a) 50 Member idealization –36 Nodes

(b) 128 Member idealization–81 Nodes

Fig.50 CIRCULAR PLATE IDEALIZATIONS

(a) Deflection profiles

(b) Elastic-plastic boundaries

(c) Distribution of circumferential moment.

(d) Distribution of radial moment.
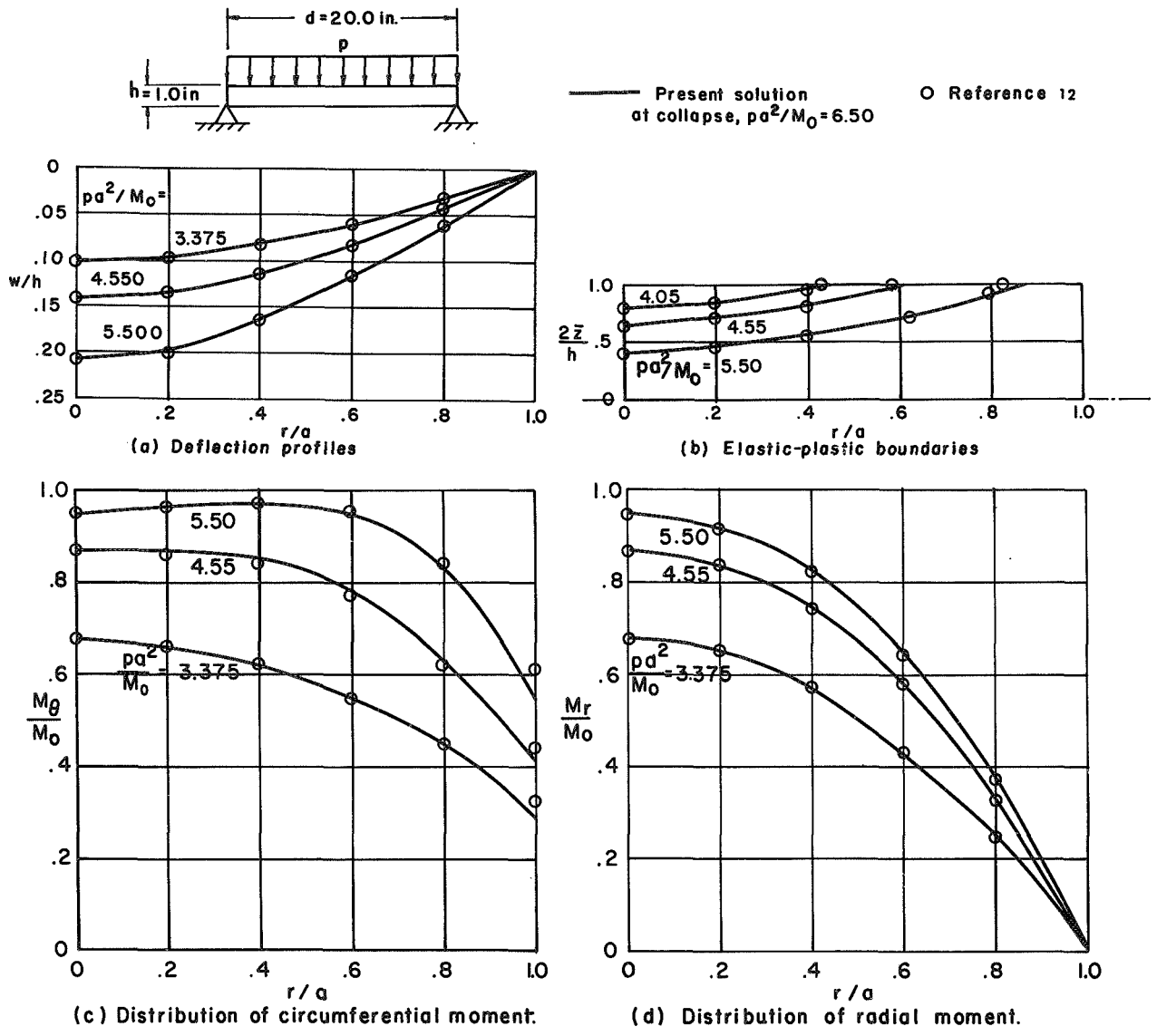
Fig. 51   UNIFORMLY LOADED SIMPLY SUPPORTED CIRCULAR PLATE:
ELASTIC-IDEALLY PLASTIC

251
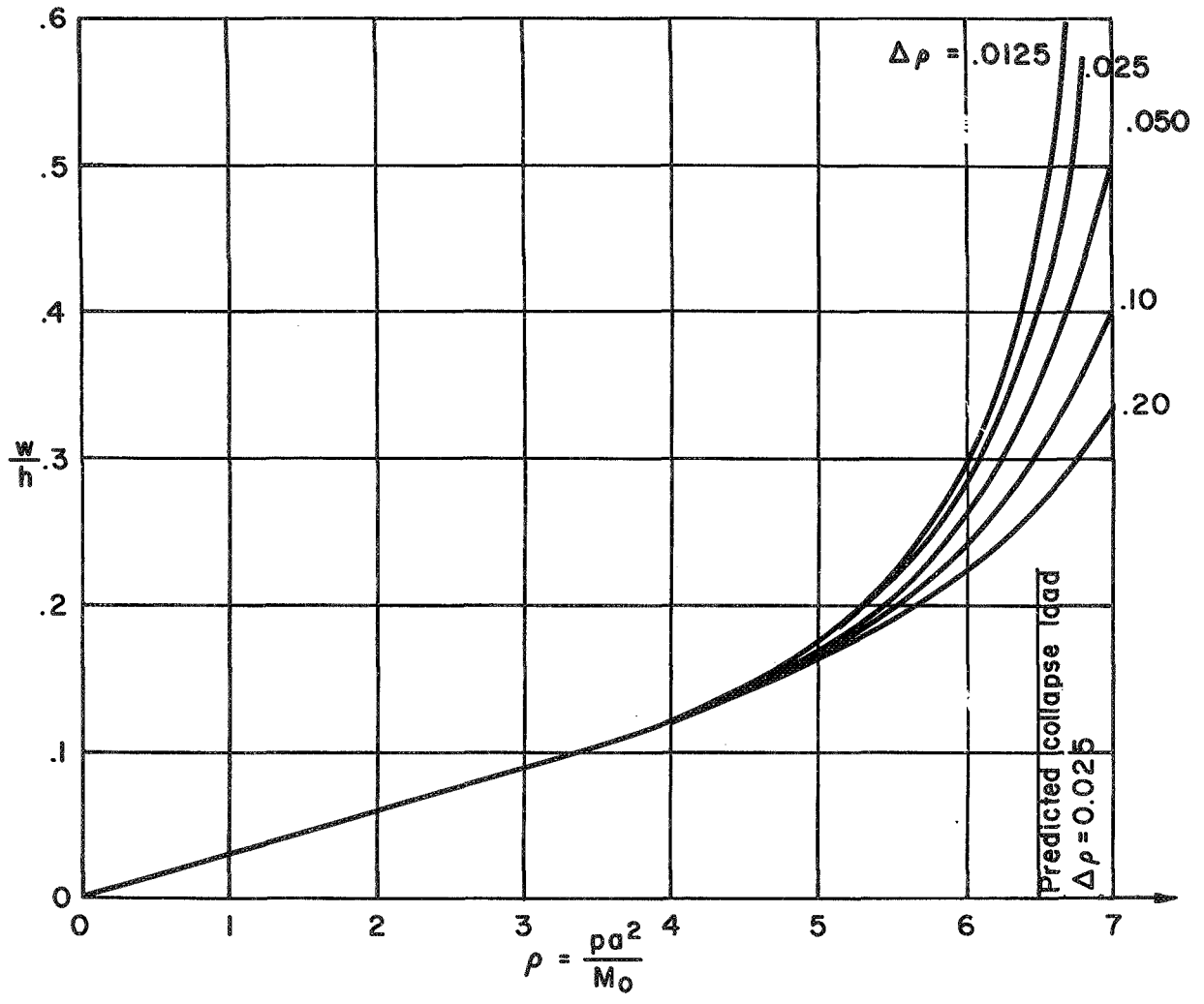
Fig.52.   UNIFORMLY LOADED SIMPLY SUPPORTED CIRCULAR PLATE:
LOAD vs CENTER DEFLECTION FOR VARIOUS LOAD INCREMENTS
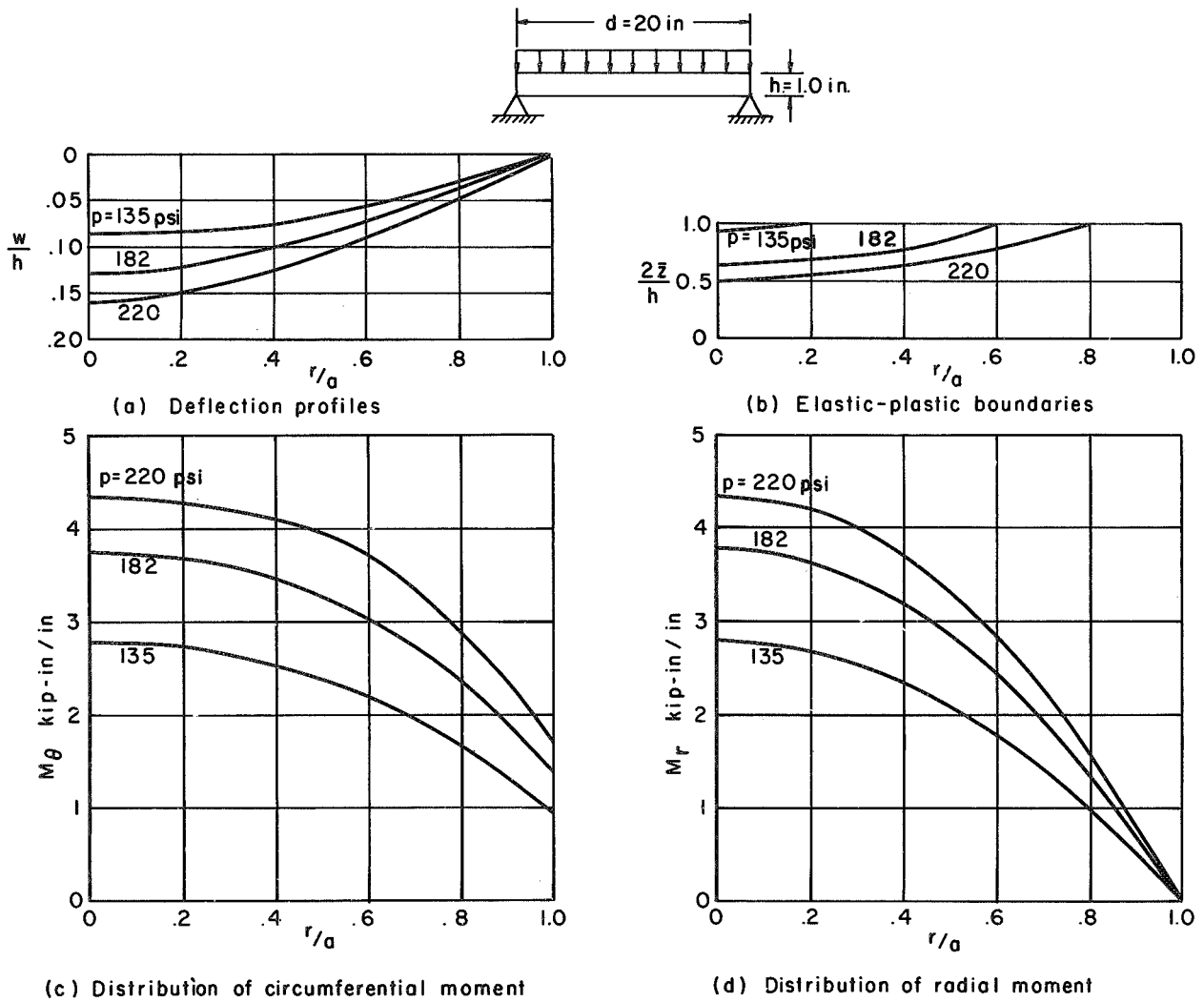
(a) Deflection profiles

(b) Elastic-plastic boundaries

(c) Distribution of circumferential moment

(d) Distribution of radial moment

Fig. 53. UNIFORMLY LOADED SIMPLY SUPPORTED CIRCULAR PLATE: ELASTIC-STRAIN HARDENING

(a) Deflection profiles

(b) Elastic-plastic boundaries

(c) Distribution of circumferential moment

(d) Distribution of radial moment
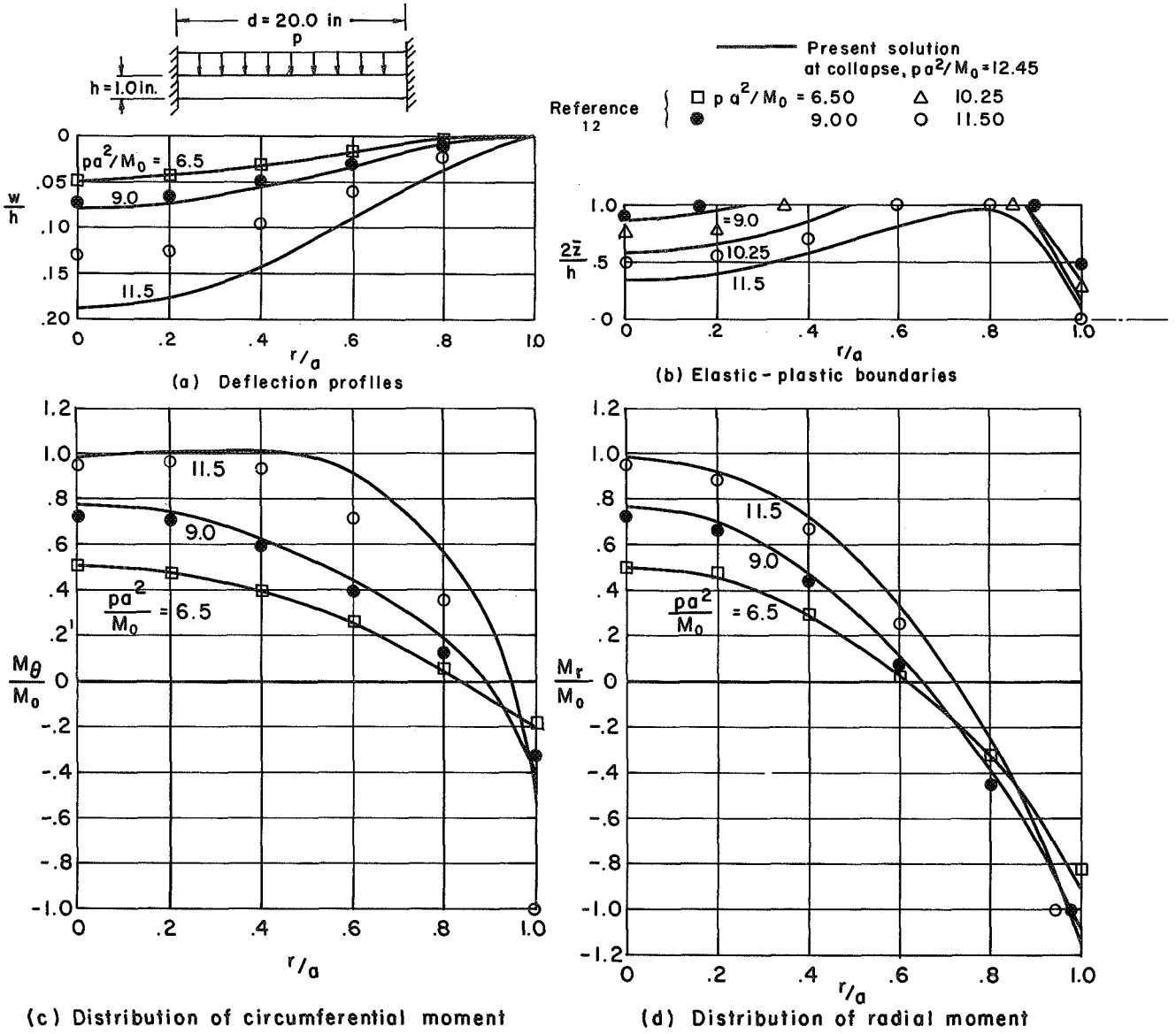
Fig. 54   UNIFORMLY LOADED CLAMPED CIRCULAR PLATE: ELASTIC-IDEALLY PLASTIC.

254

Fig. 55   UNIFORMLY LOADED CLAMPED CIRCULAR PLATE: ELASTIC-STRAIN HARDENING

255

(a) Deflection profile

(b) Elastic-plastic boundaries

(c) Distribution of circumferential moment

(d) Distribution of radial moment.

Fig. 56 UNIFORMLY LOADED SIMPLY SUPPORTED ANNULAR PLATE

256

(a) Idealization and elastic-plastic region at collapse

H = 10"

49 Members
36 Nodes
136 Degrees of Freedom

Partially yielded sections
Fully plastic sections

$P = pH^2/6M_0$

At collapse $p = 10.06$

(b) Progression of elastic plastic boundary through the thickness along y=0

(c) Deflection profile along y=0

Δ Elastic solution, Ref. 61

(d) Distribution of moment in x-direction along median

(e) Distribution of moment in y-direction along median.

Fig.57 UNIFORMLY LOADED SIMPLY SUPPORTED EQUILATERAL TRIANGULAR PLATE ELASTIC-IDEALLY PLASTIC

257
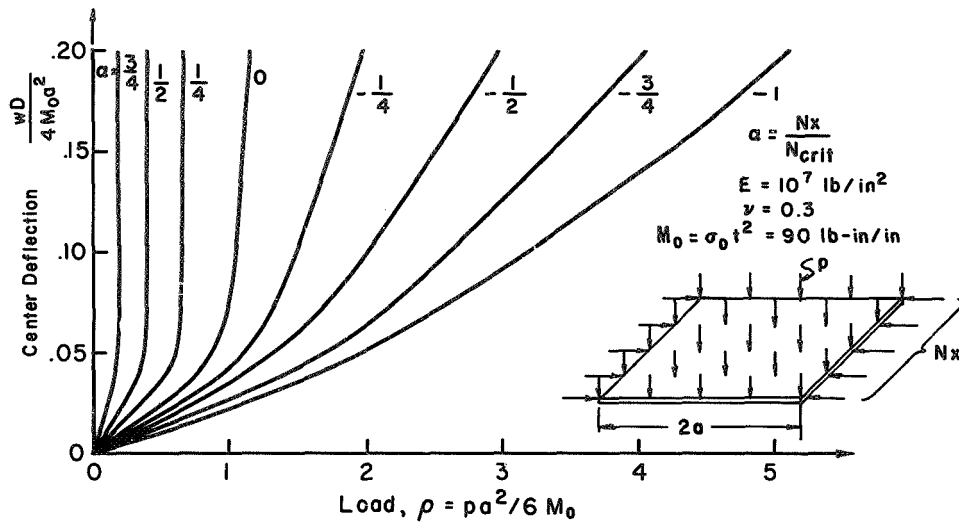
(a) Elastic-ideally plastic behavior for various values of α

elastic-ideally plastic Δ Yield load, elastic-ideally plastic
elastic-strain hardening   O Yield load, elastic-strain hardening
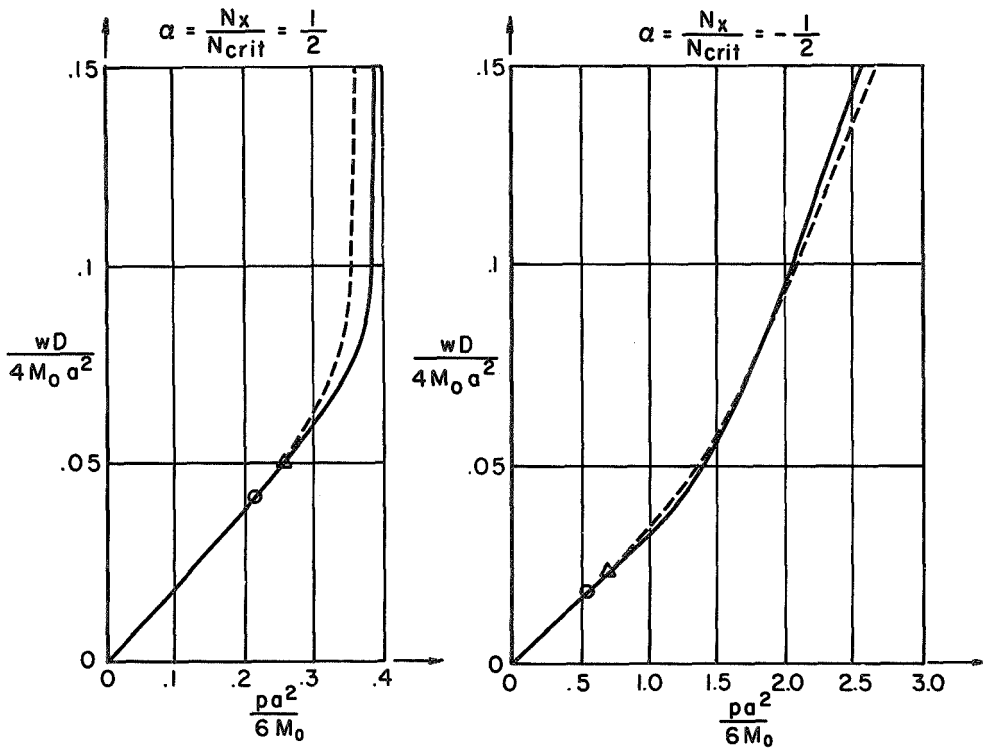
(b) Compressive membrane load   (c) Tensile membrane load

Fig.58   LATERAL LOAD vs. CENTER DEFLECTION OF SIMPLY
SUPPORTED SQUARE PLATE UNDER COMBINED LOADING
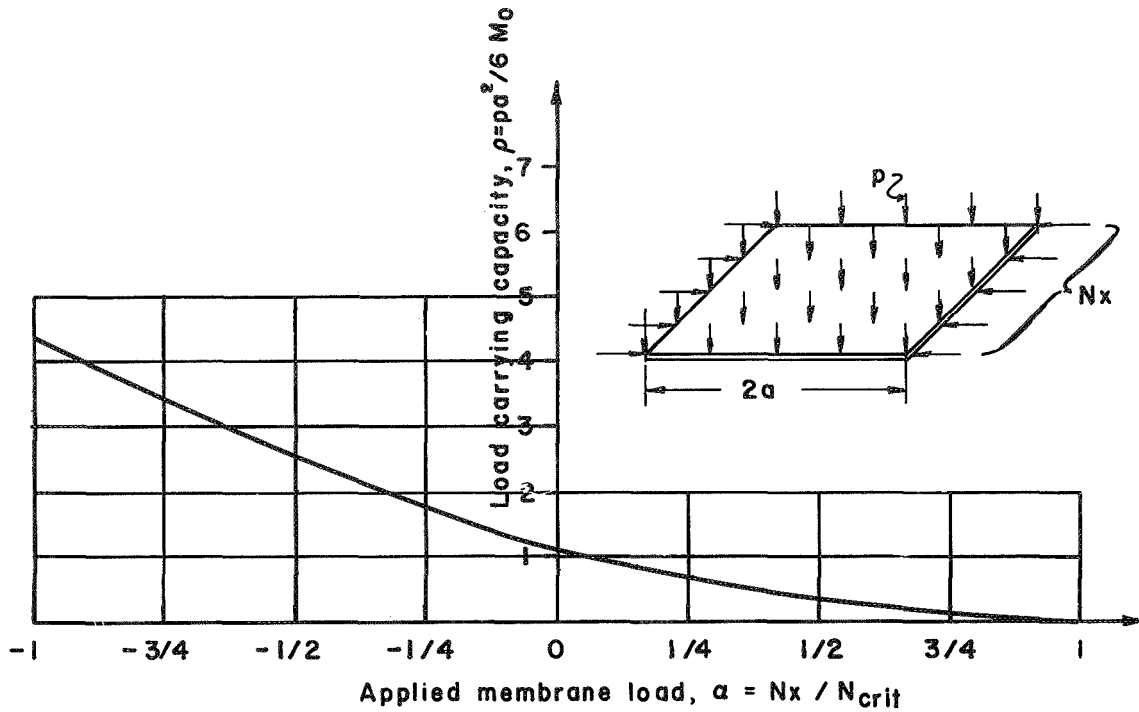
Fig.59. LATERAL LOAD CARRYING CAPACITIES OF SIMPLY SUPPORTED SQUARE PLATE SUBJECTED TO UNIFORM MEMBRANE LOAD IN ONE DIRECTION
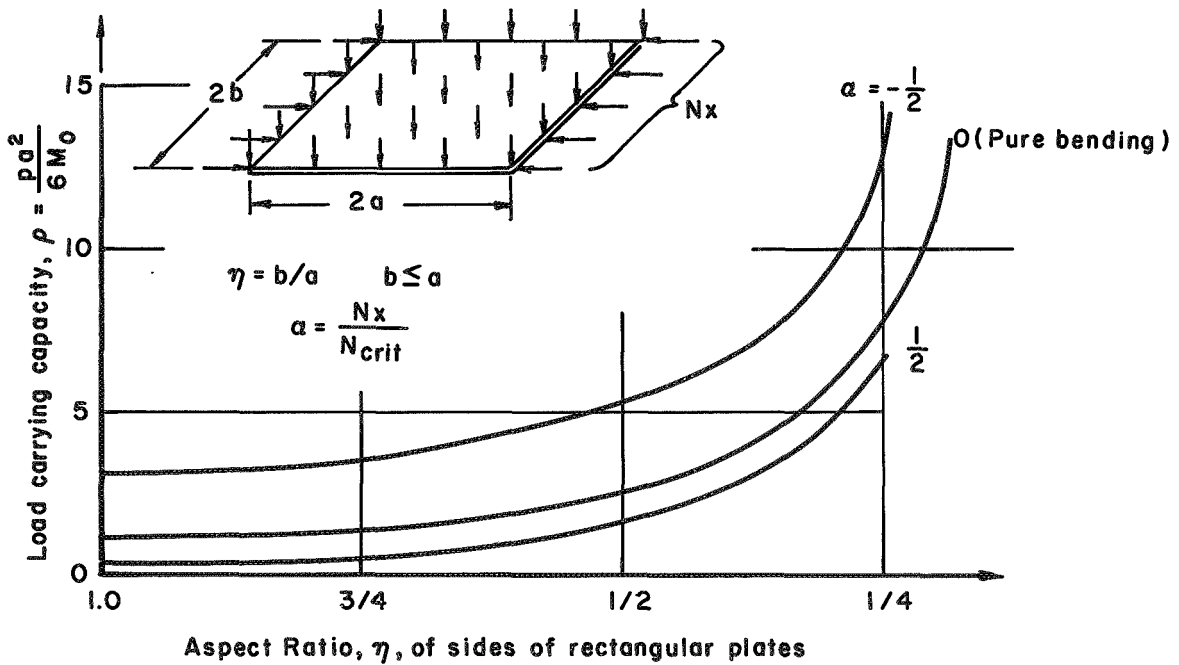
Applied membrane load, $\alpha = N_x / N_{crit}$

$\eta = b/a \qquad b \leq a$

$\alpha = \dfrac{N_x}{N_{crit}}$

Aspect Ratio, η, of sides of rectangular plates

Fig. 60. LATERAL LOAD CARRYING CAPACITIES OF SIMPLY SUPPORTED RECTANGULAR PLATES UNDER COMBINED LOADING

259

$$\gamma = \frac{N_{xy}}{N_{crit}} = \frac{1}{2}$$

$$E = 10^7 \ lb/in^2$$

$$\nu = 0.3$$

$$M_0 = \sigma_0 \times t^2 = 90 \ lb. \ in/in$$
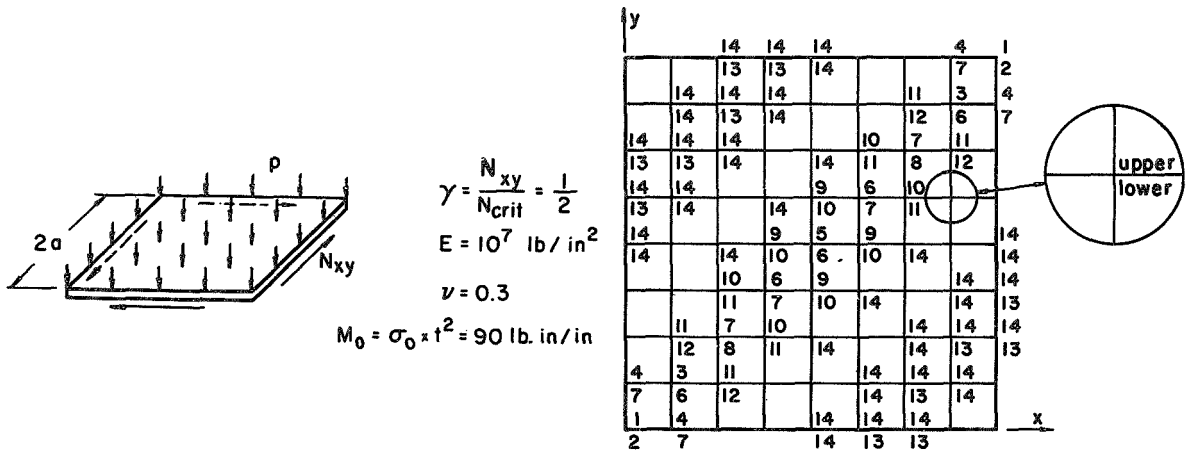
(b) Idealization and yield sequence

Sequence	Load $\frac{pa^2}{6M_0}$	Sequence	Load $\frac{pa^2}{6M_0}$
1	.239	8	.398
2	.268	9	.417
3	.278	10	.426
4	.343	11	.444
5	.370	12	.463
6	.380	13	.500
7	.389	14	.509

Collapse load $\frac{pa^2}{6M_0} = .518$
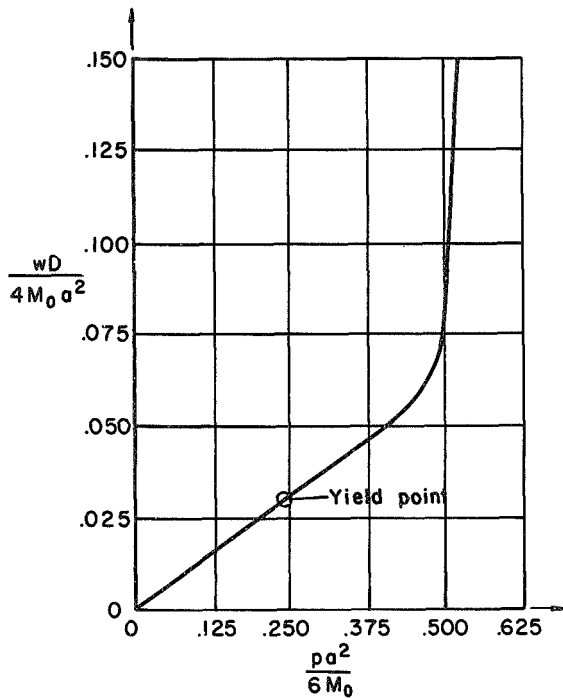
(a) Load vs. central deflection
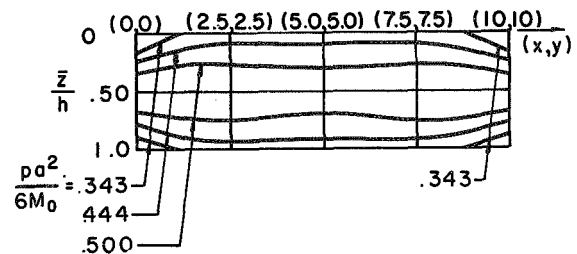
(c) Elastic-plastic boundaries along diagonal x=y

Fig. 61. SIMPLY SUPPORTED SQUARE PLATE UNDER COMBINED LOADING : IN-PLANE SHEAR

260
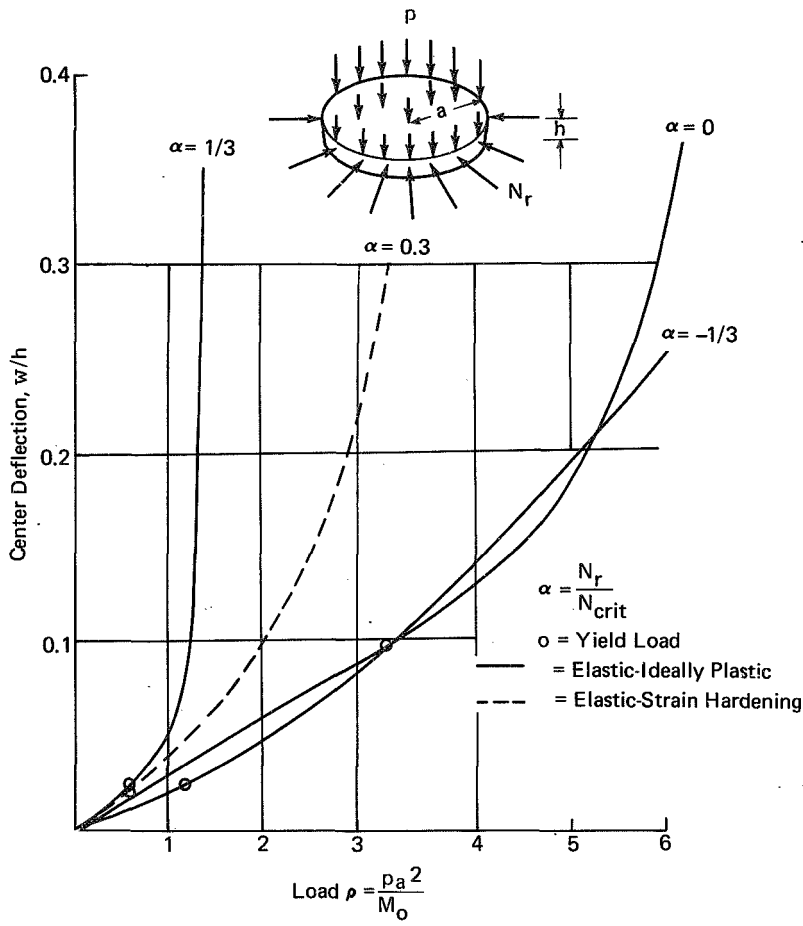
(a) Load Versus Center Deflection
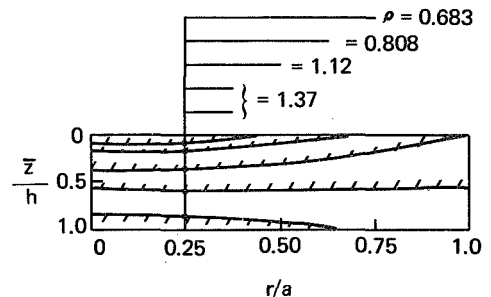
(b) Elastic-Plastic Boundaries: $\alpha = 1/3$
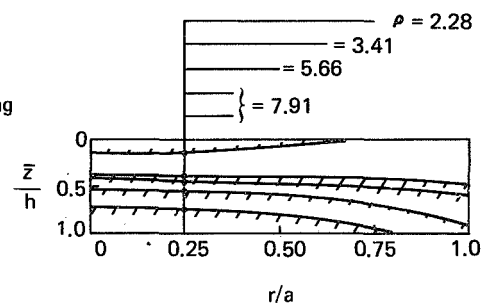
(c) Elastic-Plastic Boundaries: $\alpha = -1/3$

Fig. 62. UNIFORMLY LOADED SIMPLY SUPPORTED CIRCULAR
PLATE UNDER COMBINED LOADING

261

$\rho = 9.55$
$= 12.50$

$\rho = 12.50$
$= 15.68$

(b) Elastic-Plastic Boundaries: $\alpha = 0$

$\rho = 7.13$
$= 8.20$

$\rho = 8.73$
$= 8.20$
$= 7.13$
$= 5.53$

$\rho = 5.53$
$= 7.13$
$= 8.20$
$= 8.73$

(c) Elastic-Plastic Boundaries: $\alpha = 1/4$

$\alpha = 0$

$\alpha = 1/4$

$\alpha = \dfrac{N_r}{N_{crit}}$

$b/a = 0.375$

O - Yield Load

Load $\rho = \dfrac{Pa^2}{M_o}$

(a) Lateral Load versus Free Edge Deflection along r = b

Deflection, w/h Along Free Edge r = b
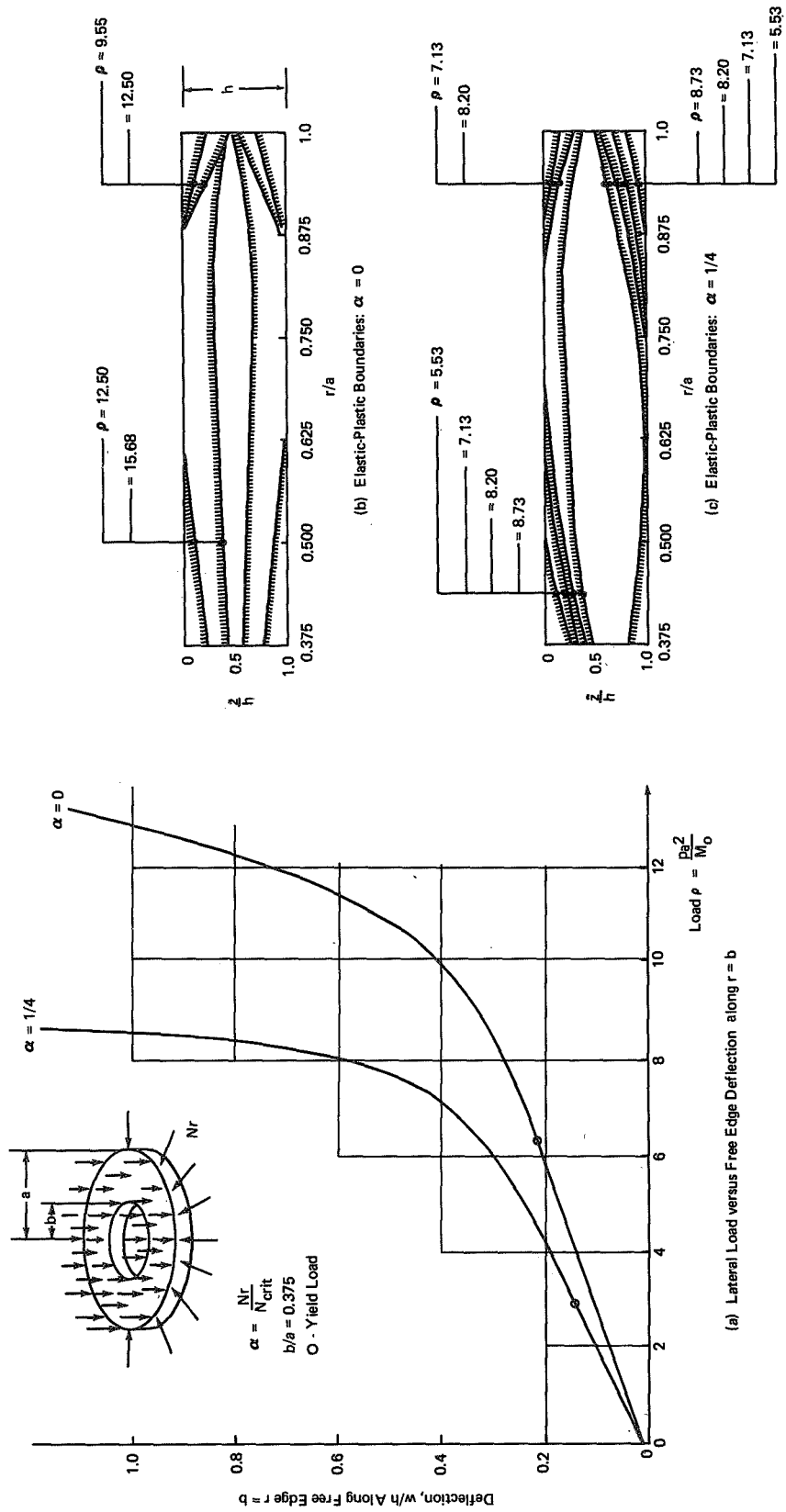
Fig. 63. UNIFORMLY LOADED CLAMPED-FREE ANNULAR PLATE
UNDER COMBINED LOADING
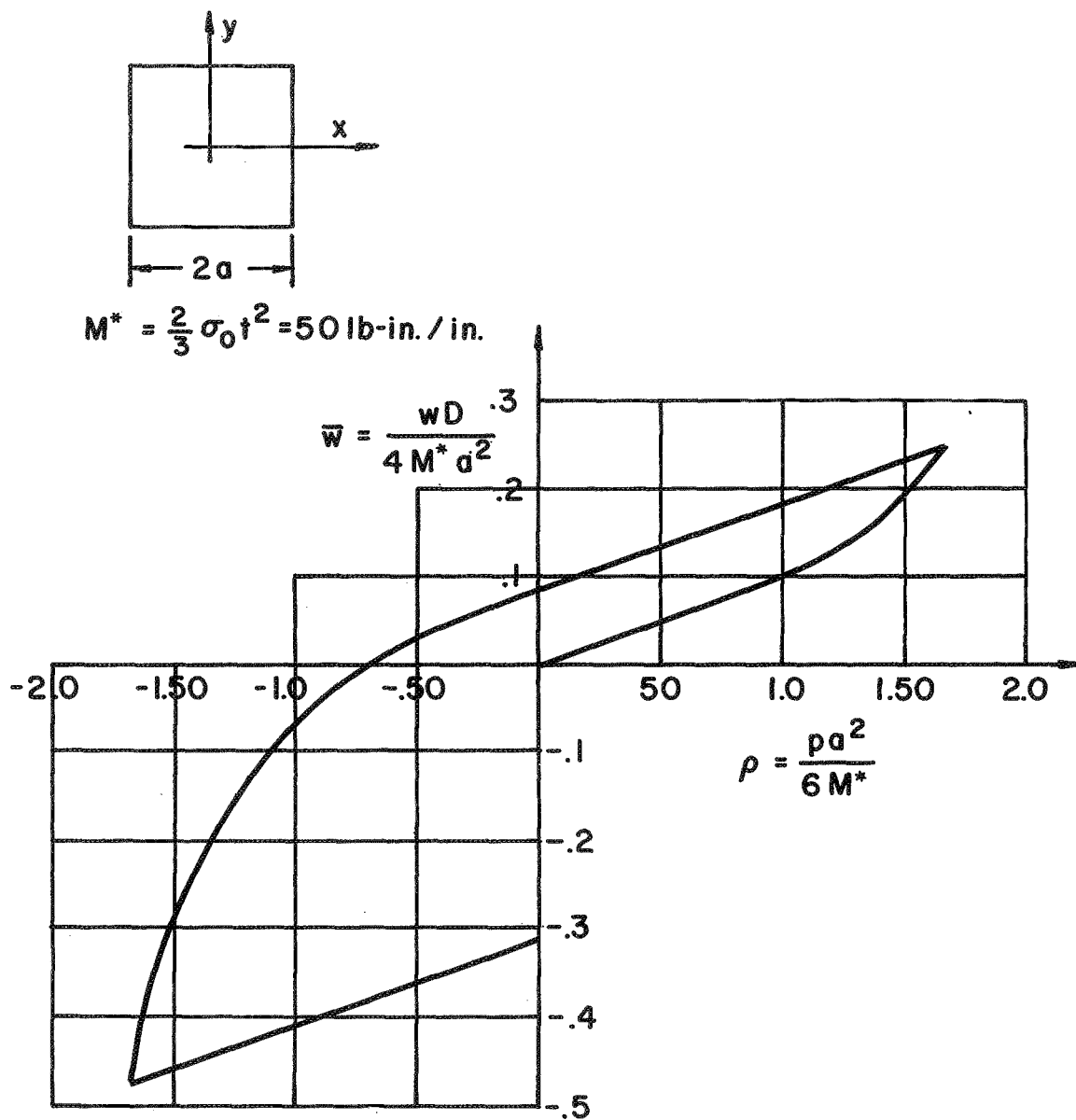
(a) Load vs. center displacement : $\rho = \pm 1.67$

Fig. 64.   SIMPLY SUPPORTED SQUARE PLATE
SUBJECTED TO CYCLIC UNIFORM LOAD
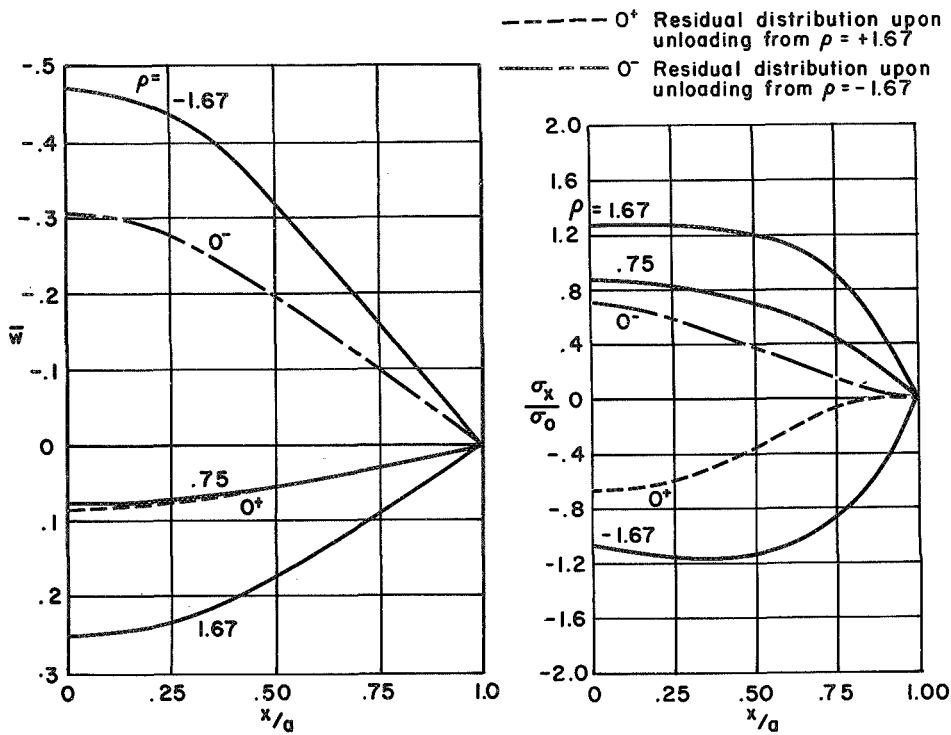
(b) Deflection profile along y=0

(c) Distribution of normal stress in x-direction along y = 0
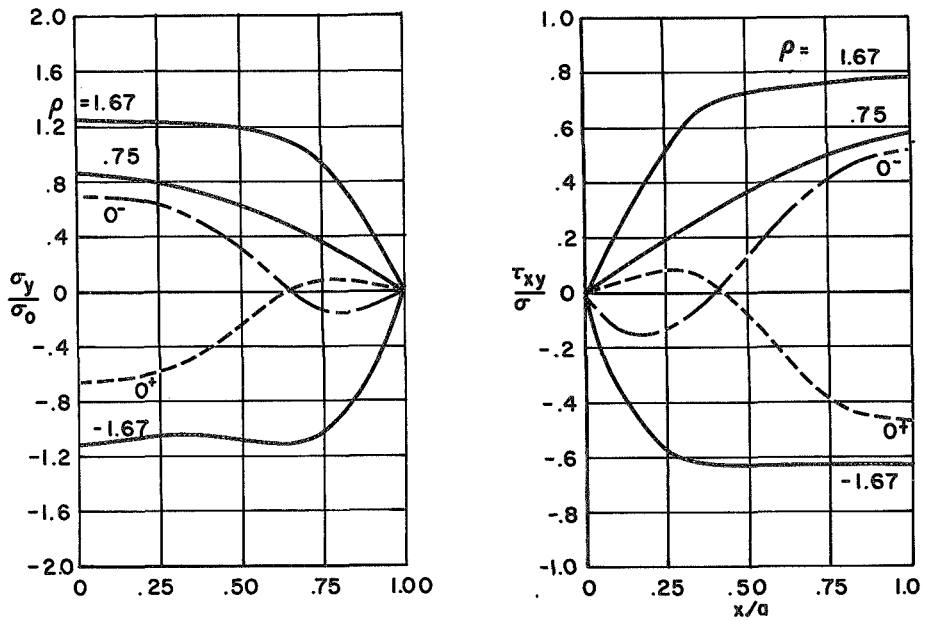
(d) Distribution of normal stress in y-direction along y=0

(e) Shear stress distribution on outer surfaces along y=±a

Fig. 64 (cont.) SIMPLY SUPPORTED SQUARE PLATE SUBJECTED TO CYCLIC UNIFORM LOAD

264
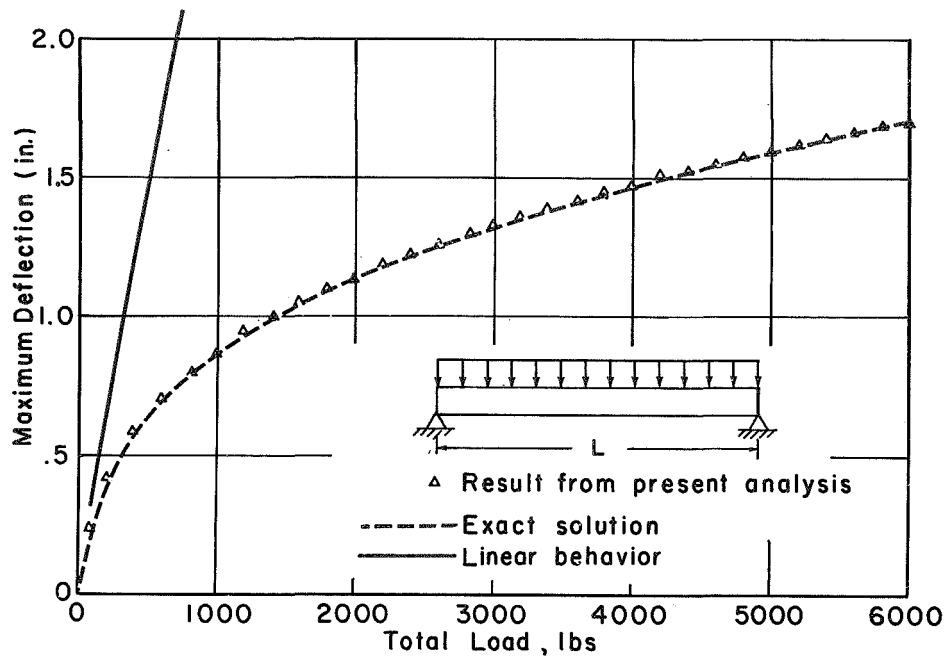
(a) Load-deflection behavior
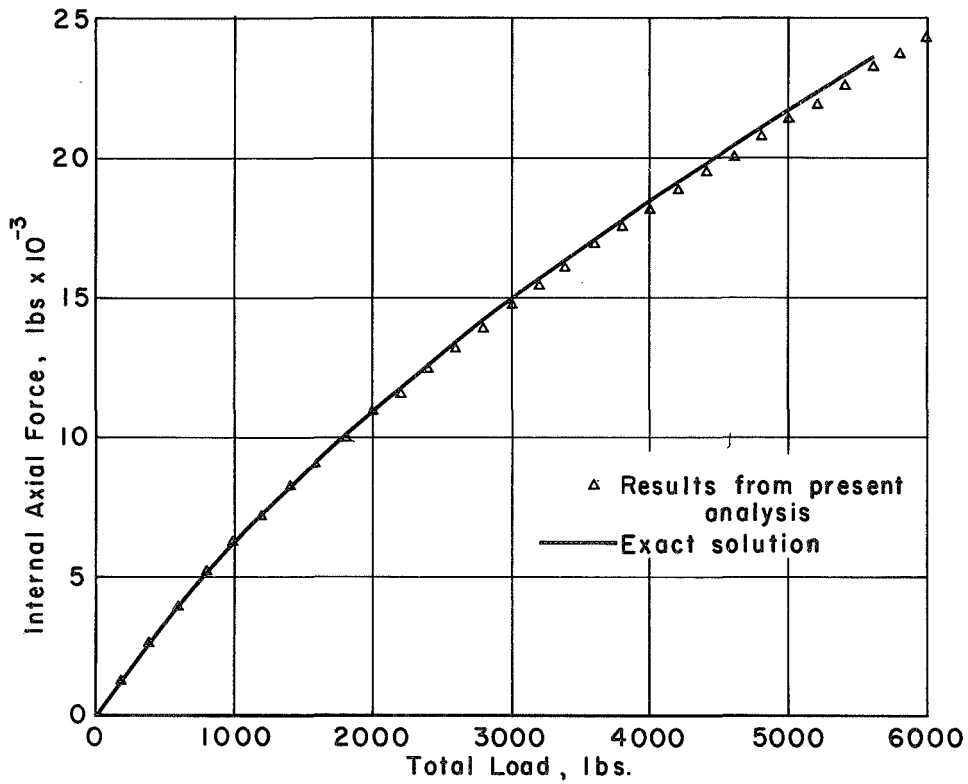
(b) Variation of internal axial force with load

Fig. 65   RESPONSE OF RESTRAINED BEAM TO APPLIED LOADING

265
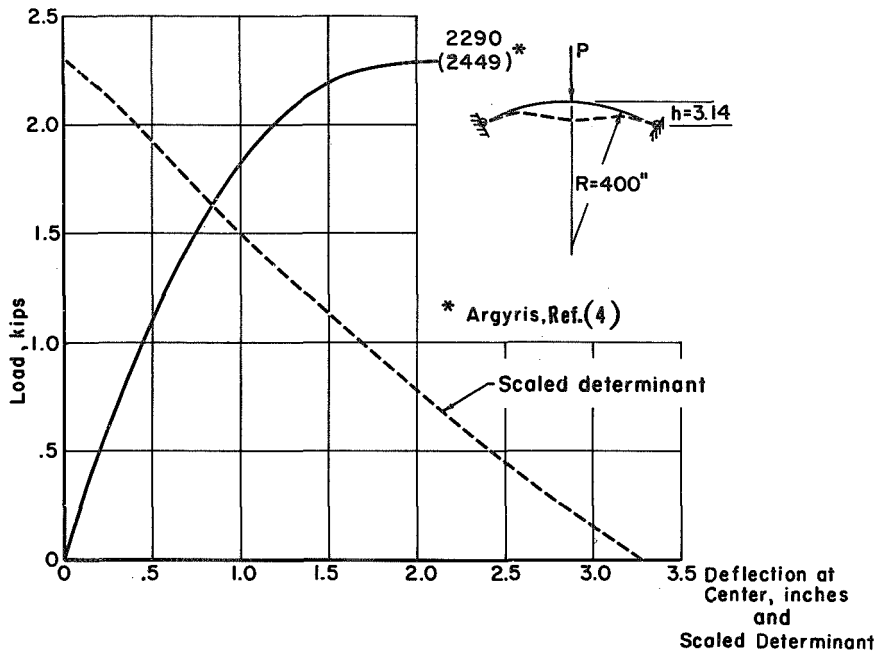
Fig. 66 LOAD VERSUS CENTRAL DEFLECTION FOR A SIMPLY SUPPORTED
ARCH SUBJECTED TO A CONCENTRATED LOAD
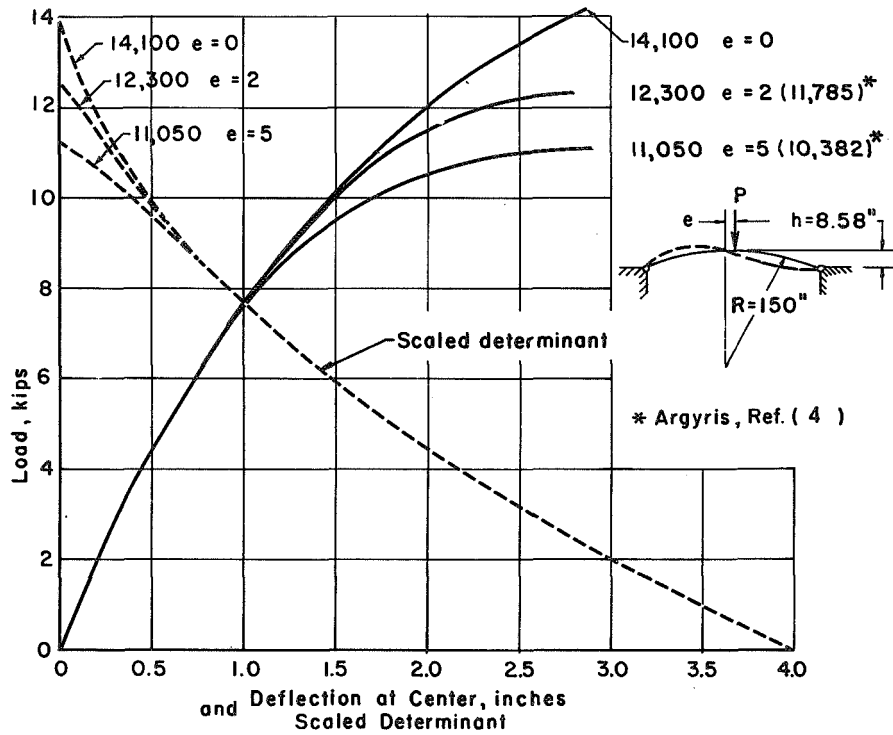
Fig. 67 LOAD VERSUS CENTRAL DEFLECTION FOR A SIMPLY SUPPORTED
ARCH SUBJECTED TO A CONCENTRATED LOAD

266
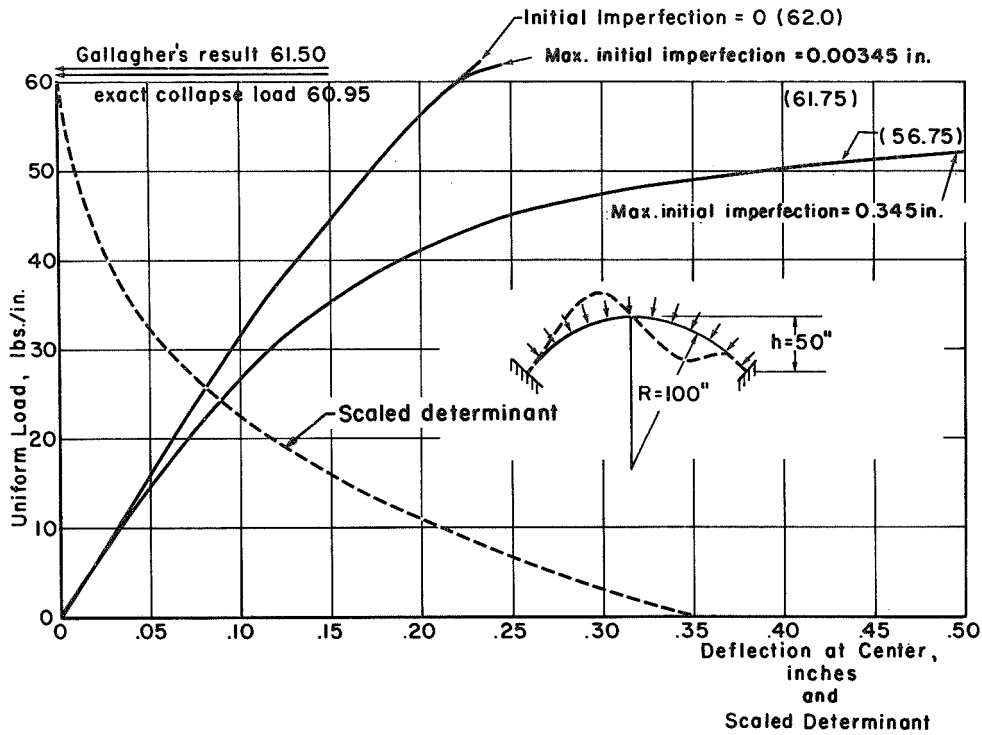
Fig. 68 LOAD VERSUS CENTRAL DEFLECTION OF A UNIFORMLY LOADED
FIXED ENDED ARCH
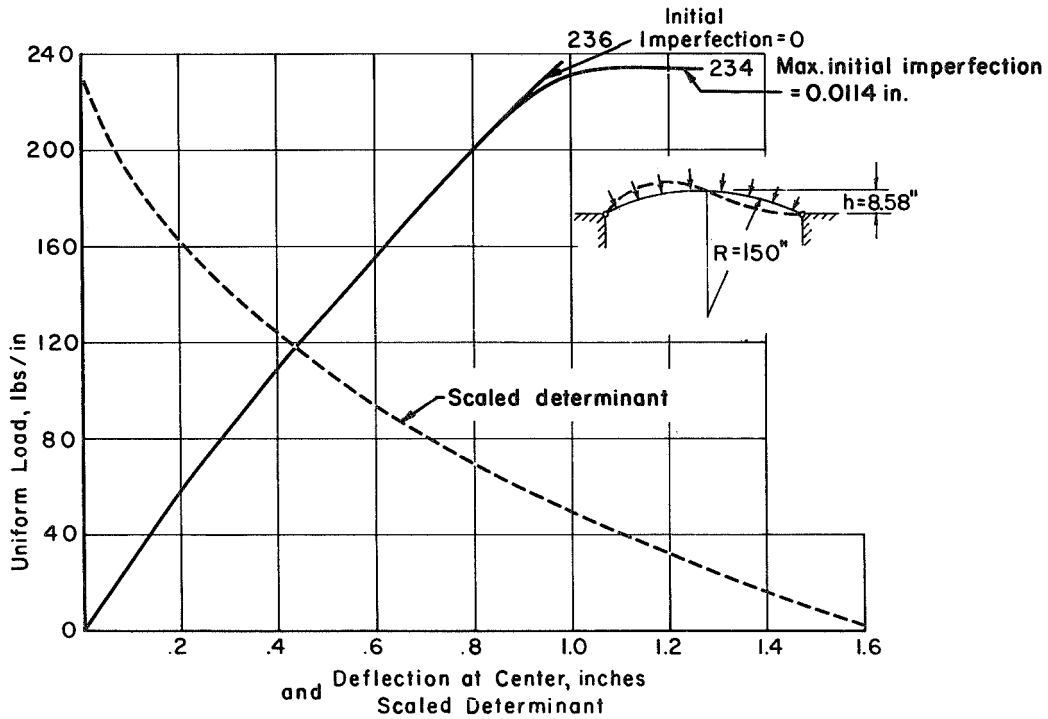
Fig. 69 LOAD VERSUS CENTRAL DEFLECTION FOR A UNIFORMLY LOADED
SIMPLY SUPPORTED ARCH

267
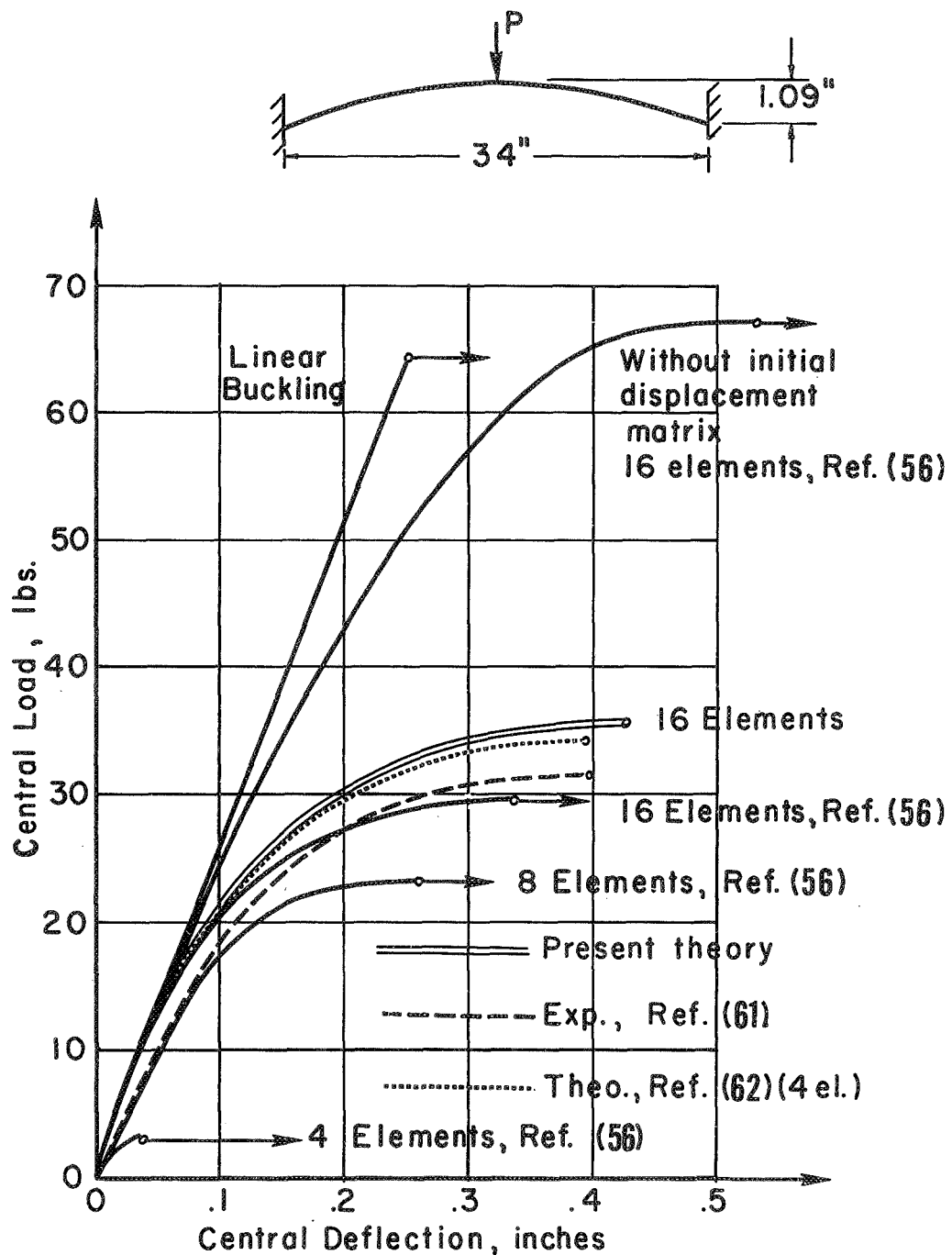
Fig. 70 COMPARISON OF RESULTS FOR A FIXED-ENDED
ARCH SUBJECTED TO A CONCENTRATED LOAD

(a) Load-deflection behavior

(b) Progression of elastic-plastic boundary
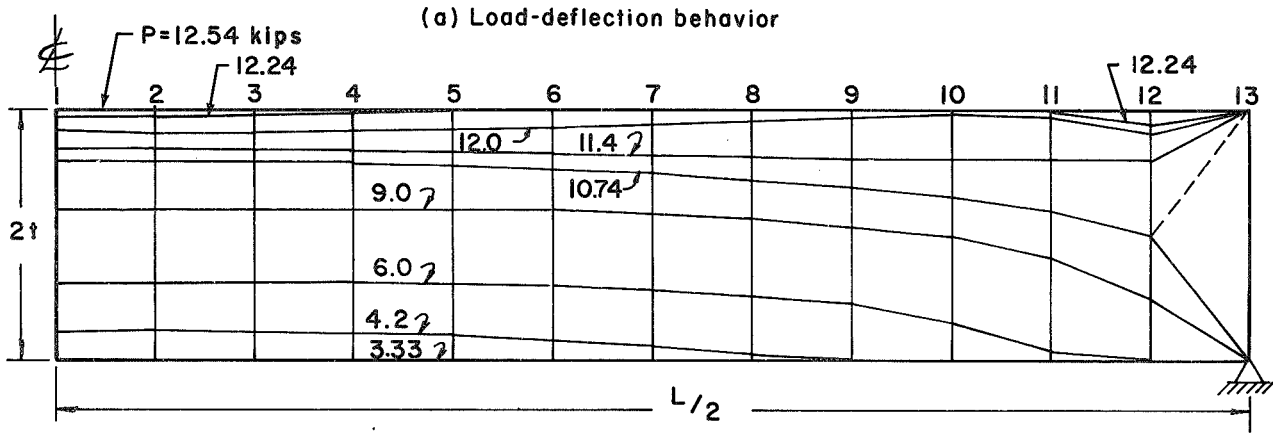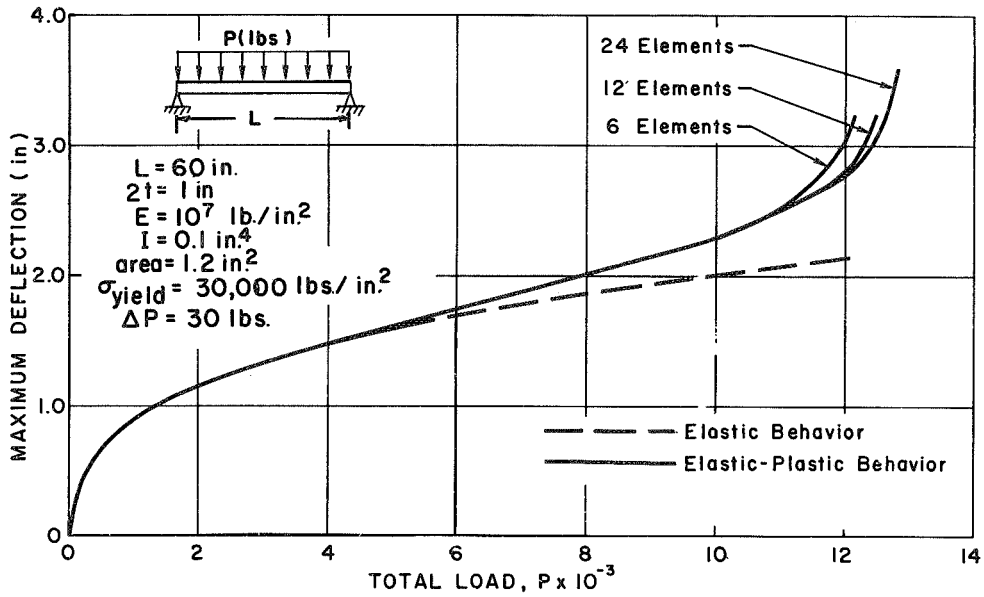
Fig. 71 ELASTIC-PLASTIC RESPONSE OF A RESTRAINED BEAM

269
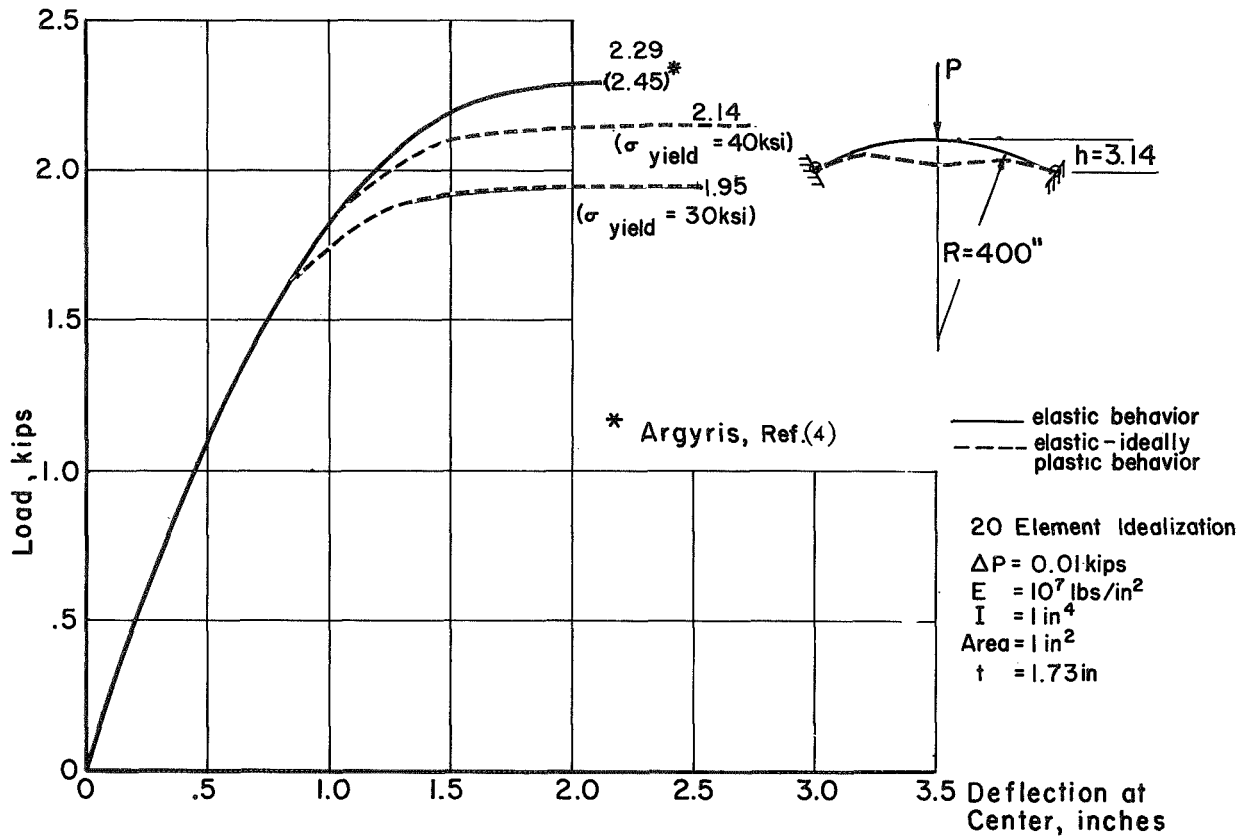
Fig. 72. LOAD VERSUS CENTRAL DEFLECTION FOR A SIMPLY SUPPORTED
ARCH SUBJECTED TO A CONCENTRATED LOAD

270
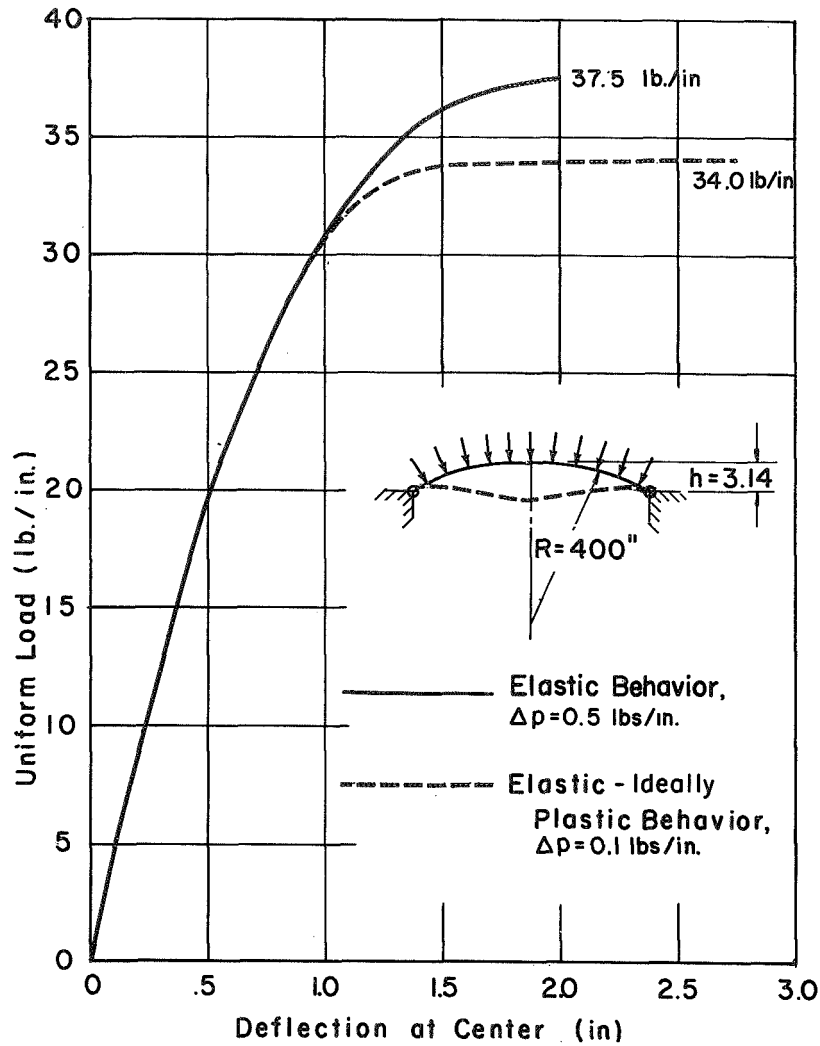
(a) Load vs. central deflection
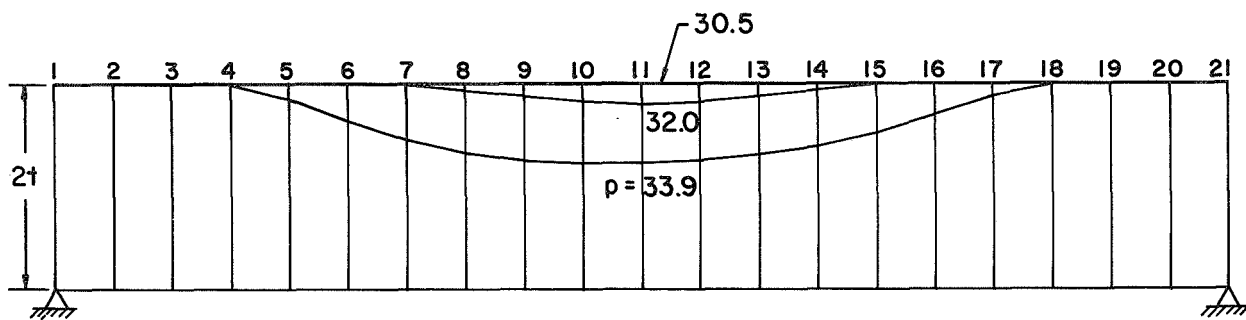
(b) Progression of elastic-plastic regions

FIG. 73   SIMPLY SUPPORTED ARCH SUBJECTED TO A UNIFORM LOAD
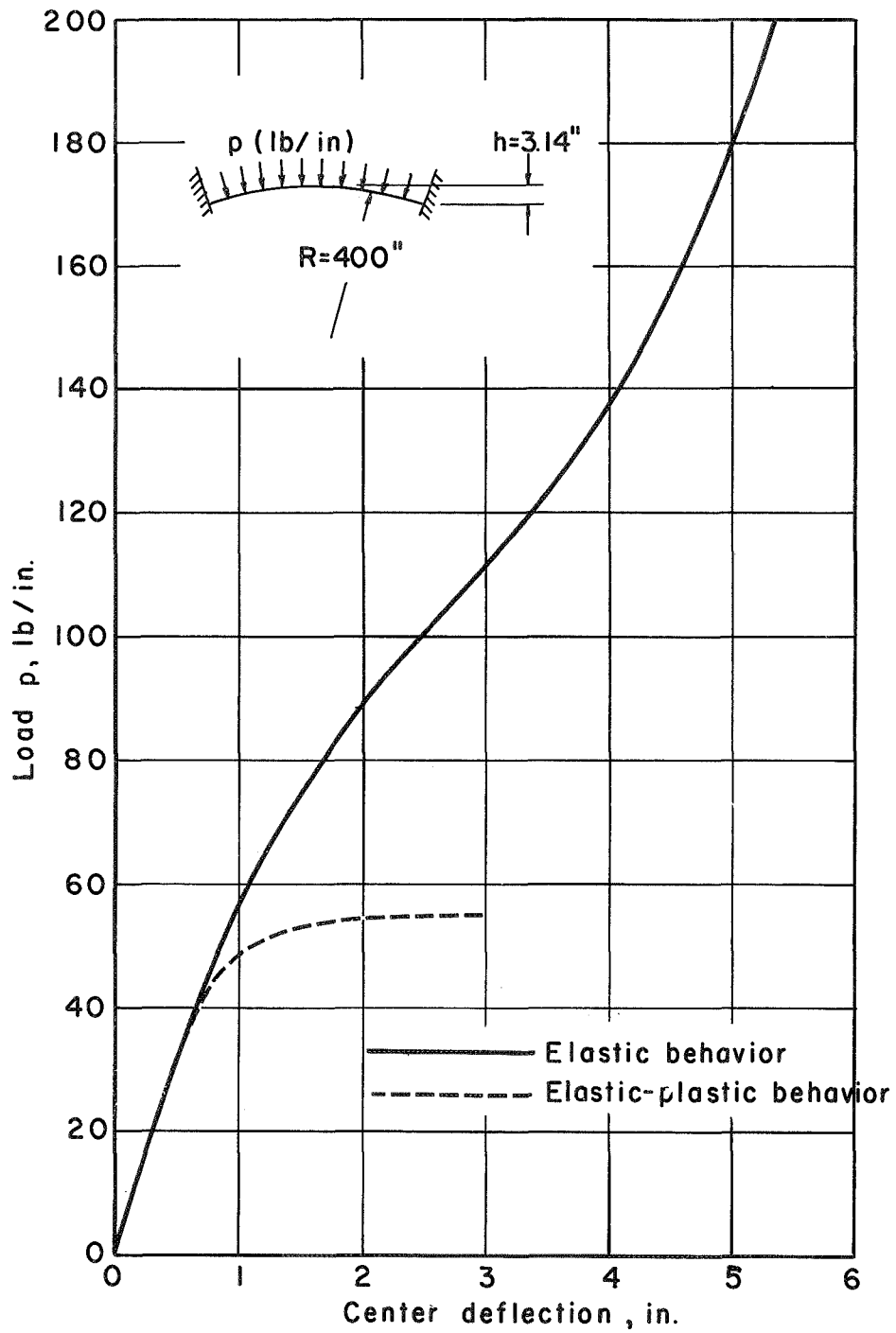
Fig. 74. LOAD VERSUS DEFLECTION OF A
UNIFORMLY LOADED FIXED ENDED
ARCH.
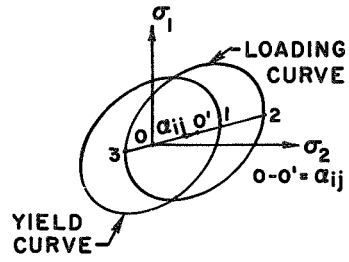
Fig. 75 KINEMATIC HARDENING
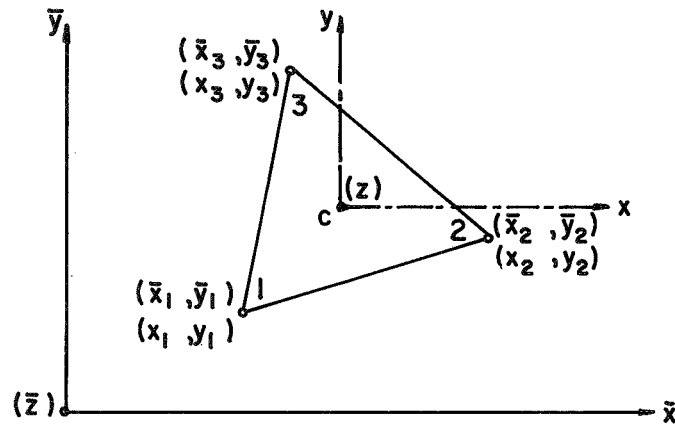
Fig. 76. GLOBAL AND "LOCAL GLOBAL" CARTESIAN SYSTEMS
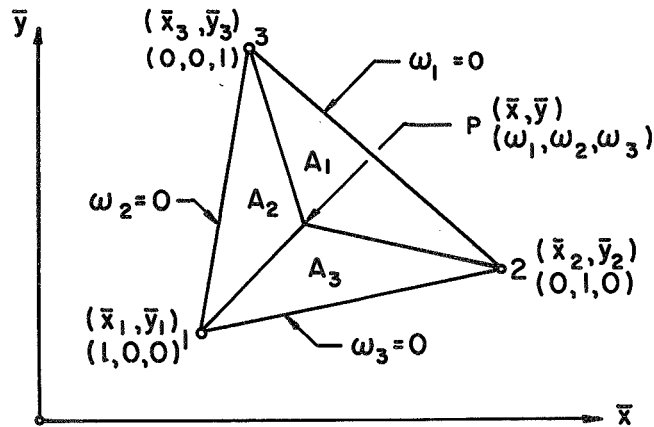
Fig. 77. AREA COORDINATES
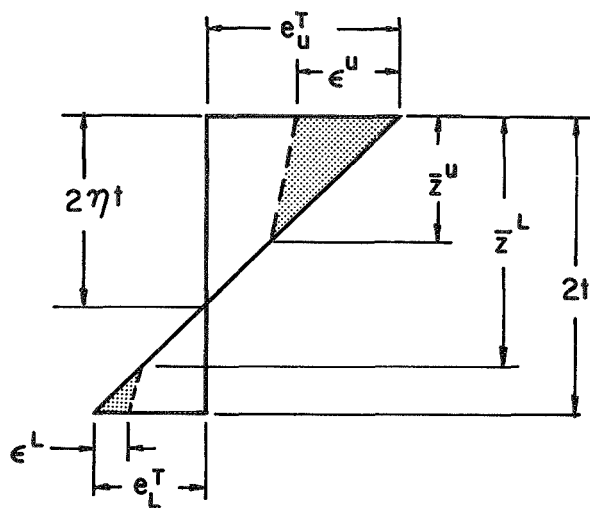
(a) UPPER AND/OR LOWER SURFACES
PLASTIC-TOTAL STRAINS OF OPPOSITE
SIGN.
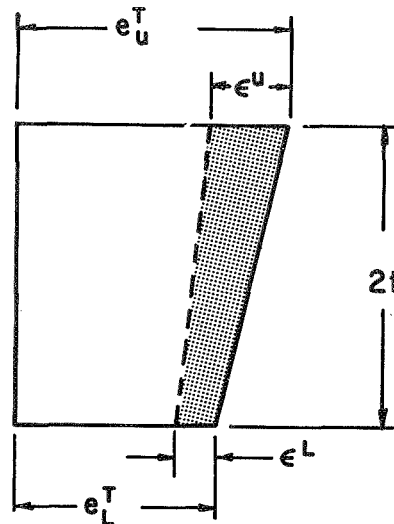
(b) FULLY PLASTIC SECTION-TOTAL
STRAINS OF THE SAME SIGN.
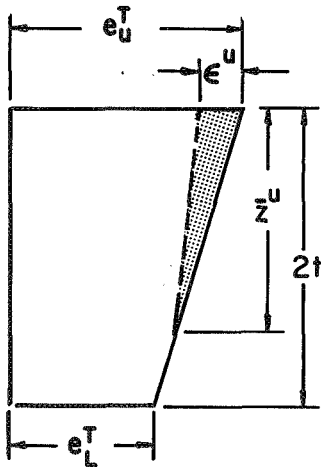
(c) UPPER SURFACE
PLASTIC-TOTAL STRAINS
OF THE SAME SIGN.
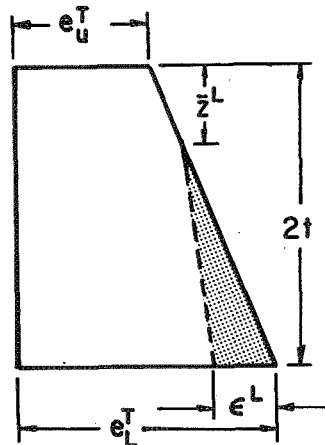
(d) LOWER SURFACE
PLASTIC-TOTAL STRAINS
OF THE SAME SIGN.
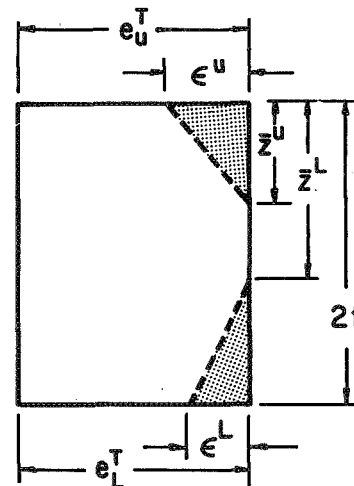
(e) UPPER AND LOWER
SURFACES PLASTIC-TOTAL
STRAINS OF THE SAME SIGN.

Fig. 78. POSSIBLE STRAIN STATES FOR USE IN COMPUTING
MEMBRANE STRESS RESULTANTS

274
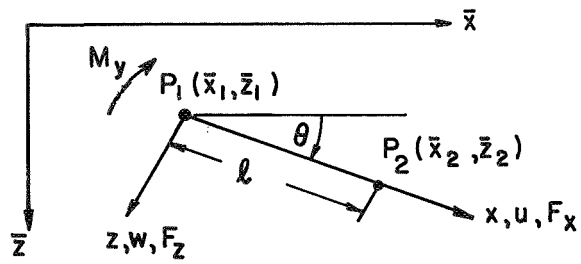
Fig.79. LOCAL AND GLOBAL COORDINATE SYSTEMS FOR
BEAM COLUMN ELEMENT.
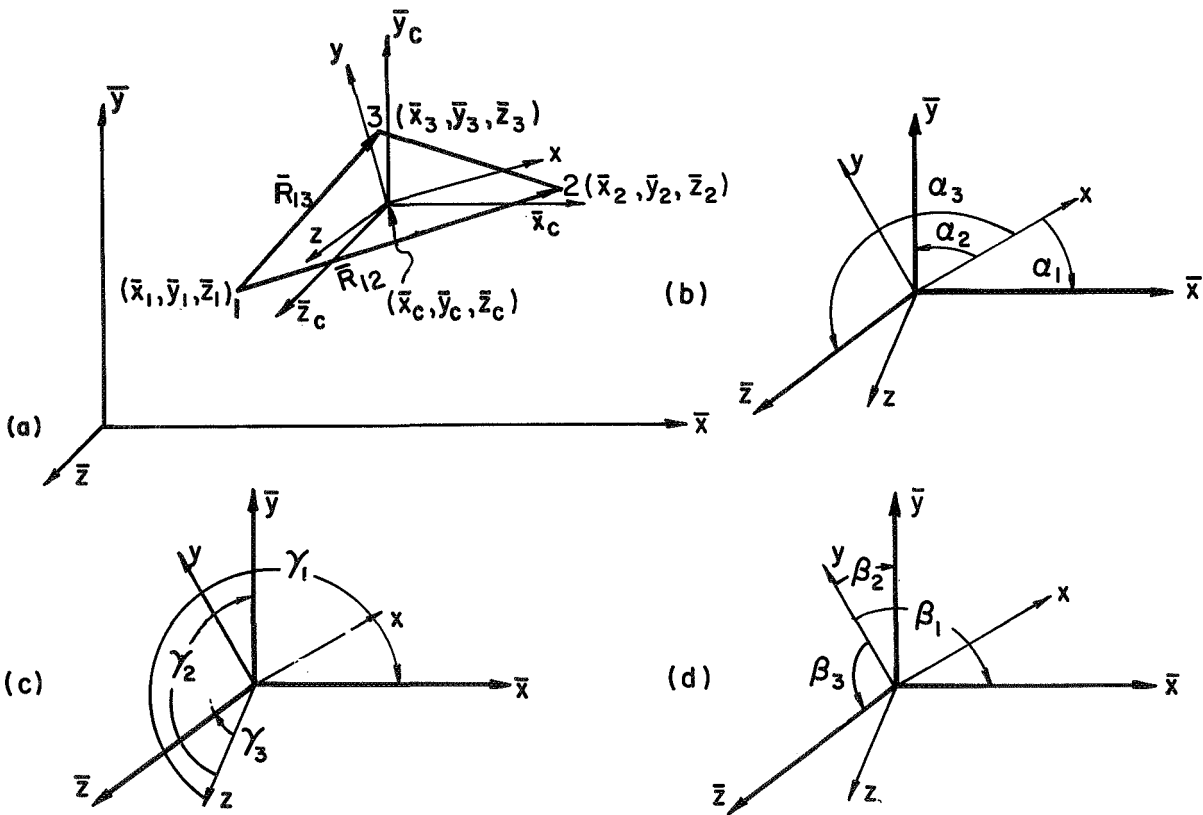
Fig. 80. LOCAL," LOCAL GLOBAL", AND GLOBAL COORDINATE
SYSTEM FOR PLATE ELEMENT.

FIRST CLASS MAIL

"The aeronautical and space activities of the United States shall be conducted so as to contribute . . . to the expansion of human knowledge of phenomena in the atmosphere and space. The Administration shall provide for the widest practicable and appropriate dissemination of information concerning its activities and the results thereof."

— NATIONAL AERONAUTICS AND SPACE ACT OF 1958

NASA SCIENTIFIC AND TECHNICAL PUBLICATIONS

TECHNICAL REPORTS: Scientific and technical information considered important, complete, and a lasting contribution to existing knowledge.

TECHNICAL NOTES: Information less broad in scope but nevertheless of importance as a contribution to existing knowledge.

TECHNICAL MEMORANDUMS: Information receiving limited distribution because of preliminary data, security classification, or other reasons.

CONTRACTOR REPORTS: Scientific and technical information generated under a NASA contract or grant and considered an important contribution to existing knowledge.

TECHNICAL TRANSLATIONS: Information published in a foreign language considered to merit NASA distribution in English.

SPECIAL PUBLICATIONS: Information derived from or of value to NASA activities. Publications include conference proceedings, monographs, data compilations, handbooks, sourcebooks, and special bibliographies.

TECHNOLOGY UTILIZATION PUBLICATIONS: Information on technology used by NASA that may be of particular interest in commercial and other non-aerospace applications. Publications include Tech Briefs, Technology Utilization Reports and Technology Surveys.

Details on the availability of these publications may be obtained from:

SCIENTIFIC AND TECHNICAL INFORMATION DIVISION

NATIONAL AERONAUTICS AND SPACE ADMINISTRATION
Washington, D.C. 20546